Effect of silica particles on foam stability

by

Shih-Chi Chu

A thesis submitted to
The University of Birmingham
for the degree of
Doctor of Philosophy

School of Chemical Engineering
The University of Birmingham
February 15, 2012

UNIVERSITY OF
BIRMINGHAM

University of Birmingham Research Archive

e-theses repository

This unpublished thesis/dissertation is copyright of the author and/or third parties. The intellectual property rights of the author or third parties in respect of this work are as defined by The Copyright Designs and Patents Act 1988 or as modified by any successor legislation.

Any use made of information contained in this thesis/dissertation must be in accordance with that legislation and must be properly acknowledged. Further distribution or reproduction in any format is prohibited without the permission of the copyright holder.

Abstract

This thesis investigates how the properties of foams can be modulated by the addition of particles to the foam solution. As a model system hydrophobic and hydrophilic silica particles were used. The de-agglomeration of hydrophilic silica particles in water and surfactant solutions was studied. Two methods are investigated: ultrasound cavitation (UC) and mechanical agitation (MA). The efficiency of these two methods was compared with respect to their ability to produce foams and to de-agglomerate particles. The results show that MA is more efficient when the aggregates size is larger than 1 μm. However, UC broke the aggregates into smaller sizes when the aggregate size was smaller than 1 μm.

In the de-agglomeration of hydrophobic silica particles in water and surfactant solutions, only UC was used. The higher the hydrophobicity of the silica the more energy input was required to break down the aggregates has been found. Slightly hydrophobic particles were broken down to micron size while the most hydrophobic particles could not be broken down into micron-sized particles. The hydrophobic particles were easier to separate at higher pH values but pH had no effect on hydrophilic silica particles.

The same particles were used as additions to protein and surfactant foaming solutions. In the experiments, the amount and types of particles, proteins and surfactants were varied in the foaming dispersions. Then UC and MA were used to foam the dispersions and the drainage, breakage and microstructure of the resulting foams were examined.

Proteins: both casein and whey protein foams were considered. In the protein solution with hydrophilic particles, foam stability and foam life increased with increasing silica particle concentration. At lower concentrations of silica, a wetter foam was produced and less energy input was needed when using UC than MA. Hydrophobic particles acted as an anti-foaming agent in the protein solution. At pH 7, the foam made by MA collapsed suddenly 30 minutes after formation, but not in UC. The results showed that the addition of hydrophilic particles only increased stability in whey protein foam but not in casein foam.

Sufactant: C12LAS and CTAB were used to study the surfactant solutions with particles. In Cl2LAS (anionic) foam, a low concentration of added particles destabilized foam whereas high particle concentrations stabilized foam. Foam stability increases with all types of silica particles in CTAB (cationic) foams. The pH has no significant effect on C12LAS foam but has a strong effect on CTAB foam. From observations of the foam microstructure, the bubble size increased with increasing pH. An increase in bulk viscosity contributed to the reduction of drainage but also led to a great reduction in foamability.

Comparing foam generation methods and varying viscosities: Partially hydrophobic silica particles were used in pure water to generate foam. Foamability and foam stability both increased with increasing concentration of particles. Moderately hydrophobic particles gave optimum foamability whilst no foam could be produced with fully hydrophilic particles. Foams generated by UC are drier and the bubble size is larger than in the ones made by MA. The particular foams produced by MA exhibited an ultra high stability with no drainage or change in foam height and bubble size over a month. A much less stable foam was generated at pH 10 and much wetter and denser foams were obtained in higher viscosity systems. In the foam rheology test, a transition from solid-like to liquid-like behaviour was found while the foam with addition of SCMC exhibited no such transition.

Acknowledgments

我要特別感謝我的家人，謝謝我的爸爸媽媽妹妹弟弟們一路上給我的支持和鼓勵，使得我能完成這論文。

I would like to thank my supervisor, Professor M. Barigou for all his assistance throughout the PhD. I would also thank to Professor David York and the P&G Company for the materials they provided and all their assistance throughout the project. Thanks also to my friends and colleagues Karin, Hanna, Yue, Roman, Ian and Yulan.

Contents

Nomenclature

A	Hamaker constant	S	skewness
C_v	coefficient of variation	K	kurtosis
C_p	heat capacity	$P(d_i)$	probability function
D	dielectric constant	Z	valency of the counterions
E	energy	a	maximum liquid level
E_V	energy dissipation rate	b	time constant
ΔG^T	total energy	d_{10}	number mean bubble size
G^d	van der Waals energy	d_{32}	Sauter mean bubble size
G^r	electrostatic energy	e	elementary charge
G^h	hydration energy	h	liquid level
G'	storage modulus	m	mass
G''	loss modulus	n_0	concentration of counter ions at infinite distance
H	foam height	k	Boltzmann constant
R	a distance R	Δp	pressure difference
T	temperature	t_d	time
ΔT	change in temperature	κ	units of reciprocal length
V_E	free energy of electrostatics repulsion	Φ	Stern potential
V_g	volume of the gas	ε_0	permittivity of free space
V_l	volume of the liquid	Υ	surface tension
M	Median	σ	standard deviation
τ	constant shear stress	$\dot{\gamma}$	shear rate

Chapter 1

Introduction

1.1 Introduction

Both suspensions and foams are disperse systems. Suspensions are solids dispersed in liquids. Suspensions are thermodynamically unstable although they can be stable over a long period of time depending on the nature of solids and liquids. Foams are gas bubbles separated from each other by thin liquid films. They are colloidal systems. In the classification based on the state of aggregation of the two phases, foams are commonly classified as gases dispersed in liquids or solids (solid foam). In the "solid foam", it can be that the liquid has changed into a gel or solid phases after making the "foam." The volume fraction of the gas and liquid can be varied, giving foams of different structure and properties. When the foam contains a very high volume of liquid, it can be called "gas emulsion" rather than foam.

Well suspended and stable suspensions are important for many processes and practical applications including pigments, printing inks, paper coating, pharmaceuticals, fertilizers, and processed foods. Foams are difficult to characterise because they are metastable and their behaviour is challenging to understand. They can be found in our everyday life, in food products, such as ice cream, chocolate mousse and instant package of cappuccino. Foams can be used in shampoo, shaving foam, and bubble bath. In addition, foams are also found in fire extinguishers and floatation.

In many contexts and applications foams are desirable, however, in others persistent foams may be undesirable. Normally stable foams are required in the food industry. A long shelf life of food

products is an important factor as well as the texture and appearance of products. In industrial contexts, it is important to control the stability of foams and the micro structure. For this reason it is of fundamental importance to understand the factors that determine foam stability.

While stable foams are sometimes desirable, in many circumstances foaming can also cause significant processing problems and product defects. For example, the presence of foams in a bio-reactor can cause operating problems in commercial fermentations and a decrease of the bioreactor efficiency. In household and personal care products consumers prefer cleaning products that produce a lot of foam which they have learned to associate with a good cleaning effect. At the same time, these foams should also be easy easy to rinse off and not be overly persistent. So in this contexts it is important to reduce foam stability, while still preserving good initial foaming.

Solid particles have been used to de-stabilize and stabilize foams for decades. Interest in this topic has been reawakened recently by the discovery that solid-stabilized foams can lead to extreme stability for foams when the solid particles are irreversibly adsorbed at the interface of air and water. This long-term stability cannot be achieved either in protein-stabilized or surfactant-stabilized foams. It was noted that the stability of solid-stabilized foams can be affected by the degree of hydrophobicity of the particles, and different environmental conditions such as pH, salt concentration, and the presence of surfactants. However, the detail of the foam microstructure (bubble size distributions) related to macroscopic foam behaviour is under-researched. Also, the rheological behaviour of these particles in suspensions and the corresponding particles stabilized foam under different conditions need further investigation.

It is the main aim of this thesis to investigate the factors that influence foaming. Specifically, in this thesis silica particles as a model system is used to understand the main factors that determine the characteristics and properties of foams. The foamability, foam lifetime, drainage and foam-microstructure depend on the type of silica particle we use (whether hydrophilic or hydrophobic), the foam generation method and the the characteristics of the suspension are investigated. With regards to the latter item the silica particles with surfactants, proteins (whey and casein) will be combined and studied the resulting foam characteristics for different pH values and viscosities. The hope is that our results will generalise and can be used to specifically regulate the desired foam

characteristics in practical applications.

An important issue in research on suspensions is particle de-agglomeration. There are a number of well researched de-agglomeration techniques. One practically important method is mechanical agitation. This method is relative well understood, including its effect on the particle sizes and their distribution in the suspension. This is particularly true for de-agglomeration studies of hydrophilic particles. Hydro-phobic particles are less studied. Another method is ultra-sound cavitation. There are only relatively few studies of de-agglomeration using ultrasound cavitation in comparison to mechanical agitation. A part of this thesis is a comparison of de-agglomeration of silica particles using those two methods: mechanical agitation and ultrasound cavitation. Specifically the achievable particle size distribution depends on the de-agglomeration method, the energy input and the hydrophobicity/hydrophilicity of the particles are investigated.

1.2 Outline of the Thesis

Each chapter of this thesis deals with a specific parameter relevant for foam stability. The literature relevant to these aspects is reviewed separately in the each chapter of this thesis. The structure of the thesis is follows: Chapter 2 gives a general background on suspensions and foams such as classifications of suspensions and foams, common preparation methods and factors determining suspension and foam stability. Chapter 3 describes the methods used in our research.

Chapter 4 studies the de-agglomeration and stability of both hydrophilic and hydrophobic silica particles in suspensions. Measurements of the median particle size and particle size distributions are used to observe the degree of de-agglomeration and the stability of the suspensions. A comparison of two de-agglomeration methods (ultrasound cavitation and mechanical agitation) is presented. The influence of particles with different degrees of hydrophobicity, and the role of pH and addition of ionic surfactants on the de-agglomeration process are also investigated.

Chapter 5 studies the effect of different foam generation methods with different energy intensities on whey protein foams. A comparison of the effect of hydrophilic silica particles on two types of protein (whey and casein) is also investigated in this chapter. The influence of different degrees of hydrophobicity of silica particles, as well as the role of the pH and the viscosity are also studied.

Chapter 6 investigates the effect of two types of ionic surfactants (C12LAS and CTAB) on foam stability. Specifically, it focuses on silica particles as a model for stabilizing or defoaming agents. The influence of different degrees of hydrophobicity of silica particles, and again the role of the pH and the viscosity are studied.

Chapter 7 presents an in-depth experimental study of the macroscopic aspects of silica particle-stabilized foams and how these relate to microscopic observations (bubble size distribution). Measurements of the surface tension and the viscosity of particle suspensions are described. Various analytical techniques are used to ascertain the stability of the particle-stabilized foam, such as the bubble size and bubble size distribution, rheological behaviour and storage stability. An elegant and time-saving foam generation method, ultrasound cavitation, is employed and compared to the conventional foam generation method, mechanical agitation. The influence of particles with different degrees of hydrophobicity, pH and viscosity on foam is investigated. The rheology of the silica particle-stabilized foams is also studied.

Chapter 8 presents the general conclusions of this thesis and outlines suggestions for future research work in this area.

Chapter 2

General Background

2.1 Suspension and Sol

Both suspensions and sols (colloids) are heterogeneous fluids (the continuous phase) which contain solid particles (the dispersed phase). In general, we can distinguish suspensions from sols by the size of the solid particles dispersed and the sedimentation in the fluids. In suspensions, the solid particles are usually larger than 1 micrometer and will eventually settle. The size range of solid particles is 10^{-9} to 10^{-6} m in sols. Due to the small size, the random motions of the particles (Brownian motion) keep the particles evenly and stably suspended in the sols over long time periods.

Getting a small and uniform size of particles is essential so that the particles fully employ their functions in the suspension and sol. Nanoscaled particles show altered properties and have widespread industrial applications in manufacturing of pigments, fillers, ceramics, catalysts, pharmaceutical, cosmetics as well as electromagnetic and optical devices. In most of those applications, the quality of the products depends on the properties of these suspensions and sols as determined by the particle size, the degree of aggregation, and the structure of aggregates.

Morrison and Ross (2002) classified two methods for the process of making suspension and sol: (i) separating agglomerates by shearing forces; (ii) comminuting aggregates by fracture. The general term is *comminution*. Energy input is needed for comminuting to break bound aggregates or shatter coherent solids. High-speed stirrers (such as blade stirrers and rotor-stator dispersers), high-shear mills (example are colloid mills, homogenizers and ultrasonic dispersers) and impact mills (for ex-

amples: ball and jar mills and vibratory mills and attritors) are commonly used in the process of producing suspensions and sols. Generally, the procedure of making suspensions and sols in these instruments can be described in four steps: (i) the wetting of the particle surfaces; (ii) the separation of agglomerations and aggregates into individual particles; (iii) possibly the attrition or fracture of individual particles into smaller particles; (iv) the adsorption of dispersant by the particle surface to obtain a stable dispersion. Higher efficiency of the process can be achieved by improving each steps. Optimum energy saving and efficiency can be achieved by choosing the correct equipment. The long-term stability of dispersion is also of great importance for the quality of the end-product. To form a stable dispersion, it is essential to prevent particles from forming aggregates. This can be done by controlling the balance of attractive and repulsive interactions between the particles as they approach each other. A well-established theory for this inter-colloidal interaction is the Derjaguin-Landau-Verwey-Overbeek (DLVO) theory (Verwey and Overbeek, 1948). In this theory, the colloidal particles are assumed to be at infinite dilution. According to the DLVO theory, the net interaction energy is the sum of electrostatic forces and the van der Waals forces as shown below (Morrison and Ross, 2002):

$$\Delta G^T = G^d + G^r \tag{2.1}$$

where G^T is the total energy, G^d is the van der Waals energy and G^r is the electrostatic energy. The van der Waals energy is also known as dispersion or Hamaker energy. For two thick, planar parallel plates separated by a distance H, the Hamaker Equation is:

$$\Delta G^d = \frac{-A}{(12\pi H^2)} \tag{2.2}$$

where ΔG^d is the free energy per unit area and A is the Hamaker constant which is specific for materials and conditions.

For two equal particles of radii a with center a distance R apart, the Hamaker Equation is:

$$\Delta G^d = -\frac{A}{6}\left[\frac{2a^2}{R^2-4a^2} + \frac{2a^2}{R^2} + \ln\left(1-\frac{4a^2}{R^2}\right)\right] \tag{2.3}$$

where ΔG^d is the free energy per unit area and A is the Hamaker constant which could be A_{111}, A_{12},

A_{121}, or A_{123} depending on the conditions. When two equal particles approach each other closely, Eq.2.3 can be reduced to:

$$\Delta G^d = \frac{-Aa}{12H} \tag{2.4}$$

$$H = R - 2a \tag{2.5}$$

where H is the distance between the surfaces of the particles. Eq.2.4 is the most commonly used equation to estimate the strength of the dispersion force attraction between suspended particles. Eq.2.3 is used for more accuracy.

The free energy of electrostatics repulsion between two flat plates as a function of the distance between the plates, H, given by the Langmuir approximation is:

$$G^r = \frac{64 n_0 kT\gamma^2}{\kappa} exp(-\kappa H) \tag{2.6}$$

where n_0 is the concentration of counter ions at infinite distance, k is Boltzmann constant (1.3810^{-23} J/K), T is the temperature (K), γ is given by Eq. 2.7 and κ is given by Eq. 2.8. Note that κ has units of reciprocal length, so $1/\kappa$ is called the Debye length or the double-layer thickness. In most systems, $1/\kappa$ varies from about 1 to 100 nm.

$$\gamma = \tanh \frac{Ze\Phi}{4kT} \tag{2.7}$$

where Z is the valency of the counterions, e is elementary charge ($1.6 \cdot 10^{-19} C$), Φ is the Stern potential which is often substituted by the ζ potential as an approximation

$$\kappa^2 = \frac{2 n_0 Z^2 e^2}{D\varepsilon_0 kT} \tag{2.8}$$

where ε_0 is the permittivity of free space ($8.85 \cdot 10^{-19} CV^{-1}m^{-1}$), D is the dielectric constant which is 80 for water.

The application of the classical DLVO theory has its limitations. When water is the dielectric medium in which colloidal particles are suspended, the theory generally fails to predict the stability of very hydrophilic and very hydrophobic particle suspensions (Yotsumoto and Yoon, 1993a). Direct

measurements of the interaction between silica (Chapel, 1994, Vigil et al., 1994) and mica surfaces (Vigil et al., 1994) in aqueous electrolyte solutions have agreed with DLVO above a few nanometers. However, a short range repulsive force was found besides the van der Waals and electrostatically forces at smaller separations. This repulsive force is also called *hydration* force or *structural* force. Vigil et al. (1994) explained that the reason for the break-down of the DLVO theory is that modified water structures exist at the solid and water interfaces. For colloids and interfaces in aqueous media the predominant interaction is attributed to the hydration of adsorbed counterions and ionic functional groups on the surface. When the particle surfaces approach each other closely during interactions, the presence of hydration-ions close to the surface leads to a repulsion. Therefore, for these colloids, the classical DLVO theory must be extended as follows:

$$\Delta G^T = G^d + G^r + G^h \tag{2.9}$$

where G^h is hydration energy.

A dispersion can be classified as hydrophobic and hydrophilic[1] in the colloid system. To maintain a stable colloid system, the repulsive force must be dominant. For the hydrophobic dispersion, adding polymers can increase the stability of the system. This is because the polymers are adsorbed on the surface and prevent the particles coming into close contact. This effect is also called *steric repulsion* force. For hydrophilic particles, the electrostatically and hydration forces keep the system stable. However, adding salt into the system can change the hydration force and thus it can destabilize the dispersion. This is because adding salt can neutralize the counterions of water and other ionic functional groups on the surface of the particles. Therefore, additive of electrolytes, acid, and base, stabilizers can alter the shelf-life of dispersions and prevent the formation of flocculation and coagulation.

[1]Some of the literature uses instead of "hydrophobic" and "hydrophilic" the term "lyophilic" and "lyophobic" respectively. To simplify nomenclature, it will not be used the latter.

2.2 Foam

Foams are colloidal systems. They can be classified into to two groups based on the state of the aggregation of the two phases. The first one compares aqueous foams which are gases dispersed in liquids. The gas bubbles vary in size from about 50 μm to several millimeters. This type of foam is a *wet foam* when it has a thick liquid film between the spherical bubbles and its density is more than 700 g/L; wet foams are also called *gas emulsions* (Morrison and Ross, 2002). When a foam is not wet then it is a *dry foam*, which is a solid foam with gases dispersed in solids. Such foams have great commercial importance, for example as foam rubber, polyurethane foam, bread, sponge cake, and so on.

2.2.1 Surfactants, Proteins and Particles

Pure water cannot foam unless a surface active material is present, due to its high interfacial free energy. Creation of a new interface needs work and is energetically unfavorable. When a gas is introduced below the surface of pure water, gas bubbles rise to the surface and escape from liquid due to the buoyancy force and rupture immediately on contacting each other in order to restore to the equilibrium state with minimum energy. For true foaming to occur, the presence of solute capable of being adsorbed at the interface between gas and liquid is required (Rosen, 1989). By adding surface active agents to water the surface energy can be altered due to the adsorption of surfactant at the interfaces which can stabilize the bubble through the Gibbs-Marangoni effect, which will be described in more detail below (see page 22).

Surface active agents can be divided into two classes with respect to their molecular properties: the first class are low molecular weight surfactants (LMW) and the second class are proteins. Recently, many studies have also demonstrated the possibility of using only particles as surface active agents to generate and stabilize foams. In what follows the current literature on those three types of surface active agents will be described.

Surfactants

Firstly the surfactants were described. Low molecular weight surfactants have a characteristic molecular structure consisting of a hydrophilic group at one end and a hydrophobic group at the other. This is known as an *amphiphilic* structure. The surface energy of pure water is a result of the van der Waals attraction between water molecules. Each molecule is pulled equally in every direction by neighbouring molecules, resulting in a net force of zero as shown in Figure 2.1. At the surface of water, the molecules are pulled inwards by other molecules deeper inside the liquid and are not attracted as intensely by the air molecules. When surfactants are dissolved in water, these surfactant molecules will adsorb at air/water interfaces where they can arrange themselves such that the hydrophilic part is in the water and the other part is exposed to the air. Therefore, this arrangement destroys the original order of water molecules. It lowers the free energy of the system and reduces the amount of energy needed for foam formation. Surface tension has the dimension of force per unit length, or of energy per unit area. The surface tension of water is 72.0 N/m and the surface tension of surfactant is lower depending on the types of surfactants.

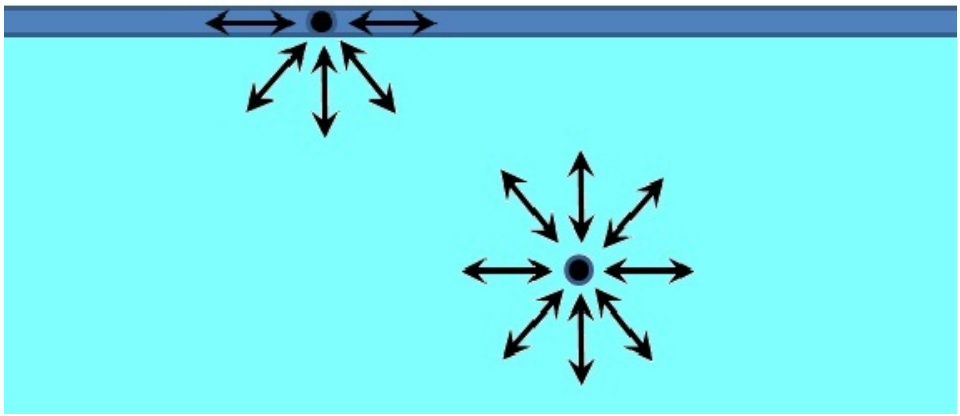

Figure 2.1: Diagram of the forces on two molecules of liquid .

As density of the surfactants molecules at the interface increases with increasing concentration of surfactants, the surface free energy (surface tension) decreases. Once a certain threshold concentration is reached—the so-called critical micelle concentration (cmc)—the surfactants start aggregating into *micelles*, thus again decreasing the system free energy by decreasing the contact area of hydrophobic parts of the surfactant with water. Upon reaching the cmc, any further addition of surfactants will just increase the number of micelles and the surface tension stays constant at the minimum

value, as shown in Figure 2.2.

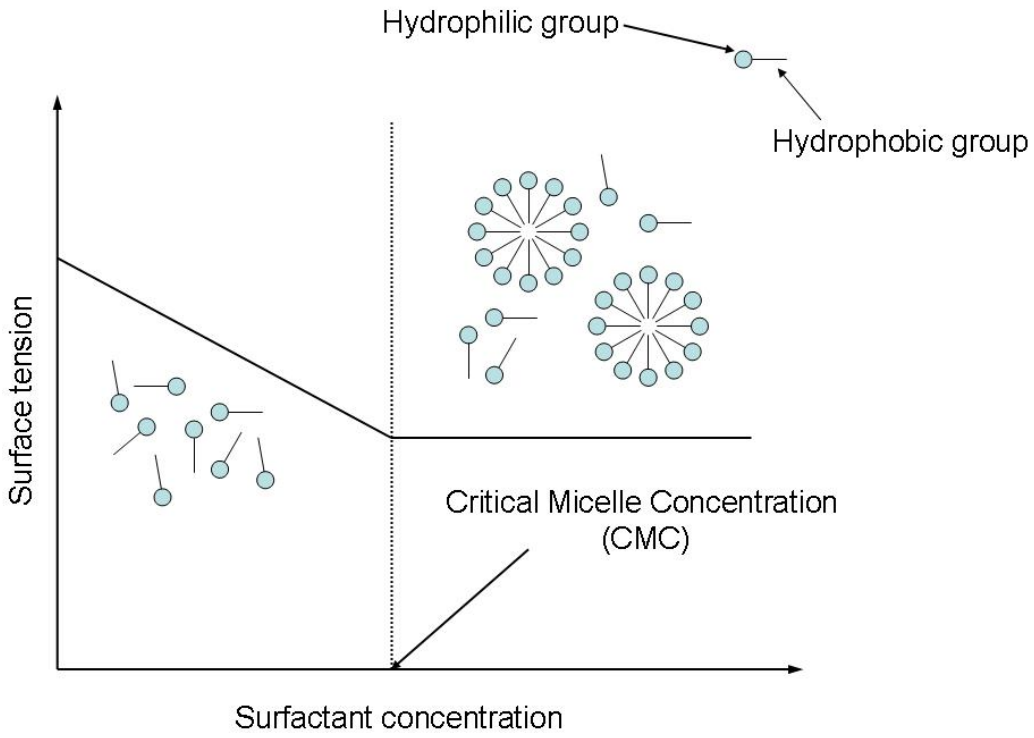

Figure 2.2: Variation of surface tension of a pure liquid with surfactant concentration

The properties of the surfactant (charge, molecular structure) are important for the properties of the dispersions (i.e. quality of suspensions, aggregations etc...) and foams (bubble size, foam lifetime etc...). According to the nature of the hydrophilic group, surfactants are classified as:

1. **Anionic:** the surface-active portion of the molecule bears a negative charge.

2. **Cationic:** the surface-active portion of the molecule bears a positive charge.

3. **Zwitterionic:** both positive and negative charges may be present in the surface-active portion.

4. **Nonionic:** the surface-active portion bears no apparent ionic charge.

   Examples of these surfactants and their chemical formulae are listed in Table 2.1. The differences in the nature of the hydrophobic groups are usually less pronounced than in the hydrophilic group. Generally, they are long-chain hydrocarbon residues. However, they include such different structures as:

(a) Straight-chain, long alkyl groups ($C_8 - C_{20}$);

(b) Branched-chain, long alkyl groups ($C_8 - C_{20}$);

(c) Long-chain ($C_8 - C_{15}$) alkylbenzene residues;

(d) Alkylnaphthalene residues (C_3 and greater-length alkyl groups);

(e) Rosin derivatives;

(f) High molecular weight propylene oxide polymers;

(g) Long chain perfluoroalkyl groups Rosen (1989).

Anionic	$RC\text{-}O^-Na^+$ (soap), $RC_6H_4SO_3^-Na^+$ (alkylbenzene sulfonate).
Cationic	$RNH_3^+Cl^-$(salt of a long-chain amine), $RN(CH_3)_3^+Cl^-$(quaternary ammonium chloride).
Zwitterionic	$RN^+H_2CH_2COO^-$(long chain amino acid), $RN^+(CH_3)_2CH_2CH_2SO_3^-$ (sulfobetaine).
Nonionic	$RCOOCH_2CHOHCH_2OH$ (monoglyceride of long-chain fatty acid), $RC_6H_4(OC_2H_4)_xOH$ (polyoxyethylenated alkylphenol).

Table 2.1: Examples of different charge surfactants and their chemical formulae.

Protein

Protein plays an important role in the stabilization of the structure of many foam-based food products. Proteins are organic compounds made of *amino acids* arranged in a linear chain and folded into a globular form. The amino acids in a polymer are joined together by the peptide bonds between the carboxyl and amino groups of adjacent amino acid residues (Ridley, 2006). When air is introduced into a protein solution, new interfaces are created. The structure of the protein unfolds to a more energetically favorable conformation to adsorb at the interfaces due to the simultaneous dehydration of the hydrophobic surface and the hydrophobic portions of the protein (Dickinson, 1986). Natural flexibility within the molecules can expose the hydrophobic portion of the protein into interfaces and conformational changes can be seen as a form of interfacial denaturation of the protein (Graham and Phillips, 1979). Therefore, the adsorption of proteins at interfaces can be described in terms of three

processes, namely, transport from bulk solution to the interface, penetration into the surface layer and reorganization of structure (surface denaturation) of the protein in the adsorbed layer, as shown in Figure 2.3 (Wilde, 2000). These may lead to completely different properties of foam.

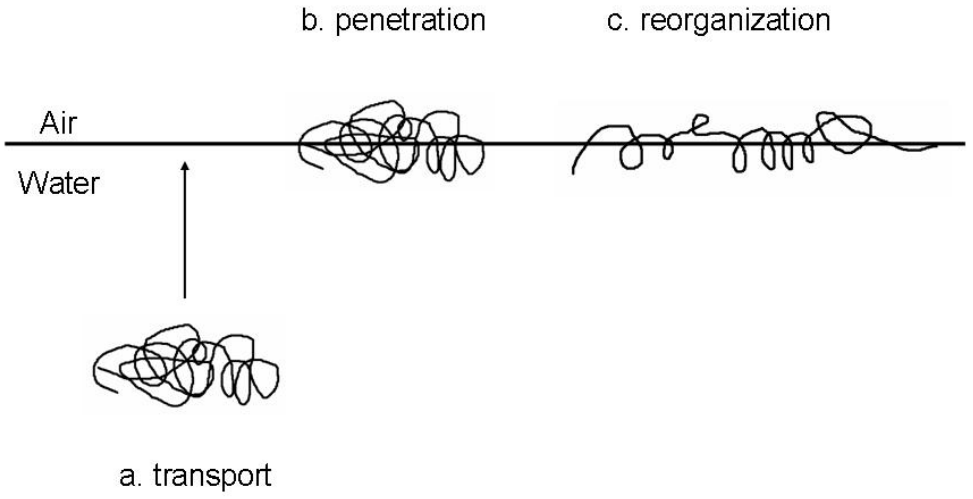

Figure 2.3: Adsorption process of proteins, (a) diffusion or transport to the interface; (b) penetration of adsorption; (c) structural reorganization (surface denaturation).

Protein may have good foamability. Foamability depends on how the protein adsorbs at the interface. A reduction in interfacial/surface tension is the most obvious outcome of protein adsorption. At equilibrium, surface tensions of concentrated protein solutions are often around 45.0 mN/m, while the surface tension of water is 72.0 mN/m at room temperature (Prins et al., 1998). The ability of proteins to adsorb and thus to lower the interfacial tension can be affected by the temperature and the pressure of the dispersions. These affect the structure of the proteins and hence the way the proteins behave at the interface.

Surfactants are relatively small and simple molecules which can move around at the interfaces to restore stability of foam films. In contrast, proteins are known (Dickinson, 1992) to form films with high interfacial elasticity, viscosity, and cross-linking between the surface adsorbed protein

molecules caused by van der Waals attraction, electrostatic repulsion, hydrophobic, hydrogen and covalent bonds (e.g. oxidation of sulphydryl group). Proteins have a distribution of both positive and negative charges throughout the molecule. Proteins with charges of equal sign will repel each other. However, by increasing the pH the net charge of proteins may be neutralized (which defines the *isoelectric* point (Graham and Phillips, 1979)), which in turn affects the protein-protein interactions in the dispersion. Protein foams are more stable around this isoelectric point, because the absence of protein-protein interactions allows a closer packing of the proteins at the interface.

When the protein molecules adsorb and unfold at the interface, they tend to associate with each other and create a network by van der Waals, electrostatic, hydrophobic forces, hydrogen bonds and even covalent intermolecular disulphide cross-linking (Hammershoj et al., 1999, Bos and van Vliet, 2001). Bos and van Vliet (2001) show that these intermolecular interactions are critical for the stabilization of the surface films between bubbles. The authors also point out that proteins are of high molecular weight compared to surfactant molecules and hence adsorp and desorp significantly slower than the latter. The stabilization of bubbles in foam is highly influenced not only by the protein-protein intermolecular interactions but also by the properties of the plateau border. Saint-Jalmes et al. (2005) reported that protein foams coarsen more slowly than the surfactant ones due to the highly viscoelastic interface and high surface shear viscosities of protein films resulting in more rigid plateau border. Kloek et al. (2001) have reviewed the effects of both bulk rheology and the interfacial rheological parameters (elasticity and viscosity) on the dissolution of the bubbles (shrinkage of the bubbles). A bulk or interfacial viscosity higher than a critical value can retard the shrinkage of the bubbles. The interface can act as a mechanical barrier to stop bubble dissolution, for example in solid foams, at high bulk and interfacial elasticities.

Particles

Hydrophobic particles can be used as antifoaming agents to destabilize unwanted foam. The mechanism was proposed by Frye and Berg (1989). When the solid particles size is larger than the thickness of the foam film, the solid particles will bridge the film as shown in Figure 2.4. Hydrophobic particles can penetrate the interface of air and water and the liquid drains away in the foam films because of

the capillary force and the large contact angle($> 90°$). This is also called *de-wetting*. Theory predicts that hydrophilic particles will prevent film rupture by slowing down the process of de-wetting due to its small contact angle; also they do not attach to the surface of bubbles but tend to remain within the film.

Partially hydrophobic particles can be divided into two types. Firstly, particles whose coating is homogeneous over the surface (e.g. reaction in the vapour phase). These particles are surface-active but not amphiphilic. The second type of partially hydrophobic particle is also called *Janus* particles. The coating is restricted to parts of the surface of the particles; the particles are thus amphiphilic and can be regarded as surfactants. However, both types of partially hydrophobic particles can adsorb at the surface of bubbles.

The size of the solid particle has an important influence on foam stability and contact angle; it is thus one of the important parameters to affect the attachment of the particles into the interfaces. Garrett (1993) showed that the foam can be destabilized with diameters of particles around 1-100 μm, while Tang et al. (1989) reported that the foam becomes more stable if the particle size is below ($< 0.7\ \mu m$). In a review Pugh (2005) explained that this is because the particle size is small enough compared to the film thickness and hence they can be arranged at the liquid/gas interface and stabilize the films by the capillary mechanism.

For hydrophilic particles, the contact angle is smaller than 90 degree and a larger portion of the particle surface sits in the aqueous phase. For hydrophobic particles, the contact angel is larger than 90 degree and a larger portion of the particle surface sits in the vapour phase. Pugh (1996) explains that partially hydrophobic particles behave similar to surfactant molecules (as shown in Figure 2.4 as far as the shape monolayers is concerned. This monolayer will be shaped such that the larger area of the particle surface remains on the external side. Once the particles adsorb at the interface of air and water (often described as *solids-coated* or *armored*) the bubble is stabilized against dissolution of gas into surrounding liquid. A rigid framework can be formed because of the large stresses between particles (Kam and Rossen, 1999). Extra energy is then required to remove the adhered particles during the coalescence of gas bubbles in order to break the thin film (Pugh, 1996). Therefore, the particles in the correct size range and with the appropriate wetting properties

can become essentially irreversibly adsorbed. This can give excellent stabilization against coalescence and disproportionation (Murray, 2007).

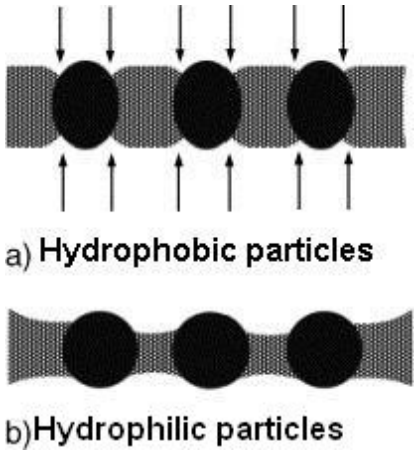

Figure 2.4: The influence of hydrophobicity of particles on the film stability as the particle size is larger than the thickness of the foam film. From Ref Pugh (1996).

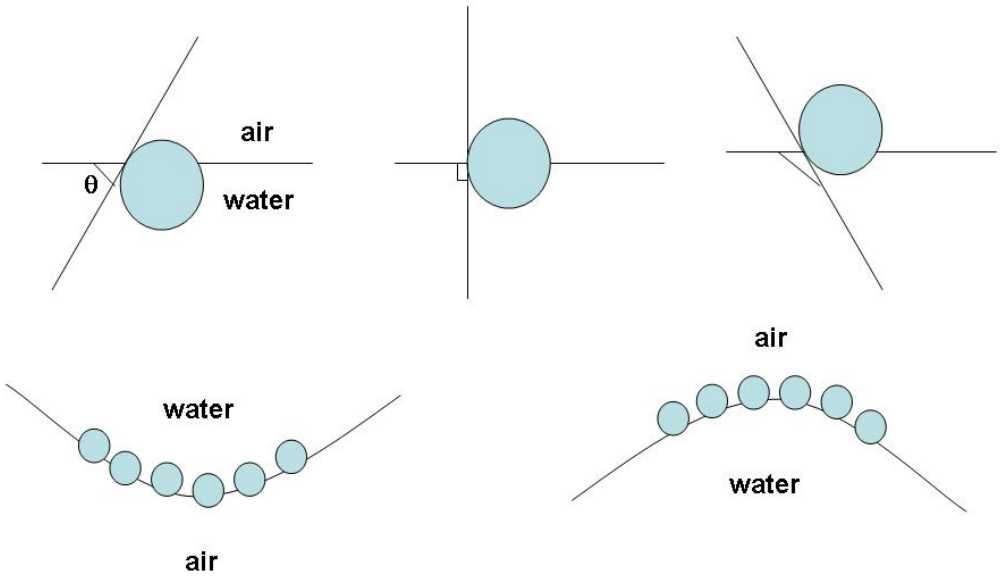

Figure 2.5: (Upper) Position of a small spherical particle at a planar air-water interface for a contact angle (measured through the aqueous phase) less than 90° (left), equal to 90° (centre) and greater than 90° (right). (Lower) Corresponding probable positioning of particles at a curved air-water interface. For $< 90°$, solid-stabilized aqueous foams (left). For $> 90°$, solid-stabilized aerosols (right).

2.2.2 Generation of Foams

Foam can be made using two methods: condensation and dispersion methods (Bikerman, 1973). In the condensation method, the foam is produced by dissolving the gas in the liquid under higher pressure in a supersaturating state and releasing it at lower pressure (such as, soft drinks, beer and Champagne) or gas *in situ* (for example, from chemical reaction, fermentation). In the dispersion method, numerous techniques have been used to generate foam. Foam can be made simply by shaking a bottle partially filled up with a solution. In the kitchen and food industry, the entrapment of air in the product results from whipping and beating. In the flotation and fractionation process, injecting gas through a single orifice or a porous plates is commonly used. Finer foam and smaller bubbles can be produced by using mixers, homogenizers and ultrasound devices.

Different methods of foam generation can alter the properties of foam. For example, size and shape of the bubbles can affect the amount of liquid in the foam. A fairly uniform bubble size can be obtained in supersaturated liquids via the nucleation of gas bubbles and by sparging the gas through a single orifice with a low and constant flow rate. With a higher flow rate or a porous disc, the resulting foam is *polydispersed* (Weaire and Hutzler, 1999), i.e. heterogenous with respect to bubble size. Foam produced by using high shear mixer and homogenizer are fairly homogenous in bubble size.

Foams occur as end products or during the processing of products in a wide rage of industries. The texture of foam is one of the vital key parameters to enhance flavours of food products and increase the smoothness of cosmetic products. Consumers have also learned to associate the detergency with foaming in personal care products. A more uniform bubble size distribution can provide a higher stability of foam, whilst the foam with broad bubble size distribution destabilizes due to coarsening and disproportionation. Therefore, a suitably bubble size distribution becomes one of the essential factors to determine the quality of the products. To prevent polydispersity of bubble sizes at an industrial scale is extremely difficult. Thus, developing methods to generate desirable foam structure is of great interest to industry.

2.2.3 Foam Structure

Foams are often classified into two types of structure according to the shape of the bubbles. The spherical bubbles in freshly made foam is also called *kugelschaums* which is often found at the lower part of the foam as shown in Figure 2.6(a). These spherical bubbles are separated by thick liquid lamellae and have fairly high liquid content. Therefore, they are often referred as "wet" foam and can be found in higher viscosity liquids. In general, the thick films between bubbles become thin and flat when the bubbles grow over time. The shape of the bubbles is changed from spherical to polyhedral and the liquid content in these films decreases dramatically until the system reaches balance. If the resulting film thickness is less than about 100 nm, these bubbles are referred to as *polyederschaum* which is normally found at the upper part of the foam in the column.

In foam, various thick and thin films meet at an angle of 120^o as illustrated in Figure 2.6(b) and the meeting point is called a *Plateau border*. The pressure in the Plateau border is lower than in other places in the bubble due to the curvature of the interface. It can be expressed by the Young-Laplace equation:

$$\Delta p = \gamma \left(\frac{1}{R_1} + \frac{1}{R_2} \right) \tag{2.10}$$

where γ is the surface tension and R_1 and R_2 are the two principal radii of curvature. For a spherical bubble, $R_1 = R_2 = R$, Equation 2.10 becomes:

$$\Delta p = \frac{2\gamma}{R} \tag{2.11}$$

Foams containing solid particles are also referred to as *froths*, hence froths are three phase systems. An important parameter for stabilizing the foam is the hydrophobicity of the solid particles. The structure of froths is shown in Figure 2.7. In froths the bubble size increases and liquid films get thinner towards the top of the foam. However, the bubbles at the top layers are typically distorted and the films are thicker. The structure of froths is similar to the two phase (air/water) foams (Pugh, 2005).

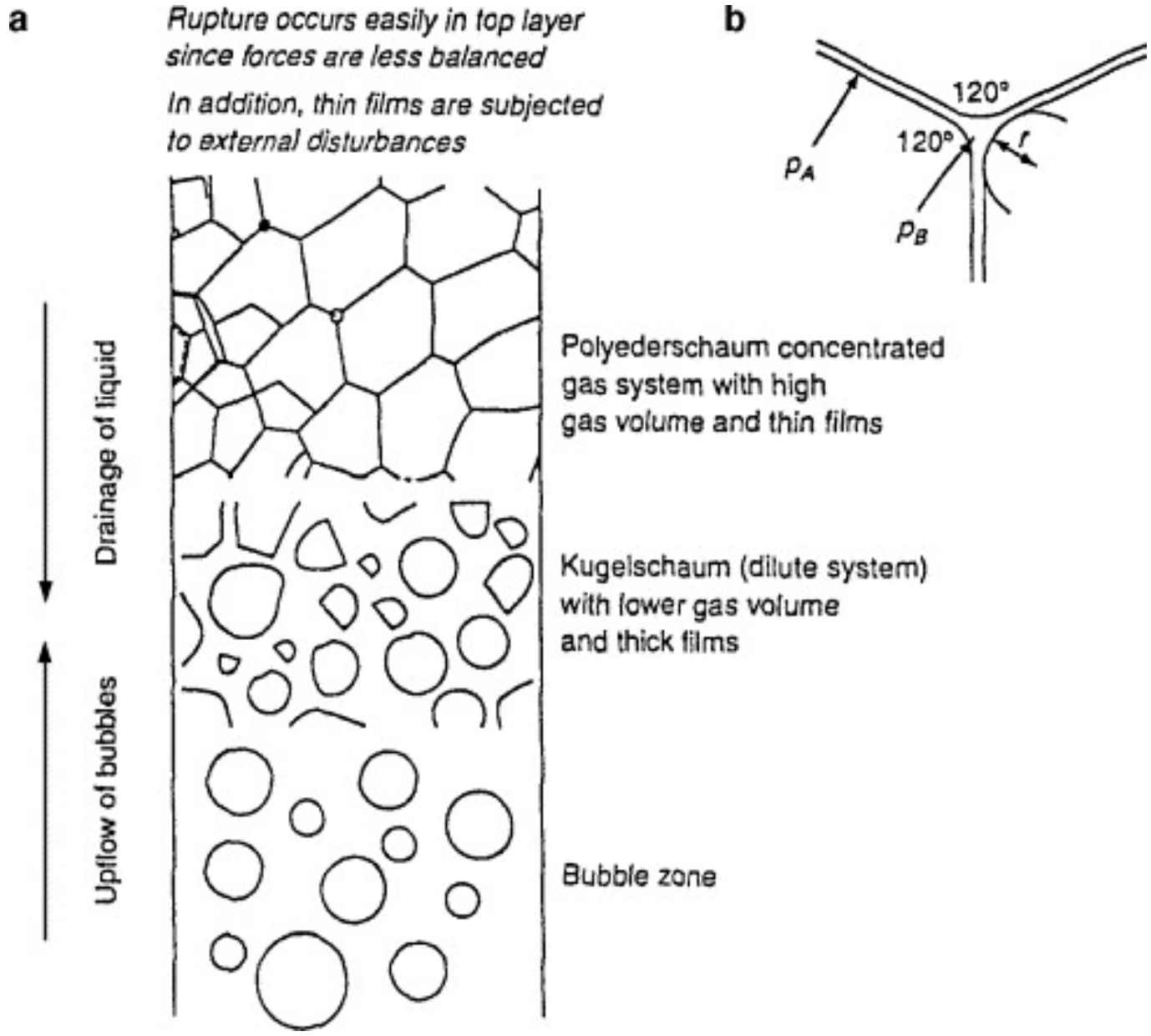

Figure 2.6: (a) Foam structure occurring during formation and drainage of foam in a column. (b) Plateau borders, capillary pressure sucks liquid into the borders. From ref (Pugh, 1996).

2.2.4 Foam Stability

Foam structure is related to bubble shape and size. Many studies have reported that the bubble size distribution has a huge impact on the stability and rheology of foams. The evolution of the bubble size has been observed in static foams during drainage. Due to film and gravitational drainage, the liquid drains away from the foam film. As a consequence the bubble size increases. However, the foam structure itself is difficult to visualize because three dimensional foams are opaque and

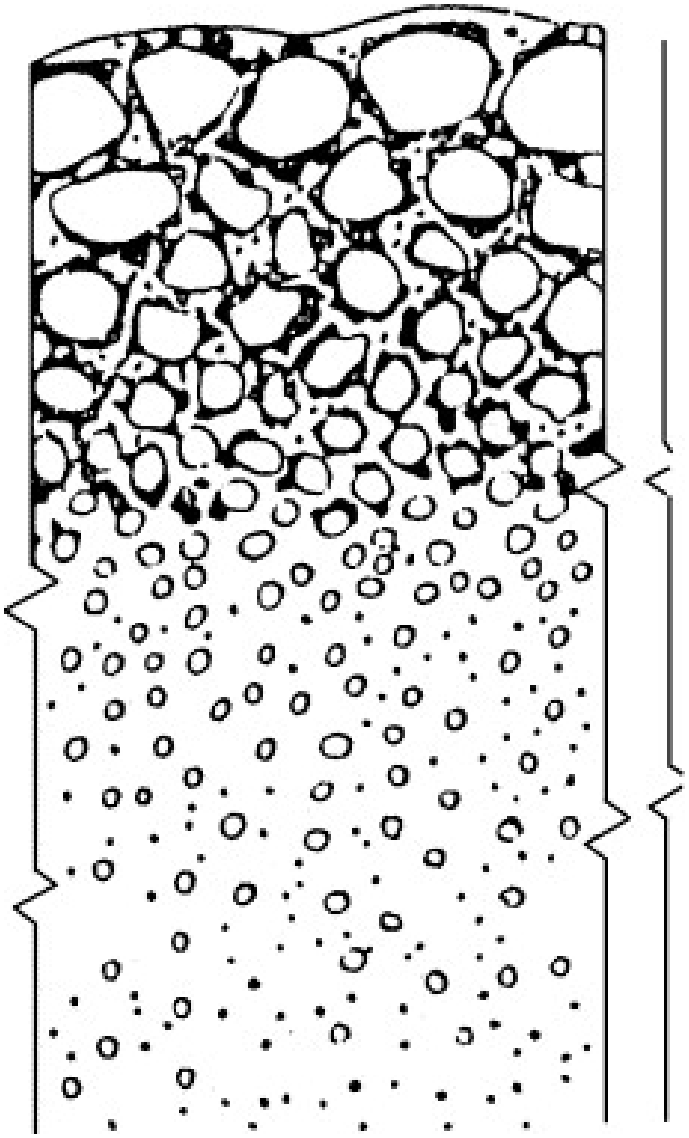

Figure 2.7: Structure of a typical three-phase froth. From ref (Pugh, 1996)

unstable. The structure of the foam is so fragile and is destroyed if probes are inserted. Therefore, optic photographic method can only obtain two dimensional information.

Foam is a thermodynamically unstable or metastable system as the individual bubble will eventually burst or disappear at some point after generation. The instability of foam can be divided into two extreme types: (*i*) unstable or transient foams with lifetimes of seconds; (*ii*) metastable foams with lifetimes which may be measured in days. Nowadays, a wide range of foam lifetimes can be accomplished by numerous types of different surfactants (Pugh, 1996).

At the moment of formation the liquid content in the foam is usually considerably larger than at *hydrostatic equilibrium*, which is reached when drainage stops. Immediately after foam formation,

the liquid starts draining out of the foam. This is caused by the effect of gravity on the liquid in the foam films. The liquid drains into the Plateau borders and then flows down through them from the upper to the lower foam layers until the gradient of the capillary pressure equals the gravitational force (Exerowa and Kruglyakov, 1998, p.381), which defines the hydrostatic equilibrium. Under a no-slip hydrodynamic boundary condition at the film surface, the drainage time t_d for a vertical film of initial thickness h_{f_0} to reach a thickness $h_f \ll h_{f_0}$ is given by:

$$t_d \approx \frac{6\eta H_f}{\rho g (h_f)^2} \tag{2.12}$$

where ρ and η are the density and viscosity of the liquid respectively, H_f is the film height, and g the local acceleration of free fall. To give an example, according to Eq. 2.12 a vertical film of height 1 mm takes about 2 months to reach 10 nm but just few seconds to reach 10 μm. However, many foams will not live for a few months. One important factor determining the lifetime of foams is the interactions between colloids (Dickinson, 1992).

Coalescence, also called film thinning, can occur because of drainage of the intervening fluid between bubbles followed by the close approach of the surfaces and therefore form a larger bubble. It can lead to foam collapse (Dickinson, 1992).

The diffusion of gas from small bubbles at high pressure in the plateau border (so-called *Laplace pressure*) into big bubbles at low pressure leads to the coarsening of the foam. The effect is called *disproportionation*, and is analogous to Ostwald ripening in emulsions. According to Henry's law, more gas dissolves near the small bubbles than near the large ones, and so the latter grow at the expense of the former.

Assuming that gas transport takes place by diffusion through the continuous phase, the radius r of a small bubble can be given as a function of time t

$$r^2 = r_0^2 - \frac{4RTD_1 S_\infty \gamma}{p\lambda} t \tag{2.13}$$

where r_0 is the bubble radius at $t = 0$, D_1 is the diffusion coefficient of the gas in the liquid, S_∞ is the gas solubility as a planar interface ($r \to \infty$), γ is the surface tension, p is the pressure and λ is

the distance over which gas diffuses from the small bubble to one with an infinite radius of curvature. R and T are the gas law constant and temperature, respectively. From Eq. 2.13, the radius can be calculated in different conditions (Dickinson, 1992). Coarsening of the bubble size distribution can also accelerate drainage and coalescence. Drainage, coalescence and disproportionation are three mechanisms of foam instability. Therefore, stopping or slowing down these three processes will be a solution to prolong shelf-life of foam.

The Gibbs-Maragoni effect can explain the stability of foam films, such as metastable foams generated by proteins and detergents. During drainage, the liquid in the foam film flows around the bubble surface towards the Plateau border and the surfactant molecules at the interface flow away with the liquid. This causes a gradient of the surfactant concentration which leads to a surface tension gradient in the liquid film. The part of the interface with higher surface tension moves the surfactant molecules to the area with lower surface tension. In the Gibbs-Marangoni effects these two effects are superimposed and together re-equilibrate the surface tension at the bubble interface; these mechanisms are illustrated in Figure 2.8. A stronger Gibbs-Marangoni effect can restore efficiently the thickness of the lamellae and prevent further film thinning resulting in slower drainage. One way to increase the Gibbs-Marangoni effect is by using a type of the surfactant with a higher rate of diffusion and adsorption at the surfactant molecules to the interface. Another way is to increase the concentration of the surfactant in order to provide a sufficient number of surfactants molecules to form a tighter packing on the interface. However, a concentration above cmc (critical micelle concentration) can cause the surface tension to relax too rapidly, resulting in a film rupture.

In general, the more viscous the liquid, the slower the drainage between the layers of bubbles. Increasing the bulk viscosity of the solution by adding a solute (such as glycerol, liquid paraffin, or polyoxyethylene) or generating a gel network by an additive of electrolyte in the liquid resulting in a decrease of the rate of drainage. Alternatively, drainage can be slowed down by increasing the surface viscosity and elasticity. A higher surface viscosity and elasticity can be caused by an inter-particle interactions due to locally higher concentrations of surfactants in the interface (Pugh, 1996); these interactions can lead to the formation of local gel-networks.

Tamura et al. (1998) investigated the influence of surfactant structure on the foam stability by ob-

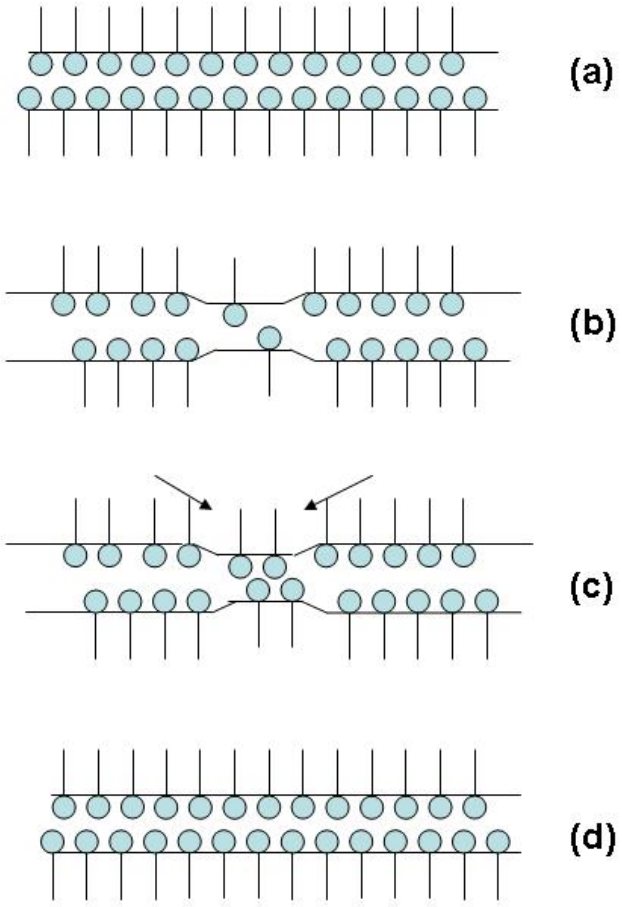

Figure 2.8: Illustration of the Gibbs-Marangoni effect in a thin liquid film: (a) Original state of film. (b) Higher local surface tension developed. (c) Action of elasticity pulls back surface molecules into thin section; returning surfactant molecules drag back underlying layers of liquid with them. (d) Surface film repaired by surface transport mechanism.

serving the drainage in foam films. A longer life of foam film can be obtained by non-ionic surfactants with longer hydrocarbon chain length due to an increased intermolecular hydrophobic interaction. In contrast, increasing the size of hydrophilic groups causes a less structured surface coverage resulting in less foam stability. Bergeron (1997) has found a similar result, i.e. the surfactant chain length can have a significant effect on foam film stability by using cationic surfactant (CTAB). For highly purified surfactants an abrupt increase in film stability is seen when extending the chain length from C_{12}TAB to C_{14}TAB. When an uncharged cosurfactant is present, a similar abrupt increase of the film stability takes place between C_{10}TAB and C_{12}TAB. Beneventi et al. (2001) have also observed the same effect of the length of the hydrophobic chain by using anionic surfactants with a sodium sulphonate hydrophilic group and cationic surfactants with a trimethylammonium bromide hydrophilic group. They conclude that the stability of a given foam depends on the surface tension which in turn is modulated by the surface activity of their surfactants, namely the adsorption kinetics between the head group and hydrophobic chain length. Neither surfactant molecules with a particularly short hydrophobic chain nor an exceedingly long hydrophobic chain can provide sufficient surface tension for foam stability because the adsorption is either too fast or too slow.

In contrast, proteins are good foaming agents because they are strongly adsorbed to the interfaces, provide steric and electrostatic stabilization, and create the network in between the films once they are adsorbed at interfaces (Hammershoj et al., 1999, Bos and van Vliet, 2001). Foaming properties of protein strongly depend on the nature and the extent of protein-protein interactions, as well as other processing and environmental parameters such as pH, temperature and the viscosity in the continuous phase. Moreover, films with higher viscosity and elasticity (such as protein films near the isoelectric pH or when the protein concentration is high) gave complete monolayer coverage resulting in a better foam stability (Patino et al., 1995). Murray (2007) has pointed out that an overall increase of the molecular weight caused by the interaction between the proteins and other components in the bulk will slow down the adsorption whilst other interactions may affect the inherent surface activity of the complexes. For example, the state of aggregation and the concentration of caseinate can affect the rate of diffusion to the interface which correlates with foaming ability (Sanchez and Patino, 2005). Protein adsorption and foam formation both can be slowed down by the complex formation between

beta-lactoglobulin and pectin (Ganzevles et al., 2006).

A uniform bubble size can eliminate the effect of disproportionation (which is the result of differences of pressure found in bubbles of different sizes, as discussed above). Monsalve and Schechter (1984), Pugh (1996) and Magrabi et al. (1999) also reported the importance of the bubble size distribution on the stability of foams. To avoid foam developing into a polydisperse foam, it is important to stop gas migration between bubbles. It can be retarded by using less soluble gas or tighter packing of surfactants, polymers and particles. For example, nitrogen has a low water solubility and decreases the rate of gas molecules transport across water film. Liquid evaporation can also destroy the foam and the rate of evaporation can be affected by the surfactant monolayers. Langevin (2000) suggested fatty alcohols which can reduce dramatically water evaporation because of the compact monolayers and its viscoelasticity change. Recently, there are several studies which showed that partially hydrophobic particles can form extra stable bubbles as these particles adsorb at the interface of gas and liquid irreversibly

2.2.5 Foam Applications

Foams are used as intermediates and end-products in numerous different applications ranging from mineral separation or flotation, textile industries, food and beverage manufacturing, cosmetic formulations, personal care products and drug delivery system (Cooke and Hirt, 1995, Rieger, 1995, Prud'homme and Khan, 1995, Bikerman, 1973). They are mixtures of immiscible fluids in which a gas phase consisting of millimetersized bubbles is dispersed in the continuous phase of a liquid (Exerowa and Kruglyakov, 1998). Not only liquid foams but also solid foam are widely used. The foams can be classified into different groups as their properties serve different purposes in different applications. The low heat conductivity and density of foams is a reasons to use them in many applications which need thermo-insulating materials. Apart from foam concrete, foam glass and polymers foam, liquid foams are also used as thermo-insulators in hothouses. The ability of a foam to adsorb various gases, liquid, solid particles and to isolate from the medium has been applied in the firefighting, dust protection and collection, purification from solid and liquid pollutants, isolation of hazardous gases and aerosols from the electrolysis baths, and water basin protection (Briggs, 1995,

Exerowa and Kruglyakov, 1998).

In the oil industry, a strong hydrodynamic resistance of foams and their stability at high capillary pressures are especially important in enhancing oil recovery. Beside that, one of the specific properties of foams—their large specific surface area—is also providing faster absorption and purification of gases in foam devices, accelerating vacuum drying[2] and degassing oil. The process of foam flotation of suspensions, ion flotation, foam separation as well as the water waste treatment are using the difference in the compositions of the initial foaming solution and liquid phase in the foam (Rossen, 1995, Exerowa and Kruglyakov, 1998).

Also, foam films are used as models in the study of various physicochemical processes, such as thinning, expansion and contraction of films, formation of black spots, film rupture, molecular interactions in films (Exerowa and Kruglyakov, 1998). Many other everyday processed products apply particle stabilized foam systems, which ensure long-term foam stability. Partially crystalline solid oil droplets accumulate at the interface and stabilize the foam. Whipping cream is one of the examples in the dairy industry (Dickinson, 1992). The rheological properties of foams are important for determining the texture of the food products. There are many examples of particle stabilized foaming processes in both aqueous and nonaqueous environments, with and without surfactant addition (Alargova et al., 2004, Binks, Duncumb and Murakami, 2007, Binks and Horozov, 2005a, Binks and Murakami, 2006, Binks, Murakami, Armes, Fujii and Schmid, 2007, Dickinson, 2010, Gonzenbach et al., 2007, 2006a,c,b, Lan et al., 2007, Binks and Horozov, 2005b, Tang et al., 1989, Zhang, Lan, Liu, Xu and Sun, 2008, Zhang, Sun, Dong, Li and Xu, 2008).

2.2.6 Research Needs and Problems

In suspension, nano-particles are widely used in cosmetics, pharmaceuticals, paints, pigments, catalysts and devices for electromagnets and optics. However, to be able to fully use the large surface area of these particles in these applications, it is essential to ensure that these particles disperse well in the suspensions and stay homogeneous and stable. In the de-aggregation process, interacting particles can differ in their nature, size, shape, and degree of hydrophobicity. Therefore, there are

[2]For the absorption of water it is equally important the foam possess high capillary pressure (high expansion ratio)

still aspects unexplored in particles (transient particle distribution) on the de-agglomeration process using ultrasound cavitation and also in comparison to a conventional mechanical agitation.

In foams, both protein and surfactant foams are widely used in our daily life. Although many studies have investigated the properties of protein and surfactant foams, addition of particles into the foam system to stabilize foams has not yet been fully studied. Further research into the stabilization of particles in these foams may yield results of great significance. Overcoming the lack of stability of surfactant and protein foams may be achieved by using particles in addition to or as a replacement for proteins and surfactants. This is because particles may cause stability over and above generally used surfactants and also because of the benefits of reducing the proteins and surfactants.

Chapter 3

Experimental Materials and Methods

3.1 Introduction

This chapter describes the materials and methods used in this PhD study. The process of de-agglomeration of silica particles in suspensions and foam producing from these suspensions are illustrated. The energy dispassion of ultrasonic probe and high shear mixer are explained. The experimental techniques used to characterize the physical properties of the suspensions using surface tension meter and rheometer are illustrated. The suspensions was analyzed using HPPS and Mastersizer. The details of these techniques are described. The methods used for measurements of foam properties such as foam drainage, foam breakage, foam microstructure, as well as foam rheology are illustrated.

3.2 Materials

Surfactants, proteins and regents

Solutions were prepared using double-distilled and deionized water. To prepare this, the water was passed through a double distillation unit (Aquatron, BIBBY, UK) and then a deionzer. C12LAS (Sodium dodecylbenzene sulfonate)-anionic surfactant was used, given by P&G;; CTAB (Cetyl trimethylammonium bromide)-cationic surfactant, Sodium hydroxide, hydrogen chloride, sodium carboxymethyl cellulose (SCMC, low viscosity) were purchased from BDH. Whey from bovine milk

and casein were supplied by Sigma (UK). Ethanol (99.99%) was obtained from Fisher.

Particles

Four different fumed silica particles were evaluated in this study. Hydrophilic silica particles were supplied by Sigma and the hydrophobic silica particles were supplied by Degussa. The particles differ with respect to their degree of surface modification, achieved by controlled reaction of hydrophilic silica with different chemicals. The higher content of carbon indicates the higher hydrophobicity. The properties of the silica particles are listed in Table 3.1.

Type	Primary particle size (nm)	Carbon content (wt%)	Degree of Hydrophobicity	Treated with
R972	16	0.6-1.2	Weakly hydrophobic	DDS (Dimethyldichlorosilane)
R812	9	2.0-3.0	Moderately hydrophobic	HMDS (Hexamethyldisilazane)
R202	14	3.5-5.0	Strongly hydrophobic silica particle	PDMS (Polydimethylsiloxane)

Table 3.1: Hydrophobic silica particles properties

3.3 Methods

3.3.1 Suspension studies

Surfactant solutions

Surfactant solutions were used in the experiments in Chapter4. C12LAS, SDS, and CTAB were dissolved in double distilled and de-ionized water. The concentration ranged from 0.2 to 2.0 critical micelle concentration (cmc). The following concentrations of the surfactants correspond to 1 cmc, respectively C12LAS (1.2 mmol/L) and CTAB (0.92 mmol/L)(Rosen, 1989).

Hydrophilic silica particle suspensions

1.0 wt% and 5.0 wt% of hydrophilic silica powder was dispersed into 100 ml of de-ionized and double distilled water or surfactant solutions to prepare solutions for foaming. The following procedure was

used: The mixture of hydrophilic silica particles and water was stirred intensively using a stirrer for 5 minutes followed by exposure to an ultrasonic probe using a high intensity ultrasonic processor (750 W, GENEQ, USA) which generates ultrasonic waves at a fixed frequency of 20 kHz at a net power input of up to 750 W. The amplitude of the sound wave can be adjusted from 0 to 100% of the maximum 123 μm. To keep the dispersion from overheating during ultrasonication, the dispersions were sonicated in an iced-water bath. The amplitude of ultrasound was adjusted from 30% to 95% (the amplitudes is from 36.9 μm to 116.9 μm). The processing time was varied from 10 seconds to 35 minutes. When using mechanical agitation, the suspensions were mixed using a high shear mixer (L4RT-A, Silverson, USA) at a fixed frequency of 50 Hz and power input up to 250 W. The processing time was from 1 minute to 160 minutes and the speed of rotation was 6000.

Hydrophobic silica particle suspensions

1.0 wt% of hydrophobic silica powder was wetted with 5.0 wt% ethanol and dispersed into 100 ml of de-ionized and double distilled water or the surfactant solutions describe above. The mixtures were initially stirred intensively using a magnetic stirrer for 5 minutes and exposed to the ultrasonic probe using the high intensity ultrasonic processor for 2 minutes.

Calorimetry measurements

Calorimetry measurements were carried out using a digital type K thermocouple thermometer capable of measuring temperatures ranging from -50 to $1300°C$ in 100g water. The energy generated by both processing equipments, high shear mixer and ultrasonic processor, can be obtained from Eq. 3.1 by measuring the rise in temperature in the system as shown in Figures 3.1 and 3.2. The energy dissipation rate can be obtained by knowing energy E from equation 3.2. Table 3.2 shows the data

.

$$E = mC_p\Delta T \tag{3.1}$$

where E is energy, m is mass, C_p is heat capacity and Δ T is the change in temperature.

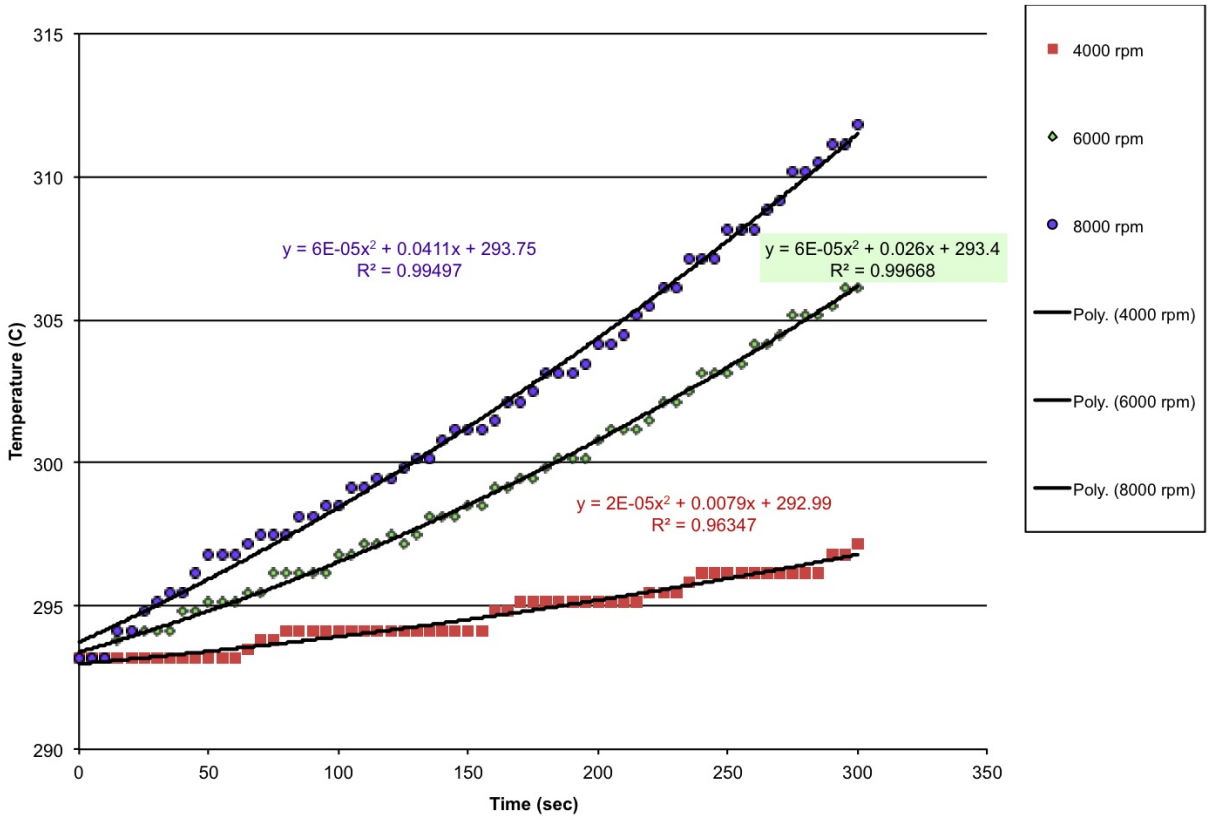

Figure 3.1: Measurement of rising temperature using in mechanical agitation.

RPM	dT/dt t =o	*E*(W)	*Ev*(W/kg)
4000	0.0079	3.3022	33.022
6000	0.0260	10.868	108.68
Amplitude	**dT/dt t =o**	***E*(W)**	***Ev*(W/kg)**
36.9 μm	0.0261	10.9098	109.098
62.5 μm	0.0599	25.0382	250.382
116.9 μm	0.1472	61.5296	615.296

Table 3.2: Parameters of equations 3.1 and 3.2.

$$E_v = \frac{E}{m} \tag{3.2}$$

where E_V is the energy dissipation rate and m is the mass. The energy dispassion rate of ultrasonic process at amplitudes of 36.9 μm, 62.5 μm, and 116.9 μm are 109.01 Wkg^{-1}, 250.38 Wkg^{-1}, and 615.30 Wkg^{-1}, respectively. In our experiment for mechanical agitation at an rpm of 6000, the energy dispassion rate is 108.68 Wkg^{-1}.

By knowing the energy dispassion rate of these two methods, the total energy input into the

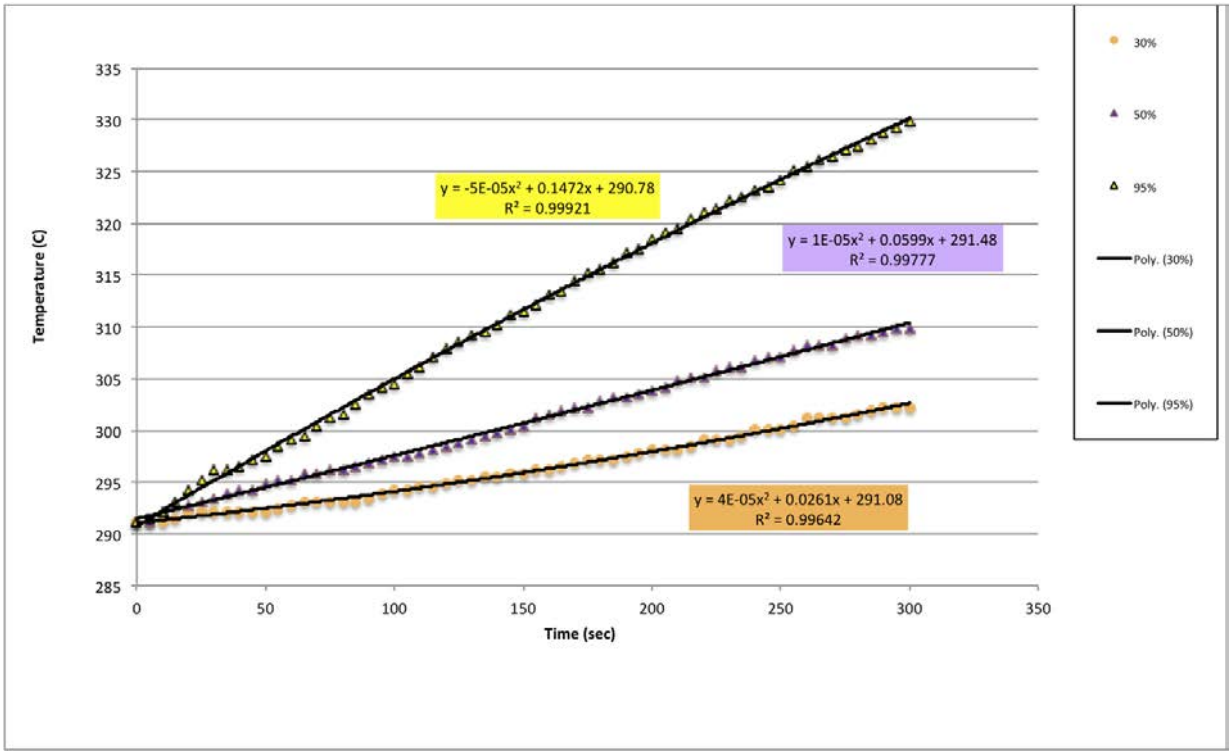

Figure 3.2: Measurement of rising temperature using in ultrasound.

system can be obtained from the equation below:

$$E_T = E_v t \tag{3.3}$$

where E_T is the total energy and t is the time.

Suspensions with different pH values

The influence of pH on the hydrophilic silica particle suspensions has been studied in the pH range from 2 to 12. To investigate the influence of pH on the properties of suspensions containing surfactant, suspensions prepared by mixing of silica powder with a surfactant solution during 6 hours were used. The pH values were adjusted with 1 M hydrogen chloride and 1 M sodium hydroxide.

Characterization of particle/aggregate size distribution

Particle size measurement of the silica suspension was mainly carried out by Mastersizer which can measure wider range of particle size. HPPS was only used to measure when the particle size is at

sub-micron range.

Laser light diffraction Laser light diffraction has become a widely used technique for particle size analysis. A laser light passing through a particle will scatter light at an angle that is directly related to their size. As the particle size decreases, the observed scattering angle increases logarithmically. The scattering intensity is also dependent on particle size, diminishing with particle volume. Large particles therefore scatter light at narrower angles with high intensity, whereas small particles scatter at wider angles but with low intensity.

Although the supplier claims that the sub-micron range (from 20 nm to 2000 μm) of particles can be measured by a Mastersizer, there is a limitation to this measurement (Mastersizer does not show differences in particle size distribution while HPPS does). There are three regimes to describe the size-wavelength relationship theoretically, depending on the ratio of the wavelength of the incident light to the size of the particle. Rayleigh theory is for the particles which are small compared to the wavelength of light; Mie and Fraunhofer theories are for particles larger than the wavelength of the light (see Figure 3.3).

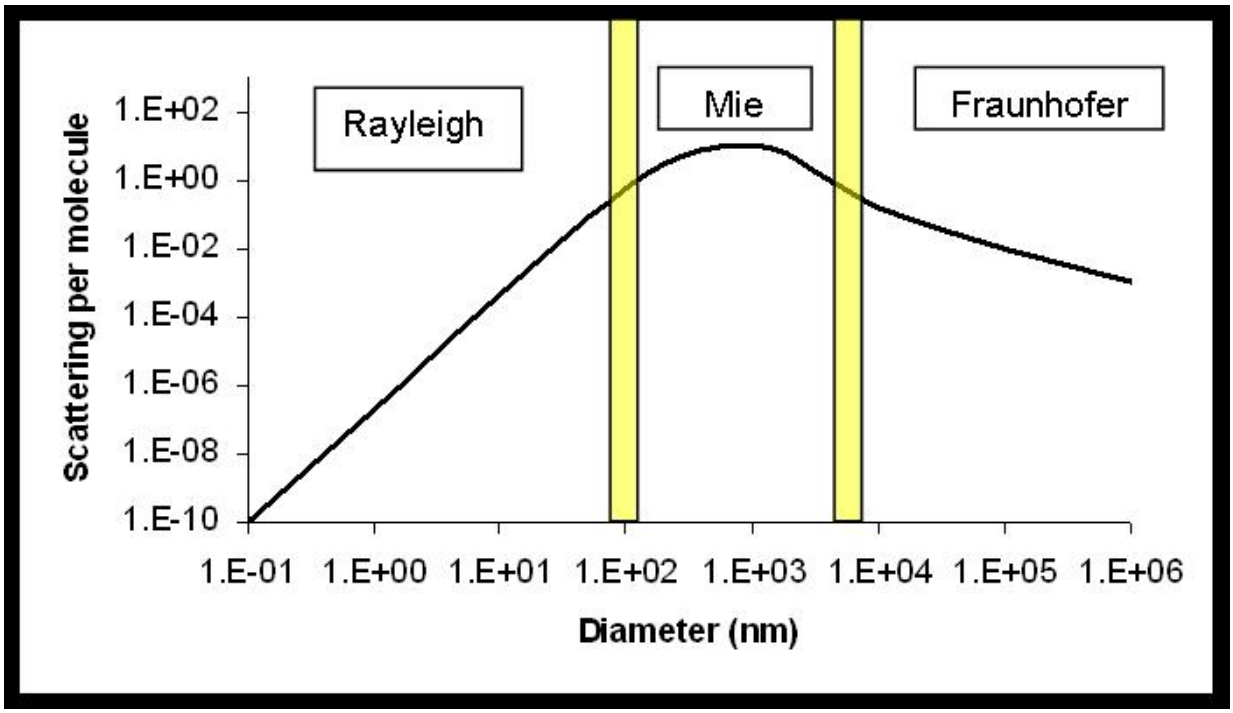

Figure 3.3: Scattering of visible light per water moleculeMorrison and Ross (2002).

The particles/aggregates were sized using a Malvern Mastersizer 2000 Malvern Instruments, UK)

designed for particles in a size range from 20 nm-2 mm. It uses a method based on volume equivalence. The particle size distribution calculated from the scattered laser light using the refractive indices of both the particle material and dispersant. A refractive index of 1.46 and 1.33 is used, respectively for particles and water. The calculation of the particle size distribution internal to the machine is based on the Mie Theory(Kippax, 2005). This instrument is equipped with an external small dispersion unit. A small quantity of particle suspension, sufficient to give the required obscuration, was added to water within the sampling unit. The suspension was then recirculated in the optical unit within the instrument. While in the sample unit, the suspension was stirred at a speed of 2000 rpm continuously throughout the measurements to ensure the sample was homogenous. Care was taken to clean the flow cell between samples by rinsing several times with double distilled water and if necessary Decon-90. All particle sizing measurements were performed in triplicated, thus the results reported are an average of 3 measurements. Figure 3.4 shows the graphical representation of the silica suspension.

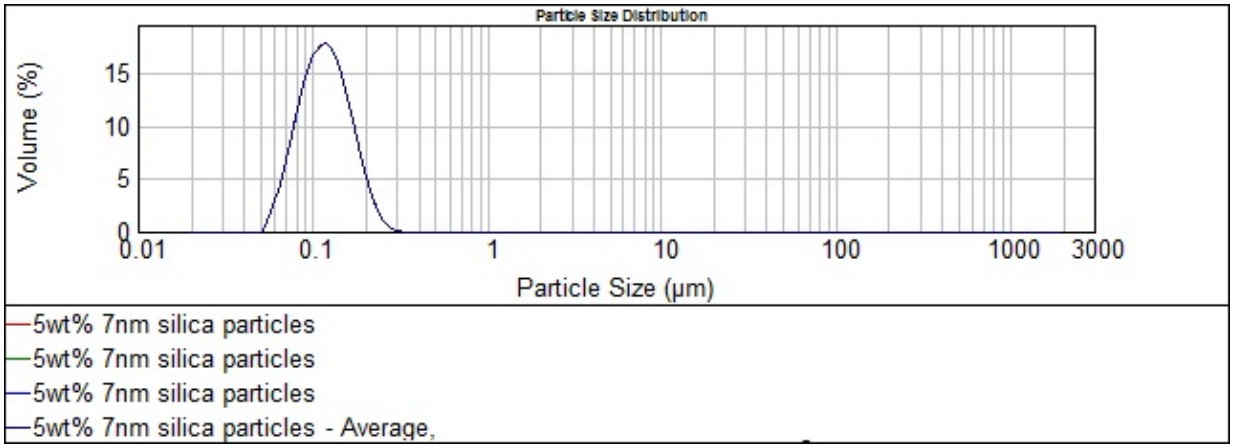

Figure 3.4: Particle size distribution of hydrophilic silica particles after ultrasonic treatment.

High performance particle sizer (HPPS)/Dynamic light scattering (DLS) The HPPS internally uses *dynamic light scattering* (DLS), also known as *photon correlation spectroscopy* (PCS) or *quasi elastic light scattering* (QELS) to determine the size distribution of colloidal particles in the sub-micron range.

When light from a laser bean hits small particles, the light scatters in all directions (Rayleigh scattering). The intensity of scattering light fluctuates due to the random movement of particles in the

suspension, also known as Brownian motion, and the distance between the scatterers in the solution is constantly changing with time. An important feature of Brownian motion for DLS is that small particles move quickly and large particles more slowly. The Z_D (Z average), the intensity weighted mean hydrodynamic size, can be derived from a cumulants analysis of the measured correlation curve.

The DLS autocorrelation function, along with the exponential fitting expression, is shown below, where $G_2(q;\tau)$ is the autocorrelation function at a particular wave vector, t_i is the initial time, τ is the delay time, and I is the scattering intensity, A is the amplitude or intercept of the correlation function, B is the baseline, D is the diffusion coefficient, q is the scattering vector, λ_0 is the vacuum laser wavelength, n_0 is the medium refractive index, θ is the scattering angle, k is the Boltzmann constant, T is the absolute temperature, η is the viscosity of the medium, and R_H is the hydrodynamic radius.

$$G_2(\tau) = \langle I(t_i)I(t_i+\tau)\rangle = A[1 + B\exp(-2\Gamma\tau)] \tag{3.4}$$

$$\Gamma = D_a q^2 \tag{3.5}$$

$$q = \frac{4\pi n_0}{\lambda_0}\sin\left(\frac{\theta}{2}\right) \tag{3.6}$$

$$D = \frac{kT}{6\pi\eta R_H} \tag{3.7}$$

In the Cumulant approach, the exponential fitting expression is expanded to account for polydispersity of peak broadening effects, as shown below.

$$G_2(\tau) = A[1 + B\exp(-2\Gamma\tau + \mu_2\tau^2)] \tag{3.8}$$

The expression is then linearized for τ using a Taylor expansion. Then the data fitted to the approximated formula below, where the D subscript notation is used to indicate diameter. The 1st Cumulant or moment (a_1) is used to calculate the intensity weighted Z average mean size and the

2^{nd} moment (a_2) is used to calculate a parameter defined as the polydispersity index (PdI).

$$y(\tau) = \frac{1}{2}\ln[G_2(\tau) - A] = \frac{1}{2}\ln[AB\exp(-2\beta\tau + \mu_2\tau^2)] \approx \frac{1}{2}[AB] - \Gamma\tau + \frac{\mu_2}{2}\tau^2 = a_0 - a_1\tau + a_2\tau^2 \quad (3.9)$$

The coefficient a_1 is now the mean particle size and a_2 is a measure of the standard deviation of the distribution. By comparing the coefficients a_1 and a_2 with the expansion, the mean value of the particle radius R_H can be determined and is $\frac{1}{2}Z_D$.

$$Z_D = \frac{1}{a_1}\frac{kT}{3\pi\eta}\left[\frac{4\pi n_0}{\lambda_0}\sin\left(\frac{\theta}{2}\right)\right] \quad (3.10)$$

$$PdI = \frac{2a_2}{a_1^2} \quad (3.11)$$

$$B = \frac{\exp(2a_0)}{A} \quad (3.12)$$

The particles were sized using a Malvern HPPS designed for particles in a size range of 0.6-6000 nm. The samples for analysis were diluted in double distilled and deionised water to obtain a suitable concentration range. The samples were then placed in a disposable polystyrene cuvette in the sample chamber. All measurement were made at $25°C$ and an angle of $90°$, and all readings were repeated three times. Data produced by the instrument included the intensity mean diameter of particles (Z-average) and a polydispersity index (PI) that is a measure of size heterogeneity. PI values can range from 0 to 1, where low values are associated with small size distributions, and higher values indicate polydispersity.

Zeta potential measurement Zeta potential is a physical property which is exhibited by any particle in suspension and is widely used to quantify the magnitude of the electrical charge at the double layer which arises as follows: Particles carry a charge in aqueous media which could be positive or negative depending on the pH of the solution and its isoelectric point. The particles attract oppositely charged ions which lead to the establishment of an electrical double layer at the

solid-liquid interface.

Measurements of zeta potentials are used to characterize the surface of colloid particles and to understand colloidal stability. The magnitude and range of the forces between the liquid and the particles depends on the ionic strength of the surrounding solution and the difference in electrical potential between the solid and the liquid phases. Figure 3.5 shows a schematic diagram of the electrical forces around a negatively charged particle.

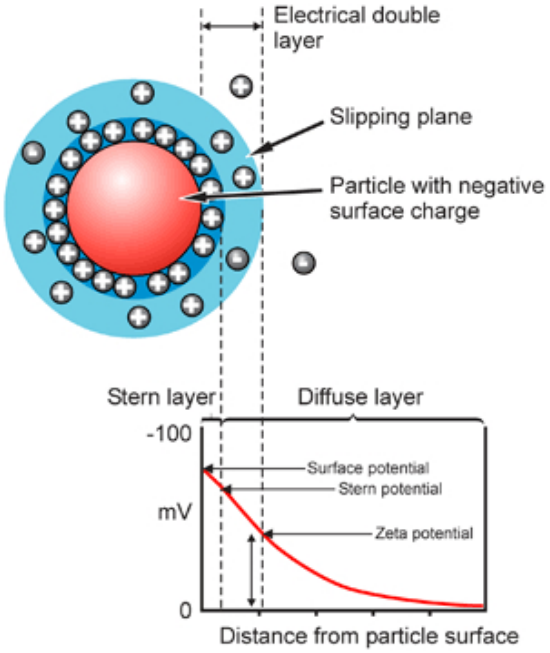

Figure 3.5: Schematic diagram showing the nature of electrical forces around a negatively charged particle in bulk solution.

Dispersion zeta potentials were determined using a Malvern Zetasizer (Malvern Instruments, U.K.). The samples were diluted in 50 ml pH-controlled double distilled and de-ionized water and injected into the Zetasizer sampler unit, taking care not to introduce any air/bubbles into the unit. Ten measurements were taken for each sample, thus the results reported represent averages over 10 measurements.

Surface tension measurement Equilibrium surface tension was measured for freshly prepared solutions by a goniometer (Easy drop, Kruss) using the pendant drop method. The solutions and suspensions were loaded into a syringe. The syringe was used to obtain a drop with a defined liquid volume from the sample. The surface tension was determined by fitting the shape of the drop (in a

captured video image) to the Young-Laplace equation which relates surface tension to drop shape. The software (Drop Shape Analysis) does this automatically. The syringes and needles used in the measurements were rinsed with concentrated HCl, NaOH and double distilled water prior to each measurement to prevent possible contamination. All measurements were made at room temperature, repeated 3 times and an average surface tension value was calculated with an error range of ± 5%. All surface tension of the suspensions and solutions were checked before using in all foam experiments. More details and samples measurements can be found in 7.2.1 in Chapter 7.

Viscosity measurement "TA AR-1000" controlled-stress rheometer (TA Instruments Ltd, UK) was used to measure the viscosity of the solutions and suspensions. A parallel plate geometry was used for the solutions and a cone and plate geometry was used for suspensions. The most appropriate size for the diameter of the plate was 60 mm because it was appropriate for low viscosity samples as it had a large geometry. Thus it maximized the contact area and hence the torque to generate a given stress. The samples were placed in the rheometer measuring device at 25 $^{\circ}C$ and left to equilibrate for 1 minute before any subsequent tests were carried out. The samples were covered with a moisture trap which contained water to prevent moisture loss. The measurements were repeated 3 times. The viscosity values were calculated and the measurements were repeated if the error range (the difference between the highest and lowest result) was greater than ±5.0 %.

Microscope Imaging Transmission electron microscopy using an Environmental Scanning Electron Microscope (ESEM, Philip XL30) was adopted to examine the size of agglomerates/particles. A drop of particle suspension was placed onto a steel plate. The sample was dried and viewed in high-Vac mode.

3.3.2 Foam studies

In this section, the methods to produce foam are described and the method to measure foam properties are illustrated. The surface tension of the double distilled and deionized water, and all the suspensions used in the foam studies were checked

Ultrasound cavitation

The local pressure in the expansion phase of the cycle falls below the vapour pressure of the liquid, causing tiny bubbles to grow. These bubbles are created from existing gas nuclei within the fluid. However, the most important effect in high power ultrasonics is the phenomenon of cavitation. The condition within these imploding bubbles can be dramatic, with temperatures of 5000 K and pressure of up to 1000 atmospheres, which may create new reaction pathways, break down and dislodge particles or even generate different products (Suslick, 1988, Patist and Bates, 2008). The same concept applies to making foams. Therefore, in our foam experiments, high intensity ultrasound was employed to generate foams. To avoid over heating the foam, the time ultrasound which was minimized was applied once the foam had been generated.

For all protein experiments, the protein solution was kept in a closed 2 litre glass jar and replaced after two days. 30 ml protein solution was prepared in a 70 ml sample bottle (height 60 mm and diameter 45 mm) with a known amount of whey and casein protein. A 13 mm standard probe was inserted into the protein solution. The protein foam was produced by using the high intensity ultrasonic processor (750 W, GENEQ, USA) which generates ultrasonic waves at a frequency of 20 kHz at a net power output of up to 750 W. The protein solutions were sonicated for several seconds (the precise period of time depending on the intensity (amplitude) of ultrasound; see figure 3.6).

For the hydrophilic silica particles, a known amount of silica powder was placed into a 70 ml sample bottle and added to 30 ml double distilled and deionized water or protein solution. For the hydrophobic silica particle, the dispersions were prepared from 0.1 wt% to 1.0 wt% of silica particles dissolved into 5.0 wt% ethanol and added to 30 ml distilled and deionized water or 5.0 wt% protein solution in a 70 ml sample bottle. For better mixing in the silica nano-particle dispersions, the dispersion was mixed by a magnetic stirrer for 10 minutes. A 13 mm standard ultrasound probe was inserted into the dispersion and the protein foams with silica particles were generated by sonicating for several seconds at an amplitude of 95% until foam was formed (the precise time depended on the concentration of the silica particles).

The same procedure was followed in all cases, that is for protein, surfactant, particles and detergent mixtures. All the solutions and dispersions were placed in an ice bath while they were

sonicated.

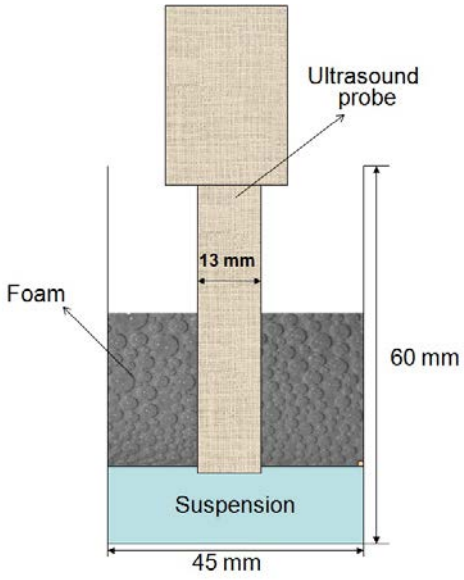

Figure 3.6: Experimental set up for ultrasound cavitation.

Mechanical agitation

For all experiments, the protein and surfactant solutions were kept in a closed 2 litre glass jar and replaced after two days. The foams without silica particles were prepared by placing the protein or surfactant solutions into a 250 ml sample bottle (height 105 mm and diameter 60 mm). A laboratory mixer (SL2T, Silverson, USA) was used for 1 minute at a frequency of 50 Hz at a power up to 50 W and a speed of 6000 rpm (see figure 3.7).

In the foams with added hydrophilic silica particles, the desired amount of silica particle was placed into a 250 ml sample bottle and then the liquid was added (either pure water, or surfactant or protein solution). For a better silica particle dispersion in the suspension, the samples were sonicated for two minutes using the high intensity ultrasonic processor at an amplitude of 95% (116.9 μm). In the foams with addition of hydrophobic silica particles, the suspensions were prepared by adding a desired amount of silica powder into 5.0 wt% ethanol upon continuous stirring which was then added to 100 ml liquid (protein or surfactant solution or double distilled and deionized water) in a 250 ml sample bottle (height 105 mm and diameter 60 mm). For better silica particle dispersion in the suspension, the sample bottles were sonicated for 2 minutes using the high intensity ultrasonic

processor at an amplitude of 95%. In those cases sonication did not lead to foam formation because of the large quantity of the liquid. After this the pH was set to its desired value and equilibration was assured by stirring the suspension for approximately 30 minutes. The suspensions were mixed using the Silverson mixer for 1 minute at a frequency of 50 Hz, a power up to 750 W and a speed of 6000 rpm. All the solutions and dispersions were placed into an ice bath while they were sonicated and mixed.

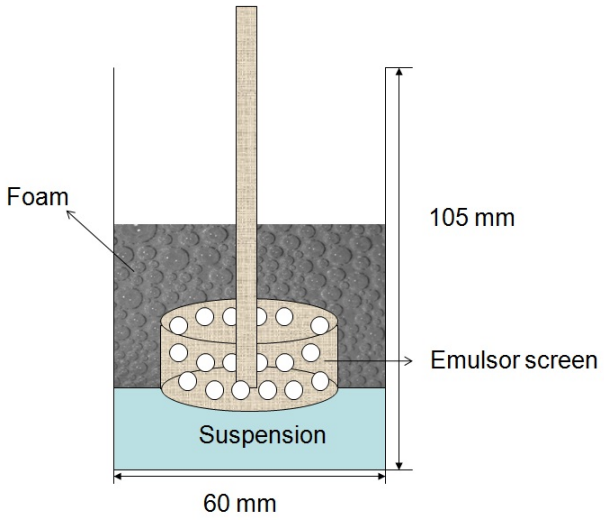

Figure 3.7: Experimental set up; Mechanical agitation.

Characterization of foams

Foam drainage and collapse In each experiment, foam volumes at different times were determined by measuring the height of the foam generated. During the first 5 minutes, foam drainage change was recorded directly via a digital camera, and foam collapse was measured by monitoring the decline in foam height with time. Two measurements were recorded: h, the liquid level and H, foam height as shown in Figure 3.8. The drainage curves were fitted to Eq. 3.13; this fit gave the values of a and b. The duration of the experiment depended on the nature of the foam and its stability.

$$h(t_d) = a(1 - e^{-\frac{t_d}{b}}) \tag{3.13}$$

Where h is the liquid level, and t_d is the time. The value of a indicates the maximum liquid level and $\frac{1}{b}$ can be regarded as a time constant.

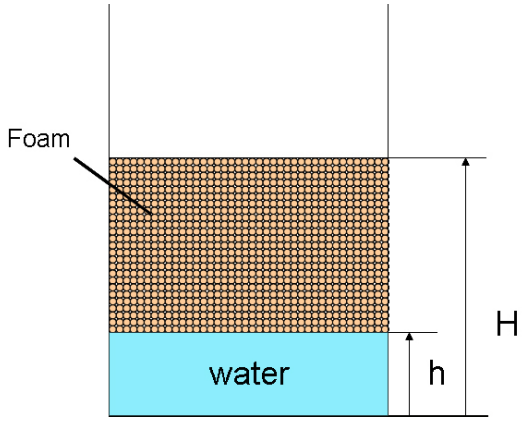

Figure 3.8: Measurement of foam drainage (h) and foam height (H).

Gas volume fraction The gas volume fraction is known to be an important parameter in various applications of foam in petroleum and chemical engineering (Assar and Burley, 1984).

$$\text{Gas volume fraction} = \frac{V_g}{V_g + V_l} \tag{3.14}$$

where V_g is volume of the gas and V_l is the volume of the liquid. When drainage almost stops and the system reaches equilibrium then the liquid holdup in the foam can be inferred from the measurement of drainage and foam volume.

Liquid holdup Liquid holdups were usually reported in terms of foam quality given as Burley and Shakarin (1992):

$$\text{Liquid Holdup} = \frac{V_l}{V_g + V_l} \tag{3.15}$$

where V_g is the volume of the gas and V_l is the volume of the liquid. When drainage almost stops and the system reaches equilibrium then the liquid holdup in the foam can be inferred from the measurement of drainage and foam volume.

Foam cell size distribution The cell size distribution was determined by photographing the foam through the transparent sample bottle wall using a stereomicroscope (SZX12, Olympus, Germany). Photographs were taken using fibre-optics front-lighting, approximately 5 bubble layers above the liquid surface inside the bottle. Because of the transparent nature of the foam, the image contrast was not sufficient to enable automatic identification of most bubble contours by the image analysis

software. Thus, the bubbles at the wall, which were clearly visible to the naked eye, were traced manually and analyzed by Droplet Detect System software as shown in Figure3.9.

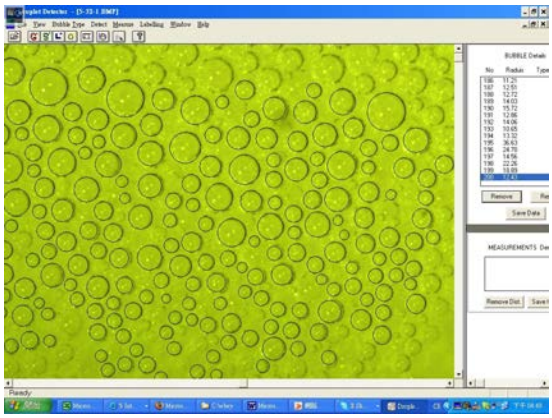

Figure 3.9: Foam image traced manually and analyzed by Droplet Detet System software.

In analyzing the foam pictures to characterize the bubble size distribution, the software Minitab was used. A number of statistical parameters were used and are defined as follows (here d_i is the equivalent circular diameter of an individual bubble i, and n is the number of bubbles in the sample):

1. Number mean bubble size:

$$d_{10} = \frac{1}{n}\sum_{i=1}^{n} d_i \tag{3.16}$$

2. Sauter mean bubble size:

$$d_{32} = \frac{1}{\sum_{i=1}^{n} {d_i}^2}\sum_{i=1}^{n} {d_i}^3 \tag{3.17}$$

   While the d_{10} gives the average bubble size, d_{32} is considered to be a better representative of the mean bubble diameter as it is directly related to the ratio of gas hold up and interfacial area in the foam.

3. Standard deviation:

$$\sigma = \sqrt{\frac{\sum_{i=1}^{n}(d_i - d_{10})^2}{n-1}} \tag{3.18}$$

4. Whereas σ gives a measure of how different the values are from each other and from the mean (d_{10}), the coefficient of variation is a measure of the spread of the distribution relative to its mean and is defined as.

$$C_v = \frac{\sigma}{d_{10}} \tag{3.19}$$

5. Median: this is the middle number, M, in the data set when the data points are arranged from low to high,

6. Skewness:

$$S = \frac{n}{(n-1)(n-2)} \sum \left(\frac{d_i - d_{10}}{\sigma} \right)^3 \tag{3.20}$$

Skewness characterizes the degree of asymmetry of a distribution around its mean. Positive skewness indicates a distribution with an asymmetric tail extending towards more positive values. Negative skewness indicates a distribution with an asymmetric tail extending towards more negative values. Normal distributions have a skewness of zero.

7. Kurtosis:

$$K = \left[\frac{n(n+1)}{(n-1)(n-2)(n-3)} \sum (\frac{d_i - d_{10}}{\sigma})^4 \right] - \frac{3(n-1)^2}{(n-2)(n-3)} \tag{3.21}$$

Kurtosis characterizes the relative peakedness or flatness of a distribution compared to the normal distribution. Positive kurtosis indicates a relatively peaked distribution. Negative kurtosis indicates a relatively flat distribution. A histogram with a normal distribution has $K = 0$.

8. Normal distribution: A normal distribution in a variate d_i with mean d_{10} and variance σ is a statistical distribution with probability function $P(d_i)$, as follows:

$$P(d_i) = \frac{1}{\sigma\sqrt{2\pi}} e^{-(d_i - d_{10})^2/(2\sigma^2)} \tag{3.22}$$

9. Log Normal distribution: A log-normal distribution is the probability distribution of any random variable whose logarithm is normally distributed

$$P(d_i) = \frac{1}{d_i \sigma\sqrt{2\pi}} e^{-(\ln(d_i) - d_{10})^2/(2\sigma^2)} \tag{3.23}$$

Foam rheology Foam rheological tests were performed using a "TA AR-1000" controlled-stress rheometer. A parallel acrylic plate geometry with a diameter of 40 mm was employed in all experiments. A light geometry material like acrylic is essential because it offers a good measurement

sensitivity due to its low inertia.

Foam stabilized by silica particles was made on site at every test run and the sample was transferred from the sample bottle to the lower plate using a spatula. The upper plate was lowered at a very low speed to minimize any damage to the sample. All rheological tests were performed at a controlled temperature of 25 $\pm$ 0.1 $^{\circ}C$. A solvent trap was placed around the test cell to prevent evaporation from the foam sample. Every test was repeated three times and the reproducibility of measurements was always within $\pm$ 10 %.

Test of wall slip Before any rheological experiment was performed, it is important to rule out the effect of wall slip, which is a common phenomenon in the flow of two-phase dispersed systems. The wall slip test was carried out using the acrylic plate geometry with different gap sizes. If there is wall slip, there will be differences in the measurements, but the data curves will coincide if there is no wall slip. A constant stress of 70 pa was imposed on the foam sample for 5 minutes at gap sizes of 800 µm, 1000 µm, 1200 µm, and 1500 µm, using a fresh sample in each test.

Constant shear stress tests Foams are time-dependent materials because the structure of the foam is likely to evolve with time. Therefore, the conventional method of imposing a ramp of shear stress is not valid to obtain the steady shear flow behaviour of foam, and hence the rheological tests were carried out under a constant stress for a certain period of time. The evolution of shear rate and instantaneous viscosity were monitored as shown in Figures 3.10(a) and 3.10(b). A fresh sample was used for every shear stress imposed.

Steady shear flow curves From the above tests, a series of shear rate and viscosity data for different constant shear stress values can be obtained within the range specified as shown in Figure 3.10(b). Thus the flow curves can be constructed by extracting the data of shear rate ($\dot{\gamma}_1$, $\dot{\gamma}_2$, $\dot{\gamma}_3$, and $\dot{\gamma}_4$) corresponding to shear stress (τ_1, τ_2, τ_3, and τ_4) at specific time of shearing (t_1, t_2, t_3, and t_4) as shown in Figure 3.10(c).

Dynamic stress sweep tests Foam is known as a viscoelastic material. A rheological dynamic test can be used to study the properties of viscoelasticity. This test is performed by imposing an

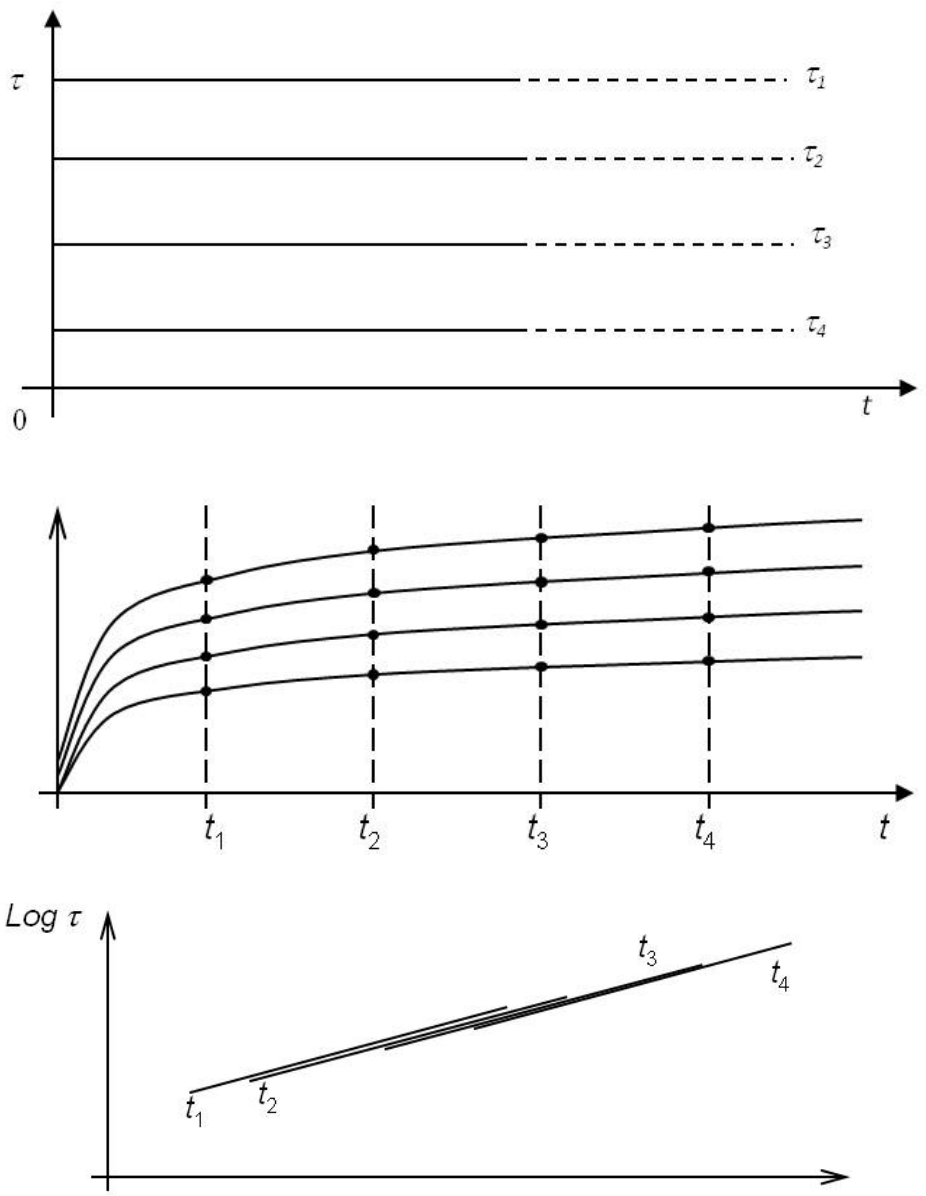

Figure 3.10: Schematic diagram showing the procedure of obtaining steady shear flow tests; (a) constant shear stress τ imposed throughout the test duration t; (b) evolution of shear rate $\dot{\gamma}$ at constant τ; (c) flow curves corresponding to different shearing time.

oscillating strain or stress which varies with time. When a sample is subjected to an oscillating strain or stress then the viscoelastic parameters can be extracted by comparing the strain with the resultant oscillating stress. The two viscoelastic parameters are: the storage modulus (elastic modulus), G' and loss modulus (viscous modulus), G" and they are used to determine the viscoelastic properties of a material.

The dynamic stress sweep tests were carried out to determine the linear viscoelastic region of the

foams. This was done by imposing a range of oscillating stresses to the foam samples at a constant oscillation frequency. Both storage modulus, G', and loss modulus, G", of foams at each oscillating stress were recorded. In this study, the range of shear stress used for foam stabilized by only R812 particles and the foam stabilized by only R812 particles with SCMC were from 0.1 to 60 Pa and 0.001 to 100 Pa, respectively. The test was done at a constant oscillation frequency of 1 Hz and it lasted for 10 minutes.

Chapter 4

De-agglomeration and Stability of Silica Particles in Suspension

4.1 Introduction

Particles have wide industrial applications in cosmetics, pharmaceuticals, catalysts, silicons, paints and pigments and devices for electromagnets and optics. Many of these applications require the particles to be processed as suspensions, hence, it is essential to ensure that the aggregates in suspensions are broken into a range of nano size particles to maximise the specific surface area and have homogenous and stable suspensions.

The fragmentation can occur either by erosion or fracture. Erosion refers to particle size reduction due to the loss of primary particles from the surface of the agglomerates. The breakup of an aggregate into particles is fracture (Kusters et al., 1994). Breakage of these aggregates requires high energy input in order to overcome the adhesion force. The interaction forces is the van der Waals (dispersion-force attraction) and forces of repulsion between particles, either electrostatic or steric (Morrison and Ross, 2002). When the hydrodynamic forces exceed the cohesive interaction between particles, the larger aggregates are broken into smaller aggregates/particles.

Depending on the different nature of the particles and dispersants, different instruments are used to obtain the suspensions. Rotor-Stators dispersers and stirred media mills (also called attritors), and ultrasound are used. The processes illustrated in Figure 4.1 are the most commonly used systems

for the dispersion of particles (Sauter et al., 2008).

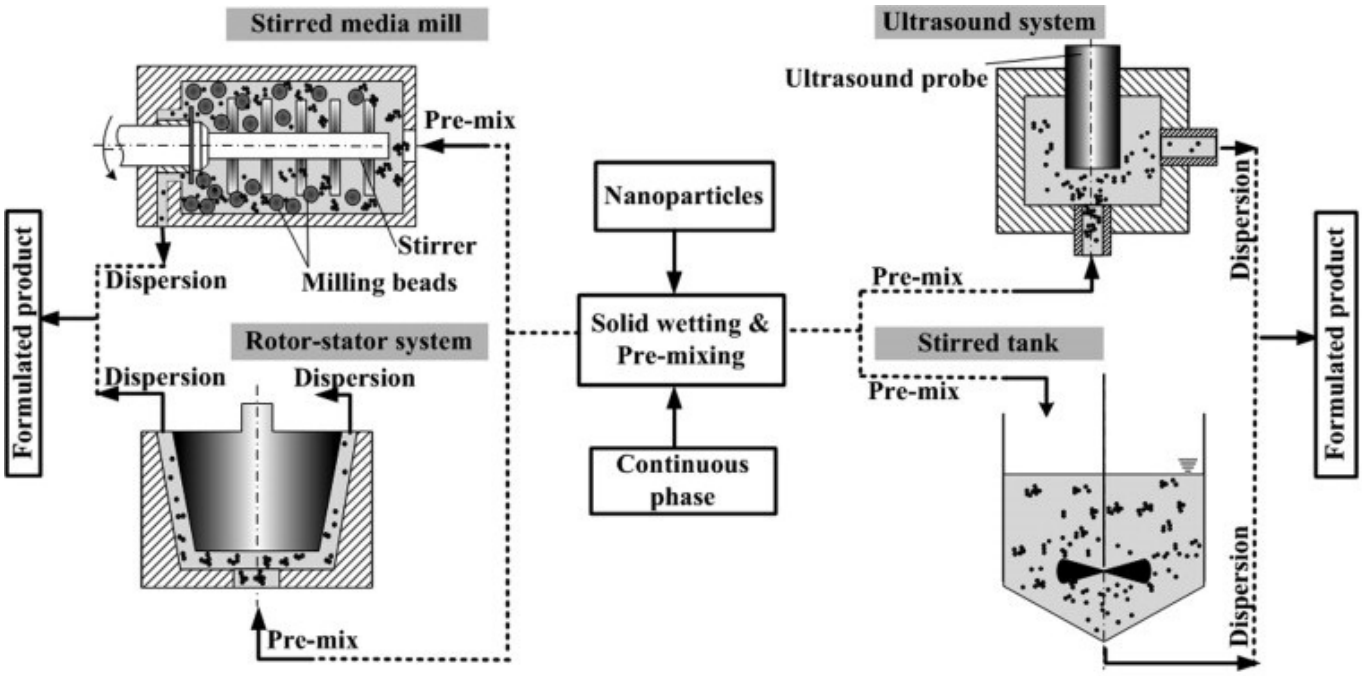

Figure 4.1: Common mechanical devices for dispersing particles in aqueous solutions Sauter et al. (2008).

Rotor-Stators dispersers are continuous mixers using a high-speed rotor turning within a stator. A stator can either be simple with circumferential slots or more elaborate with tortuous channels. With the extra stator, the rotor-stator dispersers can produce much higher shear rates than high-speed stirrers. However, a limitation of the rotor-stator is that it can only be used in low viscosity dispersions because the flow of fluid into the spinning rotor and out through the stator (Morrison and Ross, 2002).

Stirred media mills use a series of staggered horizontal rods attached to a central shaft to move the grinding media. Shear forces are generated by the motion of the rotating rods, leading to more efficient power consumption, finer grinding and shorter grinding time in comparison to the ball mill, however, contamination happens easily in the dispersion in this process (Morrison and Ross, 2002).

Ultrasonic processes have been used for the break-up of aggregates by ultrasound cavitation. Ultrasound is transmitted via waves which alternately compress and stretch the molecular spacing of the medium through which it passes. Cavitation is the production of the micro-bubbles which are created when the pressure decreases below a critical value called cavitation threshold. They

collapse when the pressure increases again at the compression cycle of the wave. This creates strong forces that act on the aggregates resulting in their disruption (Timothy and Dietmar, 2002, Mason, 1999). It has been demonstrated that higher amplitude values result in an increased probability of cavitation and more violent collapse of the bubbles as the internal pressure is raised (Sauter et al., 2008). The first stage of cavitation, i.e., the creation or the birth of cavities is called as *nucleation*. In order to initiate the cavitation, energy input is needed since cavity formation involves the creation of new interfaces. The input energy causes a local pressure fluctuation. Under such conditions vapour cavities form to counter-balance the local pressure gradient. When cavities are brought to a relatively high pressure region in the liquid, they collapse, releasing high energy in a short time period (milli- or micro-seconds).

Research indicates that at the moment of cavity collapse, the local conditions could reach 100-5000 atm and 1000-5000 $^{\circ}C$. Such high energy release produces intense shock waves with velocities exceeding the speed of sound, causing liquid microjets and interfacial turbulence (Suslick and Grinstaff, 1990). The local high temperatures can enable chemical reactions not possible at room temperature. The high speed liquid microjects disturb the boundary layer at the solid surface, leading to the increased mass transfer and fragmentation of the particles (Zhou et al., 2009). Aoki et al. (1987) studied the use of ultrasound cavitation to de-agglomerate SiC powder and organic liquids. Longer exposures of suspensions under ultrasonic process caused a coarsening of the agglomerates (i.e. increase of their size) after an initial size reduction. A model based on a rate equation was proposed to explain these competitive phenomena. Kusters and co-workers (Kusters et al., 1993) presented a semi-empirical expression for the ultrasonic fragmentation rate as a function of particle size, suspension volume and applied ultrasound power. Later it was shown experimentally that the fragmentation rate is inversely proportional to the total suspension volume (Kusters et al., 1994). The authors derived an energy consumption law for the size reduction by ultrasonic fragmentation.

Recently, it has been found that the input energy-density does not depend on the de-aggregation process (Sauter et al., 2008). The authors varied the energy density by adjusting the hydrostatic pressure of the medium, the acoustic amplitude of the sound wave, or the gas content of the pre-mix. They found that with all these methods the final particle size distribution depended on the total

energy input only.

The effects of pH and added surfactants on particles in water suspension have been studied by various researchers. Bremmell et al. (1999) studied micron sized ranges of silica particles (3.6 μm) using sodium dodeclybenzenesulfonate (NaDBS) and cetyltrimenthylammonium bromide (CTAB) to understand the adsorption of ionic surfactants in particulate systems. Adsorption and mobility data indicate that NaDBS adsorbs at the silica/solution interface, though without improving the flotation efficiency. CTAB was found to adsorb on the silica particles as a result of electrostatic interactions. At low concentrations CTAB neutralises the surface charge of silica particles which destablizes the suspension. At higher surfactant concentrations, the particle charge becomes positive thus restabilizes the suspension.

Tkachenko et al. (2006) investigated how the size, and the zeta potential of titanium dioxide particles in water depend on the concentration of non-ionic TRITON X-100 and anionic ATLAS G-3300 surfactants and the pH of the medium. It was shown that anionic ATLAS G-3300 surfactant is a more effective stabilizer of aqueous suspensions of titanium dioxide than non-ionic surfactant TRITON X-100. Synthesized hematite sols with a particle diameter of ≈50 nm (Hs50) and ≈100 nm (Hs100) revealed points of zero charge at pH 9.0. Their hydrophobic coagulation behaviour with sodium dodecylsulfate was monitored by a different group using turbidimertric titrations in the pH range between 2.5 and 7.5. Four types of aggregates (typical framboidal, compact, chain-like, and small porous aggregates) were found depending on the concentration of the SDS (Ji et al., 2007). Ding and Pacek (2008) found that the goethite nano-particles tend to re-aggregate and form weak aggregates/flocs at pH between 5 and 12.

In the de-aggregation process, interacting particles can differ in their nature, size, shape, and degree of hydrophobicity. An example is the transient particle distribution during the de-agglomeration process by ultrasound cavitation. In this chapter the effects of ultrasound cavitation in comparison to a conventional mechanical agitation on re-dispersing the hydrophilic silica particles to water is presented. Then the influence on particles with different degrees of hydrophobicity, pH values and added ionic surfactant on the de-agglomeration process is investigated. Finally the stability of these suspensions is observed.

4.2 Results and Discussion

4.2.1 Effect of Ultrasound on the Kinetics of De-aggregation of Hydrophilic Silica Particles and Compare to Mechanical Agitation

In this section, the effects of ultrasound cavitation (UC) and mechanical agitation (MA) on the kinetics of de-aggregation of hydrophilic silica particles will be investigated and discussed. The materials and methods employed were described in Chapter 3.

In UC, three different amplitudes 36.9 μm, 62.5 μm, and 116.9 μm (corresponding energy dissipation rates are 109.01 Wkg^{-1}, 250.38 Wkg^{-1}, and 615.30 Wkg^{-1}, respectively) were used to study the process of de-aggregation of hydrophilic silica particles. Figures 4.2, 4.3 and 4.4 show the size distributions of hydrophilic particles in a suspension obtained by UC at amplitudes of 36.9 μm, 62.5 μm, and 116.9 μm, respectively. The de-aggregation process started with initially large aggregates (between 5 and 300 μm). At a low energy input the larger aggregates broke into small aggregates (between 3 and 120 μm) while the peak of the (mono-modal) volume size distribution shifted to the left. At a higher energy input, the distributions became bi-modal. One peak is established in the sub-micron range (the primary and secondary peak as seen in Figure 4.2). A further increase of the ultrasound energy led to the disappearance of the right hand peak, thus, the distribution became mono-modal in the sub-micron range. In the experiments reported in this chapter, a rotor speed of 6000 rpm was chosen throughout. This corresponds to an energy dissipation rate of 108.68 Wkg^{-1}). Figure 4.5 shows the hydrophilic silica particle size distribution measured at various times in a suspension. A very similar particle size distribution change was found with increasing energy input.

Figure 4.6 shows the volume size distributions produced by UC at an energy input of 9.7 kJ/kg at different amplitudes. The same graph shows the distributions obtained from mechanical agitation at an energy input of 6.5 kJ/kg. The distribution shifts much faster to the left of the spectrum in the case of MA than in the case of UC. In the case of UC the graph shows that with increasing amplitude the shift of the distribution to the left happens faster. With increasing energy input, all the distributions started to split into bi-modal distributions.

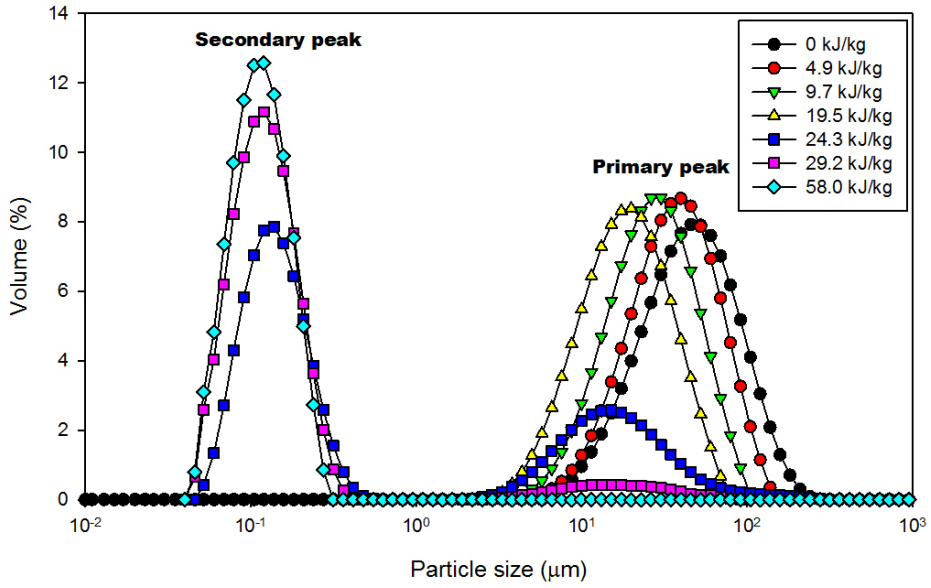

Figure 4.2: Transient volume distribution functions at an US amplitude of 36.9 µm.

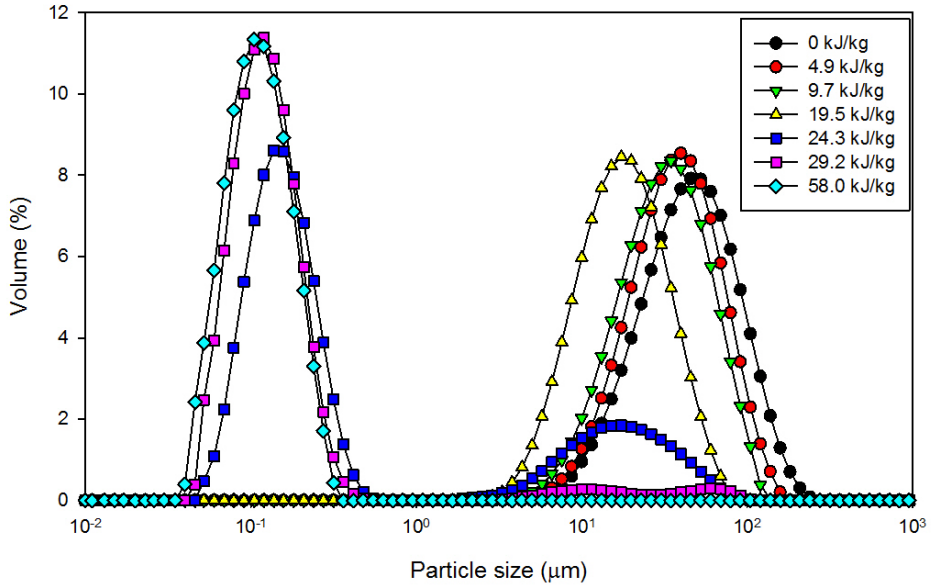

Figure 4.3: Transient volume distribution functions at an US amplitude of 62.5 µm.

Figure 4.7 shows the volume size distributions produced using ultrasound cavitation at an energy input of 24.3 kJ/kg at different amplitudes. Again, the same graph also shows the distribution obtained by using MA at an energy input of 32.6 kJ/kg. At an amplitude of 116.9 µm, an energy input of 24.3 kJ/kg was sufficient for breaking the larger aggregates into the sub-micron size range completely as there is only a single peak in the distribution which is positioned at the left hand

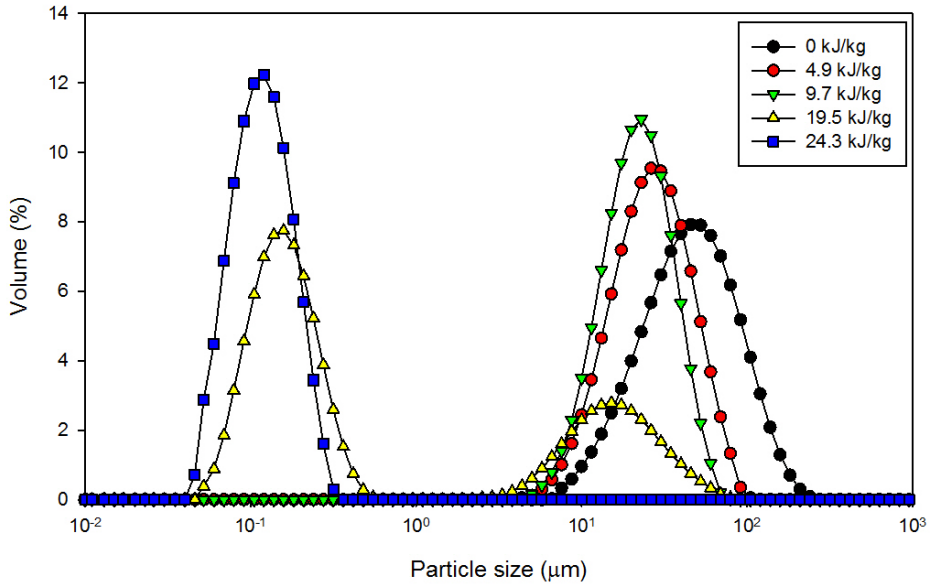

Figure 4.4: Transient volume distribution functions at an US amplitude of 116.9 µm.

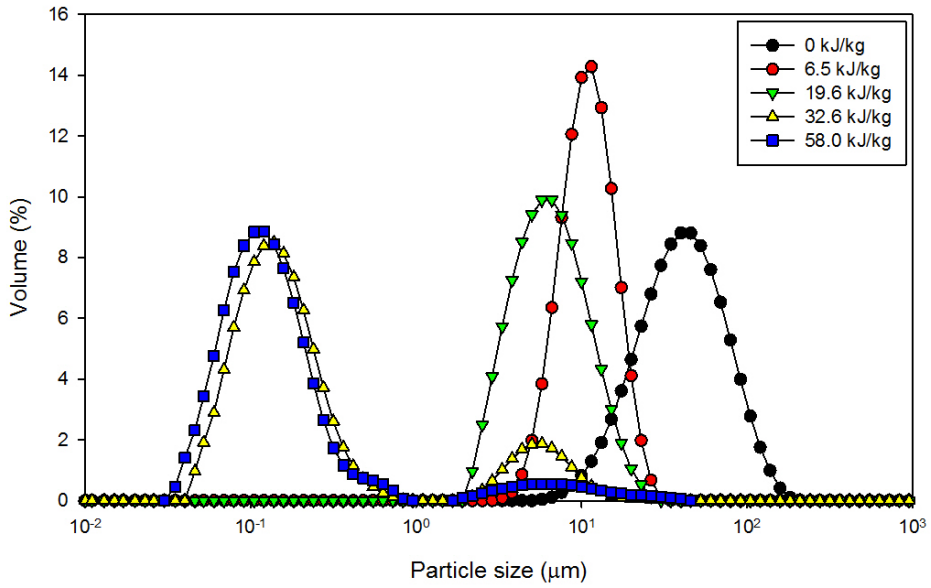

Figure 4.5: Transient volume distribution function in MA at 6000 rpm.

side of the spectrum in the micron-size range. At the same total energy input the size distributions remained bi-modal when UC amplitudes of 36.9 µm and 62.5 µm were used. The size distribution produced by MA at higher energy input also stayed as a bi-modal size distribution. This indicates that the particle dispersions produced at lower amplitudes using UC and using MA need higher energy to transform the particle size distribution from bi-modal to mono-modal in the sub-micron

range. These observations of the change of particle size distribution are consistent with the results reported by Pacek et al. (2007) who broke down hydrophilic silica particles using a high shear mixer only. In this study, both UC and MA show a similar dynamics of de-aggregation.

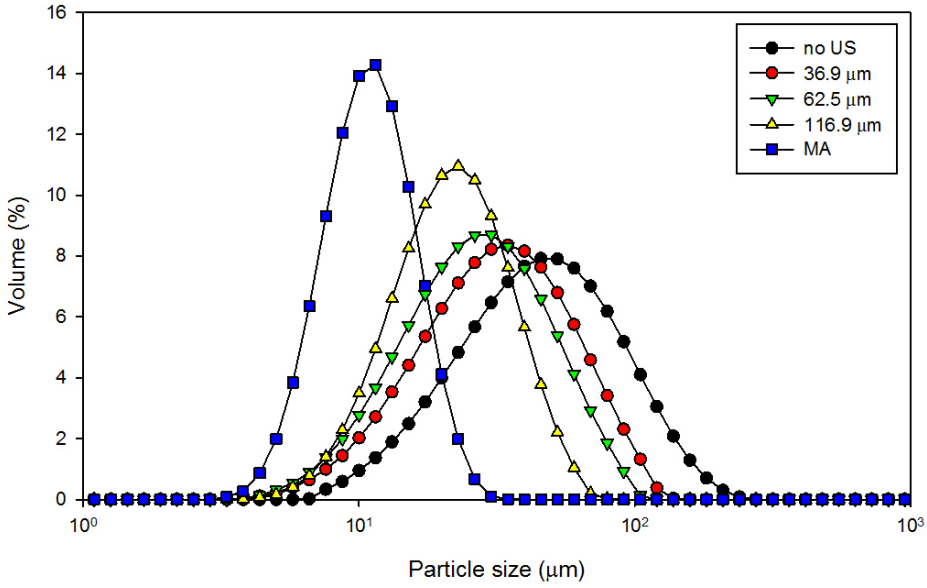

Figure 4.6: Transient volume distributions at UC amplitudes of 36.9 μm, 62.5 μm and 116.9 μm at fixed energy input of 9.7 kJ/kg; the transient volume distribution of dispersion produced by mechanical agitation is at energy input of 6.5 kJ/kg .

Figure 4.8 shows the median particle size, d_{50}, plotted as a function of processing time for different UC amplitudes and MA. It shows a sudden drop of the particle size, d_{50}. This sudden drop is a consequence of the aggregate size distribution becoming bi-modal which indicates that the aggregates split into two size groups. While the aggregate size distribution is bimodal, d_{50} is taken from the second peak of the aggregation size distribution. Therefore, the median of the aggregate size can change from micron size to sub-micron size in a very short time. The median particle size, d_{50}, decreases with increasing processing time and increasing amplitudes (both entail an overall higher energy input). Comparing UC and MA, a slower particle size decrease has been found using MA due to UC providing higher energy intensity.

In the study reported by Timothy and Dietmar (2002), high UC amplitudes lead to an increase of the intensity of a bubble collapse and consequently the de-agglomeration of particle agglomerates. A higher UC amplitude provides a larger intensity of UC and speeds up the process of de-agglomeration

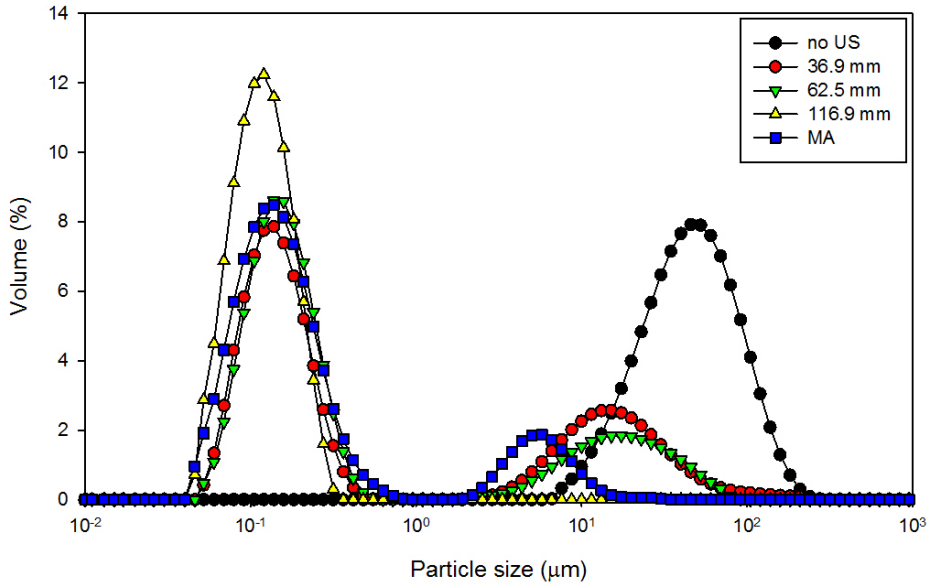

Figure 4.7: Transient volume distributions function at amplitudes of 36.9 μm, 62.5 μm and 116.9 μm at fixed energy input of 24.3 kJ/kg; the transient volume distribution of dispersion produced by MA is at energy input of 32.6 kJ/kg.

resulting in less energy input (Mason and Lorimer, 2002). Timothy and Dietmar (2002) pointed out that cavitation collapse starting from a transient bubble at 20 kHz with a maximum radius of 10-50 μm (depending on the acoustic pressure amplitude) creates a hot spot consisting of a gas filled cavity having a radius of 1 μm or less. When the aggregates are particulate in nature, cavitation can produce a variety of effects depending on the size and type of material. In a different study (Mason, 1999), he claims that the cavitation jet impact causes the fragmentation of larger aggregates/particles (> 1 μm) and the erosion of smaller particles/aggregates (< 1 μm). In these results, the higher amplitudes of ultrasound can break down the aggregates more efficiently, however, this only applies when the aggregates are larger than 1 μm. It is possible that the breakage of aggregates is also associated with the radius of the cavitation spot. When the aggregates are larger than the radius of the cavitation spot (1 μm), the aggregates are easier to break because cavitation can happen in between the gaps of aggregates. In contrast, when the aggregates are smaller than 1 μm, the jet impact is the main source for the energy input to aggregate separation. The influence of ultrasound amplitude is dependent on the the size of aggregates. Ultrasound amplitude influences only aggregate sizes larger than 1 μm.

In Figure 4.9, the median particle size, d_{50}, is plotted as a function of the specific energy input.

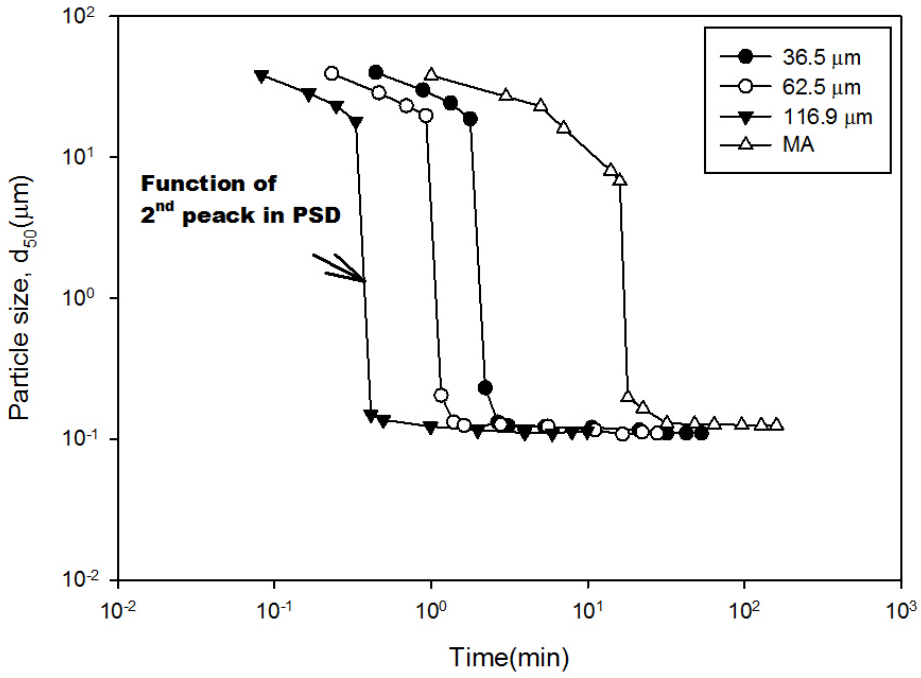

Figure 4.8: Effect of US amplitudes and mechanical agitation on particle size d_{50} as function of processing time.

The d_{50} is taken from the secondary peak of the aggregate distribution as shown in Figure 4.8. Even though previously there was a difference of the particle volume size distributions between various amplitudes using UC at the lower energy input was observed, the median particle sizes, d_{50} which show here are almost identical. In MA, the median particle size, d_{50}, decreases faster at lower energy but more energy input is needed to break down the particle aggregates into the sub-micron size range.

The relationship between the reduction of the aggregate median size and the processing time during grinding and de-aggregation is frequently described by the size-energy model (Gao and Forssberg, 1995, Mende et al., 2003).

$$X_{mean} = CE_v^{-a} \tag{4.1}$$

Where E_v is the specific energy input, the exponent a can be interpreted as a reduction rate of the mean particle size and the constant C as the aggregate size at unit specific energy input. This simple energy-size model was developed in the mid-1950s and can be used to calculate the mean (usually median) particle size in different types of grinding devices and can be used to predict and compare

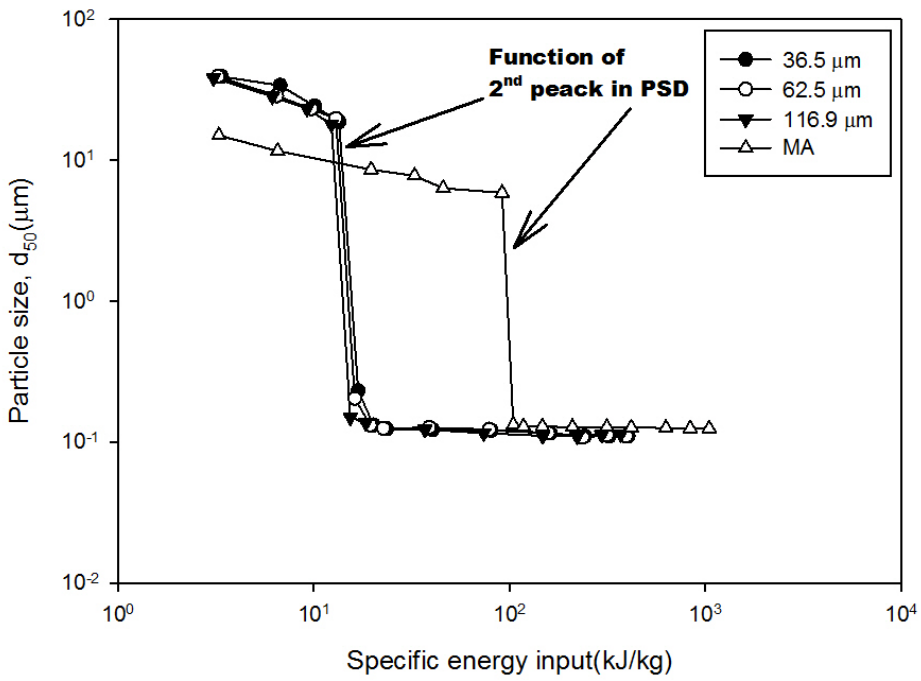

Figure 4.9: Effect of power intensity on particle size d_{50}.

the efficiency of different types of grinding devices.

In Figure 4.10, the experimental median size of aggregates is plotted as a function of specific energy input. These data are well fitted by the energy-size model Eq.(4.1). For UC, the slope is 0.54, 0.57, and 0.57 for amplitudes of 36.9 µm, 62.5 µm and 116.9 µm respectively, determined with coefficient of determination (r^2) larger than 0.99. For MA, the slope is 0.30 with a coefficient of determination (r^2) larger than 0.99. From the value of a one can conclude that UC is much more efficient at breaking down the silica particle aggregates.

The major disadvantage of the energy-size model is that it does not allow predicting the size distributions and it can only be used to model grinding processes where size distributions are mono-modal. In this study, the median aggregate size, d_{50}, of the secondary peak was used when the distributions became bi-modal. As shown in Figure 4.10, the results are in good agreement with the theoretical expectations. There is a decrease in particle size with increasing processing time due to the increase in energy dissipation which is responsible for de-agglomeration.

In previous studies (Gao and Forssberg, 1995, Mende et al., 2003, Pacek et al., 2007), the aggregate median size, d_{50}, has only been studied in a larger size range (> 1 µm). The suspensions with a

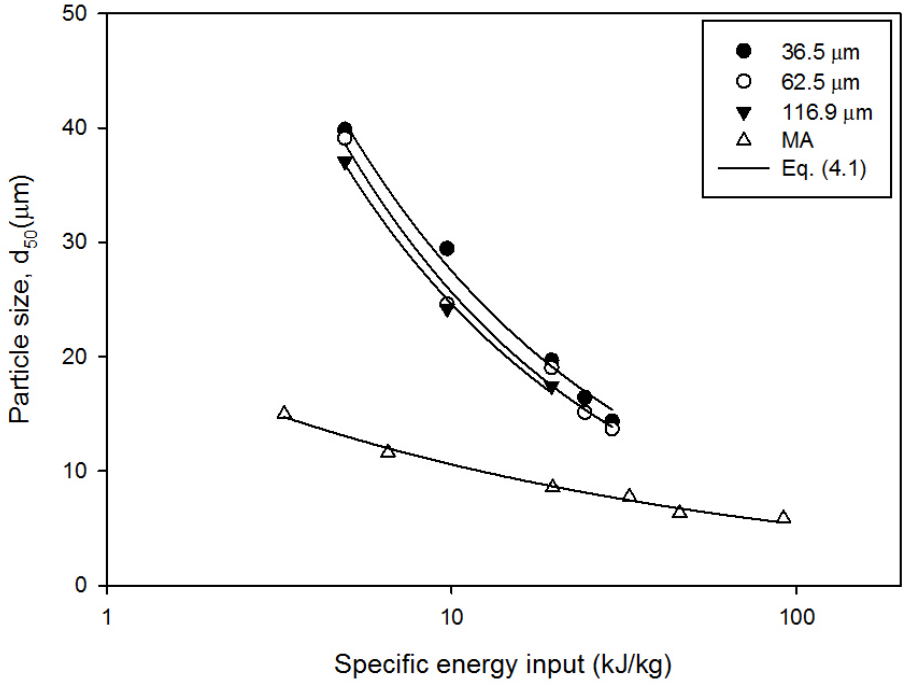

Figure 4.10: Median size d_{50} of aggregates obtained from UC and MA as a function of specific energy input.

high energy input will be looked at where the aggregate size distribution at sub-micron size becomes mono-modal again. The particle size distributions of the suspension treated by UC at an amplitude of 116.9 µm were measured in a laser diffraction method using a Mastersizer. Figure 4.11(a) shows that the d_{50} is between 110 nm and 116 nm and the volume size distributions overlap as the energy input rises from 118 to 2065 kJ.

The same suspension has also been measured by light dynamic scattering using HPPS which allows us to see the change in smaller aggregate size. In Figure 4.11(b), the z-average size of the suspensions are 141.2, 129.8, 123.9, 122.1, 120.1 and 106.5 nm for an energy input of 118, 236, 354, 472, 590 and 2065 kJ, respectively. Note that the energy input required to break down the small aggregates (i.e. 106.5 nm) is roughly twenty times higher than the energy required to break down the largest one (i.e. 141.2 nm). This clearly shows the need of a significantly higher energy input to achieve smaller aggregates.

Due to the limitation of the Mastersizer in measuring smaller aggregates (sub-micron size range) the small particles could not be resolved in detail. The light dynamic scattering method using the

HPPS machine allows more accurate measurements than the Mastersizer. In the aforementioned experiments and in what follows, therefore the particle size, z-average, was used from the measurement of HPPS. The influence of different generation methods on the particle size at high energy input is also investigated. Therefore, the particle size obtained from the suspension treated in MA has also been measured using HPPS.

Figure 4.12 shows the particle size and z-average as a function of specific energy input using UC and MA at various amplitudes. The energy-size model Eq.(4.1) was used again to fit the data. In UC, the exponent a is 0.093 with a determination of coefficient (r^2) of 0.95. In MA the particle size does not decrease with increasing energy input, but remains nearly constant, resulting in a poor fit with the energy-size model. The exponent a is 0.007 with a coefficient determination (r^2) equal to 0.28.

Compared to aggregates larger than micron size, a smaller particles (i.e. reduced by a factor of 50 or more) have a higher value of a. According to the energy-size model, this indicates that the reduction rate of the mean particle size slows down when the aggregate size decreases. The highest energy input reported here is 3800 kJ/kg and even at this energy level it was not possible to separate the aggregates into the primary size of nano silica particles. The qualitative results from the mono-modal distribution of sub-micron size aggregates after 2 minutes of UC obtained with HPPS and Mastersizer 2000 were confirmed by ESEM analysis (see the ESEM image in Figure 4.13). The suspensions were stable for months and no sedimentation occurred.

The dispersions are also observed that still have a bi-modal distribution and hence contain large as well as sub-micron sized particles. These dispersions are not stable in the sense that the aggregate size increases with time. Therefore, the stability of suspensions can be determined according to whether the particle size distribution is mono or bi-modal. Similar results have also been reported by Sauter et al. (2006).

The reason for the strong adhesion between the particles can be explained by the extended DLVO theory (Morrison and Ross, 2002) in Eq. 2.9 (See Chapter 2).

For two flat plates, the energy of dispersion-force attraction can be described by:

$$\Delta G^d = -\frac{A_{121}}{12\pi H^2} \tag{4.2}$$

where A_{121} is the Hamaker constant and the value for fumed silica reported in the literature is $0.849 \cdot 10^{-20}$ J (Morrison and Ross, 2002) and the electrostatic repulsive energy (G^d) at shortest distance H between their surface is given by Eq. 2.6.

As an additional repulsion appears at short range ($H < 3$ nm) the additional hydration energy G^h is given by

$$G^h = G_1 \exp\left(\frac{-H}{H_1}\right) + G_2 \exp\left(\frac{-H}{H_2}\right) \tag{4.3}$$

where H_1 and H_2 are decay lengths and $G_1/2\pi$ R=0.14 J/m^2, $H_1 = 0.057$ nm, $G_2/2\pi R$ =5.4 $\cdot 10^{-3}$ J/m^2, $H_2 = 0.48$ nm Grabbe and Horn (1993). In silica particles the origin of the hydration force is the interaction between the water molecules and the negatively charged silanol groups on the silica (Yotsumoto and Yoon, 1993b).

The energies of attraction and repulsion have been summarized and divided into two parts for the purpose of this discussion: the particles separated by more and less than 1 nm. In both cases, the electrostatic energy G^r can be neglected from changing pH because of the electrostatic repulsive forces which are several orders of magnitude lower than the van der Waals and hydration energies.

Figure 4.14 shows a graph of the energy landscape of interacting particles for distances closer than 1 nm according to the extended DLVO theory. To produce this graph the above parameters are used as cited in (Grabbe and Horn, 1993). The graph shows that total energy is repulsive for distances larger than 0.01 nm. Below this there is a strong attraction. This graph explains why aggregates cannot be separated into primary particles. Once particles are closer than about 0.01 nm apart the attractive force between them is very strong and it becomes practically impossible to separate them.

For distance above 1 nm the standard DLVO theory is valid and the hydration force is negligible. Following the DLVO the attractive van der Waals dominates the electrostatic repulsion at small distances. Effectively in conjunction with the hydration force this creates an energy minimum at a distance larger than 1 nm (the secondary minimum). The much stronger primary minimum at

distances smaller than 1 nm can only be reached when the hydration force is overcome. Particles can only be separated when they are within the secondary minimum.

4.2.2 Effect of Hydrophobicity on the Kinetics of De-aggregation

In this section, three types of hydrophobic particles are tested by UC only. This is necessary because the hydrophobic silica particles start to foam in the suspension when they are exposed to air making use of the mixer infeasible. The average weight carbon contents of the hydrophobic particles are 0.9, 1.5 and 4.3 for the particles R972, R812, and R202, respectively. The properties of the silica particles are listed in Table 3.1 in Chapter 3. Before applying UC, these particles are dispersed into water using a magnetic stirrer for 5 minutes. The results of these particle distributions are shown in Figure 4.15.

The hydrophobic silica cannot be broken in low pH conditions (section 4.2.3). Therefore pH 12 is chosen for all experiments discussed in this section. Figure 4.16(a) shows the size distribution for R972 particles obtained at various energy inputs at pH 12. As shown for the fully hydrophilic silica in section 4.2.1 aggregates can be broken down to sub-micron size at an energy input of 29.2 kJ/kg, but the distribution remains bi-modal which indicates that at this energy level only a fraction of the R972 clusters are broken down. A further increase of the energy input from 29.2 kJ/kg to 354 kJ/kg still leaves the distribution bi-modal. Only at the higher energy input of 472 kJ/kg, are all the larger aggregates broken into smaller ones and the average particle size , d_{50}, is about 220 nm. Further increases of the specific energy do not have significant impacts on the particle size distribution as shown in Figure 4.16(b). The particle size distributions corresponding to energy inputs of 472 kJ/kg and 826 kJ/kg are only minimally different (the small particle peak changes from 220 nm to 206 nm and is slightly lower).

Figure 4.17(a) shows the particle size distribution of R812 in a suspension obtained at various energy inputs at pH 12. The larger aggregates start to be broken down into smaller ones at a specific energy of 29.2 kJ/kg. An increase of the energy input to 118 kJ/kg leads to a reduction in the volume fraction of the larger aggregates and an increase of the volume fraction of the smaller aggregates. The particle size distribution does not change as the specific energy increases to 236 kJ/kg. When

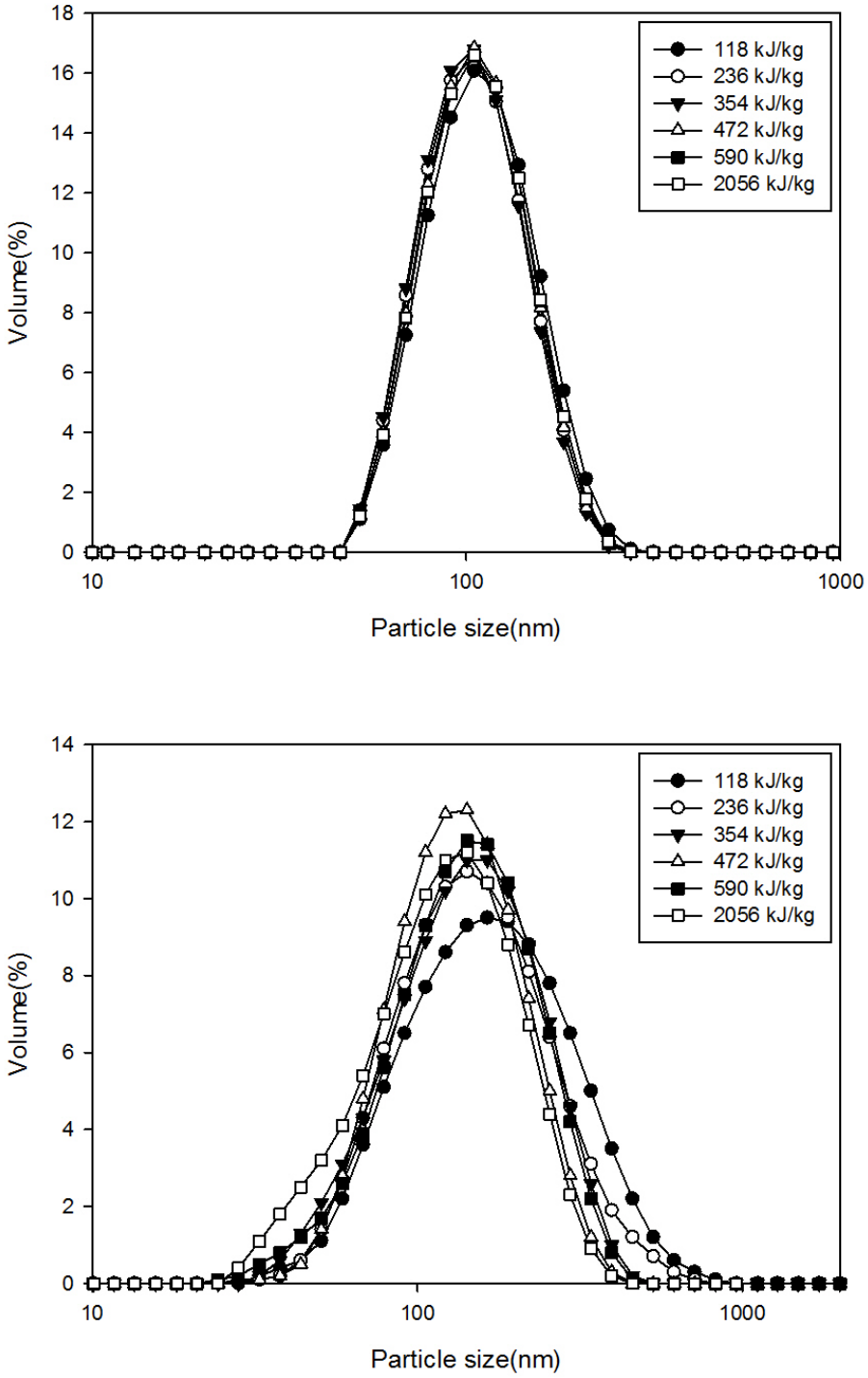

Figure 4.11: Transient volume distribution functions at various specific energy inputs measured by: (a) laser diffraction (Mastersizer) (b) light dynamic scattering (HPPS) .

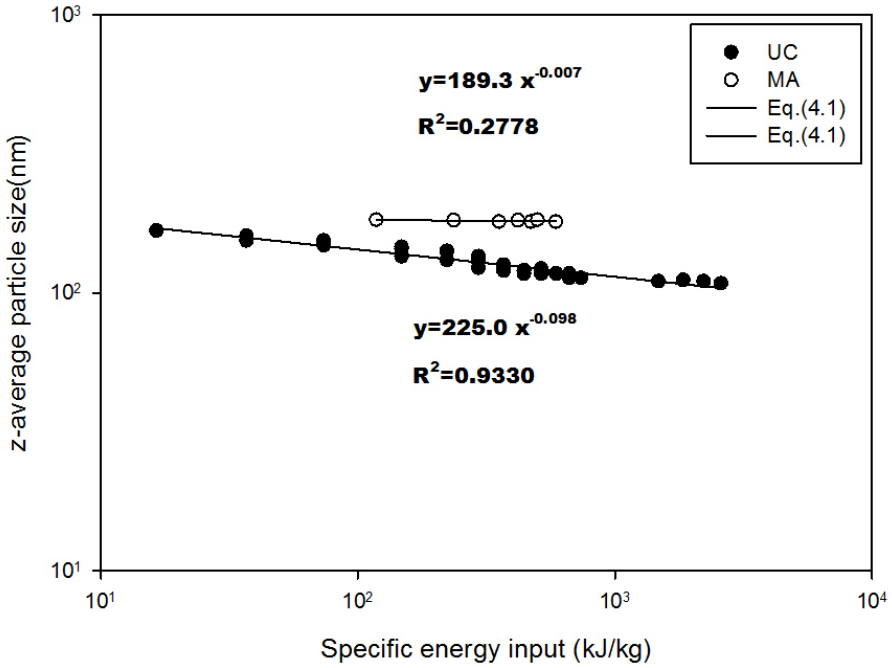

Figure 4.12: Effect of specific energy input on the z-average of particle size as a function of specific energy input.

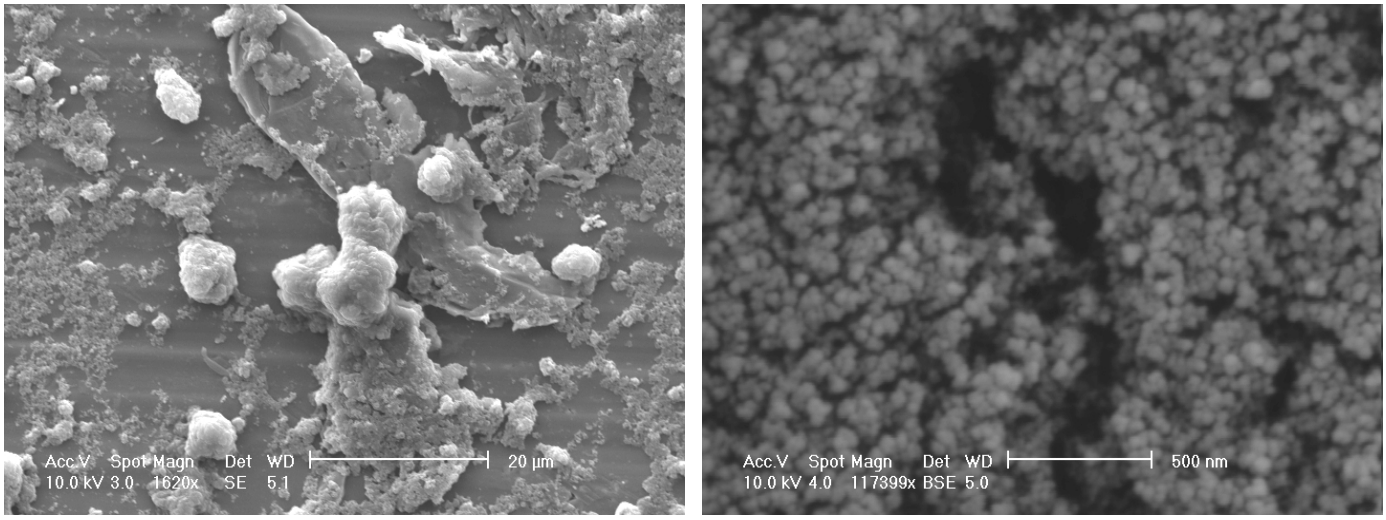

(a) *initial* (b) 2*min*

Figure 4.13: Images of silica aggregates/particles: (a) initial aggregates size after 5 min stirring, (b) aggregates after 2 min UC at an amplitude of 95%.

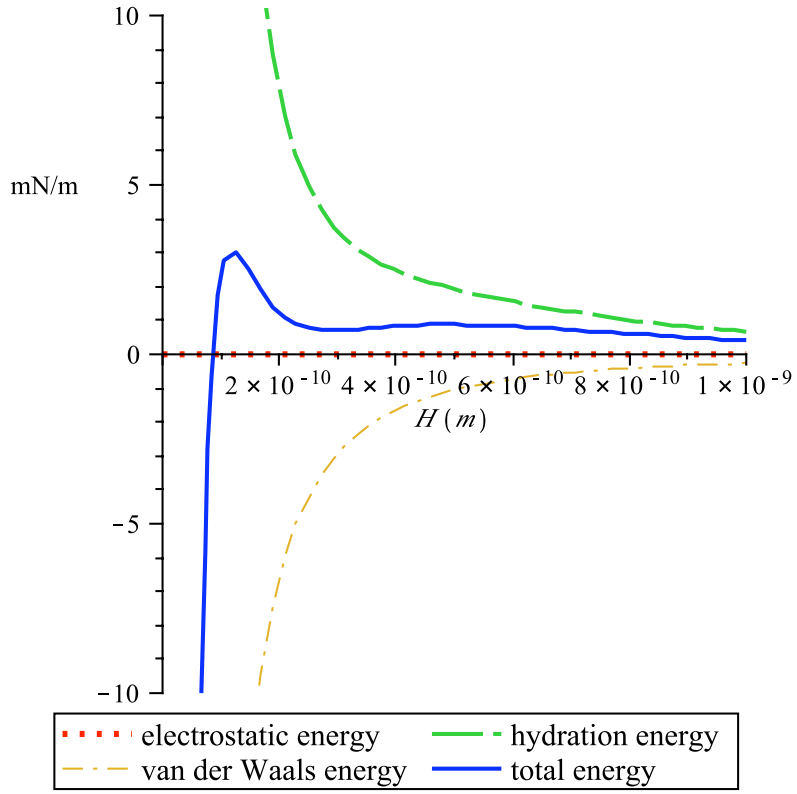

Figure 4.14: Electrostatic, van der Waals, hydration and total energy of two silica particles which their distance less than 1 nm are summarized.

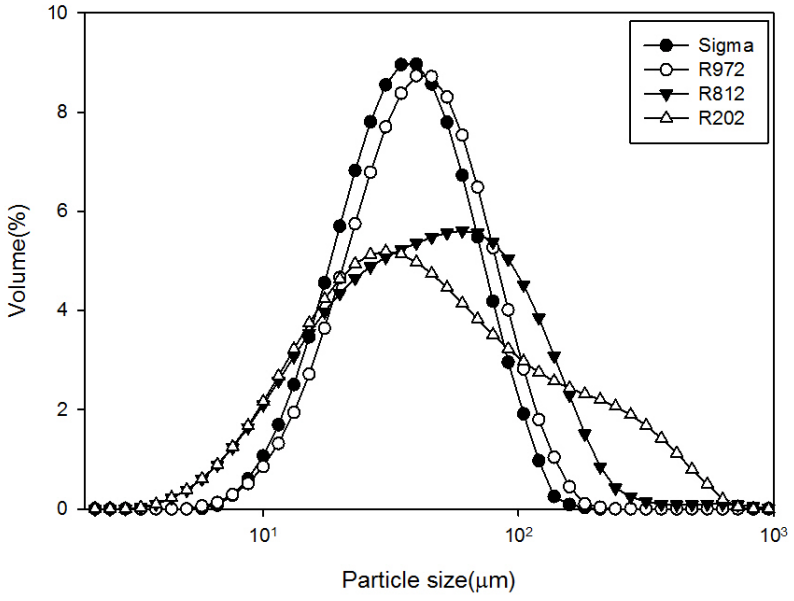

Figure 4.15: Transient volume distributions of the hydrophilic silica particles and three types of hydrophobic silica particles (R972, R812 and R202) before UC.

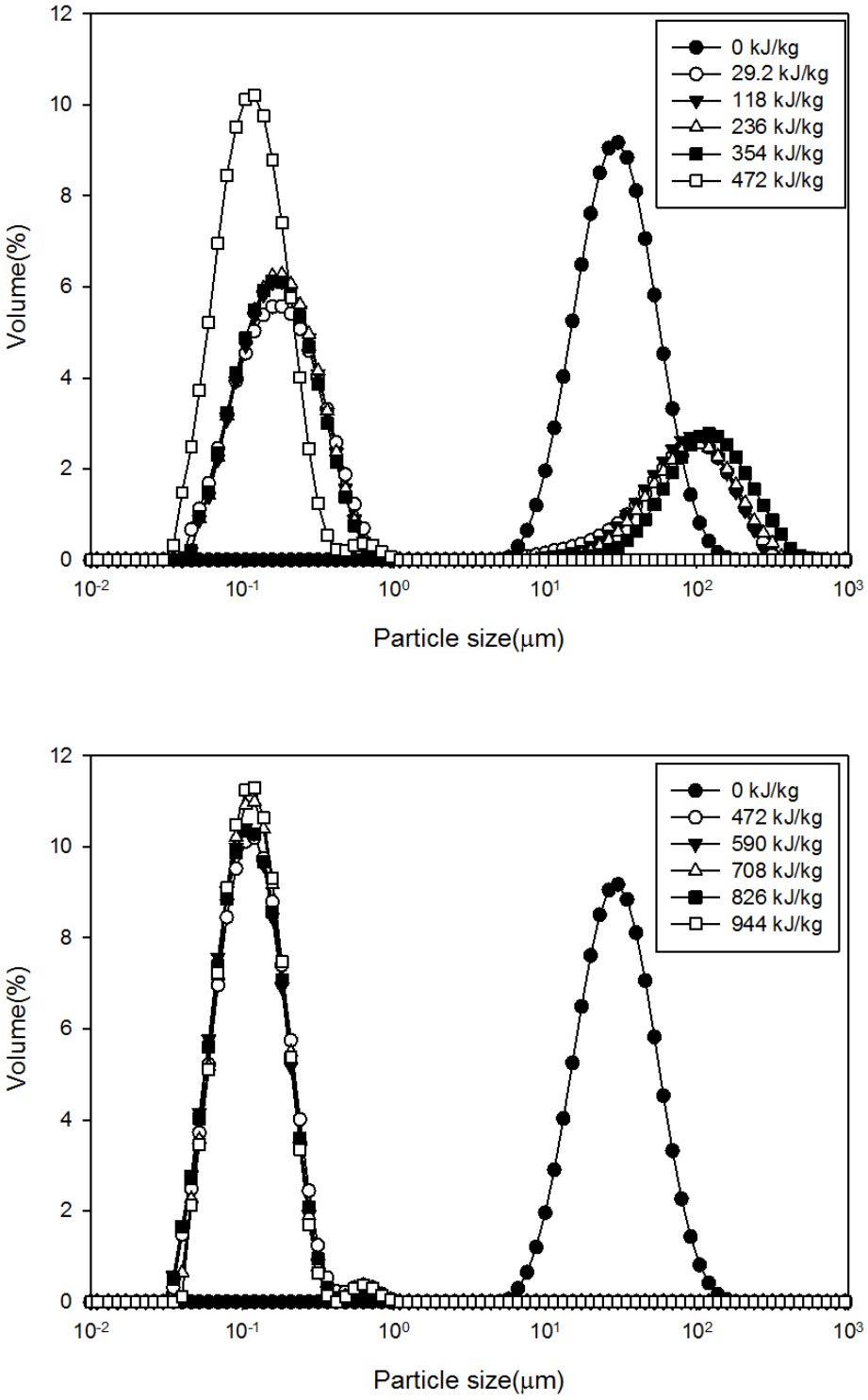

Figure 4.16: Transient volume distributions: hydrophobic particles R972 dispersions are sonicated at pH12 at energy input (a) from 0 to 472 kJ/kg (b) from 472 to 944 kJ/kg.

the energy input is over 354 kJ/kg, the particle size distribution not only has shifted to the right but the peak decreases in the sub-micron size and increases in the micron size range. This indicates that the particles start to re-aggregate after a certain energy input is surpassed. However, 120 μm size bubbles started to appear in the suspensions. This motivates the hypothesis that the increase of the large mode is due to bubbles. To what extend bubbles are measured by the Mastersizer is unclear. A further increase of energy input has no significant impact on breaking down the particles, but more bubbles were produced.

R202 particles is considered next. Figure 4.17(b) shows the particle size distribution at various energy inputs at pH 12. The particles cannot be separated with increasing energy input. 200 μm bubbles were generated in the suspension as the specific energy increased to 472 kJ/kg. A further increase of the energy input leads to no significant change in breaking the aggregates. The same is true for R812 particles, there were more bubbles produced in the dispersion. None of the hydrophobic particles could be described by the energy-size model, Eq. 4.1.

4.2.3 Effect of pH on De-agglomeration of Silica Particles

In this section, the effect of the pH on the size distribution, aggregate size and stability of the silica particle suspensions is investigate. One set of experiments with a 5.0 wt% suspension of hydrophilic silica particles is treated by UC at an amplitude of 116.9 μm specific energy input of 118 kJ/kg. The three types of hydrophobic particles (R972, R812, and R202) are also tested here. Due to the strong adhesion of these partially hydrophobic clusters, a concentration of 1.0 wt% was used and applied UC at an amplitude of 116.9 μm and specific energy input of 236 kJ/kg.

The hydrophilic particle sizes, d_{50} at pH 4, 7, and 10 are all around 120 nm immediately after the ultrasonic process and there is no significant effect of the pH value on the particle size distribution. Theoretically, a smaller aggregate size would be obtained in a higher pH environment expectedly because the highly negative charges surrounding the particles can reduce the attraction between the particles. The hydrophilic particle suspensions are stable over a period over 2 months as shown in Figure 4.18.

The relation between pH and the surface charge of the particles (zeta potential), has been mea-

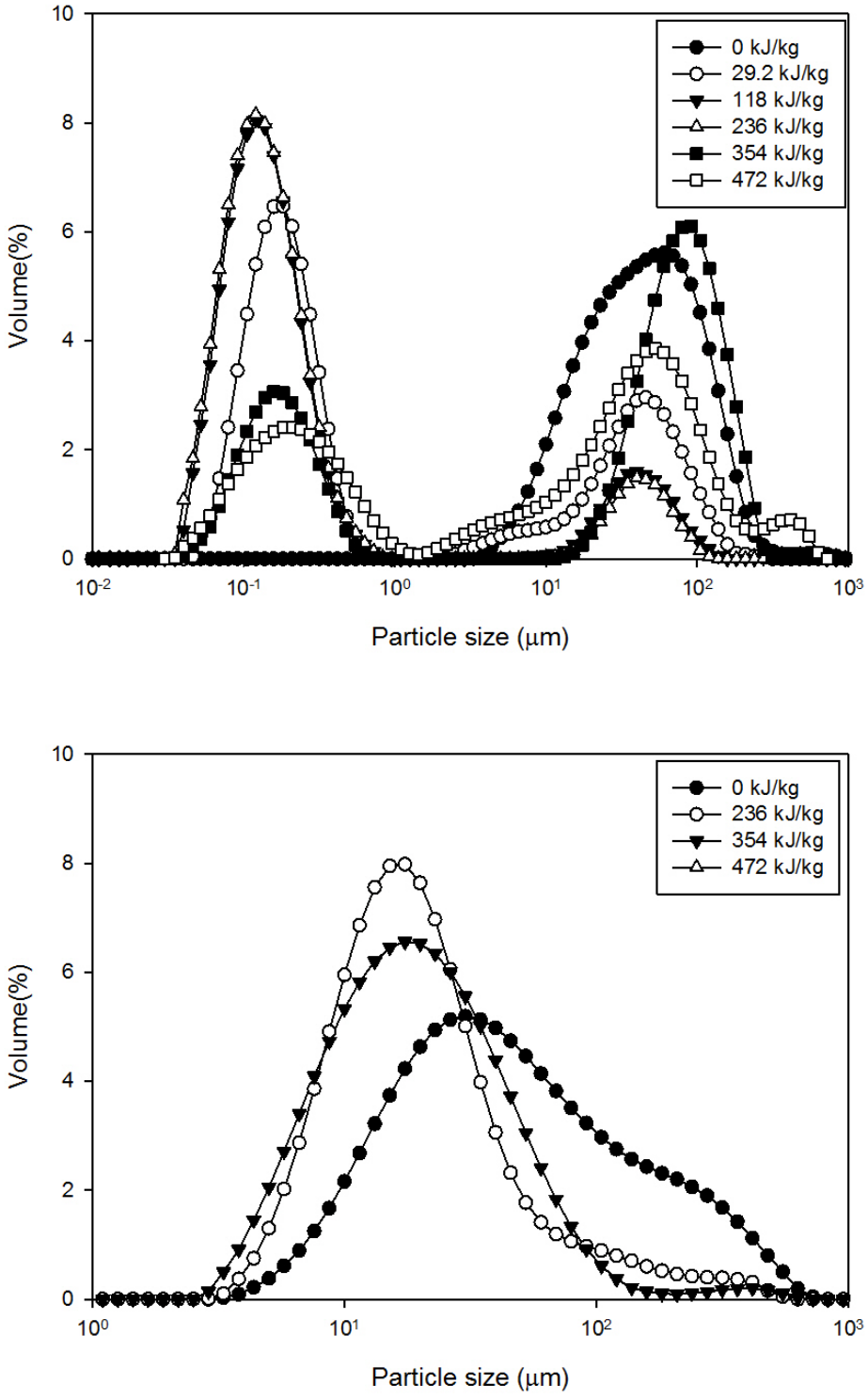

Figure 4.17: Transient volume distributions: hydrophobic particles dispersions are sonicated at pH12 at energy input from 0 to 472 kJ/kg (a) R812 (b) R202.

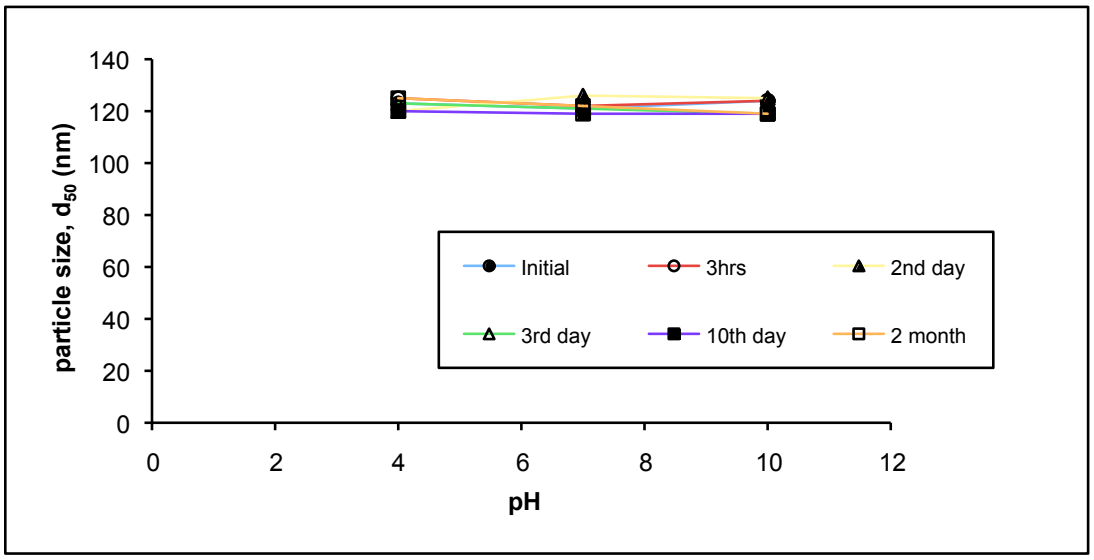

Figure 4.18: Effect of pH on the stability of 5.0 wt% hydrophilic silica suspension.

sured and the results are summarized in Figure 4.19(a). At higher pH values, the particles in the suspension possess a larger negative zeta potential which means that there is a stronger repulsive force between particles and the separation of the particles becomes easier. The zeta potential increases greatly with increasing pH. In Figure 4.19(b), the particle size, d_{50}, decreases as the pH value increases. The more hydrophobic the silica particles, the higher the pH needed to reduce the particle size.

The details of the particle size distributions of hydrophobic silica particles at different pH are shown in Figures 4.20, 4.21, and 4.22. Figure 4.20 shows the particle size distribution of R972 as a function of the pH value. At pH 2, the particle size distribution remains mono-modal but starts to shift to the left end of the spectrum over time. With increasing pH value (pH 4, 6 and 8), the distribution becomes bi-modal with one peak established in the sub-micron range. Above pH 10, the particle size distribution leads to the disappearance of the primary peak corresponding to the larger particles and the distribution becomes mono-modal in the sub-micron range. The median aggregate size of R972 are 134, 123 and 120 nm at pH 10, 12 and 13, respectively.

Figure 4.21 shows similar results for the size distribution of R812 particles. However, the larger aggregates can be broken into smaller aggregates at pH 8, 10 and 12 but not into the sub-micron size range. The particle size distribution remains mono-modal in the micron-size range at pH 4 and 6. The particle size, d_{50}, is 20.7 μm which is much larger than the corresponding values at pH 10 and pH 12 which are 193 and 288 nm, respectively (see Figure 4.19(b)). This is because at pH 8 a much larger fraction of the particles is contained in the large mode, hence the median value is high.

The R202 which has the carbon content between 3.5 and 5.0 is the most hydrophobic particle in the experiment (see details in 3.2). From Figure 4.22, it is clear that the particles cannot be dispersed into the micron size range at any pH value.

4.2.4 Effect of Ionic Surfactants on De-agglomeration of Hydrophobic Silica Particles

In this section, the effect of ion surfactants on the stability of suspensions is investigated. To do this, first 1.0 wt% of (R972, R812 and R202) hydrophobic particles is added into solutions of 0.2

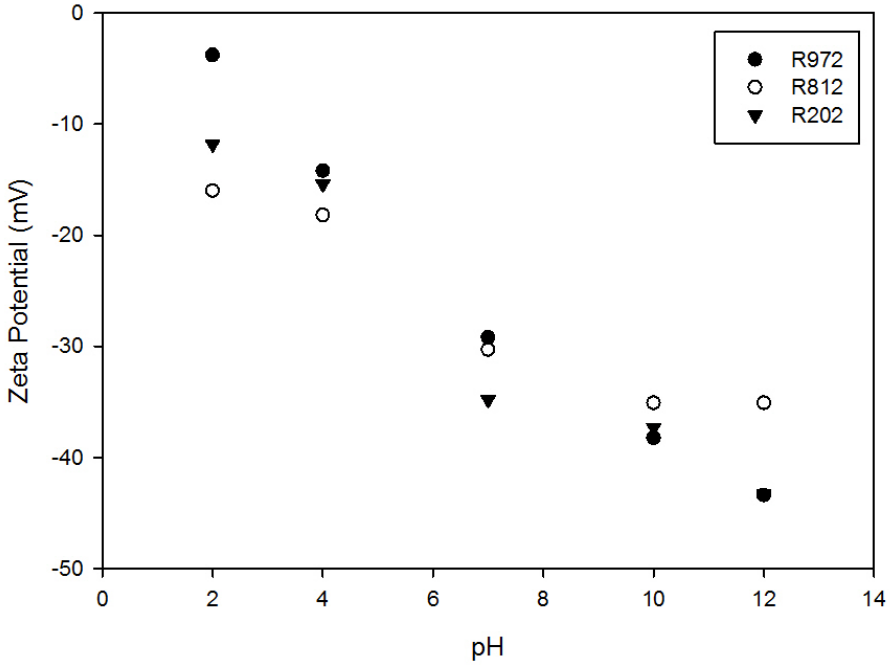

(a) zeta potential

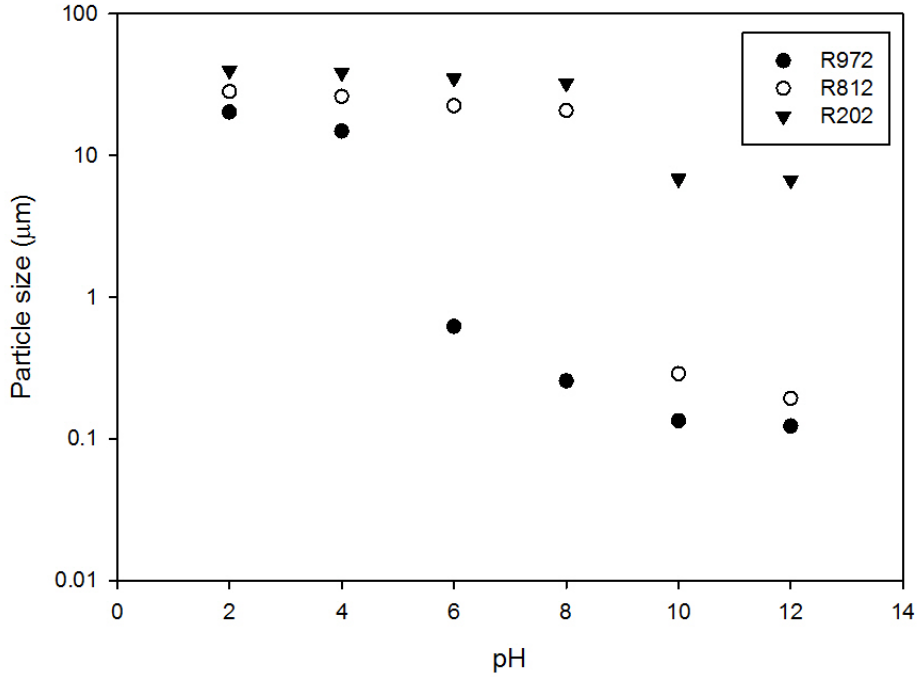

(b) silica particle size

Figure 4.19: Effect of pH on hydrophobic silica particle suspensions of (a) zeta potential and (b) mean particle size.

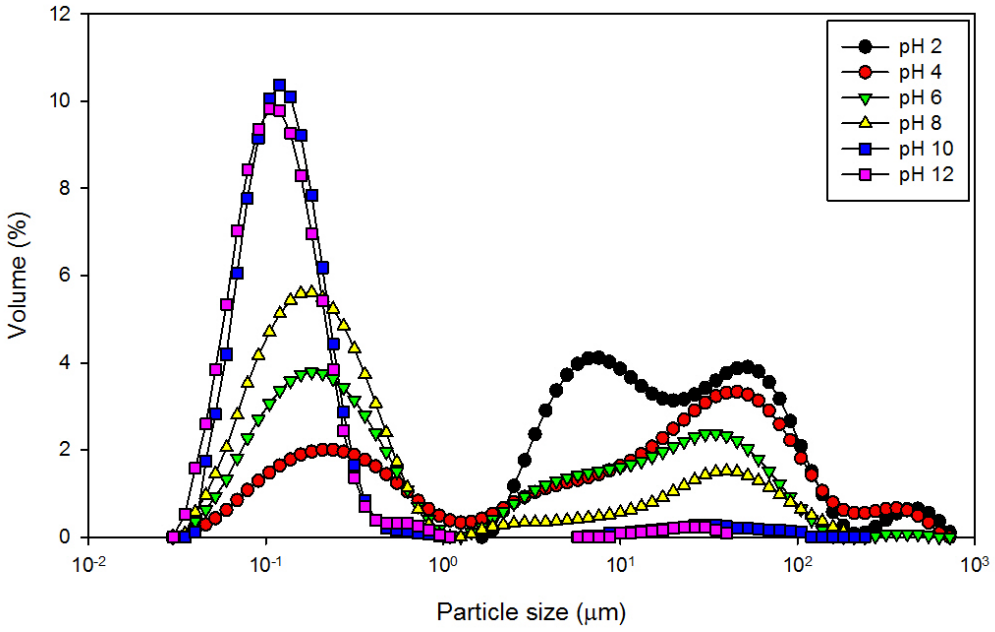

Figure 4.20: Effect of pH on 1.0 wt% R972 particle size distribution.

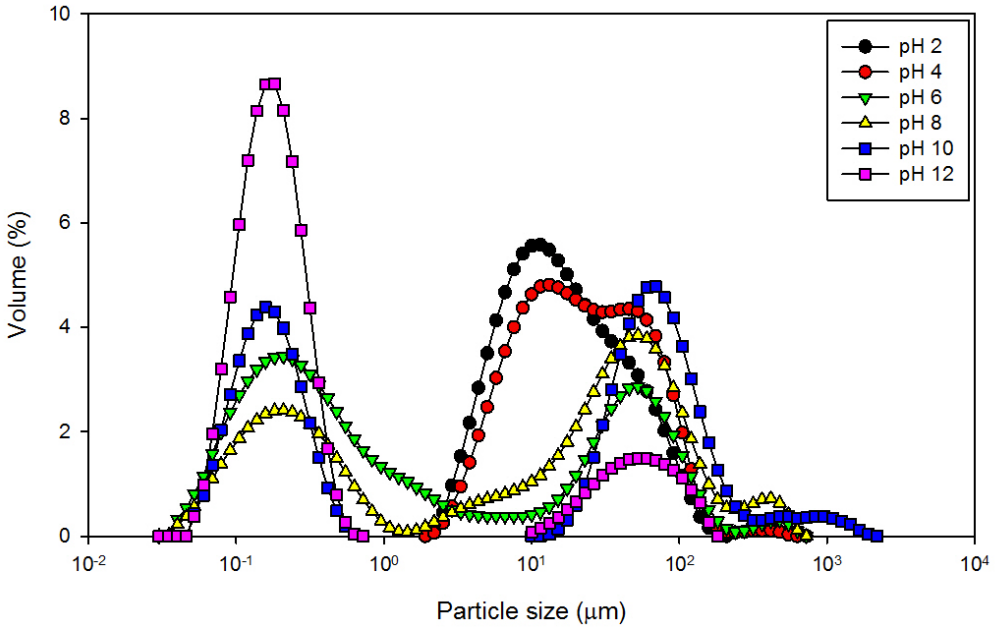

Figure 4.21: Effect of pH on 1.0 wt% R812 particle size distribution.

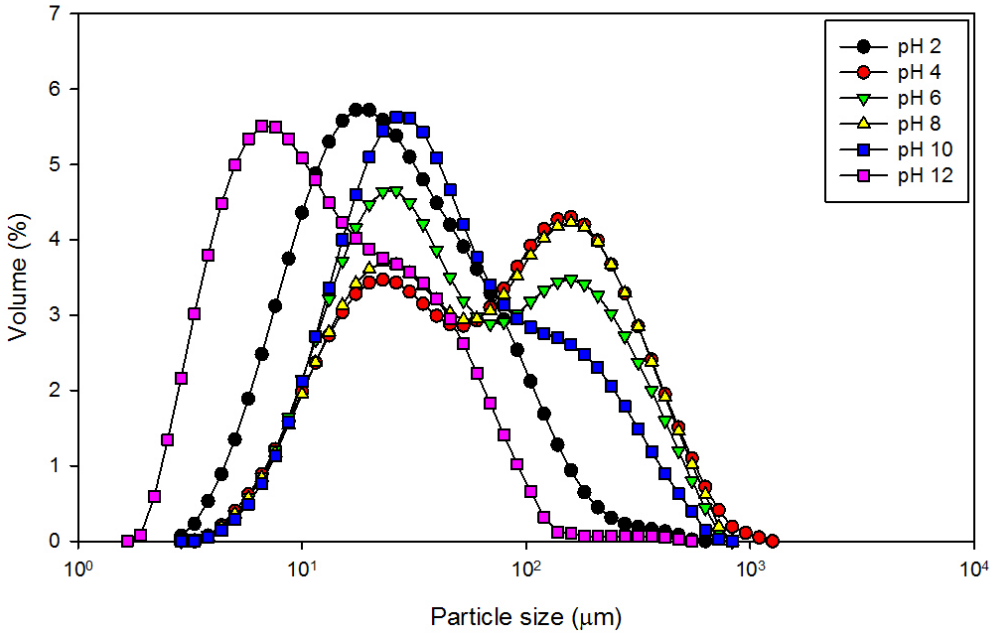

Figure 4.22: Effect of pH on 1.0 wt% R202 particle size distribution.

cmc C12LAS and CTAB. The dispersions were treated with ultrasound cavitation at an amplitude of 116.9 μm at a specific energy input of 236 kJ/kg.

The relationship between pH and the charge of the particles surface, i.e., zeta potential, has been measured and the results are summarized in Figure 4.23. The relationship between pH and the average size, d_{50}, is depicted in Figure 4.24. This shows that some suspensions are strongly affected by the charge on the particles surface. Both R972 and R812 were easier to disperse into C12LAS solution in comparison to water as we observed the reduction in particle size in C12LAS solution is greater than in water with increasing pH. This corresponds to a lower zeta potential of R972 and R812 particle suspensions with C12LAS. C12LAS has no effect on the reduction of R202 particles. The particle size of all three types of hydrophobic silica particles was not affected by the change of pH and cannot be reduced, although the zeta potential of the particles decreases with increasing pH.

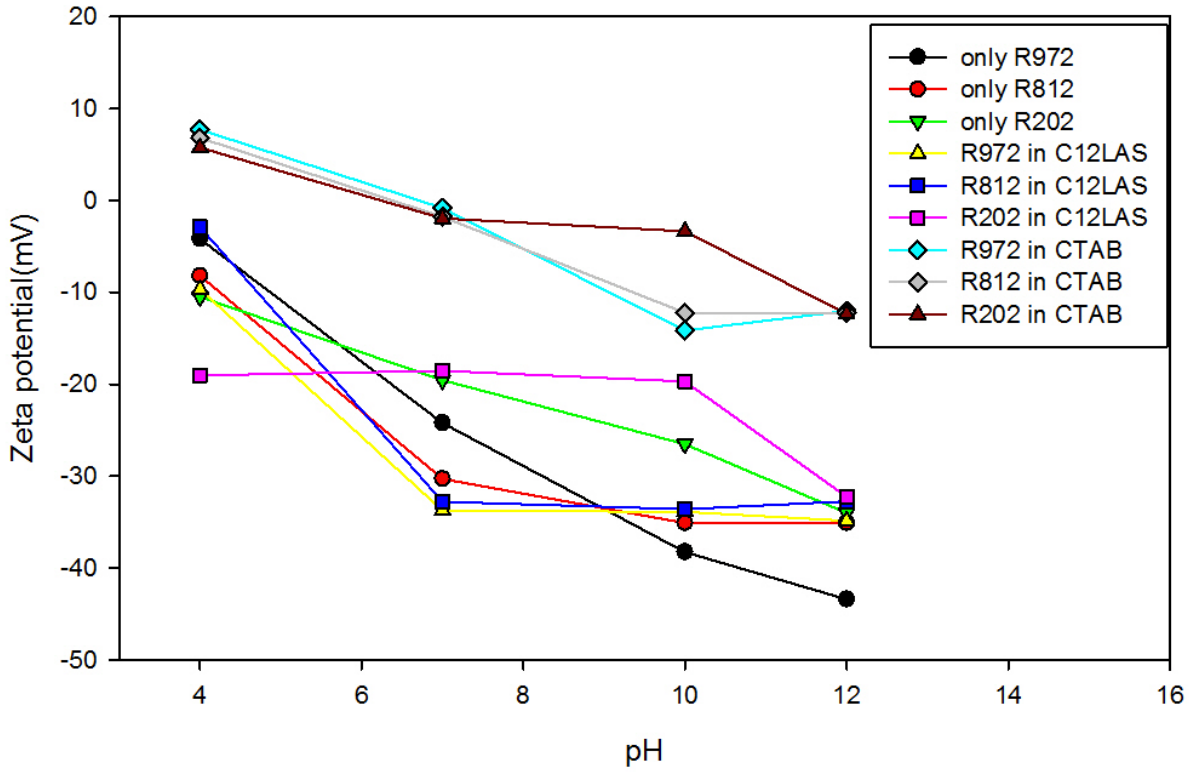

Figure 4.23: Zeta potential of (a) R972, (b) R812, and (c) R202 suspension with surfactants (C12LAS, and CTAB) at various pH.

The particle size distributions are shown in Figures 4.25(a), 4.25(b), 4.26(a) and 4.26(b). The

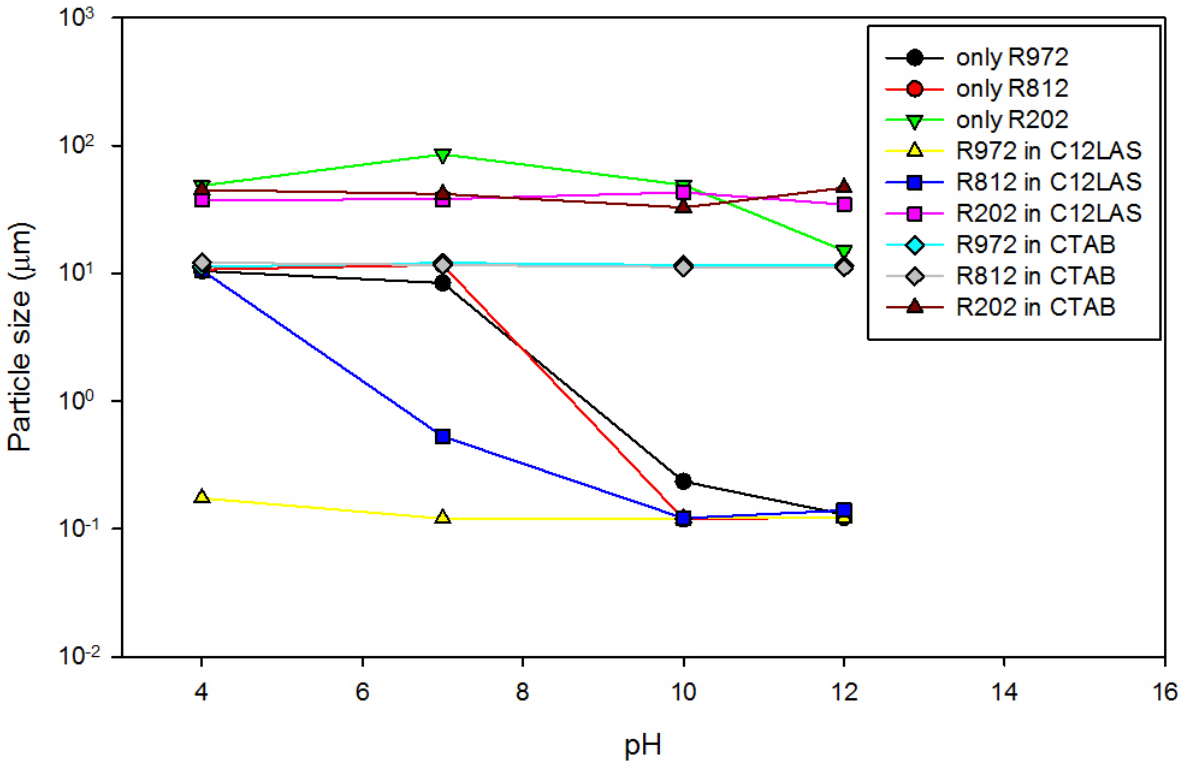

Figure 4.24: Particle size of (a) R972, (b) R812, and (c) R202 suspension with surfactants (C12LAS, and CTAB) at various pH.

large aggregates of R972 can be broken into sub-micron range in the C12LAS suspension at pH 4 to pH 12, as shown in Figure 4.25(a). At pH 4, the particle size distribution is slightly broader than at higher pH with a larger particle size d_{50}, 172 nm, while d_{50} is about 120 nm at pH 7, 10 and 12. Figure 4.25(b) shows the aggregates in a suspension of R972 in CTAB. They cannot be de-aggregated into the sub-micron size range and the particle size distribution shifts to the right of the spectrum with increasing pH. The average particle size of suspension at pH 4 and pH 7 is 10 and 12 µm, respectively, and 16 µm at high pH.

Due to higher hydrophobicity on the surface of the particles, the large aggregates of R812 were harder to break into the sub-micron range in the C12LAS suspension. Therefore, the aggregates remained in the micron size range at pH 4 but separated into smaller aggregates from pH 7 to pH 12 as shown in Figure 4.26(a). The median particle size, d_{50}, was 10 µm, 514 nm, 121 nm, and 139 nm at pH 4, 7, 10 and 12 respectively. Figure 4.26(b) shows that the aggregates in a suspension of R812 with CTAB can be separated into sub-micron size at higher pH, i.e. pH 10 and pH 12

where the mean particle size, d_{50}, is 206 nm and 123 nm. At pH 4 and pH 7, there is a mono-modal distribution throughout with overall only a minor breakup of particles; the mean particle size, d_{50}, after ultrasonication is about 20 μm for both pH values.

Anionic surfactants, owing to the presence of ionic groups, have greater possibilities in regulating colloid systems' properties (Tkachenko et al., 2006). Kosmulski (2001) reported on isoelectric point of silica of 1.7-3.5 mv and showed that at a zeta potential is larger than ±30 mv the majority of solid/liquid suspensions are stable as at this charge the electrostatic repulsive forces are sufficiently strong to overcome attractive van der Waals forces. Kosmulski's results indicate that the suspension should be stable at high pH and unstable at pH 4. Binks and Whitby (2005) report that CTAB can affect the hydrophobicity and flocculation of particles. In these experiments the zeta potential of the R972 suspension was close to the isoelectric point from pH 4 to pH 12 where larger particle sizes are observed, which is well explained by Kosmulski's finding that the stability close to the isoelectric point is poor. At higher pH the suspension of R812 resulted in a sub-micron size of aggregates. The values of the zeta potential were not changed with different pH while the average particle size increased with increasing pH dramatically, which is consistent with the findings in Binks and Whitby (2005) study.

4.2.5 Conclusions

Hydrophilic silica particles dispersed into suspensions by using both methods: UC and MA. Measurements of particle size distribution and the average of particle size have been used to determine the efficiency of separating the particles. In the de-agglomeration process, particle size distributions can be divided into three stages. The first stage is that the aggregates of particles are larger than 1 μm and the mono-modal size distribution stays in the right hand side of the spectrum. The size distribution shifts to the left but stays in single peak with increasing energy input. In the second stage, the size distribution starts to split into two peaks. One stays on the right hand side of the spectrum and the other stays the left. 1 μm is the split point. In the third stage, the particle size distribution becomes single peak again and sits only under micron size range. The single peak can shift to more left which means a further decrease of the average aggregate size with increasing energy

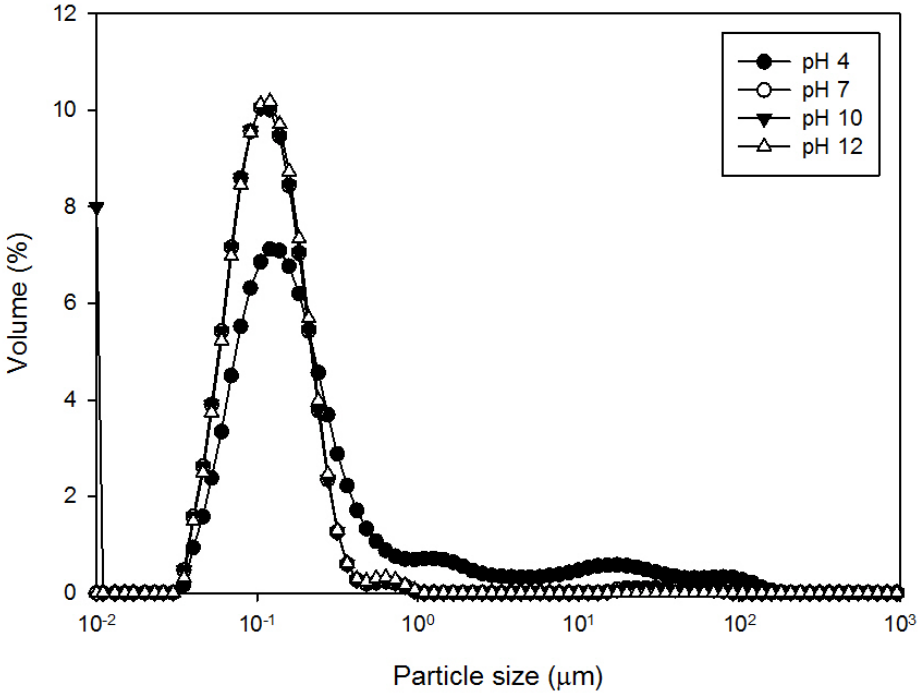

(a)

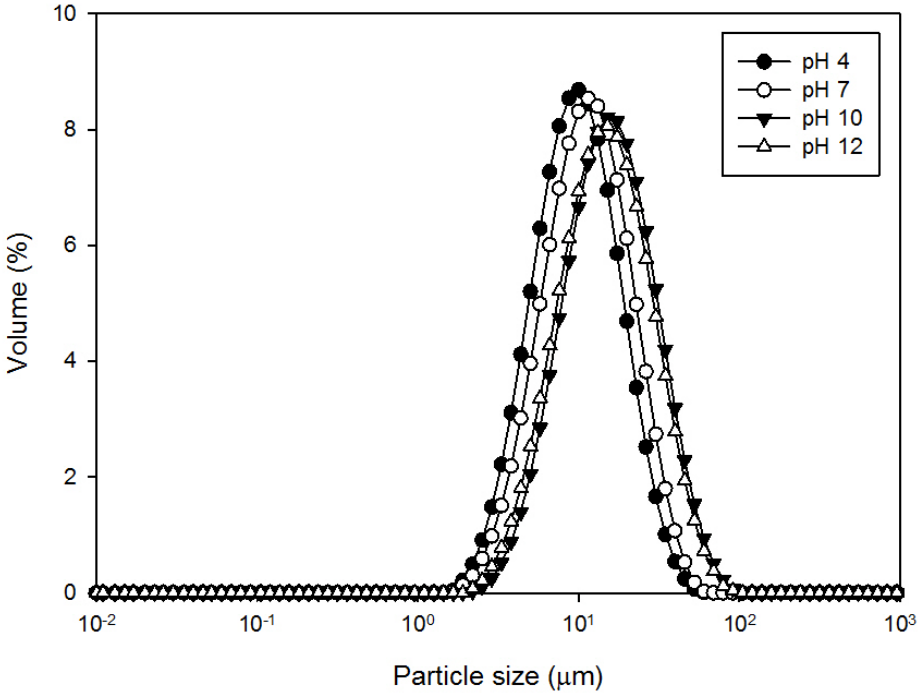

(b)

Figure 4.25: Particle size distribution of R972 suspension at various pH with (a) C12LAS (b) CTAB.

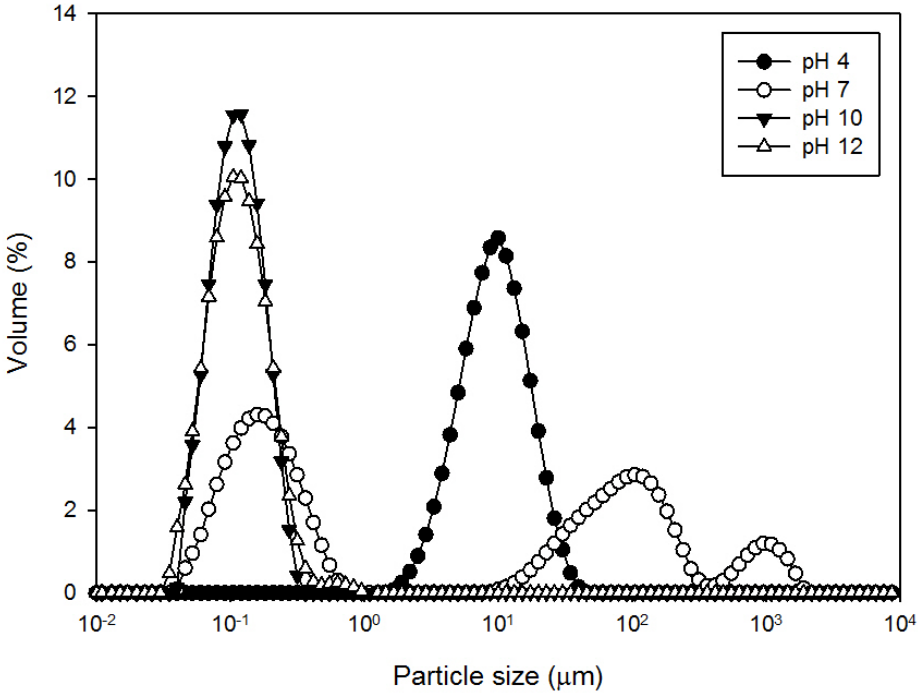

(a)

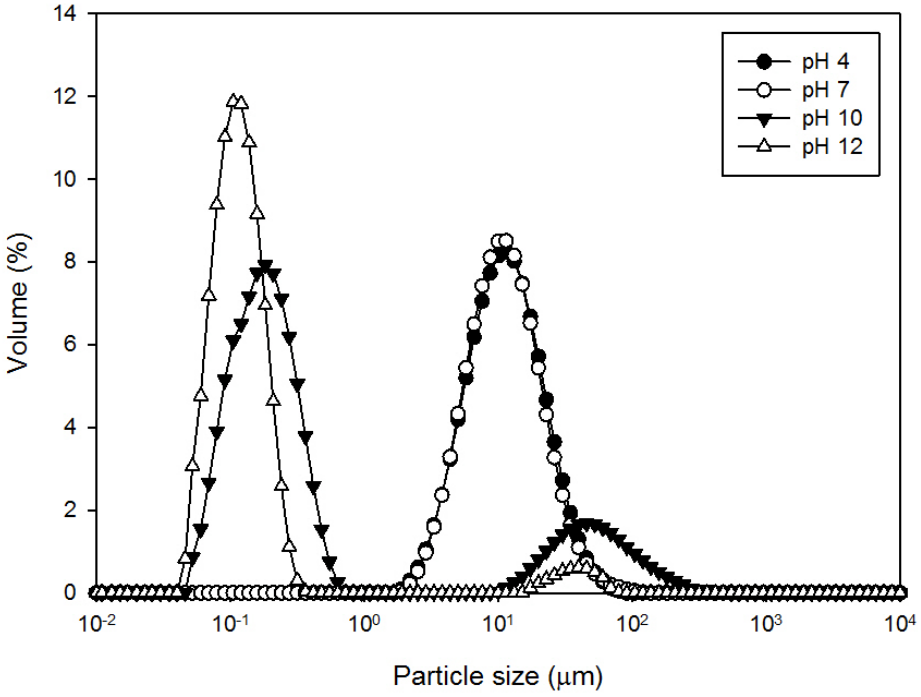

(b)

Figure 4.26: Particle size distribution of R812 suspension at various pH with (a) C12LAS (b) CTAB.

input.

In UC, the higher energy intensity (higher amplitude) has clearly a stronger power to separate the larger aggregates (> 1 μm) than the lower energy intensity at the first and second stages of de-agglomeration, but not at stage (when the particle size > 1 μm). When comparing UC and MA, MA required less energy input in the first stage and had a faster particle breakdown than UC. However, more energy input needed to get into the the third stage. After the particle size distribution becomes mono-modal with a peak in the range below 1 μm, there is no further decrease in small aggregate size using MA, but there is a further decrease by UC. However, the smallest aggregate size can be broken into is 106.5 nm using an energy input of 3800 kJ/kg and the aggregates cannot be separated to the primary size of silica particles. It is because the energy input cannot overcome the very strong bonding between particles, if the distance between these particles is less than 0.01 nm. Base on this study, combination of UC and MA methods can provide an efficient way for the de-agglomeration of hydrophilic silica particles according to the aggregate size.

The results show (see Figure 4.6) that MA can break down faster the initial micron sized silica aggregates with lower energy input than the UC. When the size of the silica aggregates reduces to less than 1 μm, UC has become more powerful to separate the silica (see Figure 4.9). Particle break-down can be made more efficient by using different de-aggregation methods during the de-agglomeration stages. Specifically, during stage 1 one should use MA to break down the large particles into micron sized aggregates; subsequently one should use UC to further break down the particles.

The de-agglomeration of three types of hydrophobic silica particles (R972, R812, and R202) has also been studied using UC. With increasing hydrophobicity of the silica, much more energy input is needed to pull the aggregates apart. The weakly hydrophobic silica (R972) which contain 0.6-1.2 wt% carbon content on the surface of the particles needs nearly 10 times more energy input to break the aggregates size to micron size range than the hydrophilic silica.

The moderately hydrophobic silica (R812) could not be fully broken into micron size range as shown in the bi-modal size distribution with increasing energy input. At an energy input of 354 kJ/kg, bubbles started to be generated and trapped in the suspensions. With the strongly hydrophobic silica (R202), the aggregate size can be reduced but the size distribution always remains mono-modal peak

during the entire de-agglomeration process. Bubbles were also generated in the suspensions.

The hydrophilic particles can easily disperse into suspension in a pH range between 2 to 12 and the stability of suspension was stable for a month. In the case of hydrophobic silica, the separation of aggregates is easier with increasing pH at a fixed energy input of 29.2 kJ/kg. The particle size distribution of R972 starts to split into two peaks at pH 4 and the aggregates can be broken into micron size completely at pH 10; while the particle size distributions of R812 hydrophobic particles only starts to split into two peaks at pH 6. Although the left peak is getting bigger with increasing pH, the aggregates cannot be broken down completely into micron size range. R202 particles cannot be broken down to micron range in any pH but the single size distribution shifted to the left. Once a suspension is broken down to a single peak of sub-micron size distribution, the suspension will then remain stable. However, the larger aggregate with bi-modal particle distribution re-aggregate after a short time.

The particle size of R972 and R812 can be altered by adjusting the pH and by adding ionic surfactant. In this study, R972 can be broken into sub-micron size at pH between 4 to 12 in 0.2 cmc C12LAS and R812 can be separated into sub-micron size at pH between 7.0 to 12.0. In comparison to only water, adding C12LAS enhanced the ability of re-dispersing these hydrophobic particles. R812 can be broken into sub-micron size by adding CTAB at pH 10 and 12.

Although only UC has shown more efficient to break down the hydrophilic silica particles under 1 µmand the possibility to separate hydrophobic silica particles, the foam study will be carried on with using MA as there is much more air draws into the suspensions during mixing and the hydrophobic silica parities can be used to form foam. There is more details on using hydrophobic silica particles to produce foam in Chapter 7.

Chapter 5

The Effects of Silica Particles on Whey Protein Foams

5.1 Introduction

Foams are often stabilized by milk protein molecules when they are used in the field of food. Liquid-like foams are metastable with lifetimes ranging from a few seconds to several days (Dickinson, 1992). Recently, there has been increasing interest in work on stabilizing foam by particles (Du et al., 2003, Alargova et al., 2004, Dickinson et al., 2004, Binks and Horozov, 2005a, Gonzenbach et al., 2006c, Horozov, 2008). In a review Murray and Ettelaie (2004) said that proteins can be considered as surface active particles in the protein-particle system which means that there can be competitive adsorption between particles and proteins. This could lead to antagonistic or synergistic effects on foam stability.

Two milk proteins were used as examples, casein and whey protein. They are both used widely in the food industry. Milk protein is of nanoscale dimension and can be classified in two groups depending on their structure: flexible and globular. Casein is in the first group. Casein includes proteins $\alpha_{s1}-$, $\alpha_{s2}-$, $\beta-$ and $\kappa-$ casein, the mixtures sodium caseinate, calcium caseinate, acid casein, etc. Casein consists of a high number of proline residues. This causes particular bonding of the peptide chain and inhibits the formation of close-packed, ordered secondary structures. There are no disulfide bridges either and this is because $\alpha_{s1}-$ and $\beta-$ casein do not have any cysteine residues.

In consequence, casein has a weak tertiary structure. Therefore, there is no denaturation from heat or other conditions because there is very little structure to unfold. Without a tertiary structure the proteins are also subjected to a considerable exposure of their hydrophobic residues (Goff and Hill., 1993).

Whey protein can be isolated after casein precipitation (e.g. in the process of cheese making). Whey protein is composed of globular proteins mainly β-lactoglobulin, α-lactalbumin and bovine serum albumin. They can be adsorbed into the interface and have good gelling and whipping properties. They preserve their globular molecular shape even after adsorption on an interface, but a partial unfolding is usually observed (Graham and Phillips, 1979). Heating can trigger denaturation of the whey protein which increases their water holding capacity. This globular protein is more hydrophilic than caseins (Goff and Hill., 1993).

Amino acids normally can be classified by the properties of its side chain. The side chain can make an amino acid a weak acid or a weak base. Also, if the side chain is polar, then the amino acid is hydrophilic; if the side chain is nonpolar, then the amino acid is hydrophobic (Creighton, 1993). Casein is very hydrophobic among all the proteins (Goff and Hill., 1993).

Dickinson et al. (2002) have studied proteins (commercial whey protein isolate (WPI), sodium caseinate, gelatin, and pure β-lactoglobulin) commonly occurring in foamed food products. They found that protein which form films with very different interfacial elasticities and viscosities appear to give fairly similar effects. None is capable of stopping disproportionation completely and none seems capable of slowing down disproportionation significantly. Within approximately 1 hour all bubbles had disappeared, having shrunk to below approximately 1 μm, so that in no cases was there evidence of stabilization via a surface rheological mechanism. The Dickinson study indicates that proteins are not capable, by themselves, of producing long-term stable foams, although it should be noted that the viscosities of the protein solutions they considered were low in all four cases. Marinova et al. (2009) have explored the foaming properties of caseins and whey protein. They found the foamability of WPC was maximal near the effective isoelectric point (pI) in contrast to sodium caseinate whose foamability was minimal near pI. Addition of salt and pH affected the stability of the films and foams. Their explanation is that the two protein types had different molecular

structures and different aggregation behaviours.

The foaming properties of protein can be altered by changing the pH. This is because protein molecules change their charge and surface activity with pH. The net charge of the molecules and the protein conformation can explain the effect of pH on protein. The hydrophilic part of protein interacts with water molecules via hydrogen bondings. Therefore, the final conformation of proteins depends not only on the amino acid side chains, but also on their interactions with water molecules (Lakkis and Villota, 1990). When the protein surface carries no net electrical charge in a particular pH, this is called the isoelectric point (pI). At pI, proteins show minimal interactions with water molecules (hydration and solubility) because there is no charge around the proteins. The attractive forces dominate the interaction between the protein molecules because of the low electrostatic and steric repulsion (Kuropatwa et al., 2009). An increase in the pH of the protein solution away from pI results in negative protein charges, however the details depend on the pI.

Paulsson and Dejmek (1992) found that the adsorption of protein at the air-water interface can be enhanced by reducing the range of repulsions between the protein molecules. They found that a pH close to the pI or at high ionic strength can enhance the adsorption. In contrast, most protein molecules possess negative net charges inducing repulsion between them, resulting in a decrease of protein-protein interactions and an increase of protein-water interactions at alkaline pH. Whey proteins cannot compact well to ensure the necessary films and foam stabilization at a pH away from their pI. However, it has to be noted here that the range of pH was only investigated from pH 3 to pH 6.4-6.8 in their study.

There are usually two main ways to make foams. One is mechanical agitation (e.g. whipping) and the other is pneumatical bubble formation by gas injection. Whipping is the traditional way to make foams from egg white or cream. Air is entrapped in the viscous liquid in the form of large bubbles, which are then broken down into smaller bubbles by mechanical agitation (Dickinson, 1989). In this study, ultrasound cavitation and mechanical agitation were used to produce protein foams. High-intensity ultrasound is rarely used as a method to generate foams but frequently used to alter the functional properties of proteins such as solubility, foaming capacity and flexibility "before" foaming (Jambrak et al., 2008).

Suslick and Grinstaff (1990) has used high intensity ultrasound to make both air-filled microbubbles and nonaqueous liquid-filled microcapsules. Gunzey et al. (2006) investigated the interfacial properties of aqueous Bovine Serum Albumin (BSA) solutions which has been treated by high-intensity ultrasound. They found that ultrasonication increased the surface activity of proteins thus lowering the surface tension of bovine serum albumin solutions; it also increases the rate of protein adsorption at the air-water interface. Gulseren et al. (2007) concluded that the magnitude of the structural and functional changes induced in proteins could be controlled by varying the sonication time. The author pointed out that potential future applications may include controlled alterations of lipid and gas interfaces in emulsions, foams and gels. Lim and Barigou (2005) demonstrated the potential of using ultrasound to generate a better foam structure (e.g. a smaller mean bubble size and narrower bubble-size distribution) during production.

There is a lot of research on protein foam stability using various proteins and under difference conditions (temperature, pH etc...). In this chapter, the effect of silica particles on the properties of foams formed by proteins is investigated as there is no research in this area. Silica particles uses as a model system for particles. Although the silica particles was used in this chapter are not food-grade ingredients, the research offers potential strategies or methodologies for developing improved particle-based systems in food product formulations (Dickinson, 2010).

The foaming experiments reported in this chapter were carried out in a small transparent column by mechanical agitation (MA) using a high shear mixer, and by high intensity ultrasound cavitation (UC) using a sonic processor. A series of experiments were carried out varying key parameters of the system including energy intensity of the foam generation methods, the concentration of the silica particles adding into the protein solutions, the type of milk proteins, the pH of protein foaming solutions, the hydrophobicity of silica particles, and the bulk viscosity of the protein solutions.

5.2 Results and Discussion

Firstly, the experiments performed to determine the concentration of whey protein using UC are shown. The optimum concentration was obtained and was used in subsequent experiments. Secondly, the effect of energy intensity, energy input and different foam generation methods (UC and MA) on

both foamability, foam stability and foam microstructure of whey protein is investigated. Thirdly, the hydrophilic silica and pH on whey protein foam is studied in detail. Fourthly, the foam produced by casein protein, is studied and compared to whey protein foam. Fifthly, the addition of three types of hydrophobic silica in the whey protein foam is studied. Finally, the effect of addition of hydrophobic and various bulk protein viscosity by adding SCMC are also studied on whey protein foam produced by using only MA.

5.2.1 Effect of Whey Protein Concentration

A few studies have reported that the foaming properties are affected by the concentration of proteins (Cherry and McWatters, 1981, Mutilangi and Kilara, 1985, Patel and Fry, 1987). In this section, the optimum concentration of whey protein (maximum foamability) is estabilished. This result is used to investigate further other effects on the foamability and foam stability of protein foam. There are four concentrations of whey protein (3.0 , 5.0, 7.0, and 10.0 wt%) and foam produced both by UC and MA.

Foamability, drainage and breakage of foam at various concentrations of whey protein produced using UC are summarized in Figures 5.1(a) and 5.1(b). The foam height and liquid level which used to plot in these Figures are defined in Chapter 3 (see section 3.3.2). Figure 5.1(a) shows the initial foam height immediately after foam formation plotted against protein concentration. A higher concentration of whey protein tends to give a higher foamability. The initial foam height at 5.0 wt% is the same as at 7.0 and 10.0 wt% but is higher than at 3.0 wt%. A previous study (Britten, 1992) found that the foamability was highest at 8.0 wt% . However, they did not show any data points between 4.0 and 8.0 wt%. Therefore, the maximal foam expansion happens at 5.0 wt% as observed in this experiment. The measurements of the surface tensions in Britten (1992) study also correspond to these results which are 45.3, 40.3, 39.8, and 39.3 for 3.0, 5.0, 7.0, and 10.0 wt%, respectively. Note that the results of the foam height are reflected by the surface tension results. The 3.0 wt% foam has a much higher surface tension, than the 5.0, 7.0 and 10.0 wt% foams which are very similar with respect to their surface tension. Figure 5.1(b) shows the liquid level and foam height plotted as a function of time. The drainage of whey protein foam at 3.0 wt% is somewhat faster than at

other concentrations which are very similar to one another. The foam curves start to decrease 10 minutes after foam formation at all concentrations. The foams almost collapse at the same time (approximately 6 hours after foam formation).

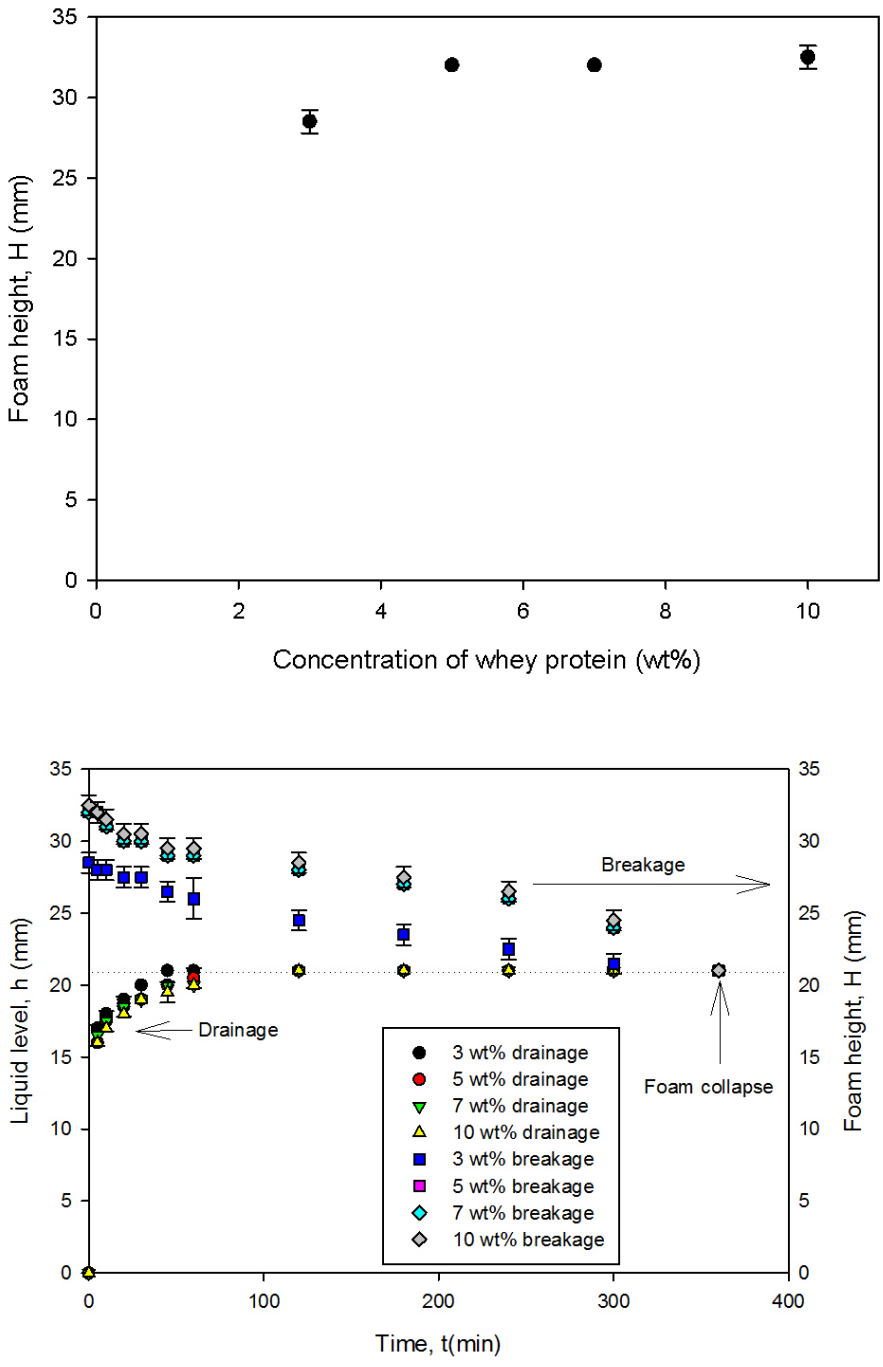

Figure 5.1: (a) Foamability of various concentration of whey protein (b) Drainage and breakage of foam at various concentrations of whey protein; UC.

The mean bubble size grows approximately linearly in time, as shown in Figure 5.2. The mean

bubble size of whey protein foam at a concentration of 3.0 wt% is larger than at 5 wt%. After that, no further increase was found with increasing concentration.

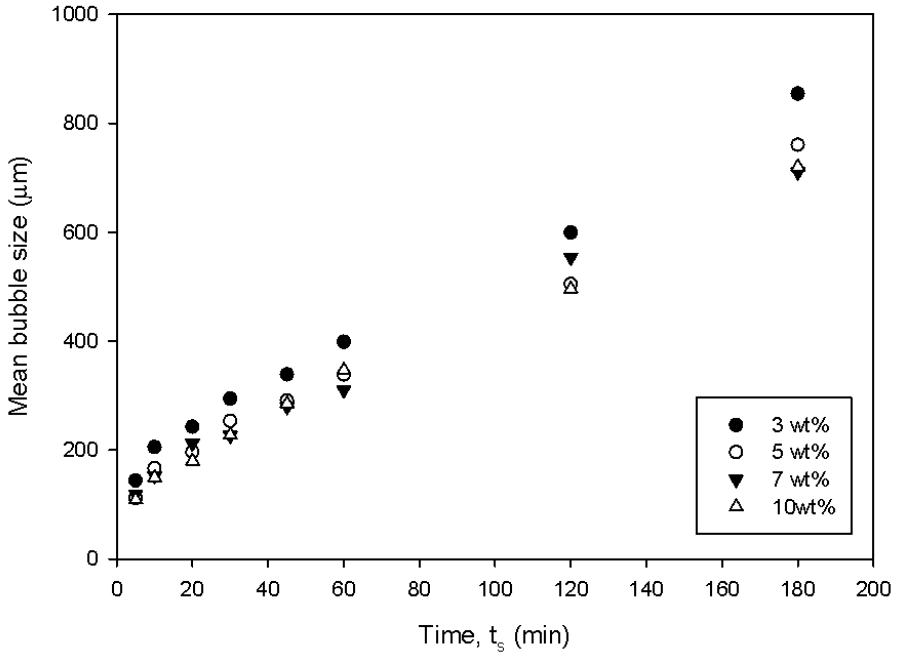

Figure 5.2: Mean bubble size as a function of time at various concentrations of whey protein; UC.

Similar results were found when foam produced using MA. Less foamability, faster drainage and foam collapse was observed at 3.0 wt%. This finding establishes that UC has not changed the functional properties of protein in this case. This is possible because it only took a few seconds to generate the foams by UC and the temperature does not rise high enough during this short treatment time to change the functional properties of protein.

The two important factors for providing a better foamability and foam stability in the foam stabilized by whey protein only are:

- A sufficient number of whey protein molecules to stabilize the foam film.
- A higher interfacial viscosity to obtain a thicker and more elastic interfacial films and to prolong the foam life time.

The bulk viscosity is the same for all four concentrations considered here, however, the foamability of the 3.0 wt% foam was different from the other three concentrations. A possible explanation for

this is that there are not sufficient protein molecules to complete surface coverage. Hence the foam quality suffers. The foamability of the other three concentrations was the same. This could be because these higher concentrations were at or above the CMC and the interface of the bubbles had full surface coverage from the protein molecules above 5.0 wt% whey protein. Therefore, 5.0 wt% whey protein was chosen in all experiments that follow because it gives the same quality of foams at higher concentrations, but better foam than at lower concentrations.

5.2.2 Effect of Energy Intensity and Energy Input

UC

In this section, three amplitudes 86.1 μm, 98.4 μm, and 116.9 μmwere chosen, corresponding to energy dissipation rates of 436.81, 488.64 and 615.30 Wkg^{-1}, respectively. A lower amplitude implies a lower intensity of power in the ultrasonic processor and therefore a longer time is needed to achieve the same energy input in the process of UC. To avoid the ultrasonic probe overheating the ultrasonic device was stopped immediately once the foam is formed. Therefore, the foams are produced by treating with UC for 5 seconds, 4 seconds, and 3 seconds at the amplitudes of 86.1 μm, 98.4 μm, and 116.9 μm, respectively. The energy inputs to produce the foam are 66 J, 59 J, and 55 J, respectively.

Figure 5.3(a) shows the foam height as a function of the amplitude of ultrasound. The foam height slightly increases with increasing energy intensity. The liquid level and foam height are plotted against time in Figure 5.3(b). Drainage is almost completely finished 5 minutes after foam formation and there was no significant difference between different amplitudes in the first 5 minutes drainage. Foam breakage starts 5 minutes after foam formation. The foam drainage curves almost overlap and so do the breakage curves. The statistics are summarized in Table 5.1. It is clear from the table that both the initial mean and the Sauter bubble size (d_{10} and d_{32}) decrease and skewness increases with time at different energy intensities. A slow growth in mean and Sauter bubble size with increasing energy intensity is observed. Skewness increases with increasing energy intensity. A positive and higher skewness value above zero indicates the presence of some large bubbles in the foam resulting in the median being greater than the mean bubble diameter d_{10}. All this indicates that in UC the mean bubble size increases over time. The rate of bubble size growth decreases as

the energy intensity increases. A smaller initial skewness also indicates a more symmetric bubble size distribution and hence a more homogeneous foam is produced by higher amplitudes than lower amplitudes.

The kurtosis increases with time, but also tends to increase with increasing energy intensity. A higher positive kurtosis means the bubble size distribution is more leptokurtic in comparison to the normal distribution and this indicates that the bubbles are more uniform. It has to be noted here that the values of the kurtosis cannot be compared at different times. This is because these bubble size distributions are based on different ranges of bubble sizes. The same applies when a low kurtosis is observed with increasing energy intensity.

From the above experiments, whey protein foam can be produced by UC. At an amplitude of 116.9 μm, it only takes 3 seconds to generate the foam and less total energy input than at lower amplitudes. The protein foam made at a high amplitude shows a better foamability and a longer foam life with slower bubble growth and smaller initial bubble size. However, there is no clear reduction in drainage. Jambrak et al. (2008) showed that high-intensity ultrasound has a major effect in changing whey protein functional properties like solubility and foamability. In their study, they noted that ultrasound may lead to protein denaturation. However, in their experiments, they did not vary the intensity, but only the treatment time. However, it has to be addressed here the treatment time was 15 and 30 minutes in Jambrak's study. They chose this long treatment time in order to denature the protein. In the experiments, treatment times was a few seconds only and probably no protein denaturation.

MA

In the MA experiments, 3 rotor speeds were chosen with energy dissipation rates at 33, 108, and 184 Wkg^{-1} for 4000 rpm, 6000 rpm and 8000 rpm, respectively. For this experiment, foams were produced using a high shear mixer for 1 minute and therefore the energy inputs are around 198, 648, and 1104 J for 4000 rpm, 6000 rpm and 8000 rpm, respectively. Protein solutions are easy foaming agents. The use of 1 minute agitation time was based on the trial results. At protein concentration of 5.0 wt%, the foamability does not improve when the mixing time is over 1 minute.

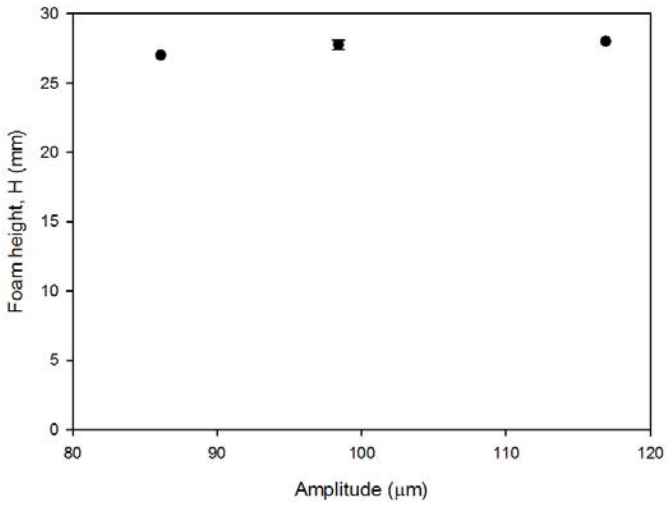

(a)

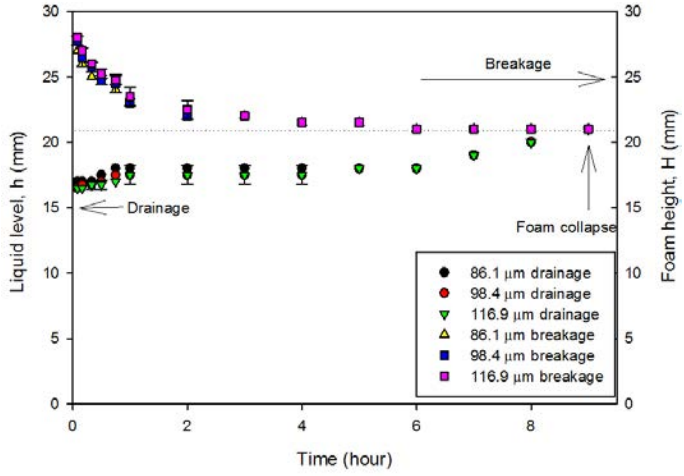

(b)

Figure 5.3: (a) Foamability of 5 wt% whey protein foam (b) Drainage and breakage of 5 wt% whey protein foam generated at at various amplitudes of 86.1 μm, 98.4 μm, and 116.9 μm; UC.

In Figure 5.4, foam height and liquid level are plotted against time. The drainage curves overlap for all three foams produced with different energy inputs. The initial foam height increases with increasing energy input. The collapse is fastest in the foam produced with the lowest energy input. However, after ten hours all foams in the sample have the same foam height.

The statistics are summarized in Table 5.2. In general, the mean bubble size of foam increases with time. In comparison to the foam produced at the speed of 4000 rpm, smaller initial mean bubble sizes with narrower bubble size distributions are obtained at the speed of 6000 rpm and 8000 rpm.

	d_{10}(μm)	d_{32}(μm)	S_t	Min(μm)	M(μm)	Max(μm)	S	K
86.1 μm								
5 min	116.81	139.32	37.40	39.78	115.14	237.38	0.26	-0.45
30 min	256.67	336.94	105.35	68.78	251.35	652.17	0.44	-0.10
60 min	358.60	682.19	206.10	116.30	306.10	1883.50	2.90	15.47
120 min	597.70	1544.69	481.00	206.00	451.00	2723.00	2.56	6.46
240 min	709.60	1532.15	487.00	223.30	578.10	2795.90	2.40	6.31
98.4 μm								
5 min	117.52	136.98	36.72	41.72	112.33	244.56	0.24	-0.22
30 min	245.34	311.61	95.22	64.26	240.78	549.74	0.49	-0.08
60 min	365.10	737.32	228.70	102.50	315.60	1744.80	2.63	9.35
120 min	604.30	1688.26	513.10	154.50	438.50	2956.70	2.73	7.75
240 min	655.30	1550.85	448.10	219.70	536.40	2998.10	3.40	13.38
116.9 μm								
5 min	112.11	129.29	32.08	34.92	110.02	200.43	0.12	-0.37
30 min	232.20	294.75	87.46	56.87	224.65	521.22	0.48	-0.27
60 min	386.40	664.60	238.30	103.80	324.80	1850.00	2.30	8.65
120 min	651.50	1311.10	531.20	126.90	412.90	3066.90	1.80	3.48
240 min	694.70	1283.88	428.7	204.70	554.70	2380.30	1.78	3.29

Table 5.1: Statistic parameters for foam bubble size distribution of protein at various amplitudes of 86.1 μm, 98.4 μm, and 116.9 μm; UC

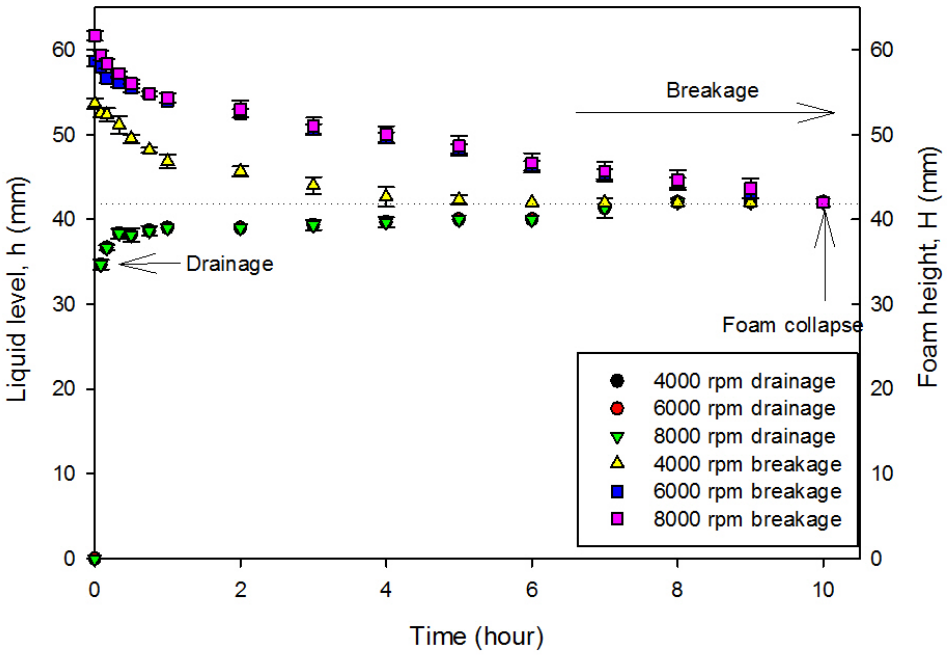

Figure 5.4: Drainage and breakage of whey protein foam produced at different speeds; MA.

The growth of the mean bubble size after foam formation is also greater at 4000 rpm than 6000 and 8000 rpm. 4 hours after foam formation a decrease of Sauter bubble size, d_{32}, was obseved in the foam generated with the lower energy input (4000 rpm). This can be interpreted to indicate that at first there is an increase in the size of individual bubbles, leading to a growth in the mean bubble

size; however, once these bubbles have reached a certain size, they burst, which leads to a decrease of the mean bubble size during later stages of the foam lifetime.

During the first hour after foam formation, the foam produced at 8000 rpm is similar in terms of bubble size to the foams produced at 4000 rpm and 6000 rpm. After that a larger Sauter bubble size was observed than in the case of 4000 rpm and 6000 rpm. It is possible that the foam produced suffers from "overbeating". The proteins become aggregated into insoluble particles that have little water-holding capacity because the prolonged whipping causes excessive coagulation of protein molecules at the air-water interface. Therefore, it leads to foam collapse. The faster bubble growth is caused by mechanical deformation of the foam and bubble rupture caused by the higher degree of mixing (Dickinson, 1992). Therefore, throughout this study, 6000 rpm is used in the mechanical agitation experiments to avoid the possibility of overbeating at 8000 rpm which anyway gives similar results.

Table 5.2: Statistical parameters for foam bubble size distribution: whey protein foam generated in different energy input; MA.

	d_{10}(μm)	d_{32}(μm)	S_t	Min(μm)	M(μm)	Max(μm)	S	K
4000 rpm								
5 min	138.16	161.85	41.71	62.48	138.59	242.97	0.21	-0.74
30 min	544.70	636.43	157.50	258.40	522.90	1018.80	0.67	0.32
60 min	887.50	1516.32	519.30	258.80	729.80	3097.70	1.36	2.02
120 min	1009.60	1777.98	600.10	229.80	825.70	3650.60	1.57	2.86
240 min	1091.80	1606.80	482.00	445.10	975.70	3360.00	2.07	6.10
6000 rpm								
5 min	123.26	140.50	33.64	53.24	120.69	215.79	0.10	-0.62
30 min	450.20	572.19	165.90	192.30	432.60	936.40	0.76	0.13
60 min	585.50	736.68	211.70	262.80	540.80	1212.90	0.68	-0.16
120 min	972.20	1930.59	670.30	239.60	751.40	3545.10	1.57	2.49
240 min	1121.40	2262.05	783.20	291.40	828.20	4180.80	1.61	2.38
8000 rpm								
5 min	124.82	141.25	33.41	54.55	126.94	196.00	-0.08	-0.80
30 min	447.00	567.58	170.20	183.80	424.70	831.50	0.37	-0.82
60 min	604.80	914.86	297.90	156.20	552.90	1806.30	1.30	2.26
120 min	1201.70	2211.78	820.30	237.30	925.50	4113.70	0.97	0.14
240 min	1303.90	2487.78	872.40	324.30	1013.10	4472.90	1.43	1.83

Comparison between ultrasound and mechanical agitation In the previous section the foam can be produced by UC using much less energy input (66 J, 73 J and 92 J for 86.1 μm, 98.4 μm, and 116.9 μm) than MA (198 J, 648 J and 1104 J for 4000 rpm, 6000 rpm and 8000 rpm). The most uniform and finest foam can be made by UC at an amplitude of 116.9 μm. In MA, a higher speed of rotation with a higher energy input does not necessarily lead to a finer and more stable foam. In this section, the effect of these two different foam generation methods on the whey protein foam

properties is investigated.

Figure 5.5 shows the gas volume fraction of whey protein foams plotted against time at various amplitudes using UC and MA (the definition of gas volume fraction can be found in section 3.3.2). In all the foams the foam volume fraction decreases with time, and a similar foam lifetime is observed in all these foams. The poorest foamability and fastest foam collapse happens in the foam made using high shear mixers at 4000 rpm with 198 J energy input. With increasing rotation speed, the foam fraction and foam stability increases. A similar result is also found with the foam produced by UC at an amplitude of 98.1 μm and 116.9 μm.

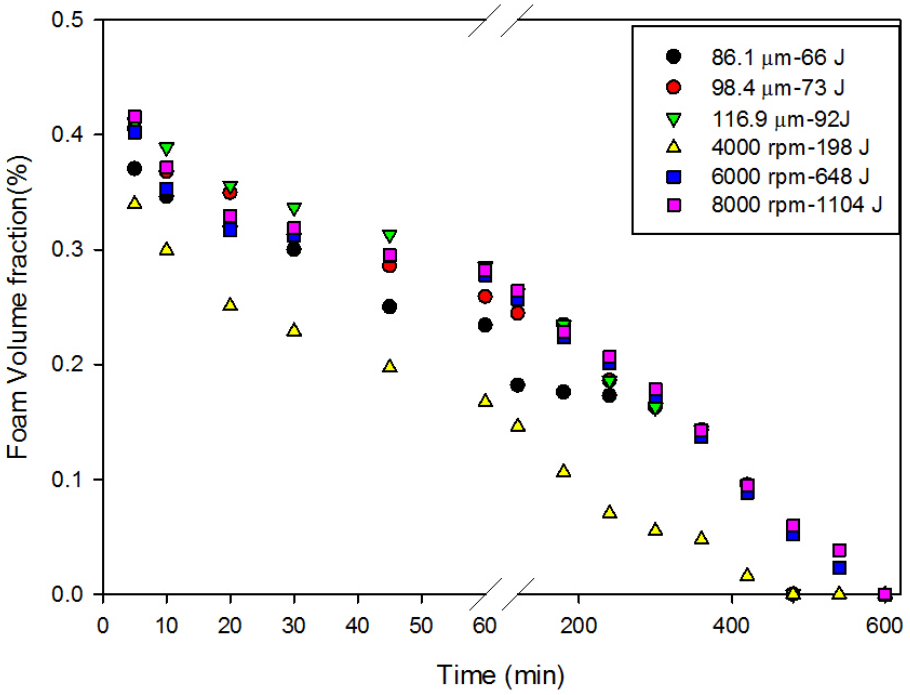

Figure 5.5: Gas volume fraction of whey protein foams produced at various energy intensities in UC and MA.

In Figure 5.6, the data showing the liquid holdup is plotted as a function of the energy input and foam generation method 1 hour after foam formation. In general, the liquid holdup is twice as high in the foams generated by UC than MA. The liquid holdup increases with increasing energy input initially and then remains constant with a further increase of energy input in the foams produced by both methods.

Figures 5.7(a) and 5.7(b) show the mean and Sauter bubble sizes, d_{10} and d_{32}, plotted against

time using UC and MA, respectively. In general, the mean and Sauter bubble sizes of foam increases with time. A slightly smaller initial bubble size and narrower bubble size distribution are obtained in UC than MA. Also a much slower mean bubble size growth is observed in UC than MA. The higher liquid holdup in the foams obtained with UC is a consequence of the smaller bubbles containing more and thicker foam films.

UC has offered an energy saving method to produce a better quality foam in comparison to MA. As the discussion above, much more energy input is required in MA than in UC. For example, 92 J is required at an amplitude of 116.9 μm in UC to produce the foam while more than 6 times (648 J) this energy is used to produce foam at a speed of 6000 rpm in MA. However, the disadvantage of UC is that it can only be used for small volumes compared to MA (as discussed above).

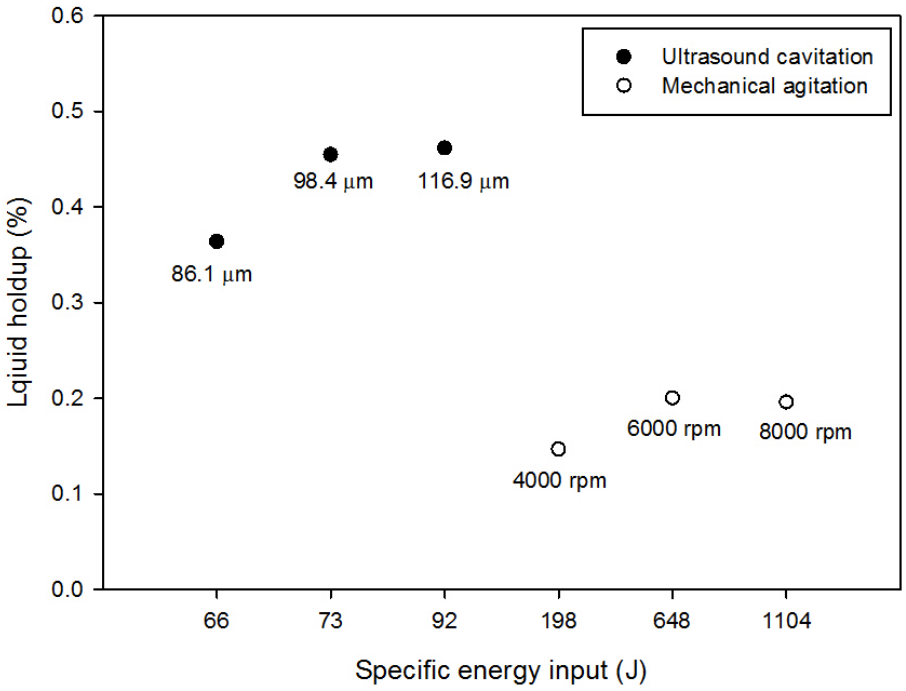

Figure 5.6: Liquid holdup of whey protein foams produced at various energy intensity in the ultrasonic processor and higher shear mixer.

5.2.3 Addition of Hydrophilic Silica Particles

In this section, the effect of the addition of hydrophilic silica on foam stabilized by whey protein is invesigated. 5.0 wt% whey protein and five different (0.3, 0.5, 1.0, 2.0, 3.0 wt%) concentrations of

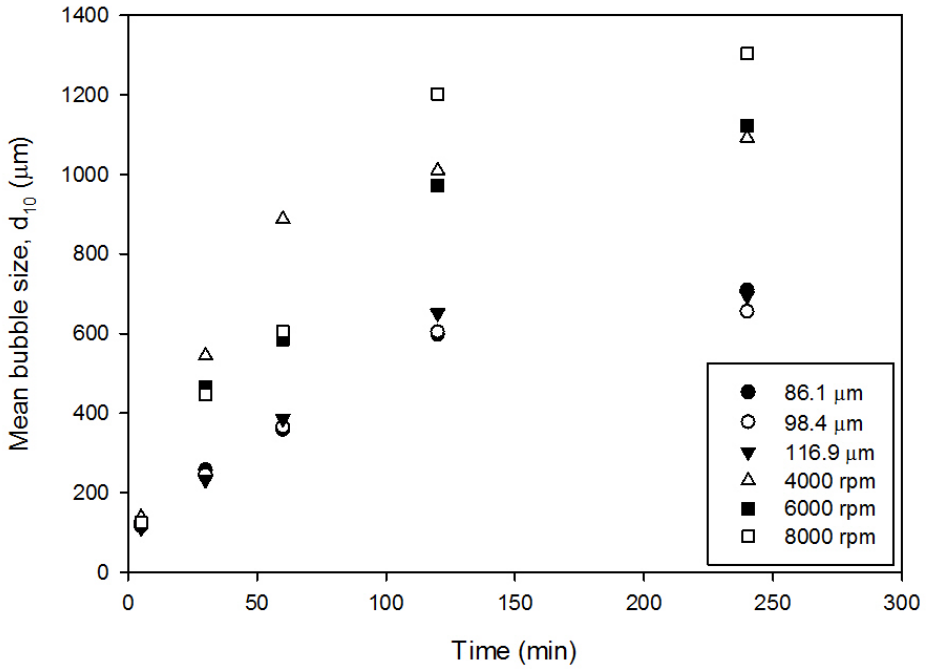

(a)

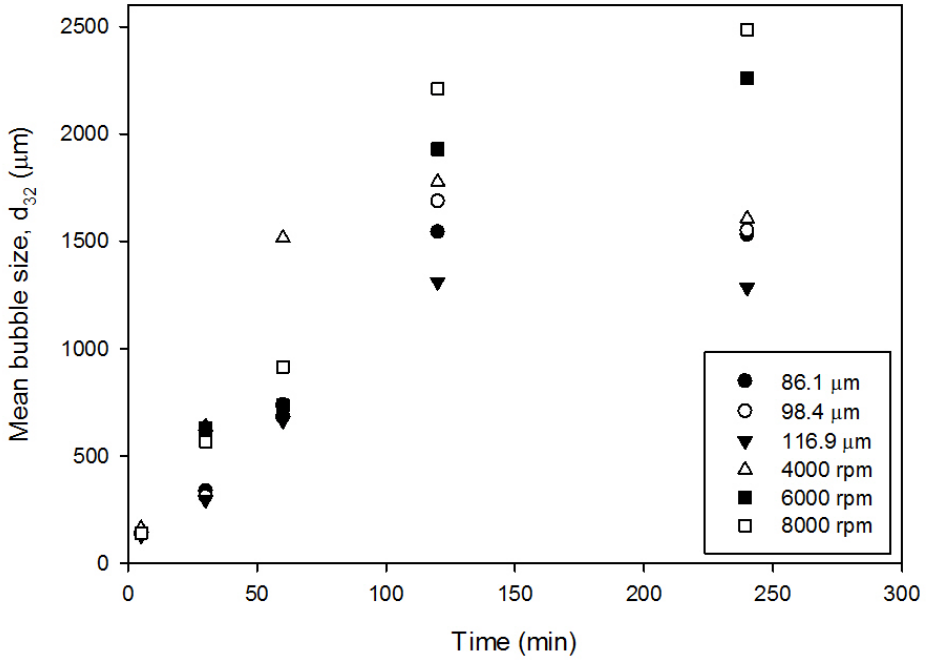

(b)

Figure 5.7: Variation of mean bubble size with foam standing time. (a) mean bubble size, d_{10}(b) Sauter bubble size, d_{32}.

silica were used for this experiment. UC and MA are both used in this set of experiments.

UC

Figure 5.8 shows the initial foam height 5 minutes after foam formation as a function of particle concentration. In general, the addition of silica in protein foam gives a slightly better foamabilty in comparison to protein only foam. However, there is a small decrease in foamability at higher particle concentrations.

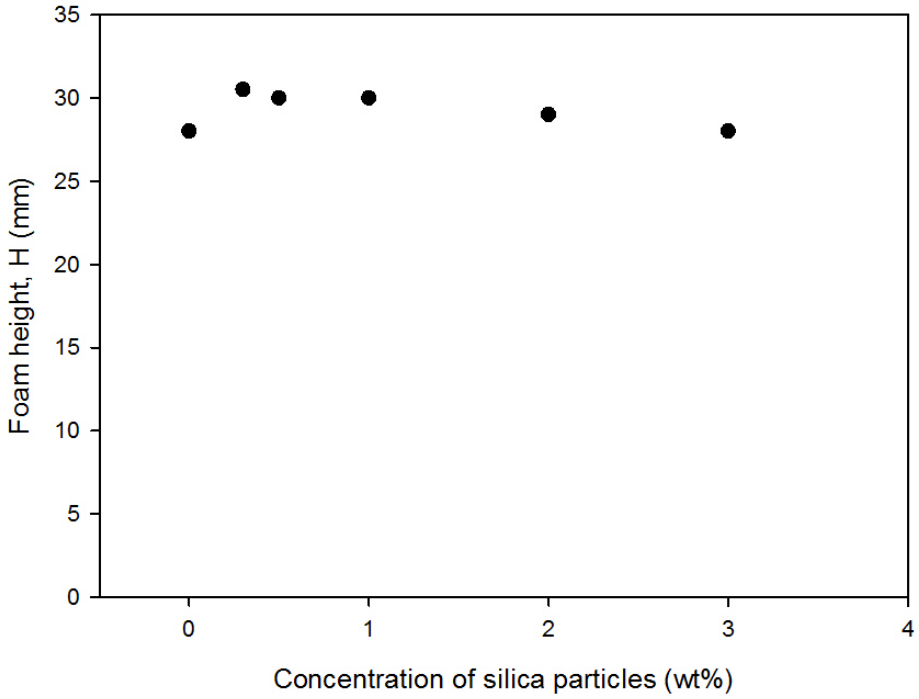

Figure 5.8: Foamability of whey protein solution with silica particles; UC.

Figure 5.9(a) shows the liquid level against foam drainage time. The drainage decreases with increasing concentration of particles. In the foam stabilized by protein only, drainage is extremely fast and ends about 2 minutes after foam formation. On the other hand, there is no drainage observed with foam stabilized by whey protein containing 3.0 wt% of particles 15 minutes after foam formation. The drainage curves can be fitted to Equation (3.13) with a determination coefficient $r^2 > 0.99$. The parameters are summarized in Table 5.3. The maximum liquid level, a, decreases with increasing concentration of particles. Figure 5.9(b) shows that drainage can be prevented at 2.0 and 3.0 wt%

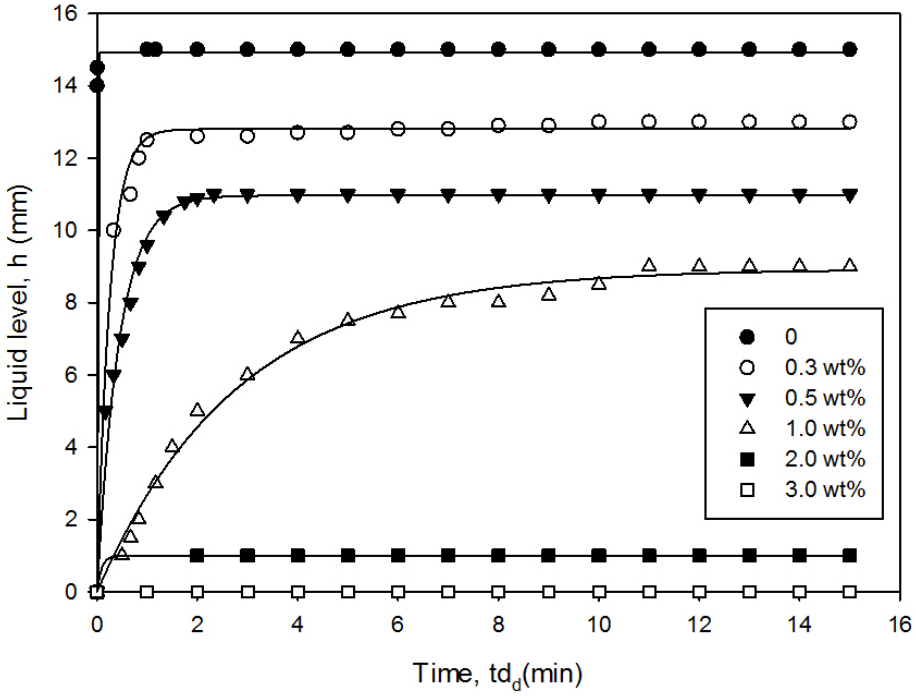

(a)

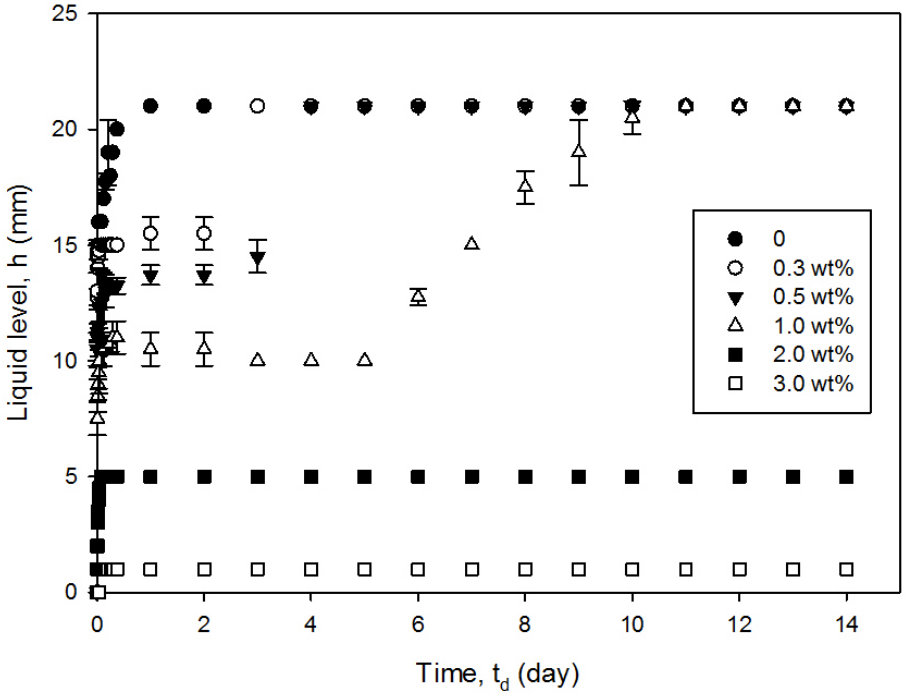

(b)

Figure 5.9: Drainage of foam with various concentration of silica particles (a) initial drainage (b) long term drainage; UC.

silica concentration and there is no drainage observed within 14 days. The viscosity of protein suspensions was $1.437 \cdot 10^{-3}$ Pa $\cdot$ s, $1.463 \cdot 10^{-3}$ Pa $\cdot$ s, $1.516 \cdot 10^{-3}$Pa $\cdot$ s, $1.922 \cdot 10^{-3}$ Pa $\cdot$ s, $2.664 \cdot 10^{-3}$ Pa $\cdot$ s and $3.689 \cdot 10^{-3}$ Pa $\cdot$ s for 0.1, 0.3, 0.5, 1.0, 2.0, and 3.0 wt%, respectively. The addition of particles slows drainage down drastically leading to extremely stable foam. The reduction in drainage may be due to the increased viscosity with increasing concentration of silica. Also, silica increase the rigidity of the foam film interfaces, thus, reducing the rate at which liquid can drain from the films to the Plateau borders. Silica can also reduced diffusion by creating a network between particles. It is also possible that some particles might accumulate in the Plateau border and thus reduce liquid flow by gravity down the network of Plateau borders, hence, slowing down drainage(Pugh, 1996).

Table 5.3: Parameters of the drainage Equation (3.13) at different concentrations of silica particles; UC

	a(mm)	b	r^2
0.1 wt%	14.92	$9.739*10^{-11}$	0.9947
0.3 wt%	12.80	0.2519	0.9897
0.5 wt%	10.97	0.4423	0.9815
1.0 wt%	8.93	2.801	0.9924
2.0 wt%	1	0.0875	1
3.0 wt%	0	NA	1

Figure 5.10(a) shows the data of foam height plotted as a function of foam standing time. The foam breakage decreases with increasing concentration of particles. Foam stabilized by whey protein only collapses within a few hours. With addition of silica, a small decrease of foam height was observed initially and foam breakage rate further decreases with increasing concentration of particles. A longer foam lifetime is obtained by increasing the concentration of particles as shown in Figure 5.10(b). The foam lifetime is 2, 3, 6, 14, and 20 days for the concentrations of 0.3, 0.5, 1.0, 2.0, 3.0 wt%, respectively.

The data of liquid holdup are plotted against the concentration of particles in Figure 5.11. The liquid holdup is unaffected at low silica concentrations, but rises significantly at higher concentration above 1 wt%.

The statistics used to describe and compare the bubble size distributions of whey protein foams with addition of silica are summarized in Table 5.4. The mean and Sauter bubble sizes, d_{10} and d_{32}, as well as skewness increase with increasing particle concentration. Positive skewness values

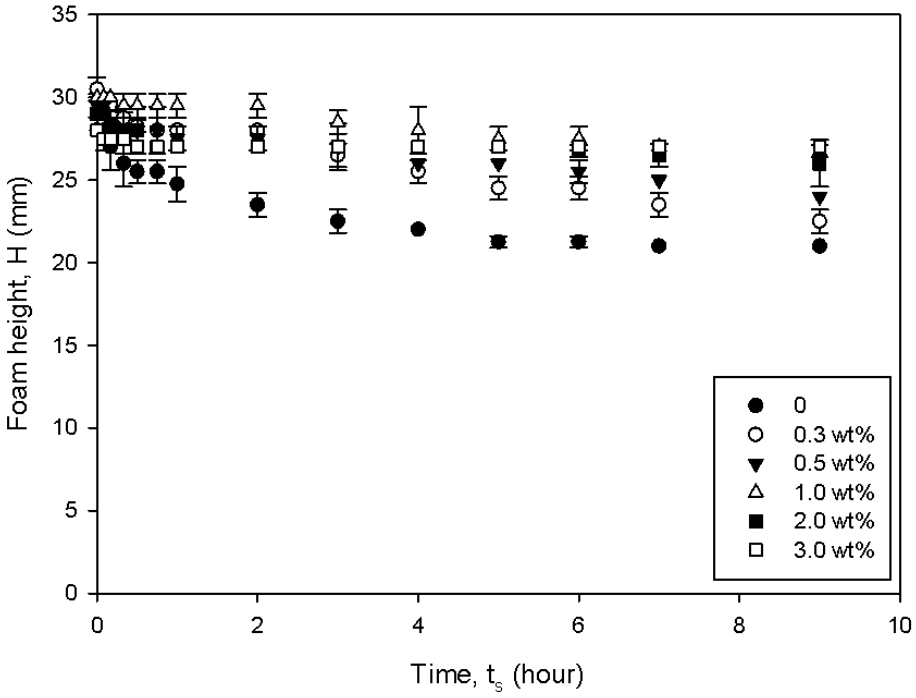

(a)

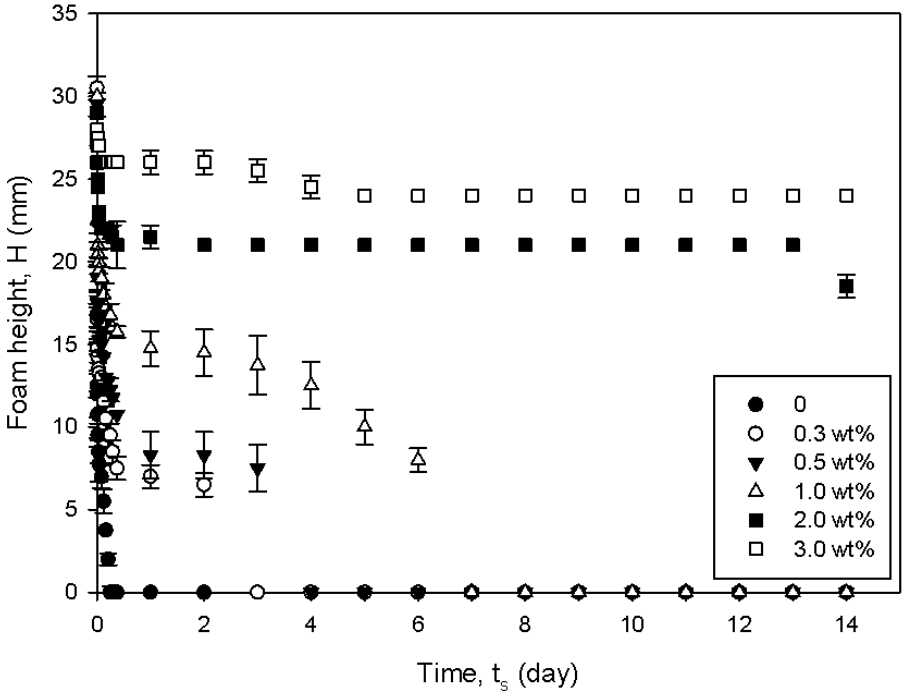

(b)

Figure 5.10: Foam height at various concentrations of silica particles: (a) in 8 hours (b) in 14 days; UC.

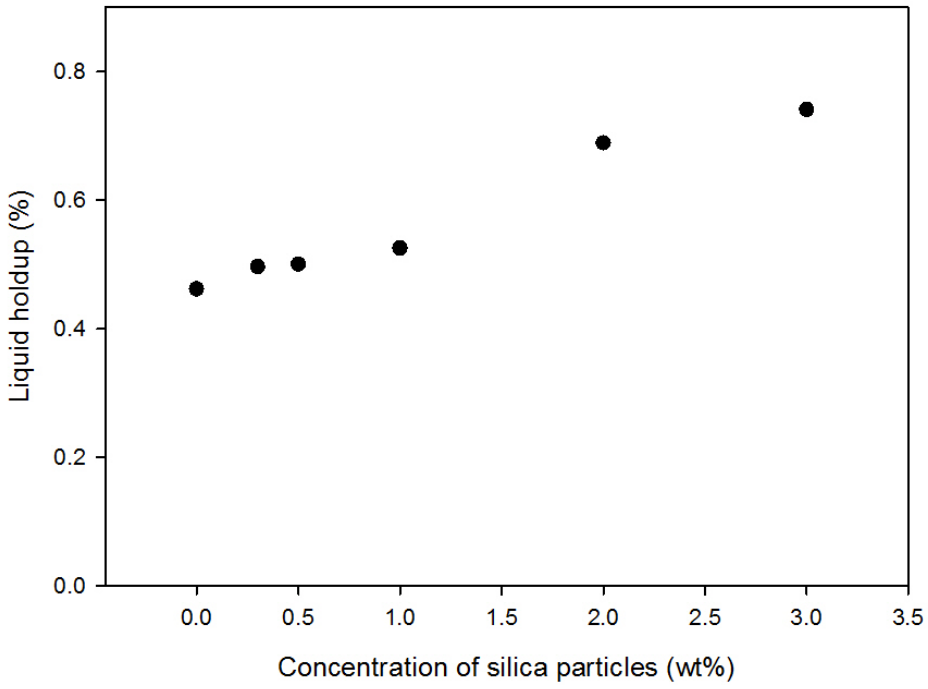

Figure 5.11: Liquid holdup at various concentrations of silica particles; UC.

indicate the presence of some large bubbles in the foam resulting in median being greater than the mean bubble diameter d_{10}. This indicates that the addition of silica led to a higher density of the dispersion which makes it more difficult to achieve evenly distributed bubble sizes immediately after foam formation. The mean bubble diameter, d_{10}, and Sauter mean diameter, d_{32} of foam increase with addition of silica (see Figure 5.19). The rate of growth of the mean bubble size decreases with increasing concentration of silica, whereas the bubble growth of the foam stabilized by whey protein increases linearly. The protein only foam also shows an increase of skewness with time. The higher the concentration of particles in the foam the slower the increase of the skewness over time. At the highest concentration, skewness remains nearly constant with only a small reduction after a long time. This is because the particles in the solution provide a gel-network to restrict the bubble growth. The kurtosis of the samples with addition of 1.0 wt%, 2.0 wt% and 3.0 wt% particles are mostly positive, which is not the case in the sample with whey protein only.

MA

Figure 5.12 shows the foam height against the concentration of particles. There is no significant difference found in foamability when the particle concentration is under 1.0 wt%. There is a small increase in foamability when the concentration of particles increases to 2.0 wt% but it falls back when the concentration increases to 3.0 wt%.

Figure 5.13 shows that the drainage of whey protein foam slows down when hydrophilic silica is added. The liquid drains fast and almost stops 5 minutes after foam formation in the foam without particles. In the foams with low concentrations of particles, there is less liquid drainage and the drainage almost stops 5 minutes after foam formation. At 1.0 wt% particles, a significant reduction in liquid drainage is observed which only stops about 20 minutes after foam formation. At 2.0 wt% particles, drainage starts 5 minutes after foam formation. At 3.0 wt% particles, there is no drainage during the first 20 minutes after foam formation. These results are similar to those found in the foam produced by UC. The same explanation applies here, the slow drainage is caused by the increased viscosity and more rigid films with increasing particle concentration.

When observed over a longer period of time, the drainage of protein foams with higher concen-

Table 5.4: Statistical parameters for foam bubble size distribution at various concentrations of silica particles; UC.

	d_{10}(μm)	d_{32}(μm)	S_t	Min(μm)	M(μm)	Max(μm)	S	K
no silica particles								
5 min	112.11	129.29	32.08	34.92	110.02	200.43	0.12	-0.37
30 min	232.20	294.75	87.46	56.87	224.65	521.22	0.48	-0.27
60 min	337.20	548.48	185.10	92.20	288.70	994.30	1.32	1.72
120 min	622.70	1311.10	468.30	126.90	412.90	2210.40	1.44	1.19
240 min	1044.80	2067.71	678.70	240.00	922.90	4097.60	2.04	5.55
0.3 wt%								
5 min	130.96	155.96	40.68	59.52	126.48	250.90	0.58	0.02
30 min	294.87	325.46	67.08	147.67	283.15	494.52	0.53	-0.02
60 min	462.08	533.05	126.53	210.59	451.37	893.73	0.78	0.78
120 min	553.90	719.57	213.30	244.70	506.50	1217.60	0.85	0.16
240 min	742.00	1323.45	439.00	214.10	629.20	2603.50	1.76	3.76
0.5 wt%								
5 min	128.70	152.92	39.54	60.07	124.24	269.31	0.63	0.17
30 min	306.20	353.95	85.36	127.12	295.89	592.60	0.63	0.17
60 min	400.04	455.47	105.01	154.90	376.27	794.90	0.61	0.60
120 min	473.00	593.94	168.60	233.30	452.20	984.30	0.79	-0.04
240 min	655.20	1194.31	392.90	237.30	522.90	2718.00	1.89	4.69
1.0 wt%								
5 min	162.77	193.38	48.70	73.00	160.17	341.44	1.01	1.47
30 min	261.01	315.90	84.34	112.96	257.68	589.70	0.73	0.63
60 min	340.97	406.29	104.07	169.59	313.15	653.42	0.85	0.14
120 min	469.70	591.76	167.50	196.10	425.50	1007.80	0.89	0.22
240 min	543.20	718.77	209.10	235.70	479.80	1353.30	1.35	1.90
2.0 wt%								
5 min	160.23	221.64	65.78	64.89	147.83	478.00	1.65	3.79
30 min	225.95	279.53	72.73	106.09	213.22	598.45	1.69	5.28
60 min	323.71	391.02	98.97	145.75	305.21	837.53	1.47	4.12
120 min	446.10	550.93	150.20	202.00	414.50	992.90	0.96	0.75
240 min	531.80	645.19	171.00	258.40	494.70	1188.20	0.90	0.79
3.0 wt%								
5 min	199.56	260.87	76.14	72.00	177.79	507.45	1.13	1.32
30 min	254.14	303.41	76.87	125.87	240.18	561.07	1.08	1.77
60 min	315.74	363.83	83.81	149.86	301.10	694.52	1.24	2.74
120 min	385.66	446.58	104.46	196.86	369.80	825.10	1.20	2.16
240 min	514.70	632.34	166.10	238.00	483.50	1251.40	1.36	2.75

tration of particles gradually increases during the first day of observation. Drainage stops after one day. These foams still contain substantial liquid even when older than 1 day. This contrasts with the foams at low concentrations that complete drainage in the first few minutes of their lifetime (see Figure 5.14).

Figure 5.15 shows liquid holdup against the concentration of particles. The liquid holdup increases dramatically with increasing concentration of particles until 1.0 wt% and it drops at 2.0 wt%. The liquid holdup increases slightly again when the concentration of particle reaches 3.0 wt%.

The foam height of the protein foam shows no change for the first 10 minutes after foam formation and then the foams start to collapse under 1.0 wt% particles. At 2.0 wt% particles, the foam height initially (i.e. during the first 3 hrs) remains constant followed by a modest foam breakage over the

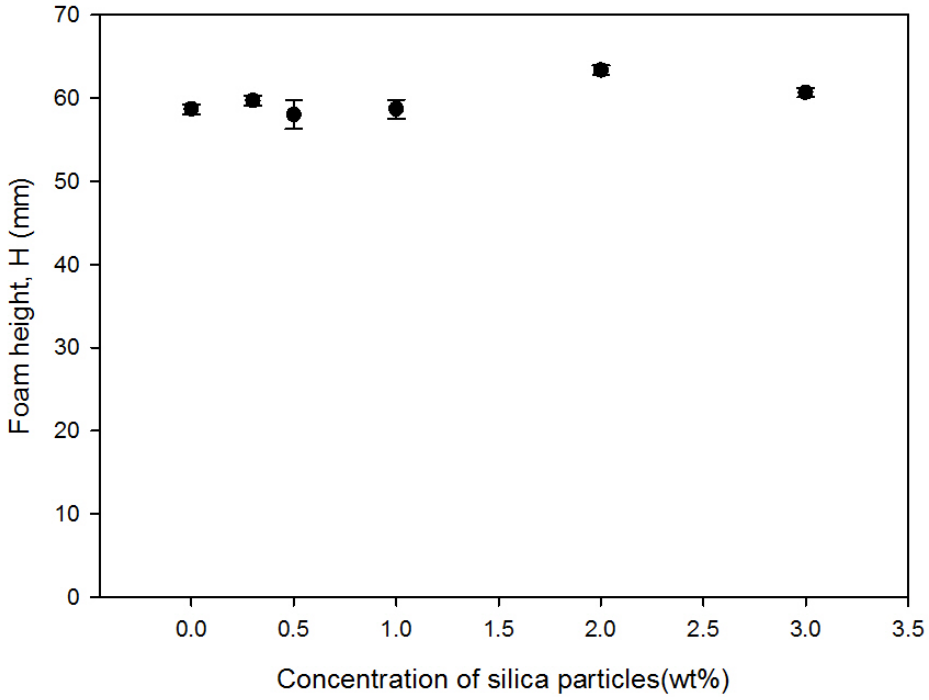

Figure 5.12: Foamability of whey protein solution with various concentrations of hydrophilic silica particles; MA.

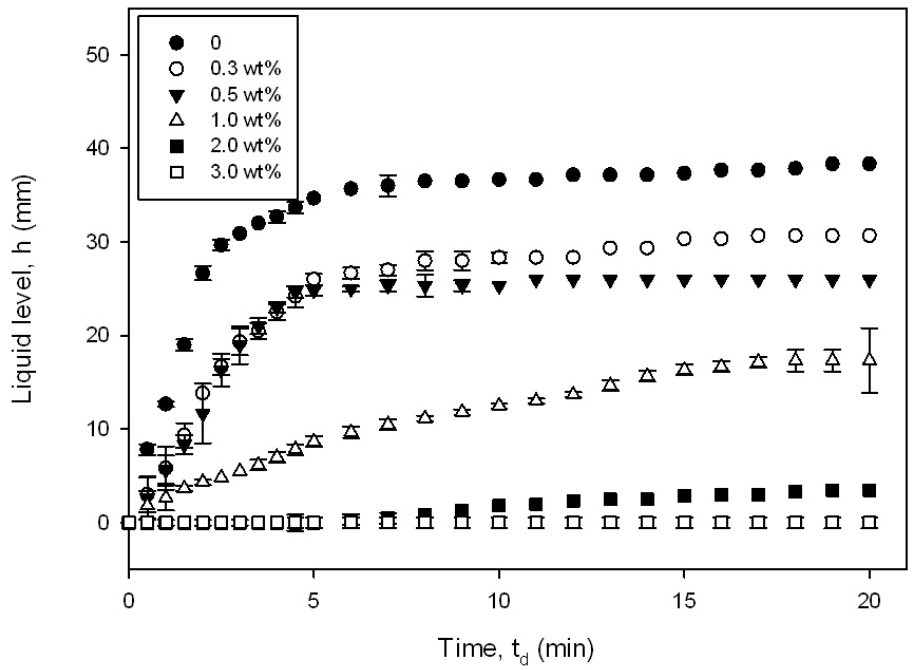

Figure 5.13: Drainage of whey protein foam with various concentrations of hydrophilic silica particles; MA.

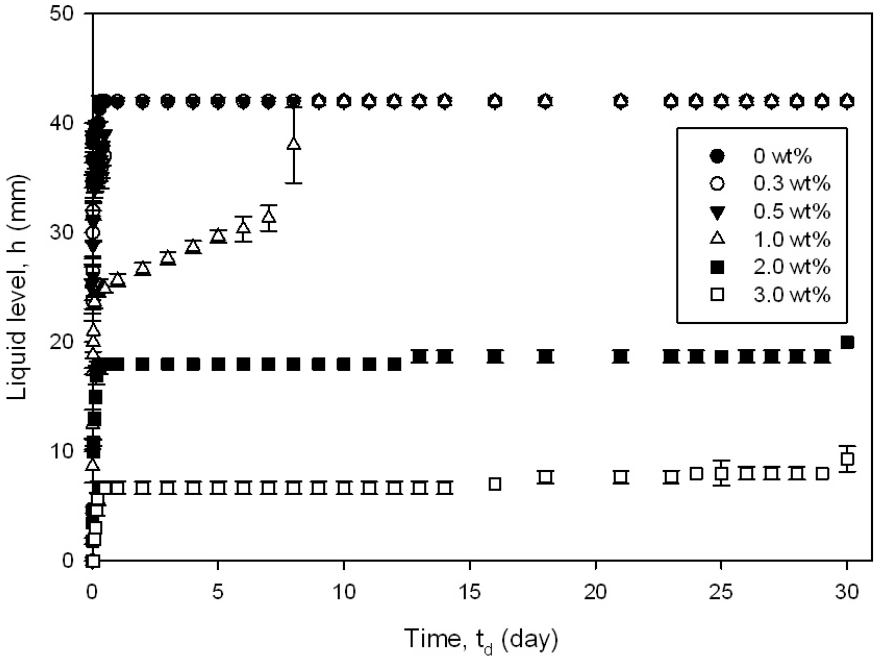

Figure 5.14: Drainage of whey protein foam with various concentrations of hydrophilic silica particles; MA.

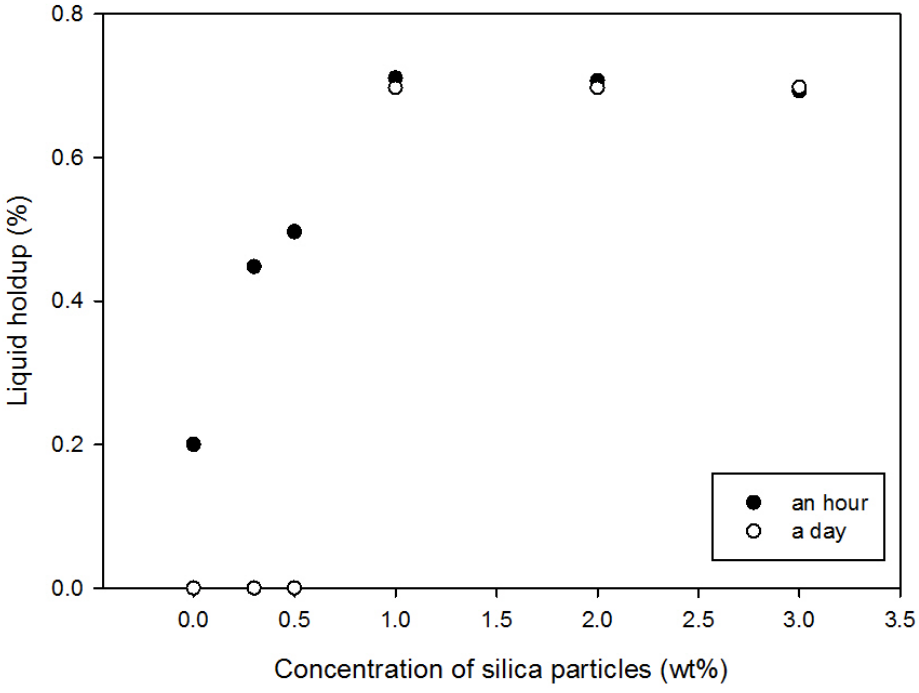

Figure 5.15: Liquid holdup of whey protein foam with various concentrations of hydrophilic silica particles; MA.

following 6 hours. Over the same period of time, there is no foam breakage in the protein foam at 3.0 wt% particles. However, above 2.0 wt% particles when the observation time is over 30 days, foam breakage starts during the first day and it stops after a few days (see Figure 5.16). The lifetime of the foam was found to be at least a month in the foam containing more than 2.0 wt% particles, while the foam life can last more than a week at 1.0 wt%, 2 days at 0.5 wt% and 0.3 wt%, less a day without addition of silica.

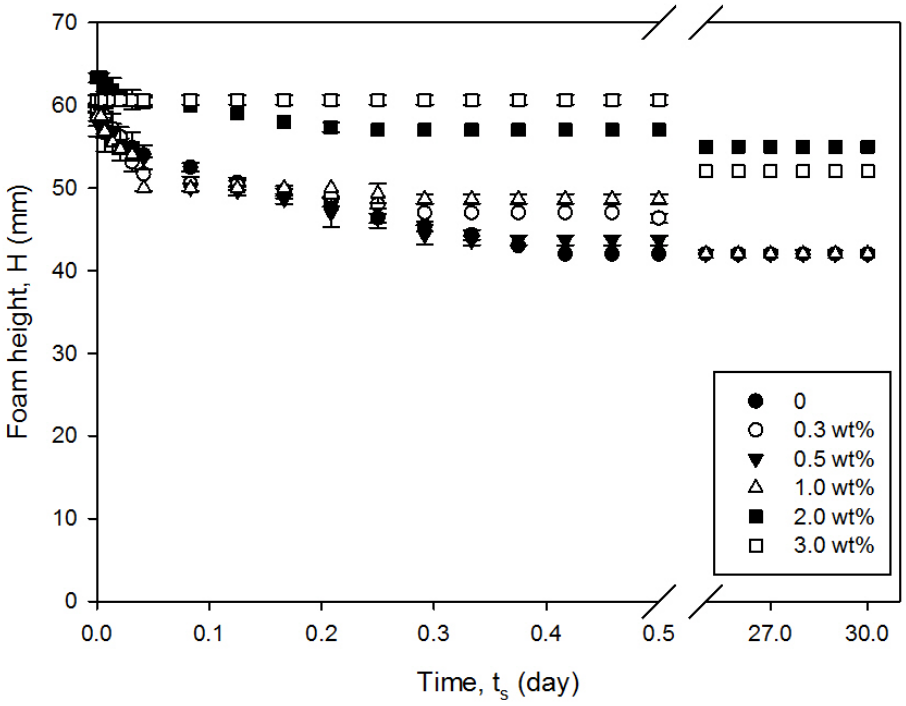

Figure 5.16: Breakage of whey protein foam with various concentrations of hydrophilic silica particles; MA.

The parameters used to describe and compare the bubble size distributions of whey protein foams with addition of silica are summarized in Table 5.5. The initial Sauter mean bubble size, d_{32}, is around 140 μm at the lower concentration of particles and increases to 150 μm when the silica concentration reaches 3.0 wt%. The rate of growth correlates negatively with the silica concentration. For example, the Sauter mean bubble size after 30 min of protein only foam is 627.94 μm and it decreases to 373.97 μm as the particle concentration is increased from 0 to 0.3 wt% particles. A further reduction in mean bubble size is found in whey protein with particle concentrations above 2.0 wt% where the mean bubble sizes are less than 200 μm.

Table 5.5 shows that skewness increases over time in foams with concentrations < 1 wt%. When the concentration of particles is higher, this is no longer true. For 2 wt% the skewness first increases and then decreases after reaching a a maximum. At 3 wt% it decreases with time. This is because the addition of particles gives a higher viscosity to inhibit the homogeneity of the bubble size immediately after foam formation, but the bubble size does not grow due to the network of particles in the foams.

Table 5.5: Statistical parameters of bubble size distribution of foam with various concentration of silica particles; MA.

	d_{10}(μm)	d_{32}(μm)	S_t	Min(μm)	M(μm)	Max(μm)	S	K
no silica particles								
5 min	123.26	140.50	33.64	53.24	120.69	215.79	0.10	-0.62
30 min	465.20	627.94	187.90	192.30	437.80	1339.50	1.26	2.38
60 min	585.5	736.68	211.7	262.8	540.8	1212.9	0.68	-0.16
120 min	972.2	1930.59	670.3	239.6	751.4	3545.1	1.57	2.49
240 min	1121.4	2262.05	783.2	291.4	828.2	4180.8	1.61	2.38
0.3 wt%								
5 min	124.68	140.62	31.96	54.69	120.21	206.07	0.33	-0.55
30 min	328.49	373.97	87.21	138.08	329.04	597.26	0.43	0.11
60 min	562.60	746.05	227.40	185.80	507.00	1276.10	0.83	0.22
120 min	615.10	1000.76	326.20	213.30	534.30	2086.30	1.65	3.43
240 min	885.80	1936.83	652.90	190.60	617.80	4516.10	1.89	5.00
0.5 wt%								
5 min	123.54	139.51	31.80	59.93	125.14	231.66	0.36	-0.05
30 min	341.79	372.69	73.14	138.63	344.52	595.34	0.36	0.56
60 min	465.00	603.94	175.90	171.20	431.40	1106.30	1.06	1.04
120 min	517.30	892.41	286.60	185.80	436.60	2147.10	2.00	6.28
240 min	682.30	1650.68	506.50	216.50	510.60	3444.30	2.73	9.43
1.0 wt%								
5 min	121.97	137.35	30.25	67.10	117.17	219.93	0.76	0.65
30 min	296.16	323.36	62.95	176.16	283.29	474.80	0.64	-0.08
60 min	335.37	376.17	83.08	160.55	330.82	586.3	0.47	0.26
120 min	402.10	563.48	166.20	170.10	360.10	1247.10	1.86	5.02
240 min	587.60	892.04	277.20	186.30	523.70	2292.20	1.84	6.84
2.0 wt%								
5 min	127.53	140.65	28.83	71.11	125.33	234.78	0.56	0.27
30 min	176.94	195.97	40.18	96.14	172.28	321.38	0.91	1.43
60 min	309.6	360.68	84.26	146.3	295.62	705.75	1.5	3.09
120 min	357.96	404.72	91.32	167.67	357.53	753.15	0.58	1.15
240 min	419.90	480.26	112.75	211.77	411.18	781.57	0.55	0.00
3.0 wt%								
5 min	127.82	150.34	36.43	62.00	123.11	303.33	1.26	3.73
30 min	176.77	198.48	43.19	80.44	175.39	388.56	0.78	2.42
60 min	282.24	316.36	69.9	128.22	279.59	494.79	0.42	0.00
120 min	320.95	355.33	74.68	167.95	317.81	526.58	0.41	-0.17
240 min	392.14	419.13	73.42	241.57	392.55	583.53	0.23	-0.26

Comparison between UC and MA

In the experimental results discussed above, the addition of silica has shown a great ability to prolong foam life and provides a much better foamability when using both foam generation methods by slowing down drainage, foam collapse and bubble growth. Here, the foam properties obtained

using UC and MA is discussed and compared in detail.

Figure 5.17 shows the foam volume fraction of whey protein foams plotted against time at various particle concentrations using UC and MA. In foams containing up to 3 wt% silica, the foam volume fraction increases from 40% to 100% 5 minutes after foam formation as the concentration increases. In general, higher foam volume fraction was produced by UC than MA. In Figure 5.18, the data for liquid holdup is plotted as a function of particle concentration 5 minutes after foam formation in UC and MA, respectively. Liquid holdup in both foams increases with increasing concentration of particles. In general, a wetter foam is obtained using UC.

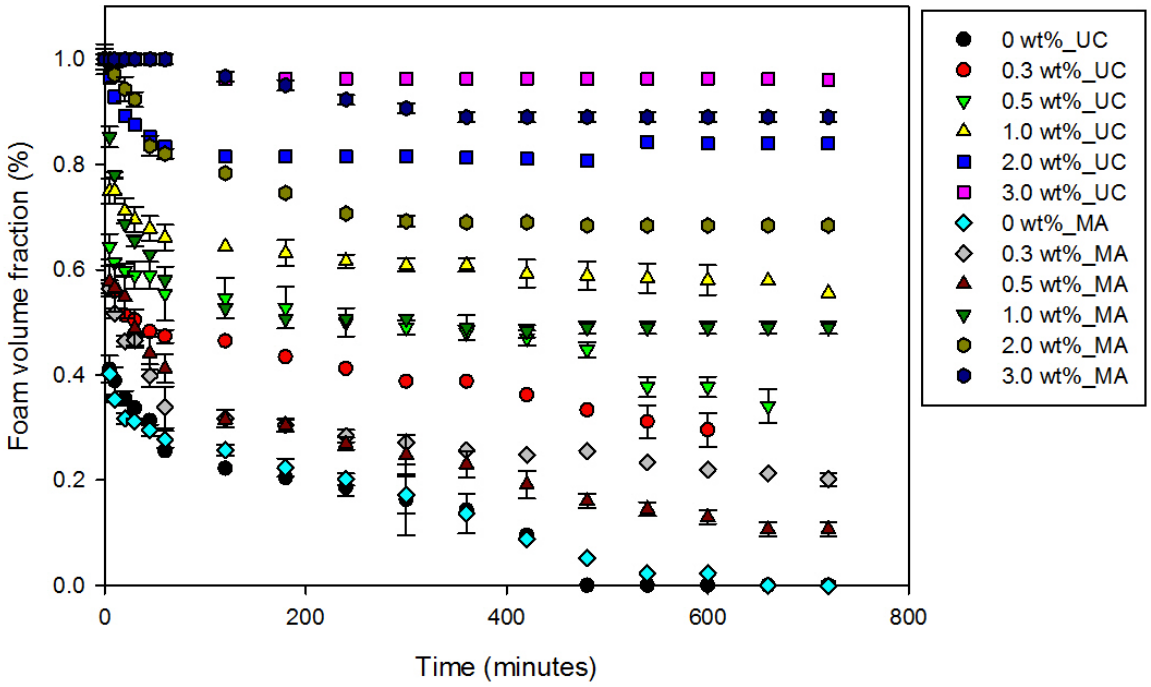

Figure 5.17: Foam volume fraction of whey protein foams produced at various concentrations of silica particles; UC and MA.

The mean and Sauter mean bubble sizes, d_{10} and d_{32}, are plotted against time in Figures 5.19(a) and 5.19(b) for the foams generated using UC and MA. The error bars were not shown in the Figures as all the data points are in an error range of ± 5.0 %. In general, both mean bubble sizes of foam increase with standing time. In the foam made by UC, a slower bubble growth was observed than MA when the particle concentration was lower than 1.0 wt%. At higher particle concentrations ($\geq$ 2.0 wt%), slower bubble growth was found in the foams produced by MA. At lower particle

concentrations ($\leq$ 1.0 wt%), smaller initial mean bubble sizes and narrower bubble size distributions were obtained in the foam produced by UC as shown in Tables 5.4 and 5.5. This corresponds to a higher liquid holdup in the foam as discussed above. However, at higher particle concentrations, a much smaller initial mean bubble size was obtained in the foam generated by MA and a very similar liquid holdup was observed in the foams made in both methods.

UC is an energy saving method to produce a better quality foam with lower concentration of silica particles in comparison to MA. There was 6 times more energy input needed in MA (648 J) than UC (92 J). However, MA is a better method to produce foam at a higher silica particle concentration. Moreover, MA can handle a much larger batch than UC.

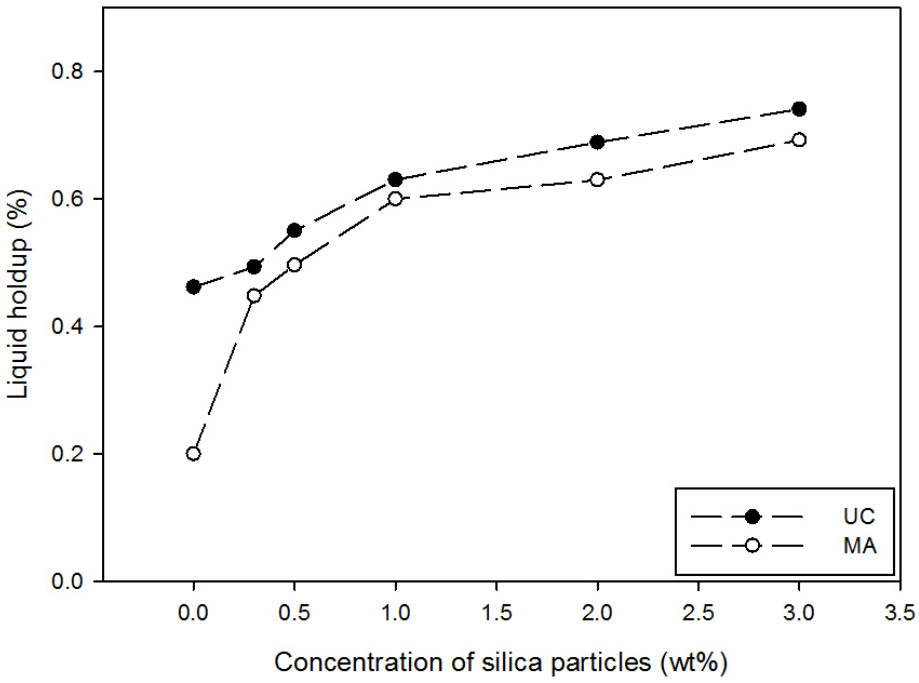

Figure 5.18: Liquid holdup of whey protein foams produced at various concentrations of silica particles; UC and MA.

5.2.4 Effect of pH

In this section, the effect of pH on the whey protein foam generated by both UC and MA is investigated. In all experiments described in this section 5.0 wt% of whey protein and 4 different pH values were used. The pH of whey protein is pH 5.55. In addition to the pH 5.55, pH 4, 7 and 10 were also

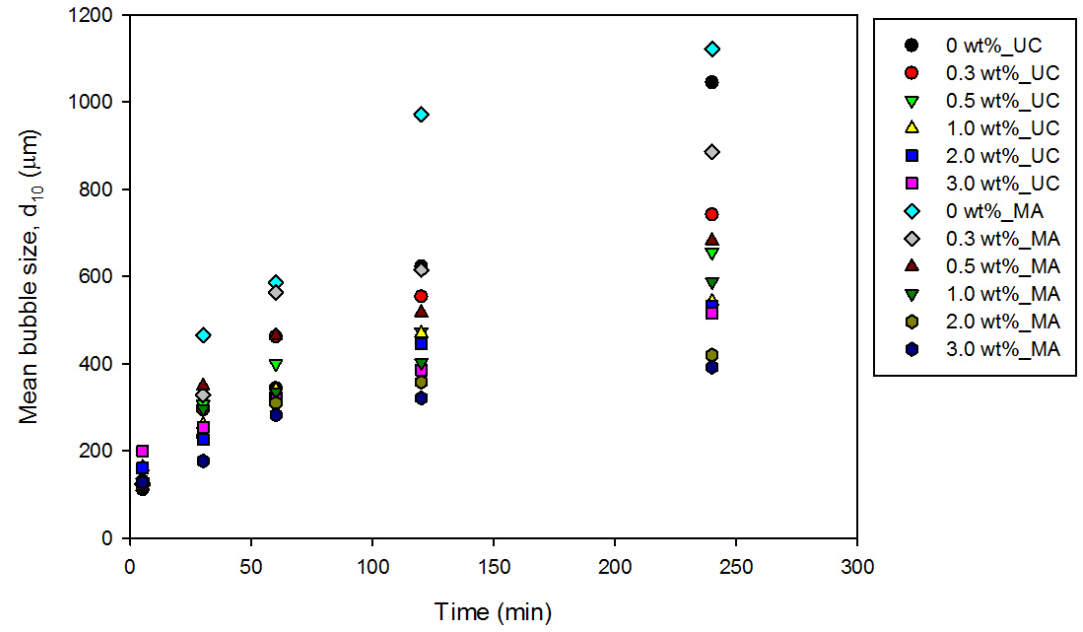

(a)

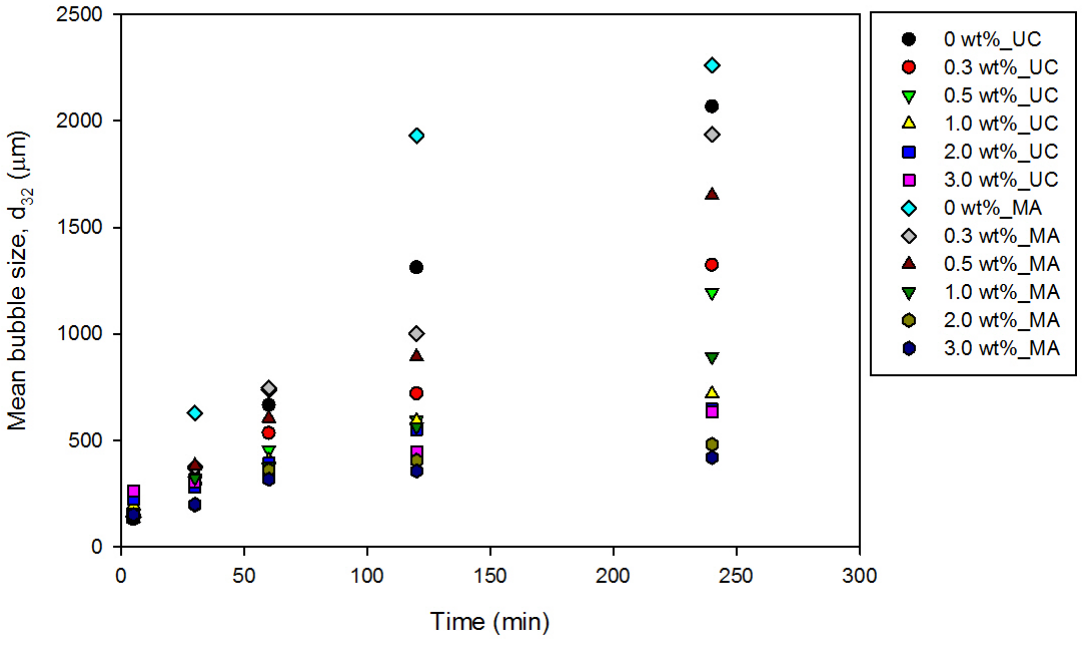

(b)

Figure 5.19: Variation of mean and mean Sauter bubble size with foam standing time: (a) mean bubble size, d_{10} (b) Sauter bubble size, d_{32}; UC and MA.

considered by adding HCl and NaOH. The addition of 0.5 wt% of silica particles was also tested to see the effect of pH on the whey protein foam with silica particles added.

UC

Foam height of the foam stabilized by whey protein only and with addition of 0.5 wt% particles is plotted against the value of pH in Figure 5.20. There is only a small increase observed at pH 10, but otherwise there is no significant difference found between various pH values both in the foam stabilized by whey protein only and foam with silica.

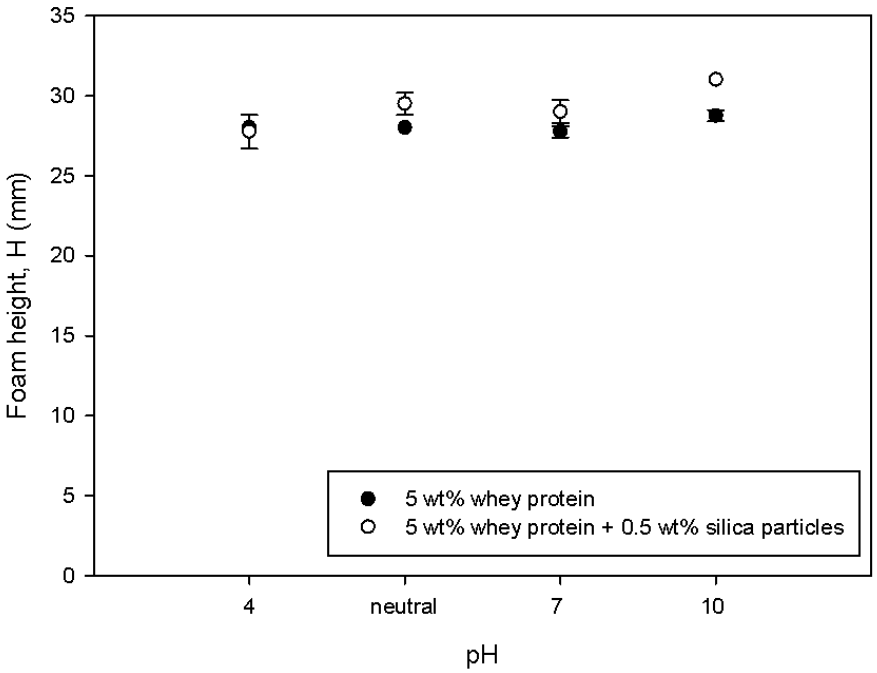

Figure 5.20: Foamability of foam stabilized by whey protein only and 0.5 wt% silica particles added at various values of pH; UC.

For foam stabilized only by whey protein at various pH, the foam height and the liquid level of foam are both plotted against foam standing time as shown in Figure 5.21. pH has no significant effect on the foam stability as the drainage curves almost overlap and foams at various pH all collapsed after 8 hours foam formation. However, a slower breakage rate of foam was observed at pH 10.

In the whey protein foam with addition of silica, the foam height and the liquid level are both plotted as functions of the foam standing and drainage time in Figure 5.22. We expect a longer

foam life for foams with silica than protein only foams. The rate of foam breakage decreases with increasing pH during the first two hours and then the foam breakage curves remain constant for another three hours. At pH 10 a sudden onset of foam collapse lasting for several hours was observed 5 hours after foam formation. The foam generated at pH 4, pH 5.55 and pH 7 are stable over the entire period of observation (for another day; data not shown). The drainage curves almost overlap at the four different pH values and they all end almost two hours after foam formation. The drainage curves remain constant for several hours.

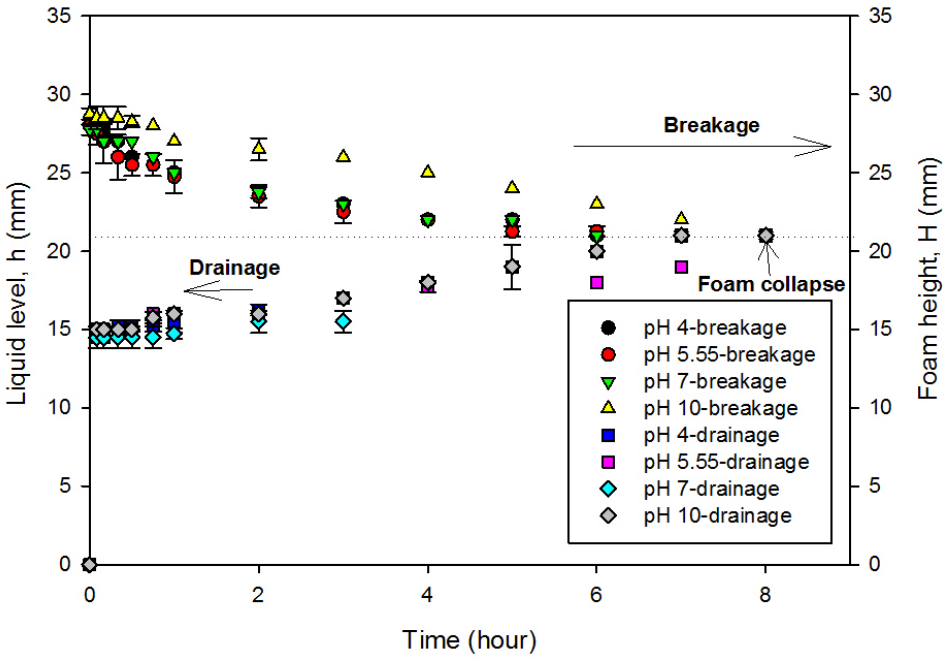

Figure 5.21: Drainage and breakage of foam stabilized by whey protein only at various values of pH; UC.

The statistical parameters of the bubble size distributions of whey protein foams only and foams with addition of silica at various pH are summarized in Tables 5.6 and 5.7. In the foams stabilized by whey protein only, the finer foam is observed at pH 5.55 but there is no great difference of the foam life time in comparison to the foam at other pH values. Similar to the foam stabilized only by whey proteins, the smaller initial mean bubble size is observed in the whey protein foam with silica at pH 5.55. However, in the latter case the rate of bubble size growth over time is slower at pH 7 than at pH 4 and 10.

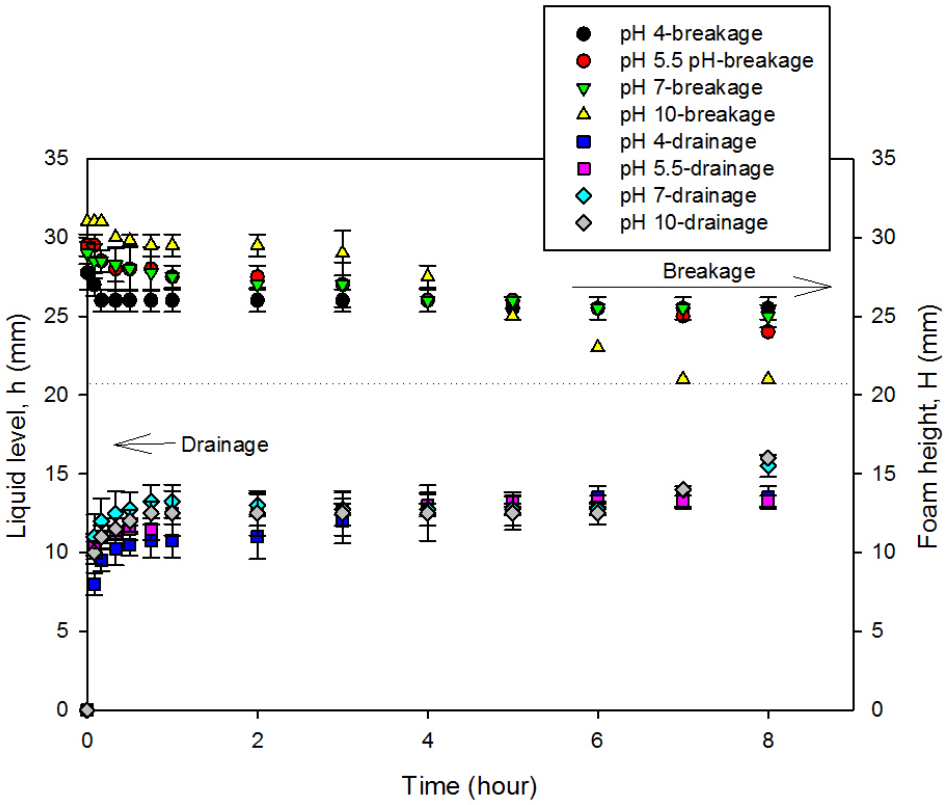

Figure 5.22: Drainage and breakage of whey protein foam with 0.5 wt% silica particles at various values of pH; UC.

Table 5.6: Statistical parameters for foam bubble size distribution: foam stabilized by whey protein only at various values of pH; UC.

	d_{10}(μm)	d_{32}(μm)	S_t	Min(μm)	M(μm)	Max(μm)	S	K
pH 4								
5 min	127.92	143.71	32.21	62.28	126.76	214.48	0.32	-0.10
30 min	346.50	429.98	118.12	154.79	336.71	775.07	0.96	1.18
60 min	488.40	638.90	189.80	178.10	442.60	1168.50	0.93	0.74
120 min	833.80	1336.24	431.30	258.80	726.30	2862.70	1.69	3.95
neutral pH								
5 min	112.11	129.29	32.08	34.92	110.02	200.43	0.12	-0.37
30 min	232.20	294.75	87.46	56.87	224.65	521.22	0.48	-0.27
60 min	337.20	548.48	185.10	92.20	288.70	994.30	1.32	1.72
120 min	622.70	1311.10	468.30	126.90	412.90	2210.40	1.44	1.19
pH 7								
5 min	123.59	146.76	38.39	42.69	117.21	249.45	0.46	-0.31
30 min	333.24	380.36	88.84	139.73	329.45	675.07	0.53	0.58
60 min	492.90	672.99	211.70	139.70	464.80	1228.80	0.84	0.49
120 min	743.10	1233.36	417.70	218.80	624.70	2889.80	1.36	2.99
pH 10								
5 min	136.60	158.63	40.07	54.76	139.00	241.10	0.15	-0.33
30 min	346.35	405.99	100.83	154.52	342.47	728.77	0.74	0.90
60 min	445.00	576.70	170.20	163.30	407.30	975.10	0.87	0.47
120 min	916.30	1472.31	497.40	231.00	865.10	3367.50	1.26	2.52

MA

Figure 5.23 shows the foam breakage of only protein foam at various pH values. The foam height remains unchanged for about 10 minutes after foam formation and then the foams start to collapse.

Table 5.7: Statistical parameters for foam bubble size distributions: whey protein foam with 0.5 wt% silica particles at various values of pH; UC.

	d_{10}(μm)	d_{32}(μm)	S_t	Min(μm)	M(μm)	Max(μm)	S	K
pH 4								
5 min	119.34	143.71	45.59	41.66	116.07	271.79	0.80	0.44
30 min	304.79	429.98	117.09	116.05	288.24	623.18	0.53	-0.50
60 min	448.70	638.90	165.70	140.00	453.60	891.20	0.23	-0.75
120 min	701.60	1336.24	328.40	207.80	634.30	2016.90	0.88	0.70
neutral pH								
5 min	128.70	129.29	39.54	60.07	124.24	269.31	0.63	0.17
30 min	306.20	294.75	85.36	127.12	295.89	592.60	0.63	0.17
60 min	400.04	664.60	105.01	154.90	376.27	794.90	0.61	0.60
120 min	473.00	1311.10	168.60	233.30	452.20	984.30	0.79	-0.04
pH 7								
5 min	125.76	146.76	34.47	52.28	122.00	213.52	0.12	-0.71
30 min	222.26	380.36	55.69	99.91	223.43	342.15	-0.04	-0.71
60 min	313.68	672.99	93.17	142.74	306.30	646.85	0.68	0.40
120 min	463.90	1233.36	306.30	163.00	394.50	2262.20	3.29	13.84
pH 10								
5 min	126.86	158.63	36.86	49.93	129.69	214.76	0.12	-0.75
30 min	291.10	405.99	98.22	113.30	279.66	635.54	0.98	1.36
60 min	633.10	576.70	235.10	206.70	612.40	1592.50	0.68	0.82
120 min	622.30	1472.31	389.30	174.00	503.00	2129.30	1.32	1.25

At pH 10, the protein foam has the best foamability in comparison to other pH values. At pH 7, the foam collapses suddenly about 30 minutes after foam formation while the foam life of the foams at other pH values lasts a few more hours. The drainage curves are nearly independent of the pH.

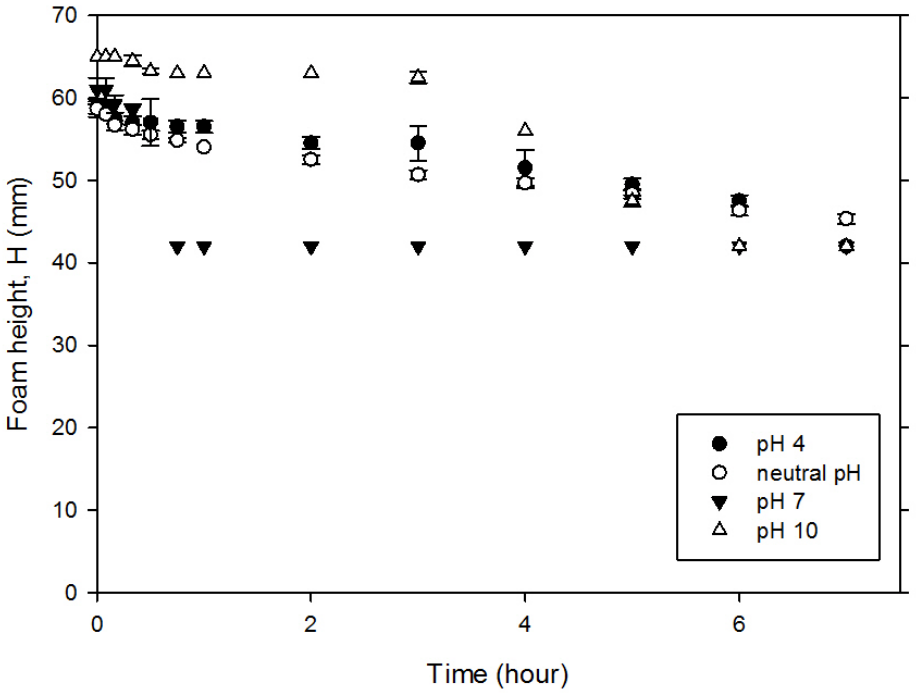

Figure 5.23: Breakage of whey protein foam at various pH values; MA.

Figure 5.24 shows the foam height against time for various pH in a whey protein foam with 0.5 wt% particles. At pH 10, it shows the best foamability, however, a faster foam collapse than other pH happens 4 hours after foam formation. At pH 4, the foam collapses rapidly initially and then remains unchanged. At pH 7, the foam life is enhanced by the addition of silica in comparison to the foam produced by only protein with a short foam life. For all pH the foam life time is approximately a day, except in the case of pH 7 foam which only lasts for about 8 hours.

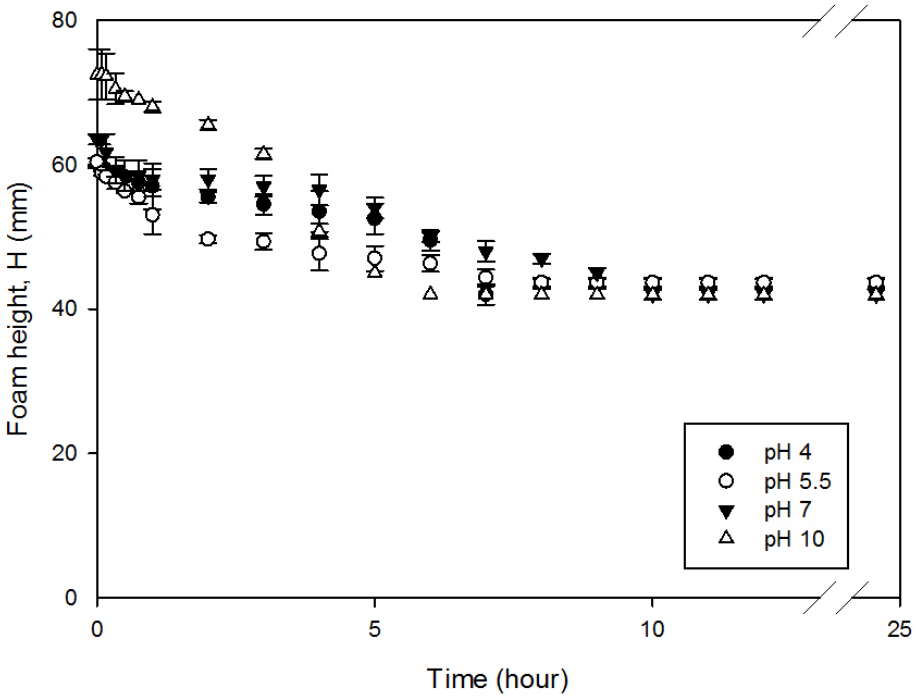

Figure 5.24: Breakage of whey protein foam at various pH values; MA.

From the foam stability test, there is a dramatic change expectiedly in the foam microstructure of foam produced by only protein at pH 7 because of its short foam life. The statistical parameters are summarized in Table 5.8. However, there is no significant difference of the mean bubble size before the sudden foam collapse at pH 7 in comparison to other pH. At pH 10, a smaller initial bubble size with a slower bubble growth is observed and this corresponds to the previous observation of the better foamability and slower rate of collapse.

With the addition of silica, the statistics used to describe and compare the bubble size distributions are summarized in Table 5.24. At pH 10, a smaller initial mean bubble size is found, however at

Table 5.8: Statistical parameters for foam bubble size distribution: foam stabilized by whey protein only at various values of pH; MA.

	d_{10}(μm)	d_{32}(μm)	S_t	Min(μm)	M(μm)	Max(μm)	S	K
pH4								
5 min	123.33	136.33	28.16	56.52	120.92	234.09	0.61	0.77
10 min	171.84	185.17	34.04	86.34	169.93	286.90	0.32	0.18
20 min	239.75	274.75	65.11	109.01	238.20	452.19	0.50	0.30
30 min	327.83	377.57	88.93	183.84	310.55	634.25	0.83	0.45
45 min	657.30	1155.26	354.60	264.70	547.60	2646.70	2.57	8.80
60 min	844.30	1352.77	449.00	223.50	737.30	2927.10	1.41	2.50
120 min	1056.40	1756.82	593.00	226.30	869.40	3346.70	1.40	2.01
240 min	1243.40	1935.62	627.00	300.00	1050.80	3332.90	1.52	2.13
pH5.5								
5 min	123.26	140.50	33.64	53.24	120.69	215.79	0.10	-0.62
10 min	156.77	184.42	47.92	59.39	153.52	276.35	0.24	-0.66
20 min	240.10	300.76	87.70	78.07	232.62	503.45	0.43	-0.37
30 min	291.52	393.47	117.73	120.52	274.34	839.31	1.26	2.38
45 min	402.80	484.71	127.86	184.11	389.86	861.64	0.74	0.35
60 min	593.40	769.89	227.50	262.80	540.80	1276.10	0.87	0.28
120 min	991.80	2298.74	743.30	239.60	751.40	5558.80	2.26	7.87
240 min	1135.20	2515.49	837.40	291.40	828.20	4965.10	2.00	4.86
pH7								
5 min	125.55	137.51	27.48	63.04	124.35	242.14	0.43	0.58
10 min	163.29	178.77	36.54	79.31	167.04	252.41	-0.01	-0.52
20 min	241.73	281.69	70.83	119.48	239.15	462.66	0.35	-0.50
pH10								
5 min	103.96	112.69	21.99	52.21	107.04	159.10	-0.13	-0.48
10 min	159.68	175.13	35.70	82.48	157.73	246.76	0.19	-0.73
20 min	264.55	299.87	69.37	92.53	264.38	456.48	0.33	-0.12
30 min	371.21	421.94	98.17	185.75	365.89	630.96	0.38	-0.30
45 min	682.70	835.11	228.70	292.60	646.30	1382.80	0.67	-0.01
60 min	659.00	899.63	278.30	177.70	612.60	1708.20	1.01	1.41
120 min	708.30	1206.96	384.60	240.00	601.40	2545.90	2.05	5.80
240 min	948.10	1794.14	626.60	229.00	754.50	3260.40	1.44	1.56

pH 5.55 the rate of bubble size growth is higher. This is related to the previously observed increased foamability at pH 10 compared to other pH values.

There is previously seen a decrease of foam stability at pH 10 compared to other conditions. At pH 4, there is a larger initial mean bubble size with a faster bubble growth than at pH 5.55. This fast bubble size growth is a reason for the fast collapse described above.

At pH 4 there is both faster foam breakage and drainage and also a coarser foam microstructure than other pH values which we studied in this experiment. Therefore, adding acid to protein to lower the pH makes foams more unstable. This is true both in cases of only protein foam and when silica is added. At pH 10, the best foamability and slowest foam collapse at first with smaller initial mean bubble size in both cases with and without silica in the protein foam was observed. However, with addition of silica, the shortest foam life was obtained at pH 10.

Table 5.9: Statistical parameters for foam bubble size distribution: whey protein foam with 0.5 wt% silica particles at various values of pH; MA.

	$d_{10}(\mu m)$	$d_{32}(\mu m)$	S_t	Min(μm)	M(μm)	Max(μm)	S	K
pH 4								
5 min	137.50	159.12	39.43	59.13	136.92	241.22	0.28	-0.53
30 min	369.14	451.47	123.68	147.67	347.81	856.16	0.66	0.52
60 min	419.40	562.36	173.70	152.90	388.60	1094.50	0.83	0.64
120 min	830.60	1416.32	456.80	312.60	711.20	3064.30	1.93	4.40
240 min	1924.10	3528.97	1293.00	370.20	1546.10	5330.60	1.04	0.27
pH neutral								
5 min	118.26	133.29	30.52	54.48	114.62	200.76	0.17	-0.66
30 min	349.46	382.24	76.42	138.63	350.14	595.34	0.30	0.18
60 min	465.00	603.94	175.90	171.20	431.40	1106.30	1.06	1.04
120 min	517.30	892.41	286.60	185.80	436.60	2147.10	2.00	6.28
240 min	682.30	1650.68	506.50	216.50	510.60	3444.30	2.73	9.43
pH 7								
5 min	112.52	126.41	27.95	59.57	109.18	204.43	0.50	-0.18
30 min	286.19	345.08	94.10	116.91	281.38	574.59	0.36	-0.53
60 min	570.80	922.05	266.00	229.40	515.70	2487.10	3.17	16.86
120 min	761.10	1906.73	538.60	267.80	633.30	4722.80	3.61	18.97
240 min	930.10	1482.26	475.50	330.20	817.10	3339.60	1.73	4.15
pH 10								
5 min	110.20	118.25	21.65	44.70	111.44	161.13	-0.12	-0.16
30 min	428.60	449.99	68.18	290.68	418.77	580.00	0.20	-0.92
60 min	803.20	894.65	191.10	480.80	786.10	1377.30	0.58	-0.13
120 min	813.30	2031.19	607.50	212.90	643.30	4456.90	2.97	11.44
240 min	2467.00	4145.31	1499.00	484.00	1970.00	5826.00	0.89	-0.41

Comparison between UC and MA

Figures 5.25 and 5.26 show the foam fraction of whey protein foam with and without addition of hydrophilic silica, respectively. In general, the foam fraction of foams produced by UC are higher

than the foams produced by MA. Higher foam fraction happens at pH 10 but the foam life is shorter at pH 10. According to Marinova et al. (2009), the maximum foamability of whey protein was obtained at pH 4.2 near its pI. This seems to contradict the results, that maximum foamability is found at pH 10 in both methods. However, Marionova only considered pH values in the range from pH 3 to pH 6.8, a range that is narrower than the results present here. While the foamability at pH 10 appears maximal, a faster foam collapse and shorter foam life were also found at pH 10.

It is interesting to note that the whey protein-only foam produced by mechanical agitation at pH 7 collapses suddenly with only about 30 minutes foam life. In UC there is no difference between the foams at pH 5.55 and pH 7. There are several studies which have demonstrated that UC can improve the functional properties before foaming (Jambrak et al., 2008) and also Gunzey et al. (2006), Gulseren et al. (2007) have suggested that ultrasonication can increase the rate of protein adsorption at air-water interface by lowering the surface tension of bovine serum albumin (the protein they considered). Therefore, UC may have altered the structure of whey protein molecule resulting in very different foam properties from the foam generated by MA. However, it is not yet clear why the whey protein foam at pH 7 collapses suddenly around 30 minutes after foam formation.

5.2.5 Effect on Different Proteins: Whey and Casein

Previously, whey protein foam have been studied and demonstrated that the addition of silica can enhance the stability of whey protein foam. In this section, a different type of protein is studied, namely casein. The effect of the addition of silica and compare this to whey protein is investigated. 5.0 wt% of casein protein and three concentrations of added hydrophilic silica are used. UC and MA are both used in this series of experiments.

Figure 5.27 shows both foam height and liquid level against time for foam generated with whey and casein protein using UC. Foam produced from casein clearly shows a better foamability in comparison to the one generated from whey protein. However, both foams collapse almost immediately and the foam life for both foams is about 6 hours. The drainage curves are almost identical. Very similar results are obtained in the foam produced by MA. In another study (Lee et al., 1992), the great difference of the molecular structure of whey and casein was pointed out. Based on this the author

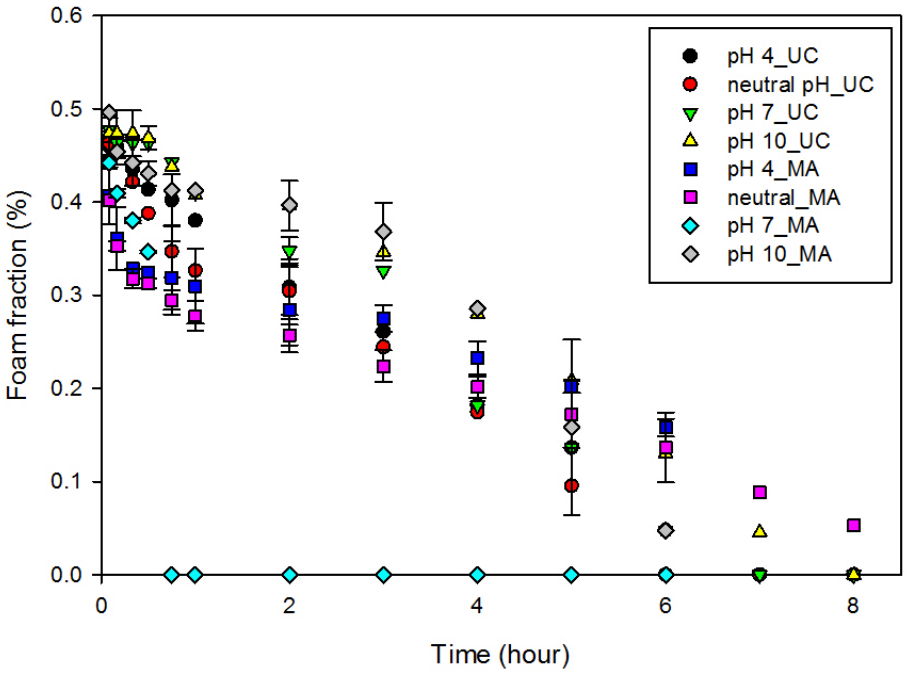

Figure 5.25: Foam volume fraction of whey protein foams produced at various energy intensities, UC and MA.

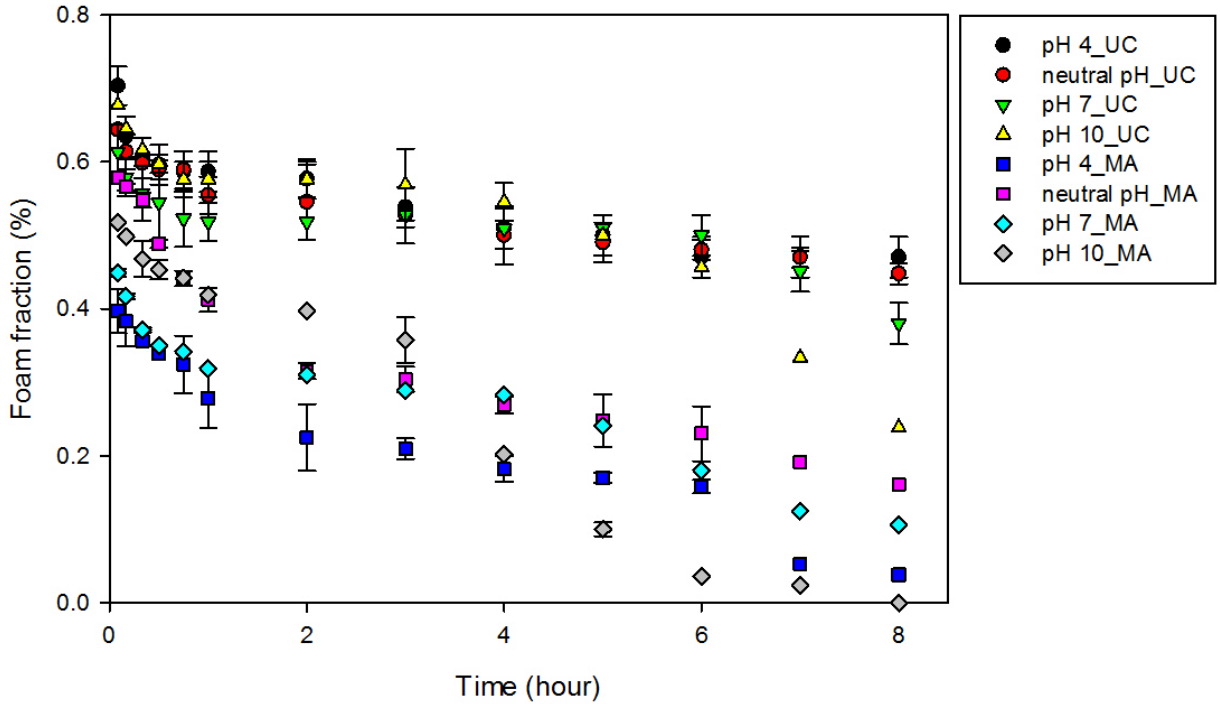

Figure 5.26: Foam volume fraction of whey protein foams produced at various energy intensities; UC and MA

expected major differences in their surface activity-related functionality. There are also other studies (Graham and Phillips, 1979, Meste et al., 1990) where it was proposed that the flexibility of protein molecules, that is the ease with which they are unfolded, is one of the important characteristics determining the foaming capacity of proteins. Therefore, casein has the better foamability than whey protein because of its more flexible molecule structure. In the latest review articles (Teilum et al., 2011), the authors pointed out that proteins rely on flexibility to respond to environmental changes, ligand bonding and chemical modifications and protein function is linked to protein flexibility.

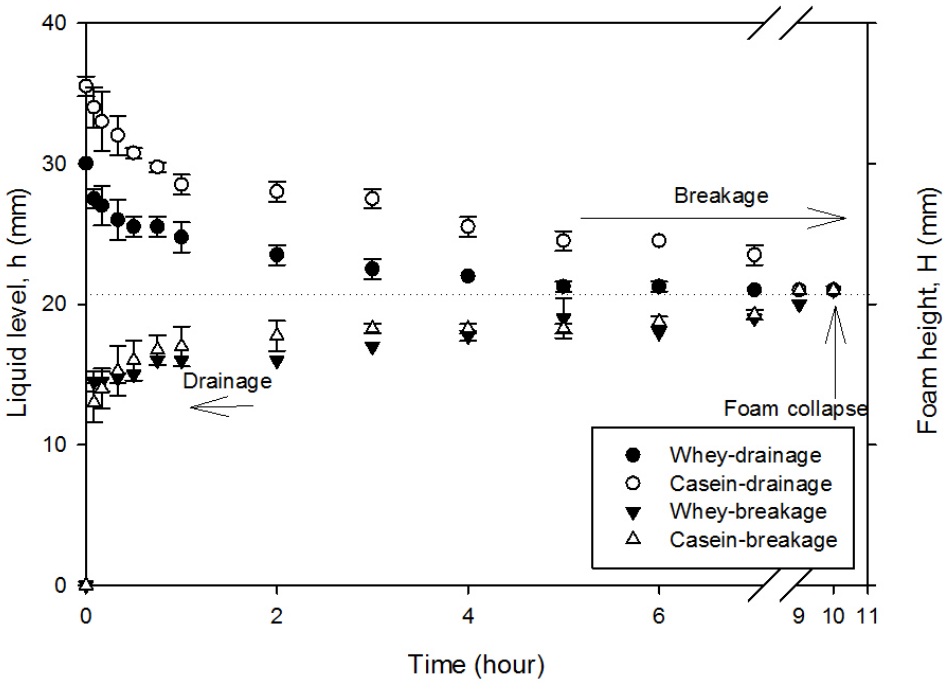

Figure 5.27: Drainage and breakage of 5.0 wt% whey and casein protein foam only; UC.

In Figures 5.28 and 5.29, the foam height and the liquid level are plotted against time using UC and MA, respectively. Foamability and drainage decrease slightly with increasing concentration of silica particles. The addition of silica particles does not lead to a significant reduction of foam collapse and foam life time. A similar result was obtained in MA.

Previously, there is great increase at foam stability by adding silica particle to whey protein foam. However, this effect was not observed in the casein foam. Therefore, the difference between these two types of protein with the silica is compared. Figures 5.30 and 5.31 show both foam height and liquid level against time for both whey and casein protein. In general, the foams produced from

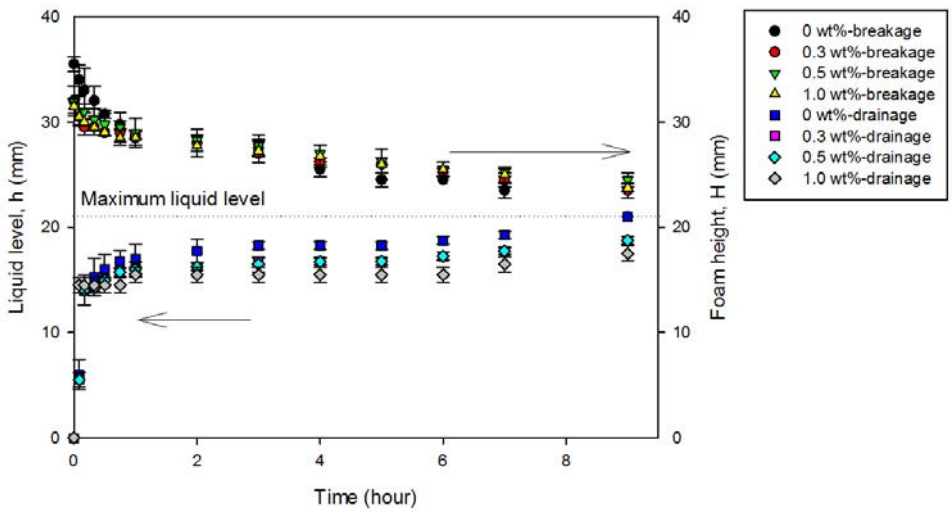

Figure 5.28: Drainage and breakage of casein protein foam with addition of hydrophilic silica particles; UC.

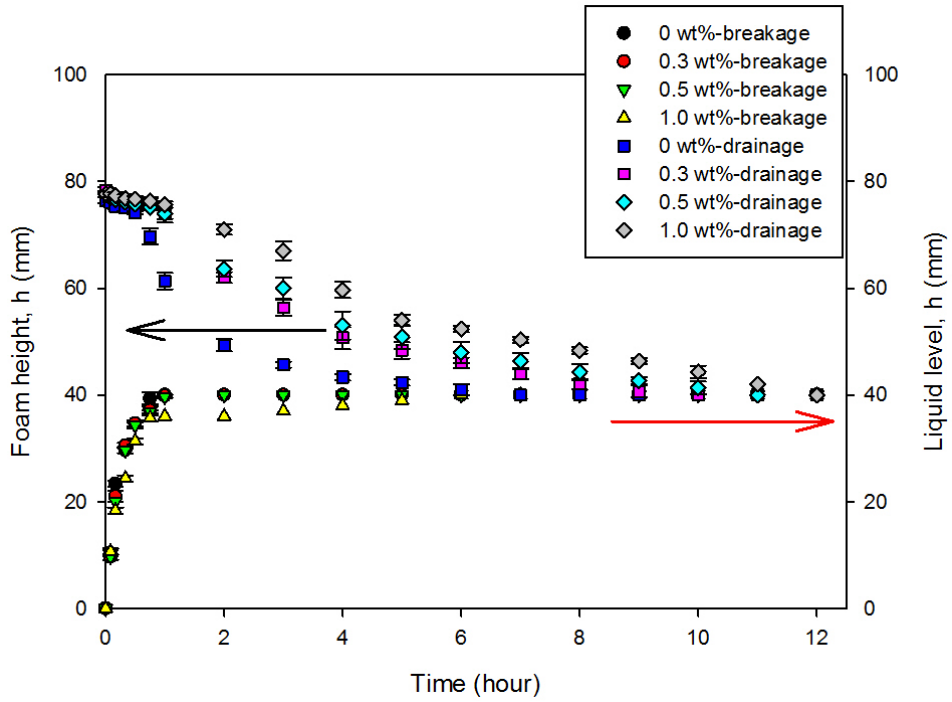

Figure 5.29: Drainage and breakage of casein protein foam with addition of hydrophilic silica particles; MA.

casein with addition of silica show better foamability than the ones produced from whey protein. Both foams made from whey and casein collapse in 8 hours after foam formation when the silica concentration is low, ie < 0.1 wt%. However, at higher concentrations of silica the foam stability is decreased in the case of casein, but increased in the case of whey protein foam. For example, the

foam life of casein protein foam with 1.0 wt% silica is less than one day while the foam life of whey protein foam can last for more than a week. Drainage clearly slows down in whey protein foam with increasing addition of silica while there is no significant drainage reduction in the foam produced by casein protein. Similar results have been found in casein foams made by MA. However, the foams made by UC have better foam fractions than MA as shown in Figure 5.32.

The statistical parameters and the bubble size distributions are summarized in Tables 5.4 and 5.10. In the original protein foams without silica, a larger mean bubble size is produced in casein foam. It also has a faster bubble growth. As discussed in the previous section, the addition of silica improves foam stability. With addition of silica, a larger mean bubble sizes are found both in casein and whey protein foams. However, the mean bubble size is much larger in whey protein foam with higher concentration of particles. The rate of mean bubble size growth decreases with increasing concentration of silica in whey protein foam while there is no such reduction in casein protein foam. A relationship between the rate of bubble size growth and foam life is observed, in the sense that a higher rate tends to correspond to a shorter foam life. This is again observed in the case of whey proteins and casein foams, where the former have slower bubble size growth and the latter have a shorter foam life. Similar results have also been found in the foams produced by MA.

Based on the arguments by Lee et al. (1992) a large difference in foamability is expected but similar foam stability between casein and whey protein because of their differing molecular structures. However, there are similar results in terms of foamability and foam stability in the foams stabilized by the proteins only in this study. However, there is difference found in terms of foam stability .

5.2.6 Effect of Hydrophobicity of Silica Particles

In this section, the effect of the hydrophobicity of silica on whey protein foam is investigated. In previous experiments, great differences was not found between the foams with silica produced by different methods. Therefore, only mechanical agitation was used as the foam generation method here. 5.0 wt% protein was used and four types of silica with different degrees of hydrophobicity were used (see Chapter 3 and Table 3.1). The concentration of these silica were chosen to be 0.3, 0.5, and 1.0 wt%.

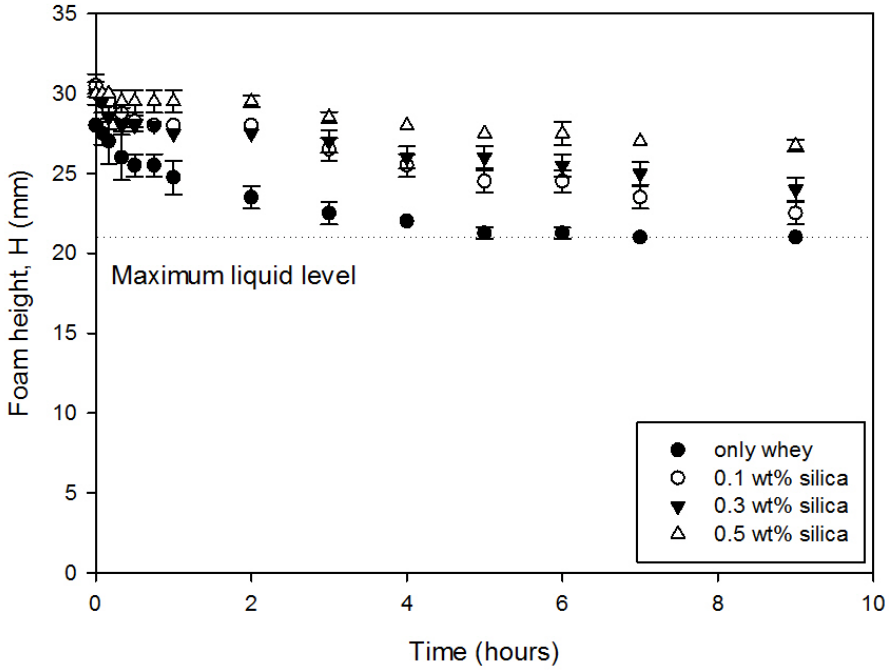

(a) Whey

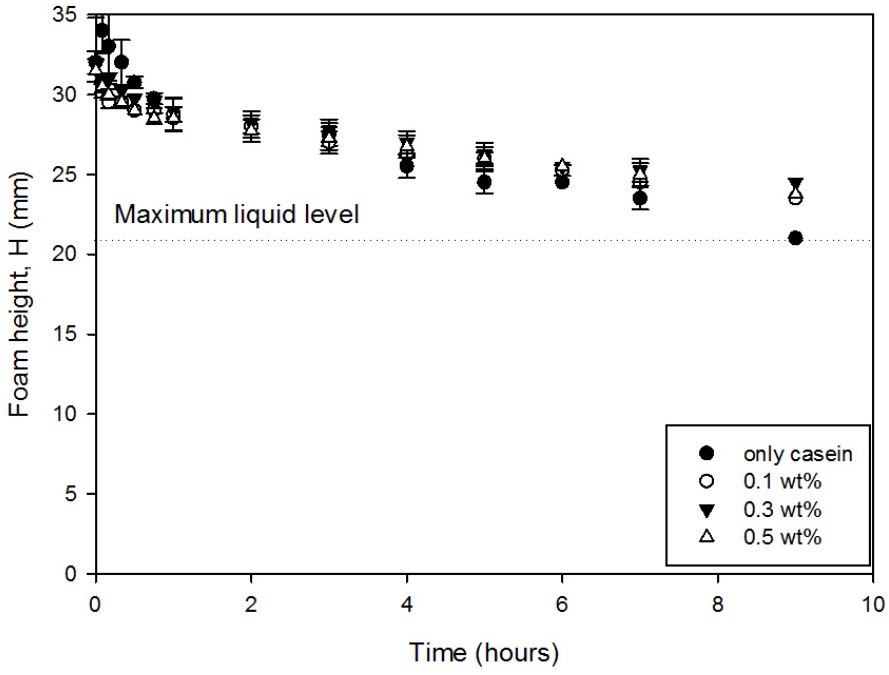

(b) Casein

Figure 5.30: Breakage of whey and casein protein foam with addition of hydrophilic silica particles; UC.

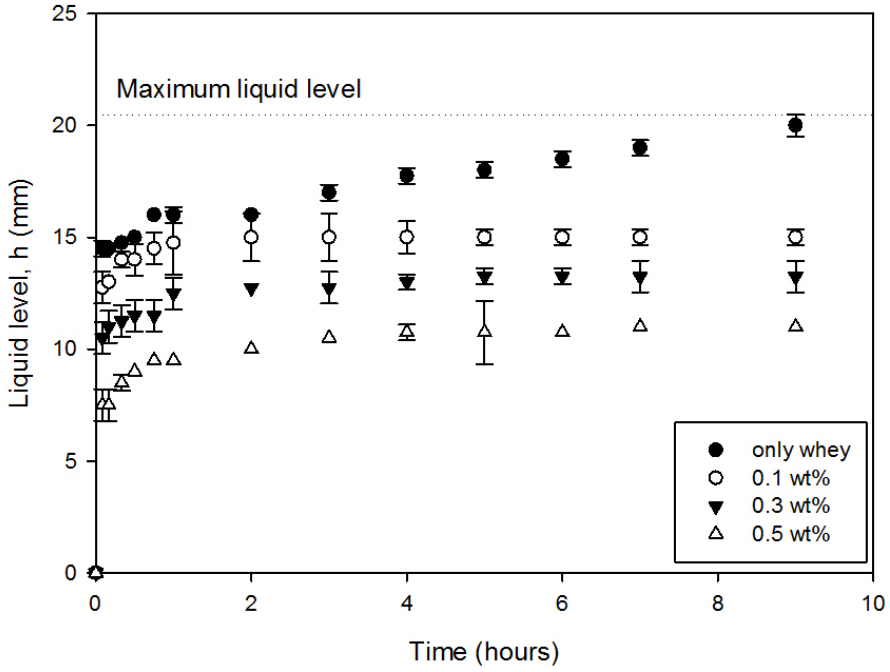

(a) Whey

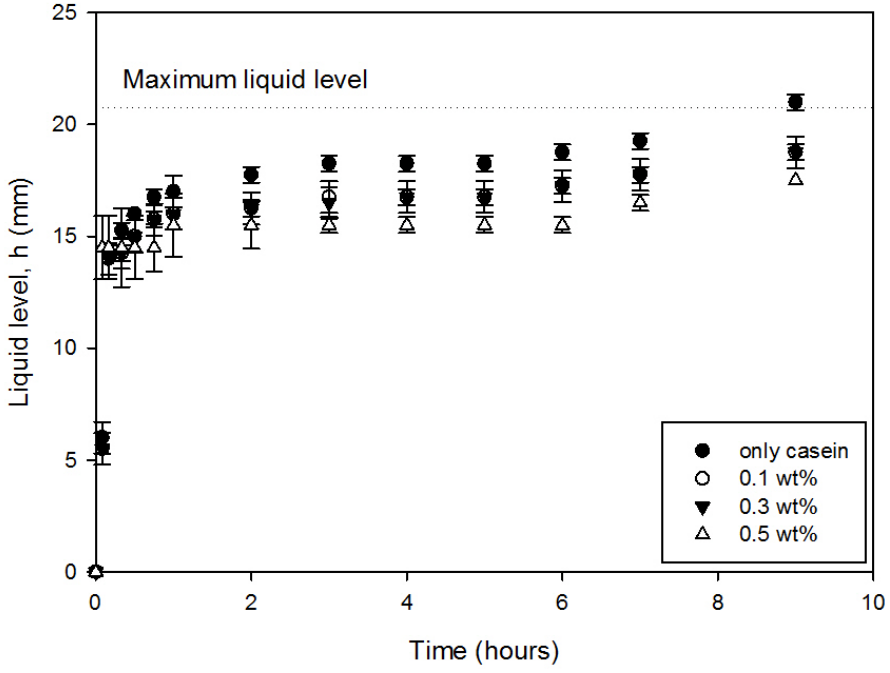

(b) Casein

Figure 5.31: Drainage of whey and casein protein foam with addition of hydrophilic silica particles; UC.

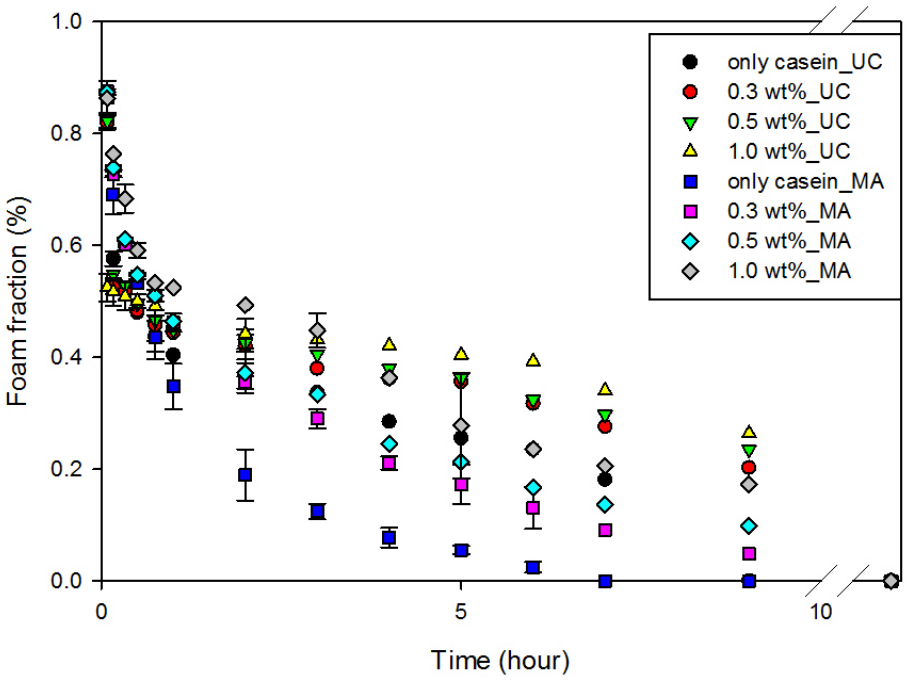

Figure 5.32: Foam volume fraction of whey protein foams produced at various energy intensities: UC and MA.

Table 5.10: Statistical parameters for foam bubble size distribution: casein protein foam with addition of hydrophilic silica particles; UC.

	d_{10}(μm)	d_{32}(μm)	S_t	Min(μm)	M(μm)	Max(μm)	S	K
no silica particles								
5 min	127.65	140.49	29.32	66.52	128.70	203.13	0.07	-0.57
30 min	313.10	361.66	89.27	104.38	314.93	532.33	0.26	-0.45
60 min	500.50	1454.76	393.10	185.90	385.30	3343.90	3.88	19.14
240 min	1100.60	1681.04	517.70	425.50	939.80	3238.80	1.98	4.54
0.3 wt%								
5 min	131.30	148.01	34.54	56.14	134.17	230.76	-0.10	-0.55
30 min	388.62	493.29	140.57	166.58	361.37	861.10	0.94	0.82
60 min	523.40	717.59	223.80	178.60	491.40	1367.90	0.97	0.80
240 min	1038.20	1890.51	657.40	258.40	852.20	3643.90	1.40	2.20
0.5 wt%								
5 min	137.67	152.24	32.30	69.30	138.00	232.52	0.17	-0.15
30 min	286.19	343.59	95.17	114.50	285.17	503.83	0.07	-0.87
60 min	411.00	579.96	157.10	140.30	393.40	837.30	0.51	-0.47
240 min	1023.40	1677.54	543.60	298.80	907.10	3820.40	1.74	5.71
1.0 wt%								
5 min	144.94	158.32	31.92	69.13	144.91	236.87	0.02	-0.06
30 min	271.36	315.13	79.57	125.49	265.75	448.93	0.16	-0.85
60 min	446.40	578.32	173.00	144.90	411.00	1044.40	0.71	0.23
240 min	910.50	1323.20	403.20	299.20	815.70	2840.00	1.77	4.94

In Figure 5.33, the foam height of the whey protein foam with addition of silica of different hydrophobicities (including hydrophilic silica) are plotted against the concentration of particles. R812 (the moderately hydrophobic silica) gives the best foamability among these silica and the

foamability increases with increasing concentration of R812 particles. R972 (the lightly hydrophobic silica) shows also a better foamability than the other two silica; R202 (the strongly hydrophobic silica) have similar foamability as the hydrophilic silica at lower concentration but a better foambility at 1.0 wt%.

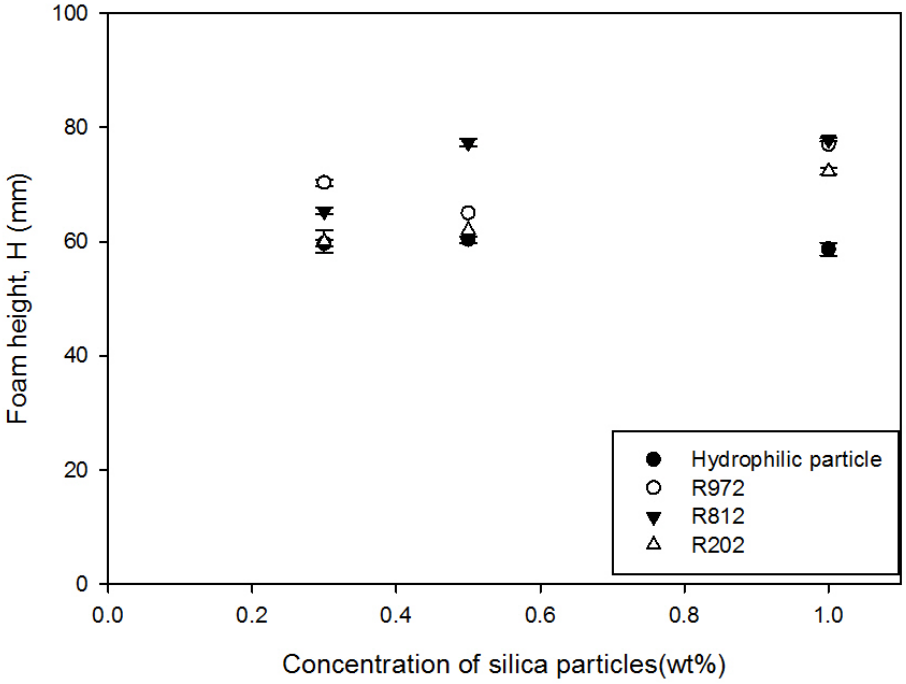

Figure 5.33: Foamability of protein foam with different hydrophobicity silica particles at various concentrations; MA.

In Figures 5.34(a), 5.34(b), 5.34(c) and 5.34(d), the drainage curves of whey protein foams produced with hydrophilic and three different hydrophobic silica particles at various concentrations are shown. Although the whey protein foam with the hydrophilic silica has the least foamability, it has shown the lowest drainage with R812 particles at 1.0 wt%. The drainage decreases with increasing concentration of hydrophilic and R812 particles. With R972 particles, addition of particles slows the drainage but there is no further reduction with increasing concentration of particles. With R202 particles, drainage increases with the addition of silica when the concentration is below 0.5 wt% and the liquid in the foam films almost drains out.

Figures 5.35(a), 5.35(b), 5.35(c) and 5.35(d) show the foam breakage of whey protein foams generated with hydrophilic, R972, R812 and R202 particles, respectively. At lower concentrations of

R972 particles, the rate of foam collapse increases with increasing particle concentrations (from 0 to 0.5 wt%) and foam life reduces from 9 hours to only 30 minutes, as shown in Figure 5.35(b). With R812 particles, the foam collapses within 30 minutes with 0.3 wt% R812 particles as shown in Figure 5.35(c). In Figure 5.35(d), the foam collapses immediately after foam formation in the case of R202, at 0.3 wt% and 0.5 wt%. However, the foam height remains constant for over a day and no foam collapse is observed with R972 and R202 at 1.0 wt% of particles and with R812 particles above 0.5 wt%. In the case of hydrophilic particles, the foam collapse decreases with increasing concentration of particles as shown in Figure 5.35(a).

The liquid holdup of protein foam with addition of silica particle at various concentrations is summarized in Figure 5.36. With hydrophilic particles, the liquid holdup increases with increasing concentration. At a concentration of 1.0 wt% a very wet foam ($\approx$ 70% liquid in the foam) is observed.

In general, adding hydrophobic silica to protein foam does not increase the liquid content of the foam. In the foam with R812 particles and a concentration of 0.3 wt% to 1.0 wt% the liquid almost completely drained. In the foam produced with the addition of the other two types of hydrophobic silica, there is less liquid remaining in the foam in comparison to the foam generated with whey protein only.

The statistical parameters of the bubble size distributions of whey protein foams with addition of silica are summarized in Table 5.11. In general, adding hydrophilic silica to whey protein foam can increase foam life, decrease drainage, and slow down the rate of bubble size growth. Adding low concentrations of hydrophobic silica leads to rapid bubble size growth or foam collapse (there is no foam for bubble size measurement). It therefore has the effect of defoaming. In the protein foam with higher concentration of silica, much larger mean bubble sizes are found and the growth of bubbles is faster in comparison to the foam with addition of hydrophilic silica.

As discussed above, a possible explanation is that more silica increases viscosity and the particles may accumulate at the plateau border to slow down the drainage and support the frame of bubbles. Partially hydrophobic silica acts like a defoamer when they are mixed with protein because they bridge the foam films. This interpretation is suggested by this finding that drainage and foam collapse are faster in these foams. This defoaming effect increases with the hydrophobicity. For

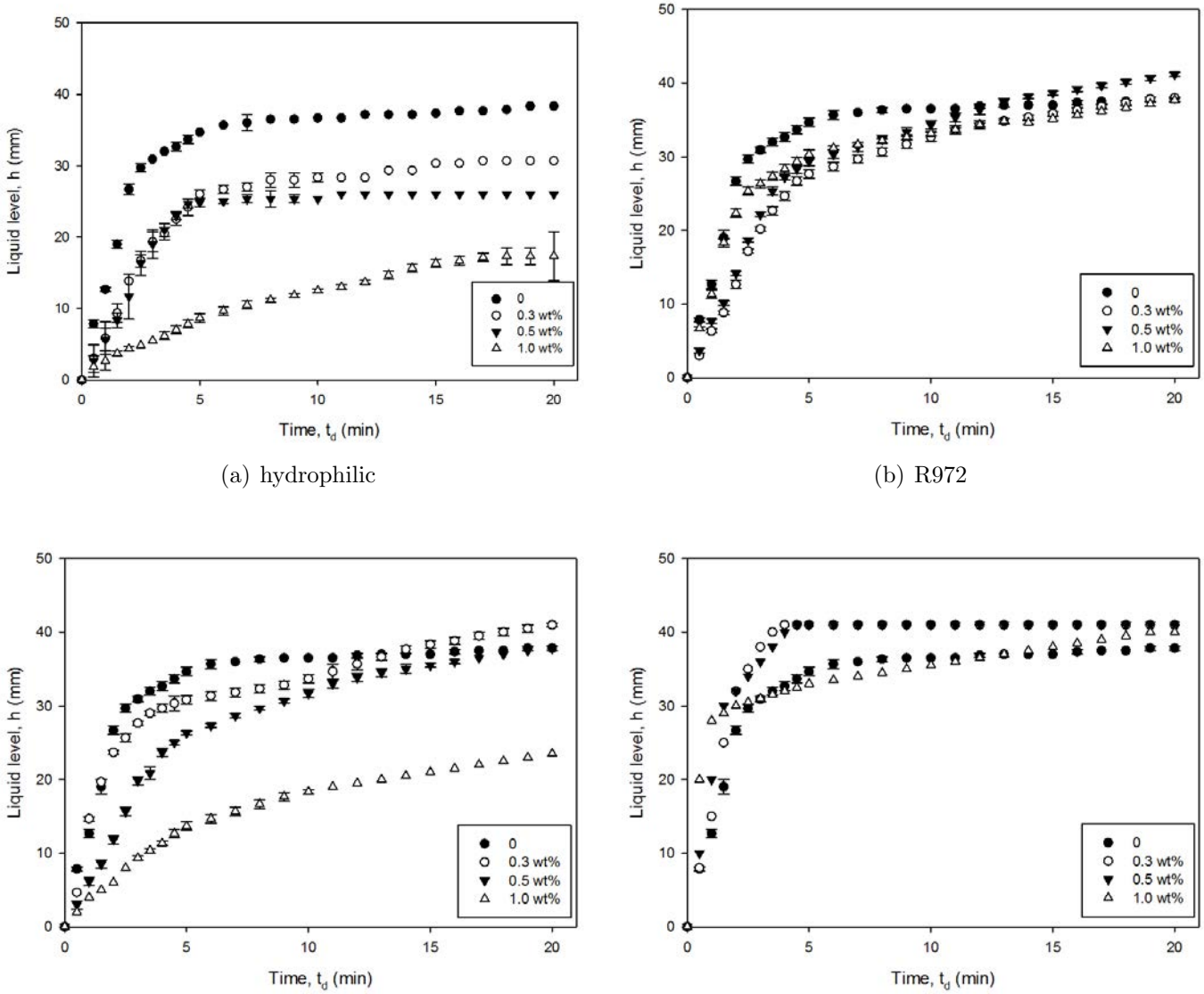

(a) hydrophilic

(b) R972

(c) R812

(d) R202

Figure 5.34: Drainage of foam with different hydrophobicity silica particles at various concentrations; MA.

example foam collapse was found within 30 minutes at lower concentrations of R202 particles. In this case also a smaller initial mean bubble size was found (see Table 5.11). This is because the hydrophobic silica starts to form bubbles and these bubbles are much smaller than the bubbles formed by the protein molecules.

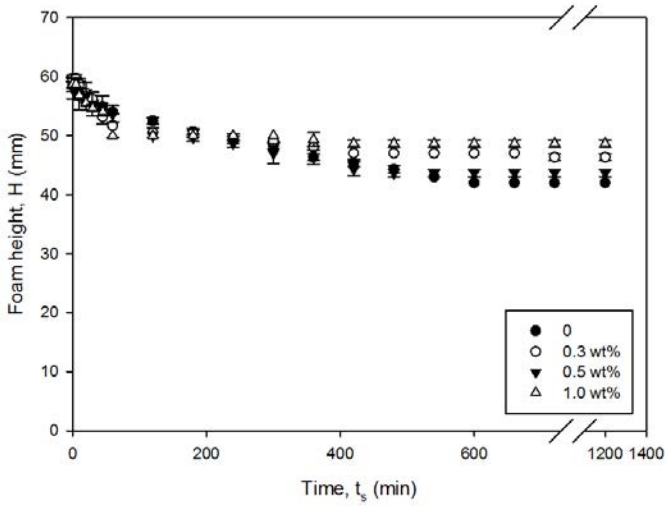

(a) hydrophilic

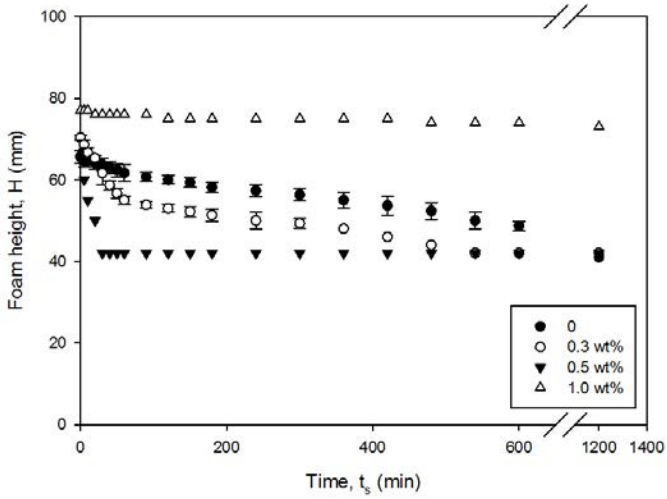

(b) R972

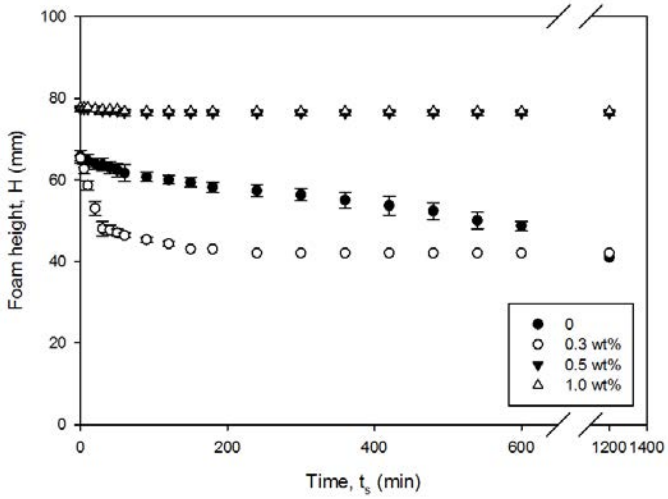

(c) R812

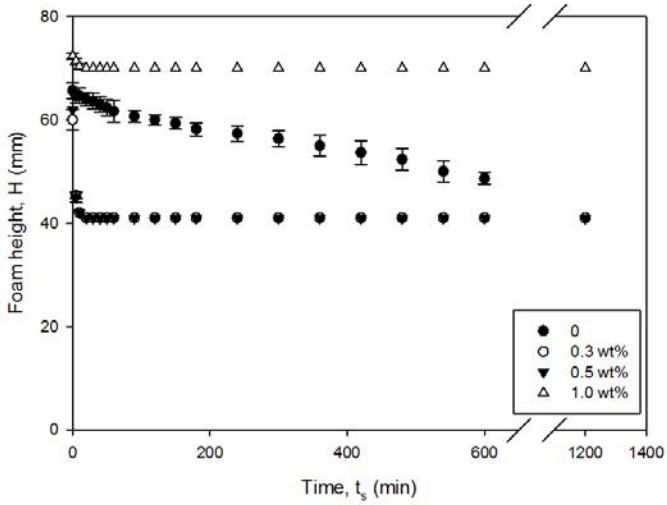

(d) R202

Figure 5.35: Breakage of foam with different hydrophobicity silica particles at various concentrations; MA.

Effect of Viscosity

In the previous section, the addition of silica particles leads to an increase of both stability and viscosity. The stability of foam increases with the concentration of silica and increasing concentration of silica provides a higher viscosity. In this section, the effect of viscosity on foam stabilized by whey protein only is investigated. SCMC is used to increase the viscosity and to compare the foam made from whey protein only with foam made from whey protein and added particles. The viscosity is varied by dissolving know amounts of SCMC (0.8 and 1.0 wt%) in 5.0 wt% whey protein solution.

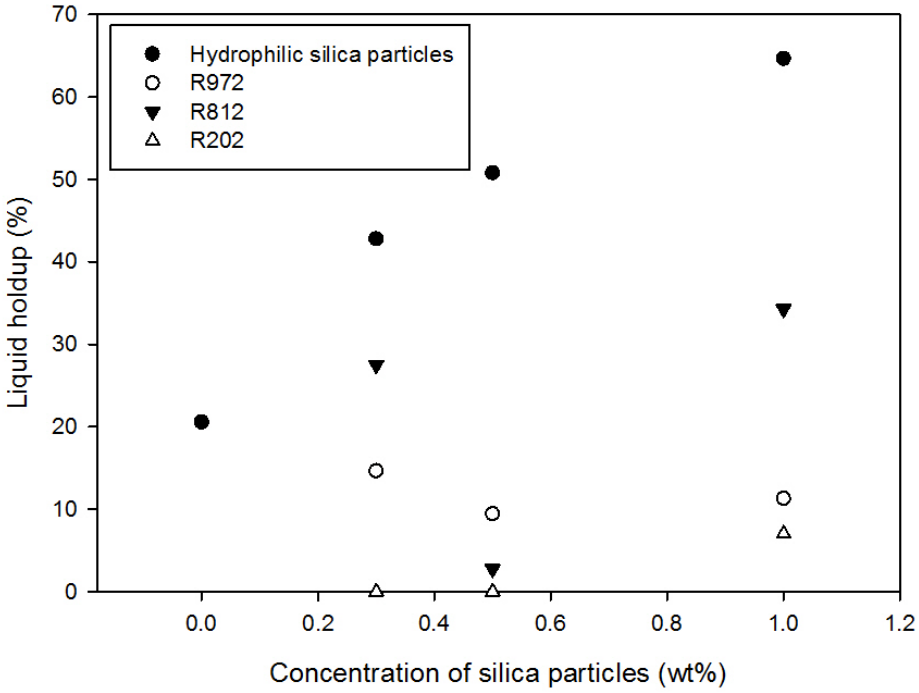

Figure 5.36: Liquid holdup of protein foam with different hydrophobicity silica particles at various silica particle concentrations; MA.

The viscosities of these two solutions are 0.024 and 0.018 Pa · s respectively.

Figure 5.37 shows the drainage of whey protein foam with different viscosities. In general, the drainage decreases with increasing viscosity. Drainage of foam produced from only whey protein starts immediately after foam formation and the liquid drains almost completely during the first 10 minutes. Drainage slows down with higher viscosity and ends about 18 minutes after foam formation at a viscosity of 0.018 Pa · s and 23 minutes at a viscosity of 0.024 Pa · s. Less liquid drains from foam produced with the more viscous whey protein solution than the whey protein only solution. However, in both solutions with SCMC there is no difference in the amount of liquid remaining in the foams.

The foam height is plotted against time as shown in Figure 5.38. Foamability and foam breakage decrease with increasing viscosity and foam life increases with increasing viscosity.

The statistical parameters to describe the bubble size distributions of whey protein foams with different viscosities are summarized in Table 5.12. The initial bubble size increases with increasing viscosity. However, similar as in the case of silica particles in the protein foam bubble growth slows

Table 5.11: Statistical parameters for foam bubble size distribution: whey protein foam with (a) hydrophilic (b) R972 (c) R812 (d) R202 particles at various particle concentrations; MA.

	d_{10}(μm)	d_{32}(μm)	S_t	Min(μm)	M(μm)	Max(μm)	S	K
R972								
0.3 wt%								
5min	115.33	121.54	19.23	61.83	116.30	176.78	0	0.29
30min	451.07	537.23	139.17	207.06	427.84	868.24	0.68	0.05
60min	688.00	1549.76	458.70	208.60	560.20	3814.50	3.16	15.88
240min	na	na	na	na	na	na	na	na
0.5 wt%								
5min	104.07	109.58	17.37	52.35	104.65	150.52	-0.21	0.26
30min	na	na	na	na	na	na	na	na
60min	na	na	na	na	na	na	na	na
240min	na	na	na	na	na	na	na	na
1.0 wt%								
5min	121.57	129.26	21.89	67.65	120.3	174.96	0.14	-0.31
30min	519	1939.88	487.5	141.6	412.5	3553.7	4.15	18.19
60min	807.8	5160.46	1215.3	214.1	442.2	8934.9	3.88	16.9
240min	2511	5490.59	2247	261	2195	8787	0.82	-0.23
R812								
0.3 wt%								
5min	116.62	123.31	20.22	62.35	116.87	161.65	-0.14	-0.15
30min	383.80	1706.71	327.30	146.30	328.40	3291.80	7.36	62.25
60min	na	na	na	na	na	na	na	na
240min	na	na	na	na	na	na	na	na
0.5 wt%								
5min	152.02	174.09	39.86	73.39	144.26	340.09	1.03	2.15
30min	4005.60	4811.16	1337.50	375.30	3816.90	7253.30	0.04	0.21
60min	4793.30	5275.31	1052.10	3086.30	4676.50	7869.80	0.91	0.89
240min	4873.00	5448.28	1215.00	2777.00	4862.00	7542.00	0.57	0.17
1.0 wt%								
5min	143.78	173.81	47.54	50.96	140.39	298.87	0.39	-0.16
30min	521.50	1081.15	335.8	161.20	404.70	2575.30	2.63	10.07
60min	315.84	412.04	115.00	149.80	295.29	855.69	1.7	4.35
240min	671.20	771.02	181.60	298.40	653.70	1359.60	0.71	0.76
R202								
0.3 wt%								
5min	na	na	na	na	na	na	na	na
30min	na	na	na	na	na	na	na	na
60min	na	na	na	na	na	na	na	na
240min	na	na	na	na	na	na	na	na
0.5 wt%								
5min	na	na	na	na	na	na	na	na
30min	na	na	na	na	na	na	na	na
60min	na	na	na	na	na	na	na	na
240min	na	na	na	na	na	na	na	na
1.0 wt%								
5min	101.32	211.62	75.84	25.39	63.43	338.87	1.41	0.7
30min	1084.6	2161.35	844.9	180.8	840.6	3828.2	0.83	-0.19
60min	1438.80	2160.79	803.5	143.1	1468.6	3534.5	0.21	-0.46
240min	3041.00	4016.54	1271.8	507.5	2947.8	6929.4	0.4	0.2

down with increasing viscosity.

In comparison to the foam stabilized by only hydrophilic silica particles, the viscosity of protein only solution with SCMC (0.024 and 0.018 Pa$\cdot$s for 0.8 and 1.0 wt%, respectively) is nearly 10 times higher than in the protein suspensions with silica particles. However, much more stable foams

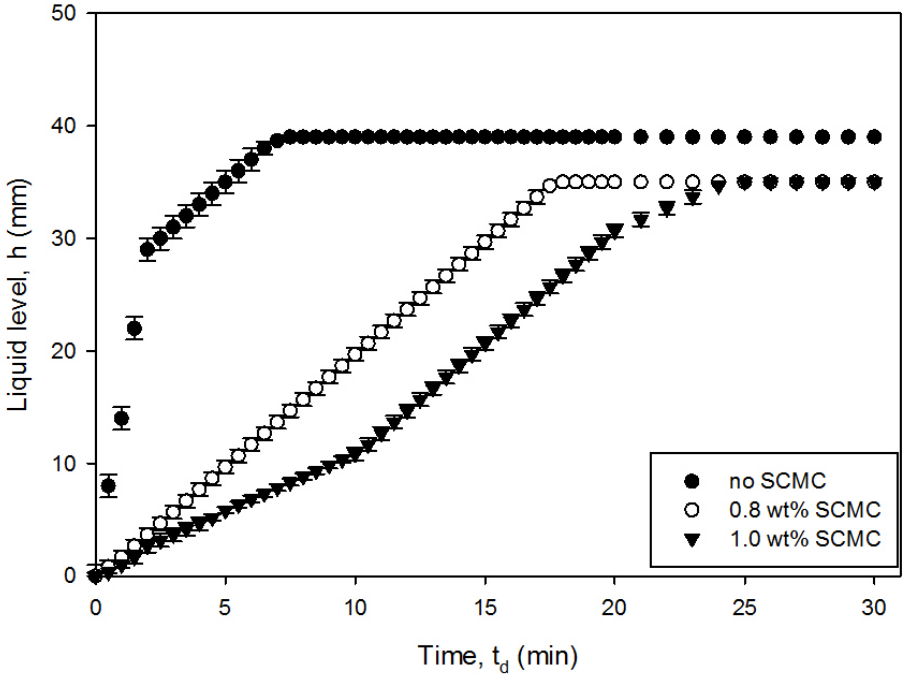

Figure 5.37: Drainage of whey protein foam with different viscosities; MA.

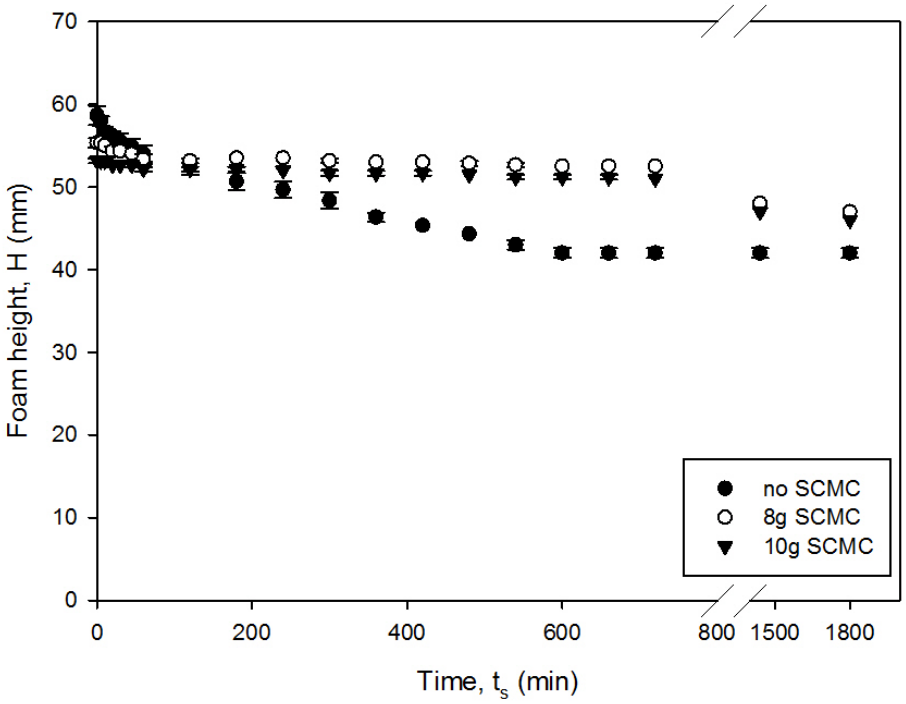

Figure 5.38: Breakage of whey protein foam with different viscosities; MA.

Table 5.12: Statistical parameters for foam bubble size distribution: whey protein foam with different viscosities; MA.

	d_{10}(μm)	d_{32}(μm)	S_t	Min(μm)	M(μm)	Max(μm)	S
no particles							
5min	119.44	142.87	38.95	44.9	120.72	214	0.16
30min	423.1	529.8271	148.4	174.5	401.8	1040.5	0.9
60min	606.3	959.64006	316.9	198.9	559.5	2099.7	1.4
240min	1188.3	2311.1455	761.7	388.2	953.5	4718	1.98
8 g SCMC							
5min	131.83	139.19532	22.36	83.65	131.57	182.78	0.04
30min	288.21	340.79112	89.08	124.97	282.41	553.52	0.33
60min	470	581.67048	165.1	103.3	448.9	972.6	0.5
240min	807.4	1255.281	413.6	254.9	717.5	2544.7	1.34
10 g SCMC							
5min	138.05	150.76518	29.6	77.22	135.61	235.04	0.5
30min	266.26	304.66115	72.84	127.17	266.83	454.21	0.3
60min	418.68	511.05379	140.66	148.77	404.25	872.33	0.56
240min	744.4	1096.5678	348.3	249	671	2282	1.39

(including reduction of drainage and slower or no bubble growth) were observed in the foam stabilized by particles. This indicates that improving foam stability is mainly dominated by the mechanism of adsorption at air-liquid interface. A higher viscosity can only improve foam stability for a relatively short period of time.

5.3 Conclusion

Firstly, the optimum concentration of whey protein for forming stable foam was investigated. Base on this 5.0 wt% of whey was chosen in all the experiments in this part of the study. Whey protein solution was treated by UC and MA at various energy inputs. This is to find the optimum energy input in both methods. 116.9 μm of amplitude and 6000 rpm were selected for UC and MA, respectively. Comparison of these two foam generation methods showed that UC can produce finer foams with less energy input into the system (see section 5.2.2).

Secondly, the effect of adding hydrophilic silica in whey protein foam is investigated. Foam stability and foam life increase with increasing concentration of silica. In the foam made by UC, a higher liquid holdup with smaller initial bubble size and slower bubble growth was obtained than in foams produced by MA at low concentrations (<1.0 wt%). Similar liquid holdup for UC with coarser foam and faster bubble growth was observed and compared to the foams produced by MA at the higher concentration of the particles (<1.0 wt%). UC offers an energy saving way to generate foams

with addition of hydrophilic silica, however, this can only apply to smaller batches and low viscosity materials.

Thirdly, whey protein foams produced by UC and MA have better foamability at pH 7 but shorter foam life than at other pH value. At pH 7, the foam made by MA collapsed suddenly in about 30 minutes, but there is no difference in bubble size in comparison to the foams at other pH. There is no such observation in the foam made by UC. UC may alter the structure of the whey protein and prevent foam collapse. Otherwise pH has no substantial effect on protein only and foams with addition of silica.

Fourthly, the difference between whey and casein protein foams have been investigated in pure protein foams and foams with addition of silica. Casein foams show a better foamability than whey protein foams both in pure foams and with addition of hydrophilic silica. However, the addition of hydrophilic silica has very little impact on enhancing the stability of the casein protein foams. These results have been shown in the foams made using both foam generation methods. The foams made by UC have higher foam fraction than the foams produced by MA.

Fifthly, hydrophobic silica acts as antifoam agents in the whey protein foam when the concentration is below 0.5 wt%. Once the concentration of particles is over 1.0 wt%, the foam stability is enhanced relative to the no silica foam. Increasing viscosity by adding SCMC has the same effect as adding hydrophilic silica to reduce the drainage. However, foam stability and foam life are much longer in foams with addition of particles. A possible explanation for these observation is that the SCMC only offers a slower drainage (via increased viscosity) whereas silica particles build up a network in between the bubbles while also increasing viscosity.

Chapter 6

The Effects of Silica Particles on C12LAS and CTAB Surfactant Foams

6.1 Introduction

Many surfactant stabilized foam studies have been carried out by using a pneumatic method (Bikerman, 1973, Bhakta and Ruckenstein, 1997a, Exerowa and Kruglyakov, 1998). Using this method, Deshpande and Barigou (1999) have established that the foam collapse history curve can be divided into three regions: (1) The curve starts with a plateau region where the foam height remains constant over a period of time ranging from a few to many minutes, varying with the nature of the foam. During this phase, most of the liquid in the foam film drains but there is no foam breakage. (2) At the end of this time-lag period, foam films have thinned sufficiently and become unstable and foam breakage starts. The foam collapses at a fast rate and foam height decreases almost linearly. (3) In the third part of the curve foam collapse proceeds, again in a linear manner, but at a slow rate.

Addition of particles can play two different roles in the stabilization of surfactant stabilized foam depending on the particle size, shape, type and hydrophobicity. Deshpande and Barigou (1999) reported that hydrophilic silica particles can enhance the stability of foam made from NaDBS. Hudales and Stein (1990) found that larger hydrophilic glass particles (diameter approximately between 1 and 10 μm) retard both cetyltrimethylammonium bromide (CTAB) foam and film drainage and increase film stability, while smaller glass particles ($<$1 μm) shorten film lifetime in foam and have no influence

on foam drainage. Tang et al. (1989) showed that hydrophobic silica particles stabilize well foams produced by sodium dodecyl sulfonate in alkaline aqueous medium. In their study, they showed that the smaller the particle size, the stronger the stabilization. On the other hand, hydrophobic particles can be good anti-foaming agents when they are larger size (micron size range) because of the particles inducing film rupture (Frye and Berg, 1989, Aveyard et al., 1994, Pugh, 1996).

Foams and emulsions are very similar systems. Many studies have revealed that the mixture of nano particles and surfactants can stabilize emulsions which were mostly produced by using a homogenizer (Midmore, 1998a,b, Binks and Rodrigues, 2007, Binks, Desforges and Duff, 2007, Binks, Rodrigues and Frith, 2007, Eskandar et al., 2007). Most of the studies focused on the influence of the interfacial synergy on the stability of emulsions. A lot of research on emulsions can be applied to foam systems as these two are very similar with respect to their stability properties. The primary processes which are induced by gravity are creaming and sedimentation for emulsions and drainage for foams (either water and oil for emulsion or water and air of foams). The secondary processes which are caused by diffusion are named 'Ostwald ripening' in emulsions and disproportionation in foams. However, foam systems are under more constraints because of the nature of the foam. In foam systems, the larger density difference between the air-water foam compare to the oil-water emulsion, the increased effect of disproportionation, and the ability of hydrophobic particles can act as a foam de-stabilizer (Hunter et al., 2008). In particular foam systems, smaller particles are needed for foam stabilization as the larger particles can pierce the bubbles. Whereas in emulsions, larger particles will tend to form larger emulsion droplets. A narrower contact angle range is required in the foam stabilization. Schwarz and Grano (2005) found the optimum particle contact angles for stability around 63 degree while Ata et al. (2004, 2002) found 66 degree contact angle gave optimum stability condition. In their studies, increasing particle hydrophobicity led to unstable foams. Aveyard et al. (1994) concluded that the range of contact angles of particles that stabilizes foam is small. They discovered that the stability of foam shows a sudden drop once the critical receding angle is reached, where particles begin to work as de-stabilizer.

The literature considered three main properties of particle and surfactant mixtures: the effect on surface tension, the contact angle and the nature of any flocculation. Wang et al. (2004), Gonzenbach

et al. (2006a), and Lan et al. (2007), found that the mixture of particles and surfactants led to system synergy in the surface tension of large drops, which is due to the attractive interaction between interfacial particles and bulk surfactant. Binks and Whitby (2005), and Zhang, Lan, Liu, Xu and Sun (2008) found that cationic surfactants can modify the surface of particles. This is because a cationic surfactant can attach to the particle surface and increase the effective hydrophobicity of the particle. Hence, the surface tension of the suspension decreases. Lastly, a small scale flocculation can cause an increase of viscosity which enhances the stability of an emulsion or a foam, but a large scale flocculation may lead to an unstable system (Binks, Desforges and Duff, 2007, Lan et al., 2007, Zhang, Sun, Dong, Li and Xu, 2008).

There are a number of recent studies that have shown that a mixture of surfactants and particles can stabilize foams (Gonzenbach et al., 2006a, Zhang, Lan, Liu, Xu and Sun, 2008, Zhang, Sun, Dong, Li and Xu, 2008). Gonzenbach et al. (2006a) used short chain amphiphiles to modify a hydrophilic particle surface, and these modified particles were used as surfactants to stabilize foam resulting in drastically improved foam stability. Zhang, Lan, Liu, Xu and Sun (2008) also showed that a synergistic effect on foam stability occurs when they mixed disk-like Laponite particles with a cationic surfactant (CTAB) or a non-ionic surfactant (tetraethylene glycol monododecyl ether, C12E4). They found that foam stability reaches an optimum at an intermediate concentration of CTAB and increases with increasing concentration of C12E4. Alargova et al. (2004) took a different approach. Their foam was stabilized only by anisotropic polymer microrod particles using hand shaking. The lifetime of the foam was orders of magnitude longer in comparison to foam stabilized with a common foaming surfactant, sodium dodecyl sulfate (SDS). However, when they added SDS to foam stabilized by the polymer microrod particles, this led to hydrophilization of the microrods and dramatically reduced the lifetime of the foam.

Here the addition of silica particles to foam stabilized by a surfactant is investigated. In the presence of silica, stability does not simply correlate to surfactant concentration but both particle concentration and surfactant concentration interact in complex ways. More detail how the stability of foam depends on the hydrophobicity of silica particles and the type of surfactant is investigated. In the present contribution, the properties of foams (foamability and foam stability) in anionic and

cationic surfactant solutions that are mixed with silica particles of varying hydrophobicity and concentration. The aim is to understand how bulk foam stability of the mixture depends on these parameters. Specifically, two concentrations of the anionic surfactant C12LAS and one concentration of cationic surfactant CTAB are considered. An extensive series of experiments varying key parameters of the system is contucted. These key parameters are the concentration of silica in the solution, the degree of hydrophobicity of the silica, the viscosity of the liquid, and the pH value. A summary of all experiments that were carried out is given in Table 6.1 below. The method of foam generation is described in section 3.3.2.

6.2 Results and Discussion

6.2.1 Effect of Surfactant Concentration

Foam height generally increases with increasing surfactant concentration below the critical micelle concentration (Rosen, 1989). Drainage plays a key factor in foam stability. There are several studies (Bhakta and Ruckenstein, 1997a,b, Patist et al., 1998) which have shown that the drainage rate becomes slower with an increase in surface viscosity and bulk viscosity. In a study by Kralchevski et al. (1990) it was reported that the number of packed micelles increases with increasing concentration of surfactant in the solution. The higher number of micelles in the foam films leads to a higher bulk viscosity. This results in a layer by layer thinning or so-called stratification and it leads to slower drainage. Moreover, Kralchevski explained that this is because an increase in surfactant (SDS) concentration increases the repulsive forces between films (film interfaces) and therefore results in an increase in liquid holdup. The surfactant concentration ranges from 3.75 to 12.5 cmc.

Laheja et al. (1998) considered a larger concentration range of SDS surfactant from 0.75 to 60 cmc. They showed that the drainage rate first decreased and then increased with increasing concentration of surfactant. The turning point was at 10 cmc. A less stable foam and bigger mean bubble size was observed at higher cmc. They explained that this was due to a change from globular to cylindrical micelles. The bulk viscosity increased with increasing concentration of surfactant as the structure of the micelles changes, however, the increase of viscosity in insignificant. (In the case of SDS, the

Table 6.1: Summary of the experiments of (a) concentration of surfactants, (b) concentration and hydrophobicity of silica particles, (c) pH, and (d) liquid viscosity.

(a)

Surfactant	Concentration of surfactant
C12 LAS	0.1 cmc
C12 LAS	0.3 cmc
C12 LAS	0.5 cmc
C12 LAS	1.0 cmc
C12 LAS	2.0 cmc
CTAB	0.1 cmc
CTAB	0.3 cmc
CTAB	0.5 cmc
CTAB	1.0 cmc
CTAB	2.0 cmc

(b)

Surfactant	Concentration of surfactant	Particle	Concentration of particle
C12 LAS	0.2 cmc	Hydrophilica silica particle	0.1 wt%~1.5 wt%
C12 LAS	0.2 cmc	R972	0.1 wt%~1.5 wt%
C12 LAS	0.2 cmc	R812	0.1 wt%~1.5 wt%
C12 LAS	0.2 cmc	R202	0.1 wt%~1.5 wt%
C12 LAS	1.0 cmc	Hydrophilica silica particle	0.1 wt%~1.5 wt%
C12 LAS	1.0 cmc	R972	0.1 wt%~1.5 wt%
C12 LAS	1.0 cmc	R812	0.1 wt%~1.5 wt%
C12 LAS	1.0 cmc	R202	0.1 wt%~1.5 wt%
CTAB	1.0 cmc	Hydrophilica silica particle	0.1 wt%~1.5 wt%
CTAB	1.0 cmc	R972	0.1 wt%~1.5 wt%
CTAB	1.0 cmc	R812	0.1 wt%~1.5 wt%
CTAB	1.0 cmc	R202	0.1 wt%~1.5 wt%

(c)

Surfactant	Concentration of surfactant	Particle	Concentration of particle	pH
C12 LAS	1.0 cmc	Hydrophilica silica particle	0.1 wt%~1.0 wt%	4, 7, 10
C12 LAS	1.0 cmc	R972	0.1 wt%~1.0 wt%	4, 7, 10
C12 LAS	1.0 cmc	R812	0.1 wt%~1.0 wt%	4, 7, 10
C12 LAS	1.0 cmc	R202	0.1 wt%~1.0 wt%	4, 7, 10
CTAB	1.0 cmc	Hydrophilica silica particle	0.1 wt%~1.0 wt%	4, 7, 10
CTAB	1.0 cmc	R972	0.1 wt%~1.0 wt%	4, 7, 10
CTAB	1.0 cmc	R812	0.1 wt%~1.0 wt%	4, 7, 10
CTAB	1.0 cmc	R202	0.1 wt%~1.0 wt%	4, 7, 10

(d)

Surfactant	Concentration of surfactant	Particle	Concentration of particle	Viscosity
C12 LAS	1.0 cmc	Hydrophilica silica particle	0.5 wt%	0.08 and 0.1 wt% CMC
C12 LAS	1.0 cmc	R972	0.5 wt%	0.08 and 0.1 wt% CMC
C12 LAS	1.0 cmc	R812	0.5 wt%	0.08 and 0.1 wt% CMC
C12 LAS	1.0 cmc	R202	0.5 wt%	0.08 and 0.1 wt% CMC
CTAB	1.0 cmc	Hydrophilica silica particle	0.5 wt%	0.08 and 0.1 wt% CMC
CTAB	1.0 cmc	R972	0.5 wt%	0.08 and 0.1 wt% CMC
CTAB	1.0 cmc	R812	0.5 wt%	0.08 and 0.1 wt% CMC
CTAB	1.0 cmc	R202	0.5 wt%	0.08 and 0.1 wt% CMC

transition in morphology of micelles occurs from the range from 18.75 to 45 cmc (Reiss-Husson and Luzzati, 1966)).

In this section, the concentrations were determined and used in the subsequent experiments with the silica, which will be the main focus of this chapter. a series of experiments using C12LAS and CTAB to generate foams without silica is conducted. The concentration of surfactant was varied from 0.1 cmc to 2.0 cmc (see Table 6.1(a)).

Foam Formation, Drainage, and Breakage

In each experiment, foam volumes at different times were determined by measuring the height of the foam generated. During the first 5 minutes, foam drainage change was recorded directly using a digital camera, and foam collapse was measured by monitoring the decline in foam height over time. Two measurements were recorded: h, the liquid level and H, foam height (more details can be found in 3.3.2).

Figure 6.1 shows the foamability at five different concentrations using two oppositely charged surfactants: C12LAS and CTAB. It shows the initial foam height against the surfactant concentration. C12LAS has better foamability than CTAB from 0.1 cmc to 1.0 cmc and similar foamability above 1.0 cmc. In the C12LAS foam, there is a small increase in foamability from 0.1 cmc to 0.5 cmc reaching saturation at 0.5 cmc. In CTAB foam, the foamability increases with increasing concentration of surfactant up to 1.0 cmc and then levels off. In the C12LAS solution, the surface tension varies from 33.84 mN/m to 40.45 mM/m for 1.0 cmc to 0.1 cmc solutions. In CTAB solution, the surface tensions varies from 39.96 mN/m to 63.82 mN/m as the concentration varies from 1.0 cmc to 0.1 cmc.

These measurements indicate that a lower surface tension correlates to a higher foamability. In C12LAS foams there is a small reduction in surface tension with increasing concentrations of surfactant. Correspondingly, only a small increase of foamability over the same range is observed. In CTAB foam, a much higher surface tension is observed at lower concentration of surface tension resulting in a lower foamability. Foamability increases with decreasing CTAB surface concentration. At higher concentrations, these two types of surfactant have similar foamability as their surface

tensions are about the same. This shows that independent of the type of surfactants used, the surface tension is an indicator of foamability, at the least in the two surfactants here.

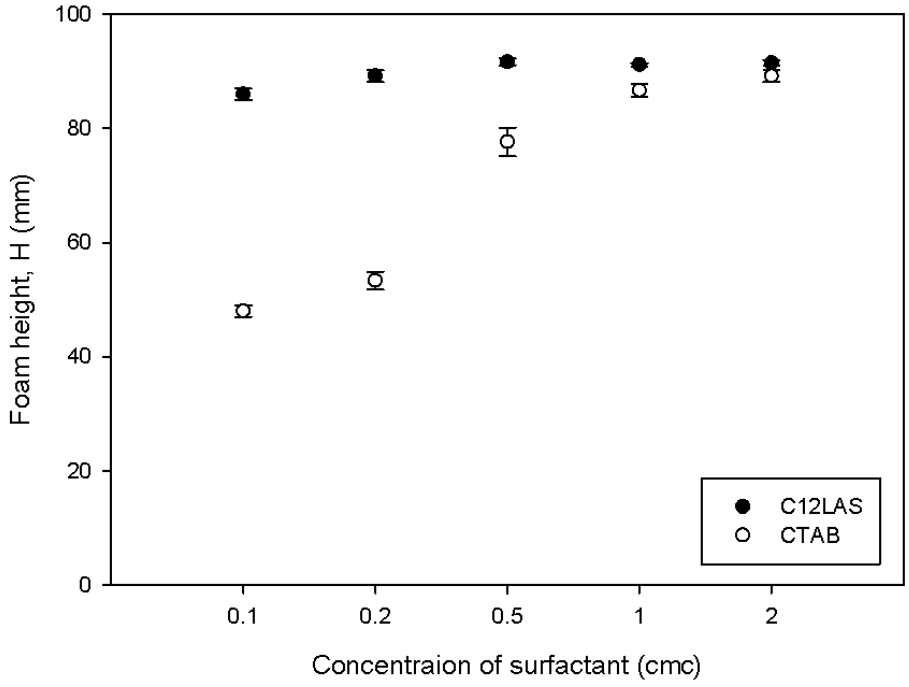

Figure 6.1: Foamability of surfactant solutions: C12LAS and CTAB at various concentrations.

Figures 6.2(a) and 6.2(b) show the liquid levels plotted against time in C12LAS and CTAB foams, respectively. The values of maximum liquid level are all around 40 mm. However, the drainage rate increases with decreasing surfactant concentration. At low concentrations, CTAB foams have a faster drainage rate than C12LAS foams because the surface tension is much higher. A higher concentrations both foams show similar drainage rate.

Figures 6.2(c) and 6.2(d) show foam heights as a function of time in C12LAS and CTAB foams, respectively. In C12LAS foam, the foam curves remain at a plateau for almost one hour; they then start to collapse. The foam breakage rate decreases with increasing concentrations of C12LAS. Contrary to C12LAS foam in CTAB foam, a substantial increase in foamability with increasing concentrations of CTAB was observed. Similarly, foam breakage decreases with increasing concentration. At low concentrations, a short foam life was observed. At high concentrations, the foam breakage rate is much slower and a much longer foam life was found. Foam life for both surfactants at high concentration is about 24 hours. According to the results, the higher the concentration the better

the foamability and foam stability in a surfactant solution and there is no further enhancement either in foamability or foam stability when the concentration is above 1.0 cmc.

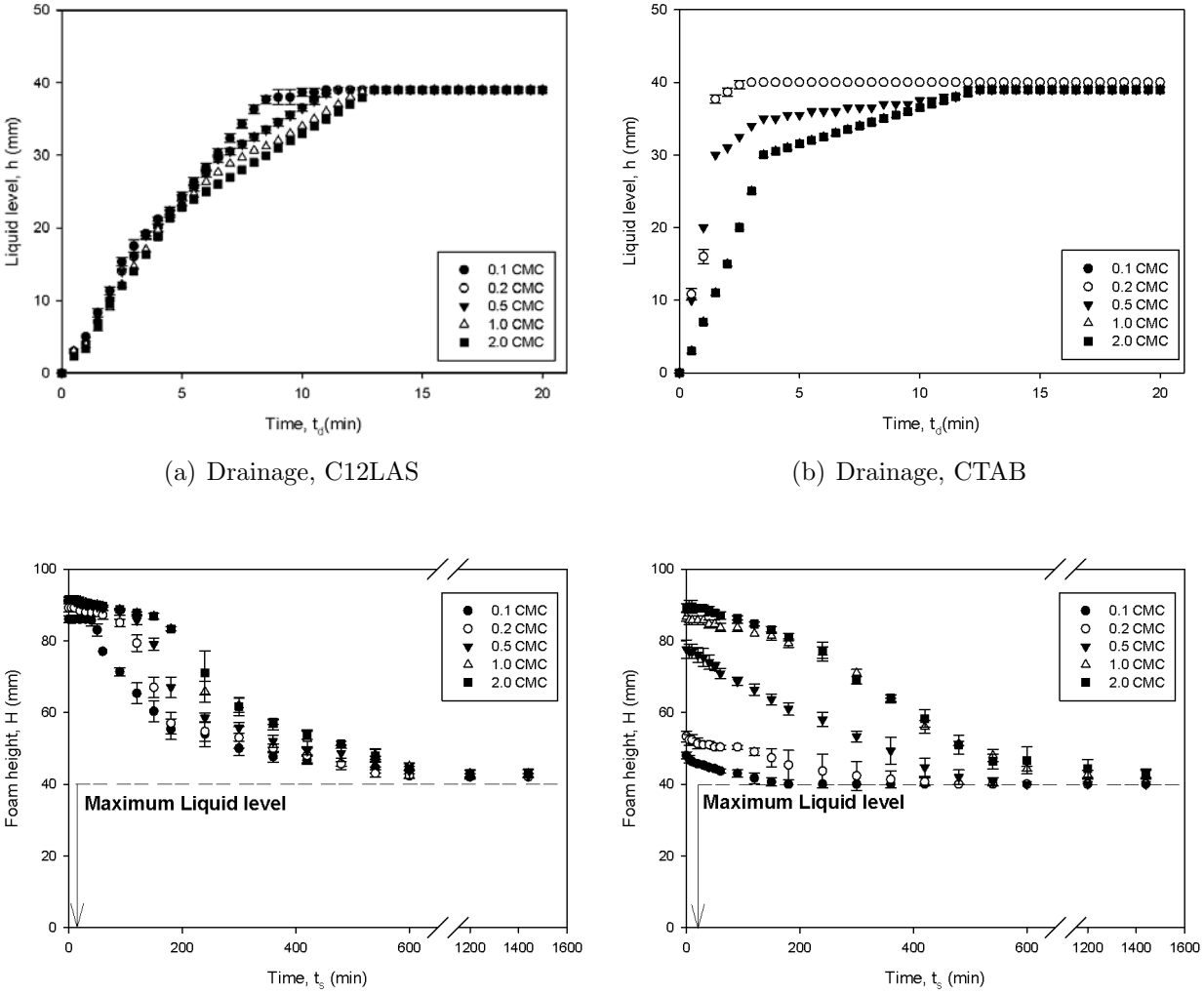

(a) Drainage, C12LAS

(b) Drainage, CTAB

(c) Foam breakage, C12LAS

(d) Foam breakage, CTAB

Figure 6.2: Foam drainage and Foam breakage at various surfactant concentrations.

Foam Microstructure

The bubble size distribution was determined by looking at 200 bubbles in each image. Firstly, the foam microstructure of C12LAS foam was discussed. Figure 6.3 shows the initial bubble size distributions of foams at five different concentrations. A long right hand side tail is found in the initial bubble size distribution at a concentration of 0.1 cmc. The distributions then shift to the left with increasing concentration of surfactant. A narrower bubble size distribution with a shorter tail

to the left of spectrum is observed in the foam at a concentration of 1.0 cmc. However, the bubble size distribution shifts back to the right hand side of spectrum when the concentration increases to 2.0 cmc. The bubble size distributions obtained 5 minutes after foam formation show a less uniform foam at the concentration of 0.1 cmc. More uniform and smaller bubbles are produced at higher concentrations. At 1.0 cmc, the smallest mean bubble size is obtained compared to the foam generated at the other concentrations.

Figure 6.4 shows how the bubble size varies with the foam standing time. The rate of bubble size growth increases first from 0.1 cmc to 1.0 cmc and then decreases at about 2.0 cmc. At all concentrations during the first hour the size of the bubbles grows linearly and then the rate of bubble growth decreases. This is because the bubbles start to burst as observed from the foam collapse experiment. The details of the bubble size distributions are shown in Figure 6.5. The bubble size distributions get broader and shift to the right side as time passes, thus resulting in a bigger and less uniform structure, as exemplified by the foam images shown in Figure 6.6 (these foams are generated by a 1.0 cmc C12LAS solution after 5 minutes, 30 minutes, 60 minutes and 90 minutes standing times).

The statistical parameters to describe the bubble size distribution of foam generated with various concentrations of surfactant C12LAS are summarized in Table 6.2. At 0.1 cmc, the skewness values are positive and much higher than at other concentrations of C12LAS. This indicates the presence of some large bubbles in the foam resulting in the median being smaller than the mean bubble diameter (d_{10}). This corresponds to the initial bubble size distribution previously. At 0.1 cmc the kurtosis immediately after foam formation was highest among all concentrations. This indicates a sharper peak and longer, fatter tails. These sharper peaks and fatter tails indicate a wider range of bubble sizes in the distribution and they also indicate a larger maximum bubble size in comparison to the other distributions at higher concentration. This can also be interpreted as to indicate that there is a large number of smaller bubbles but few larger bubbles in the foam. If the foam immediately after formation is heterogenous, then it leads to a fast rate of bubble size growth.

When the concentration is higher than 0.2 cmc, then the skewness of the bubble size distribution immediately after foam formation is just above zero. This indicates that the median and d_{10} are very

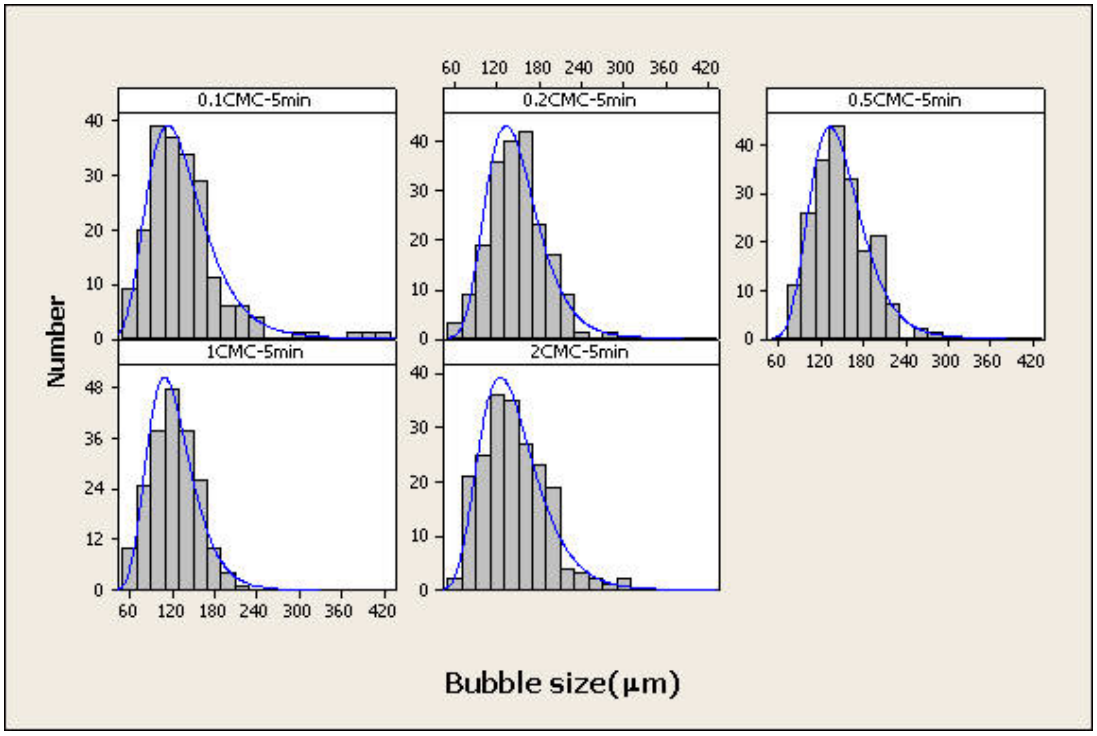

(a) individual

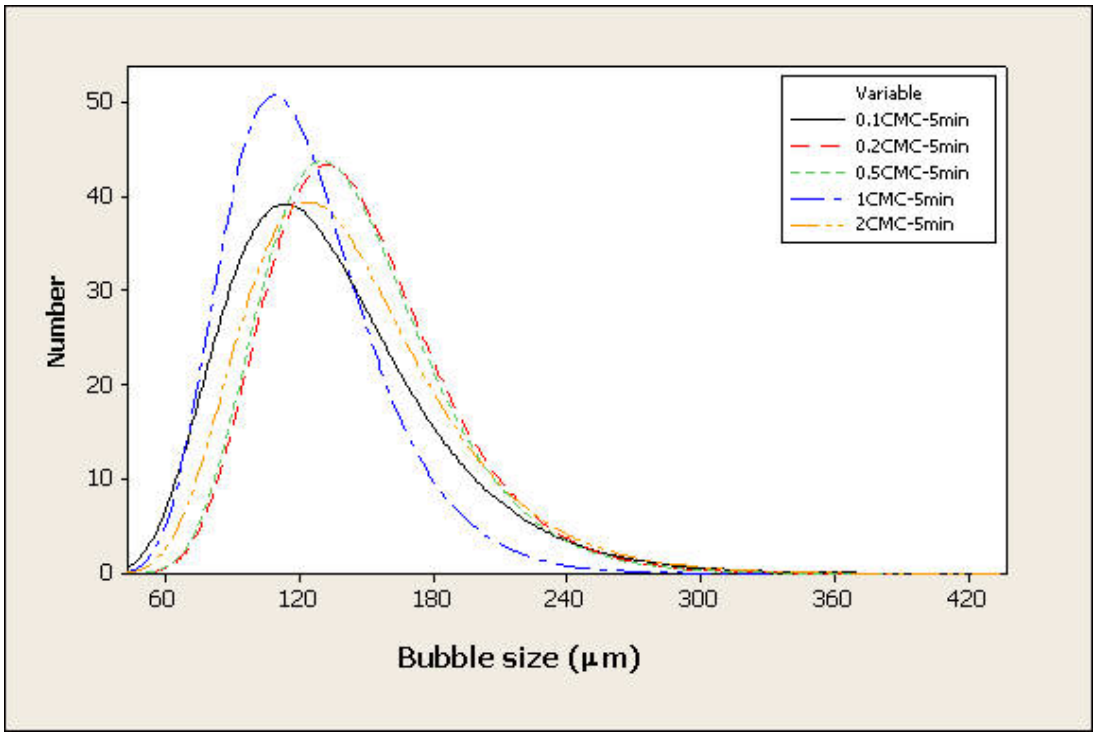

(b) in comparison

Figure 6.3: Bubble size distribution of C12LAS foam at various concentrations at 5 minutes (a) individual distribution (b) distributions in comparison.

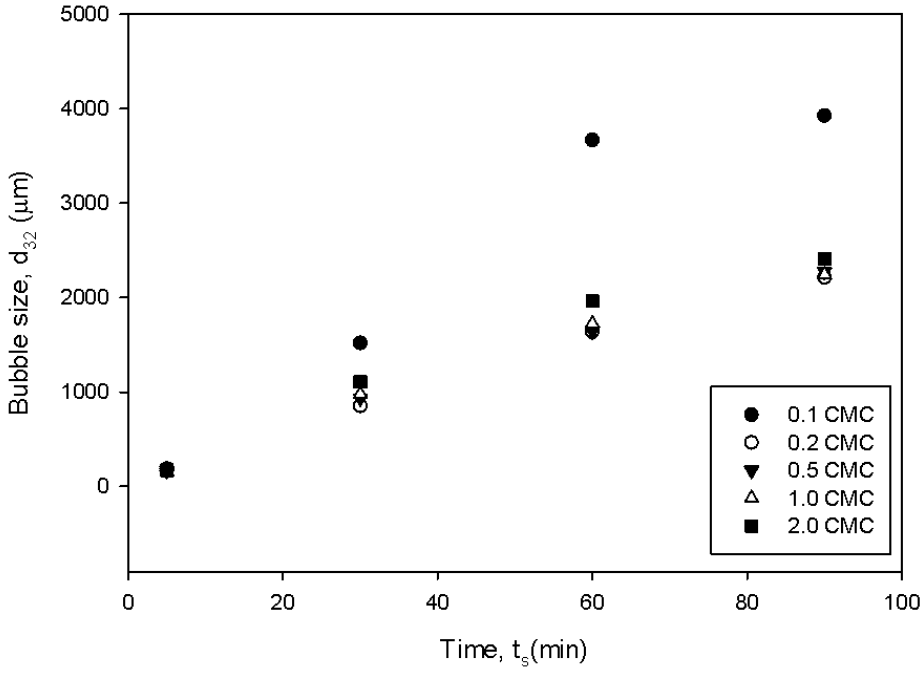

Figure 6.4: Variation of mean bubble size of C12LAS with foam standing time at various concentrations.

Table 6.2: Statistical parameters for foam bubble size distribution of C12LAS foam at various concentrations.

	d_{10}(μm)	d_{32}(μm)	S_t	Min(μm)	M(μm)	Max(μm)	S	K
0.1CMC								
5 min	135.53	186.79	53.01	62.87	127.09	411.65	2.23	8.06
30 min	818.20	1518.08	509.20	178.40	684.90	3572.20	1.75	5.08
60 min	1821.30	3668.55	1330.90	222.70	1542.00	6721.60	1.28	1.75
90 min	1775.00	3927.52	1436.00	251.00	1338.00	6455.00	1.34	1.25
0.2 CMC								
5 min	147.27	165.22	37.16	53.83	146.00	270.09	0.18	0.02
30 min	673.20	852.15	244.90	236.90	636.70	1382.70	0.79	0.35
60 min	1127.20	1637.75	530.40	231.00	1079.40	3869.80	1.09	2.84
90 min	1313.60	2214.06	764.40	233.30	1108.40	5562.40	1.25	3.53
0.5 CMC								
5 min	145.49	166.39	39.05	71.13	140.17	281.04	0.56	0.16
30 min	693.70	935.31	285.30	264.30	644.30	1800.00	1.03	0.91
60 min	1060.70	1647.11	573.80	312.20	914.70	2727.10	0.84	-0.05
90 min	1169.10	2273.47	804.90	208.20	958.40	4902.70	1.39	2.54
1.0 CMC								
5 min	139.50	158.17	36.65	69.22	139.48	241.74	0.32	-0.36
30 min	755.50	976.16	299.70	204.70	721.80	1607.80	0.40	-0.46
60 min	1039.80	1723.46	603.40	211.80	830.00	3729.80	1.08	1.56
90 min	1255.50	2243.96	802.70	210.20	1083.10	4271.40	1.14	1.49
2.0 CMC								
5 min	143.39	171.79	44.82	63.39	137.61	300.96	0.76	0.80
30 min	793.90	1105.18	358.40	226.30	754.50	1909.80	0.73	0.05
60 min	1220.90	1963.66	712.00	183.90	1132.00	3102.40	0.70	-0.10
90 min	1302.50	2409.26	869.80	223.50	1055.10	4853.70	1.16	1.18

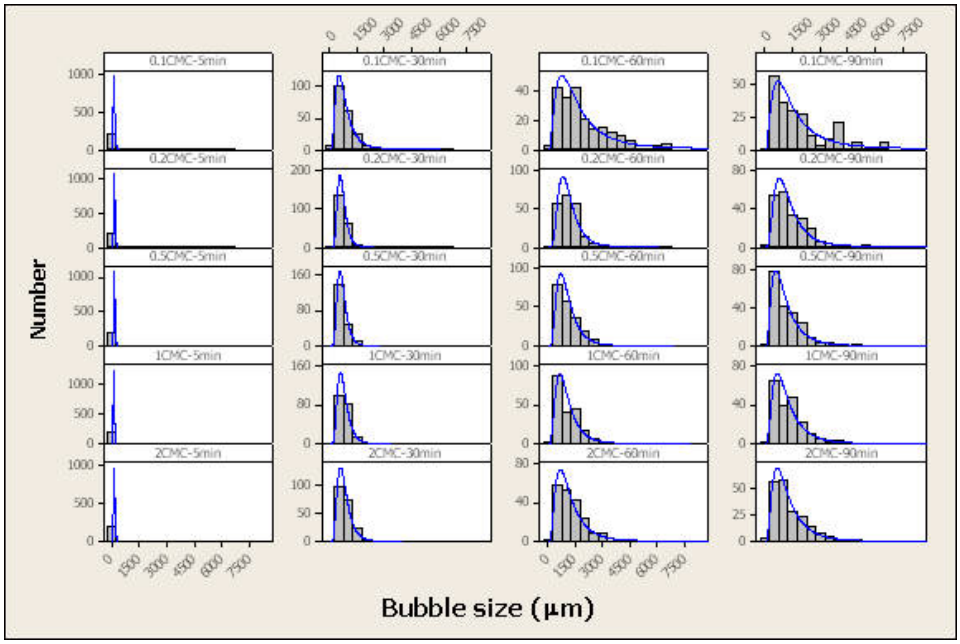

Figure 6.5: Bubble size distributions of C12LAS foam at various concentrations and different foam standing time.

similar and the bubble sizes are uniform. Positive but smaller kurtosis means a rounded peak with shorter and thinner tails. This indicates that the bubbles are more uniform and there are no larger bubbles in the foam. Therefore, a more homogenous foam initially results in a much more stable foam.

In the C12LAS foam microstructure, at a concentration of 1.0 cmc there was the smallest initial bubble size and the slowest rate of bubble size growth among all the concentrations. A possible explanation is that that there is an insufficient amount of surfactant under 1.0 cmc and an excess of surfactant molecules or micelles at 2.0 cmc (as mentioned in the last section).

The slowest bubble size growth was also observed at 1.0 cmc. Generally, when the bubble size distribution is more even, then there is a smaller tendency for disproportionation. This is because the pressure differences between bubbles is small and hence there is little net gas diffusion.

Figure 6.7 shows the mean bubble size, d_{32}, as a function of time at various concentrations in CTAB foam. The statistical parameters are summarized in Table 6.3. A much larger initial mean bubble size was obtained at lower concentrations of surfactant, resulting in faster bubble growth than at higher concentrations. At low concentrations (< 0.5 cmc), the foam collapses within two hours. Again, the same correlation between initial bubble size and rate of bubble size growth was observed

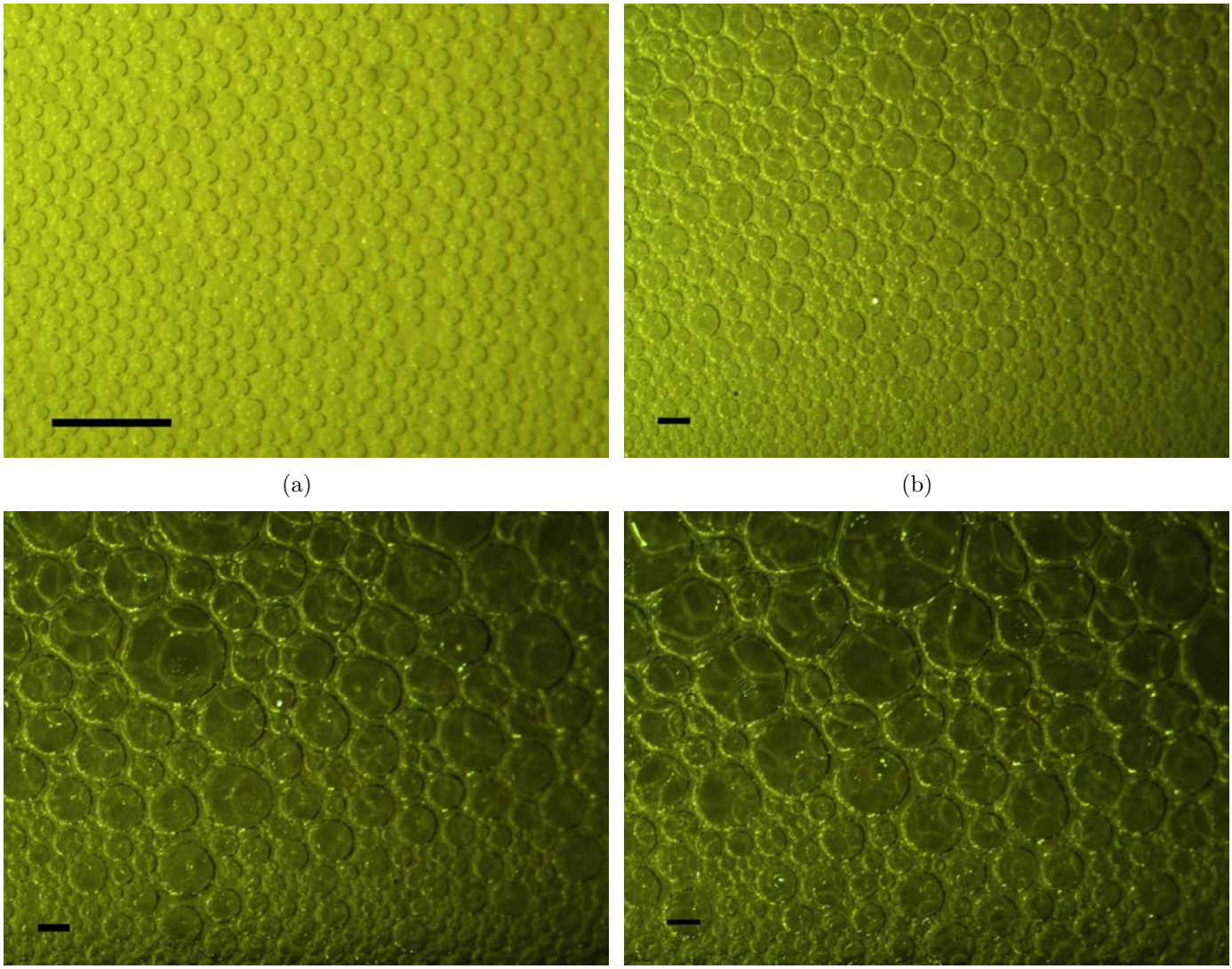

(a) (b)

(c) (d)

Figure 6.6: Foam images of C12LAS foam at concentration of 1.0 cmc at (a) t_s= 5 minutes, (b)t_s= 30 minutes, (c) t_s= 60 minutes, and (d) t_s= 90 minutes (the scale bar=500μm).

as discussed above. At higher concentrations (> 0.5 cmc), much smaller mean bubble sizes were produced and the mean bubble size grows linearly with time. The rate of bubble size growth slows down 1 hour after foam formation as in the case of C12LAS foam.

At lower concentrations (< 0.5 cmc) and 5 minutes after foam formation, the skewness and kurtosis values are positive and also higher than at higher concentrations (> 0.5 cmc). This can be explained in a similar way as in the C12LAS foam (i.e. insufficient surfactant molecules to form smaller bubbles resulting in much larger bubbles in the foam). At higher concentrations (> 0.5 cmc), the skewness values are all positive and very close to zero. The values of kurtosis are initially negative

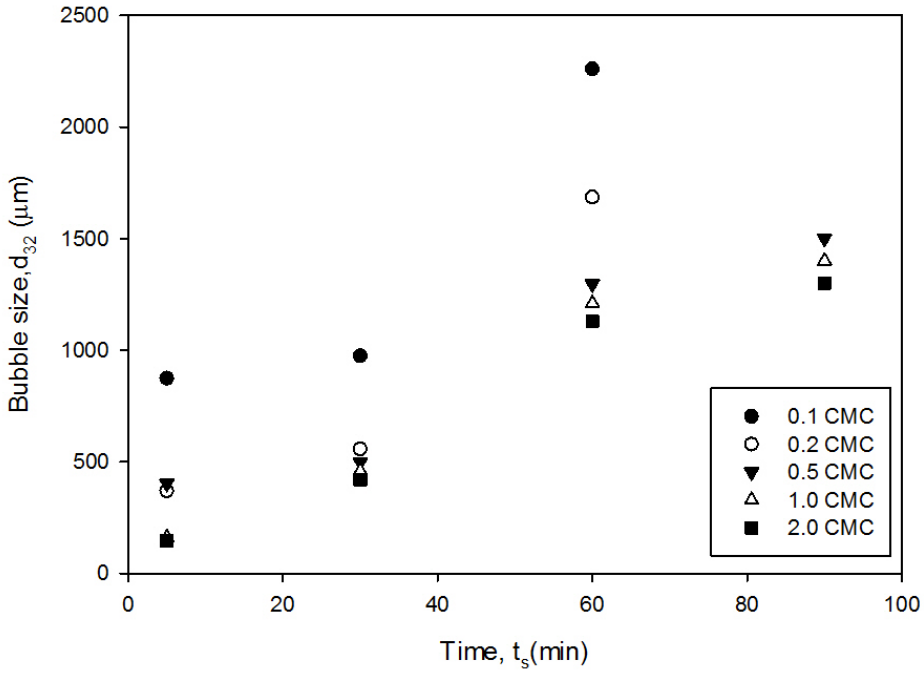

Figure 6.7: Variation of mean bubble size of CTAB foam with foam standing time at various concentrations.

and after some standing time positive kurtosis as observed. However, all the values are near zero which means that the bubble size distributions are very close to the normal distribution.

Foams made from C12LAS and CTAB at various concentrations were studied in this section to determine the optimum concentration in the subsequent experiments. From the measurement of surface tension, Cl2LAS can lower the surface tension with a low concentration (0.1 cmc) and thus it has shown a better foamability and a better foam stability than CTAB. At higher concentrations (1.0 cmc), a similar foamability and stability was found in both foams made with from these two types of surfactants. In C12LAS foam, sufficient foam volume is produced from a concentration of 0.2 cmc to 1.0 cmc. Thus, two C12LAS concentrations were chosen. Firstly, the conditions with the longest foam life (1.0 cmc) were chosen; secondly another less stable concentration (0.2 cmc) was chosen. The reason for choosing a foam with shorter life time is to see whether adding silica can enhance foam life time at this lower concentration. For the other surfactant type, CTAB, only a single concentration was chosen to be compared to C12LAS, namely 1 cmc. The reason for choosing this concentration is that CTAB foams are most stable at 1 cmc.

Table 6.3: Statistical parameters for CTAB foam bubble size distribution at various concentrations.

	d_{10}(μm)	d_{32}(μm)	S_t	Min(μm)	M(μm)	Max(μm)	S	K
0.1 CMC								
5min	603.30	873.91	265.10	257.60	544.90	1761.60	1.80	4.06
30min	999.70	974.40	435.30	327.10	913.90	2636.90	1.14	1.50
60min	1393.50	2259.98	783.80	230.60	1211.20	3544.70	1.07	0.53
0.2 CMC								
5min	329.75	369.71	80.30	161.96	327.25	701.96	0.73	2.01
30min	613.30	557.14	239.40	223.50	583.90	1578.00	0.73	0.48
60min	1161.00	1685.16	574.30	258.80	1141.20	3124.30	0.62	0.29
0.5 CMC								
5min	160.82	401.54	50.62	65.22	159.48	292.70	0.27	-0.70
30min	410.55	497.28	135.54	175.89	396.44	801.92	0.49	-0.35
60min	872.10	1296.10	432.90	214.90	812.70	2737.60	0.95	1.81
90min	1208.60	2455.52	795.50	187.80	973.30	4819.20	1.60	3.47
1.0 CMC								
5min	140.26	161.40	39.93	59.57	141.35	226.78	0.07	-0.67
30min	546.60	458.16	176.40	207.10	546.70	1022.00	0.40	-0.16
60min	805.70	1209.94	405.30	223.50	732.00	2113.70	0.99	0.58
90min	1188.00	2494.24	842.40	272.20	902.90	4488.20	1.28	1.16
2.0 CMC								
5min	126.89	145.99	35.10	59.39	121.78	232.09	0.47	-0.09
30min	505.70	418.14	154.30	211.40	482.90	1027.80	0.55	0.22
60min	771.60	1129.16	374.70	212.20	673.90	2053.30	0.91	0.39
90min	1324.40	2882.87	1029.10	321.20	970.40	5806.70	1.55	2.37

6.2.2 Effect of Particle Concentration and Hydrophobicity

Hudales and Stein (1990) reported that hydrophilic glass particles enhance foam stability with larger particles (> 10 μm) and shorten foam lifetime when the particle size is less than one micron. Two other studies (Deshpande and Barigou, 1999, Wiggers, 2001) found that nano-sized hydrophilic silica particles enhance foam stability. On the other hand, Aveyard et al. (1994) found that spherical hydrophobic particles can stabilize foam, and maximum stability has been observed at a contact angle of $< 90°$. For slightly higher angles however, foam stability falls drastically. The use of particles as foam stabilizer has been summarized by Pugh (1996): (1) For particles where the contact angle is $> 90°$, the particles will bridge between bubble films and cause de-wetting of the interface film, a positive Laplace pressure in the film adjacent to the particle and leads to greater drainage. (2) For particles with a contact angle $< 90°$, the air-solid interfaces keep steady contact angles with the particles and the drainage stops as the Laplace pressure difference reduces to zero. In this section, the effect of addition of both hydrophilic and hydrophobic silica particles in two different charged surfactant stabilized foams is investigated. Four types of silica particles in different hydrophobicity

were used to produce foam by mechanical agitation at various concentrations (see Table 6.1(b) and the details of foam generation method can be found in section 3.3.2).

Foam Formation

In each experiment, foam volumes at different times were determined by measuring the height of the foam generated. During the first 5 minutes the foam drainage change was recorded directly via a digital camera, and foam collapse was measured by monitoring the decline in foam height over time. Two measurements were recorded: h, the liquid level and H, foam height (more details can be found in 3.3.2).

Figure 6.8 shows the foamability of C12LAS and CTAB foams at different concentrations and hydrophobicity of silica. First the results of C12LA foams are presented. Figure 6.8(a) shows that foamability was inhibited by the most hydrophobic silica while other types of silica had nearly no impact on the foamability at 0.2 cmc of C12LAS.

At 1.0 cmc of C12LAS foam, adding silica had also no significant effect on foamability except for the most hydrophobic silica at higher concentration (>1.0 wt%) as shown in Figure 6.8(b). In CTAB surfactant stabilized foam, foamability increases with increasing concentration of R812 particles but decreases with increasing concentration of R202 particles while the effects of hydrophilic and R972 particles were almost negligible, as shown in Figure 6.8(c).

There is no significant variation of the surface tension with the silica concentration. For all concentrations the surface tension remains at about 33.5 mN/m. Very similar results have also been found at C12LAS concentration of 0.2 cmc (the surface tension is around 40.0 mN/m). The observation that the surface tension does not depend on the particle concentration, is in direct correspondence to the independence of the foamability of the particle concentration, as observed in Figures 6.8(a) and 6.8(b).

In the CTAB foaming suspensions, the surface tension is around 40.0 mN/m and it increases slightly when hydrophilic silica are added (see Figure 6.9). Figure 6.9 also shows that the surface tension increases to around 50.0 mN/m when hydrophobic silica are added. When silica are added under these conditions, then the surface tension only increases initially, but remains at a plateau after

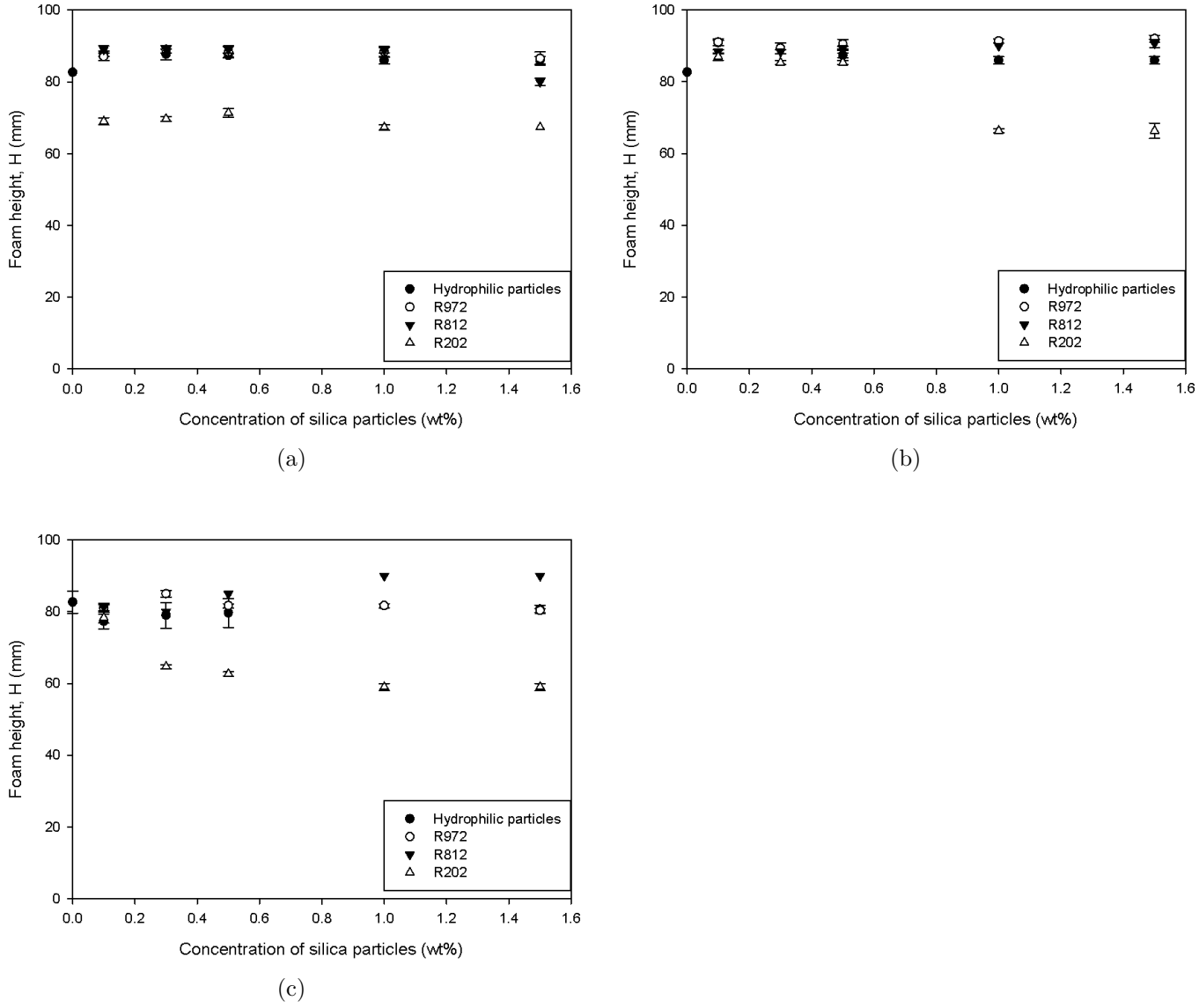

Figure 6.8: Foamability of C12LAS and CTAB foam containing various concentrations of hydrophilic and three types of hydrophobic silica particles (R972, R812, and R202) :(a) C12LAS at 0.2 cmc; (b) C12LAS at 1.0 cmc; (c) CTAB at 1.0 cmc.

reaching 0.5 wt% of hydrophobic silica. This is probably because the hydrophobic silica were not broken down to micron sized aggregates in the CTAB solutions (see the detail in section 4.2.4). Thus, the suspensions of the hydrophobic silica which were used to generate the measurements contained clusters larger than micron size.

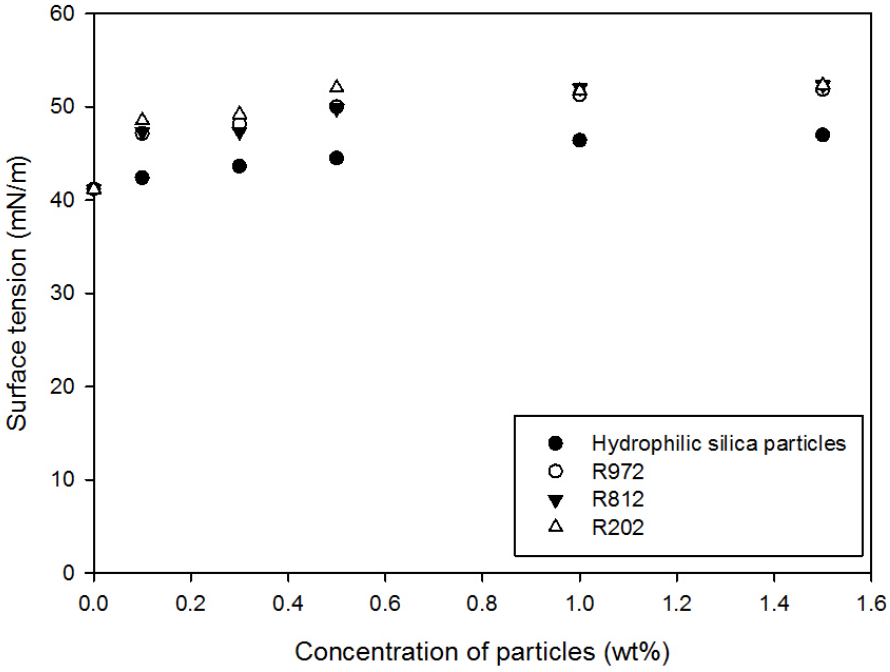

Figure 6.9: Surface tension of CTAB and silica particle suspensions.

Foam Drainage

Liquid levels were plotted as a function of time in Figures 6.10. The drainage curves in this figures shows the data for foam with various concentrations of silica in a C12LAS surfactant foam. The two particle types considered are R812 and R202. The drainage curves were fitted by Equation(3.13); this fit gave the values of a and b. The duration of the experiment depended on the nature of the foam and its stability. Following these drainage curves, the maximum liquid level, a, was obtained by Equation (3.13) (see the details in section 3). The values for all the drainage experiments are summarized in Figures 6.11(a), 6.11(b) and 6.11(c). The graph shows that drainage almost ended during the first 20 minutes after foam formation.

In both concentrations of anionic surfactant, 0.2 cmc and 1.0 cmc, the drainage decreased with increasing concentration of silica. The drainage also decreased with increasing hydrophobicity of silica. Drainage has been significantly reduced by adding R202 particles. In the 0.2 cmc C12LAS foam, the drainage can be reduced by a factor of two in comparison to the foam without silica by adding 1.0 wt% of R202 particles, as shown in Figure 6.11(a). The same drainage reduction can be achieved by adding 1.5 wt% R812 particles. However, there is only a small reduction of drainage

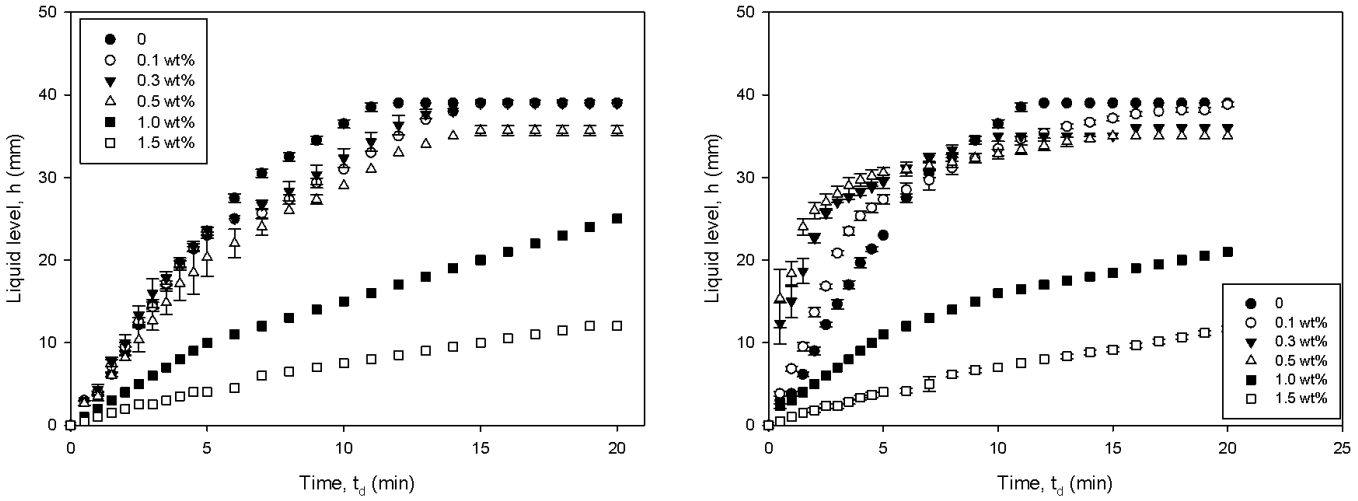

(a) R812 (b) R202

Figure 6.10: Drainage of foam containing R812 and R202 silica particles with 0.2 cmc C12LAS solution.

observed in the foam with a high concentration of hydrophilic silica and partially hydrophobic silica, R972. In the 1.0 cmc C12LAS foam, more silica was needed to reduce the drainage in comparison to at 0.2 cmc C12LAS foam. For example, drainage could only be reduced by adding more than 1.0 wt% R812 particles as shown in Figure 6.11(b). With the most hydrophobic silica, the drainage reduction was smaller, as shown in Figure 6.11(b). Similar as in the case of the 0.2 cmc foam, the addition of hydrophilic silica and R972 particles has no apparent effect on the drainage in comparison to the foam stabilized by only C12LAS surfactant. In the foam stabilized by CTAB, the addition of hydrophilic silica had a negligible effect on drainage. In general, drainage decreased with increasing silica concentration but not with the degree of hydrophobicity of silica. Drainage was significantly reduced by adding R812 particles. R812 particles were the best to slow down the drainage among the three hydrophobic silica, followed by particle R202 and R972.

In this section, both hydrophilic and hydrophobic silica were used for stabilization of C12LAS and CTAB foams. In the foam stabilized by C12LAS at two levels of concentrations, hydrophobic silica showed a limited ability to retard drainage whereas hydrophilic silica had no apparent effect. The result of hydrophilic silica on foams agreed with the studies of Tang et al. (1989) and Deshpande and Barigou (1999). Both studies have reported that addition of hydrophilic silica did not affect foam drainage. This is because the hydrophilic silica are not surface active in the liquid, therefore,

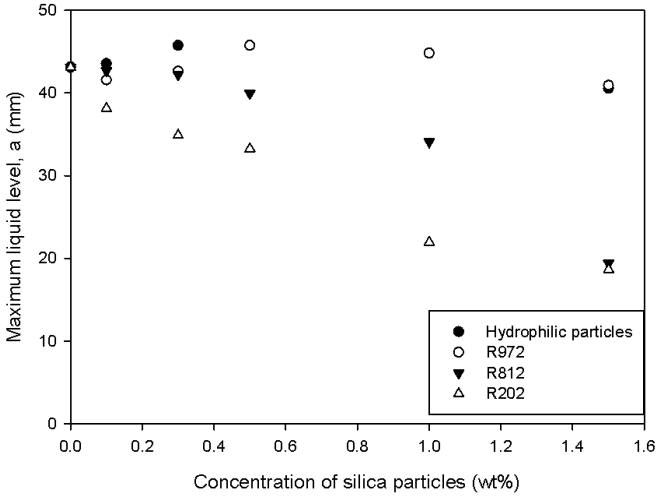

(a) C12LAS at 0.2 cmc

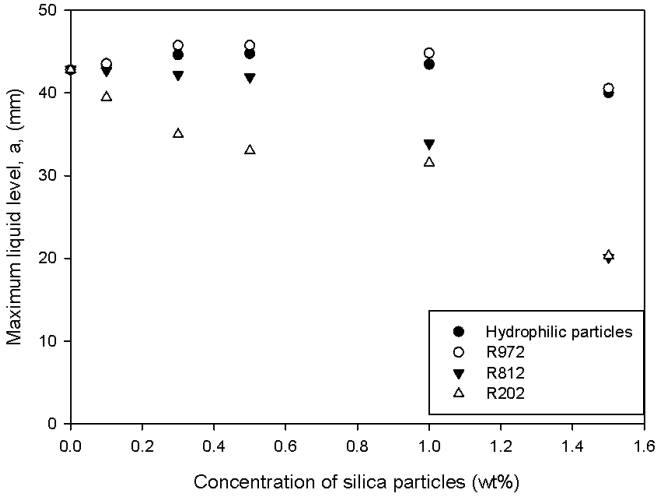

(b) C12LAS at 1.0 cmc

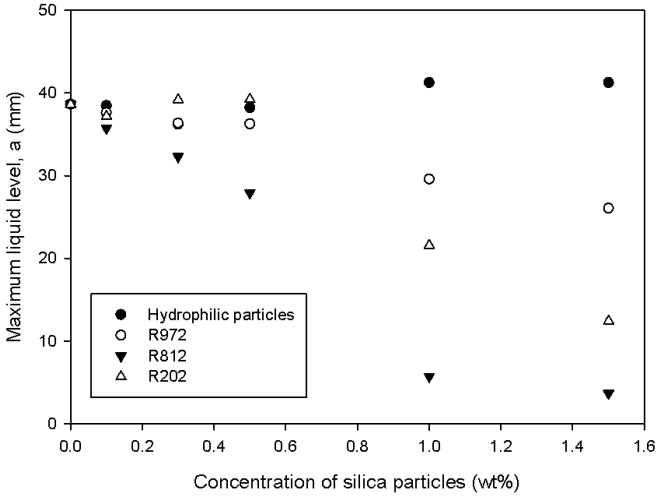

(c) CTAB at 1.0 cmc

Figure 6.11: Drainage of foams containing hydrophilic, R972, R812, and R202 silica particles.

the addition of hydrophilic silica has not much effect on the drainage.

Tang et al. (1989) showed that hydrophobic silica retarded the drainage with increasing hydrophobicity of the silica in the foam produced by sodium dodecyl sulfonate in alkaline aqueous medium. In their study, the concentration of anionic surfactant was varied from 1.0 mM to 2.0 mM which is equivalent to 0.13 - 0.24 cmc. Similar to this study, the hydrophobic silica have also effectively reduced the drainage in foam produced at 0.2 cmc of C12LAS. However, a smaller reduction in drainage was found in the foam produced at 1.0 cmc. The viscosity plays an important role to reduce the drainage. Note that in this study, the viscosity of the dispersions is almost kept constant in this

study as in the study of Tang et al. (1989). Therefore, the stabilization effect on the foam may be attributed only to the hydrophobicity of the silica.

A possible explanation for this effect (i.e. drainage lower at low surfactant concentrations) is as follows: the surfactant molecules adsorb to the interface easier than the hydrophobic particles. This is so because they are smaller. Both surfactant molecules and hydrophobic silica are surface active in the liquid. Adsorption to the interface is a competitive process between the surfactant and the silica. Hence, at lower concentrations of surfactant, there will be more silica at the interface, allowing the particles to form network. This as a reason which has been identified for stability in particle foams. Therefore, more surfactant molecules adsorption on the interface actually increase the drainage because the foam was less stable. This is also in agreement with Alargova et al. (2004) who found that the addition of SDS lead to destabilization of foam stabilized by polymer microrods.

In foam stabilized by CTAB, addition of hydrophilic silica has no apparent effect on reducing the drainage. However, the drainage reduced with increasing hydrophobicity and with increasing silica concentration was observed; see Figure 6.11(c). The highest foam stability was observed at 1.5 wt% of R812 particles. At this concentration the drainage is reduced by a factor of ten. At the same concentrations, R202 and R972 particles reduced the drainage by a factor of 4 and 1.5, respectively. It has to be noted here again that R812 is the moderately hydrophobic silica of three types of silica. Unlike the silica in C12LAS foam, the rate of drainage reduction decreases with increasing hydrophobicity of silica.

One possible explanation for this is that the CTAB surfactant molecules modify the partially hydrophobic particle by attaching to them. Among these three types of hydrophobic silica, the combination of CTAB and moderately hydrophobic silica can produce a more stable foam. Another possible explanation is that the viscosity or rigidity of the interfaces increases with the concentration of the silica. An increasing viscosity causes a slower drainage and a rigid interface can also reduce film drainage. This is also the reason for the reduced foamability when there is a higher concentration of the silica in the foams because of increasing viscosity. However, in these cases no meaningful measurement of the bubble size is possible because of the large clusters in the CTAB dispersions (see details in Chapter 4).

Foam Collapse

In many applications, the effectiveness of a foam is related to its stability, that is foam drainage and collapse. Figures 6.12 and 6.13 show foam height as a function of time at various hydrophobicities of particles at 0.2 cmc and 1.0 cmc C12LAS, respectively.

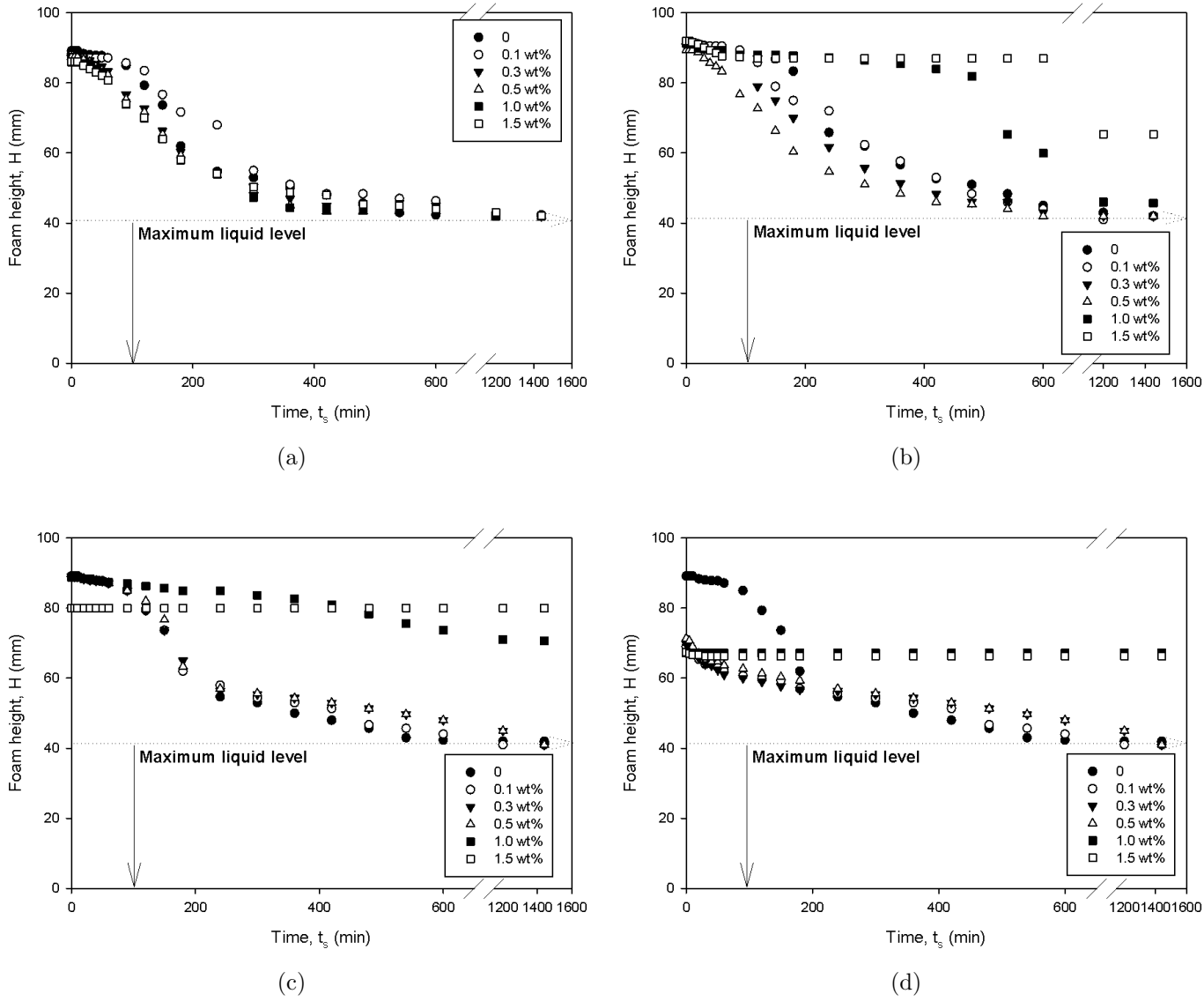

Figure 6.12: Stability of 0.2 cmc C12LAS foam containing (a) hydrophilic; (b) R972; (c) R812; and (d) R202 silica particles.

For 0.2 and 1.0 cmc C12LAS, Figures 6.12(a) and 6.13(a) respectively plot the foam height against time for different concentrations of hydrophilic silica. At 0.1 wt%, a more stable foam was found in comparison to the foam generated of C12LAS only. Above 0.3 wt%, the rate of foam breakage

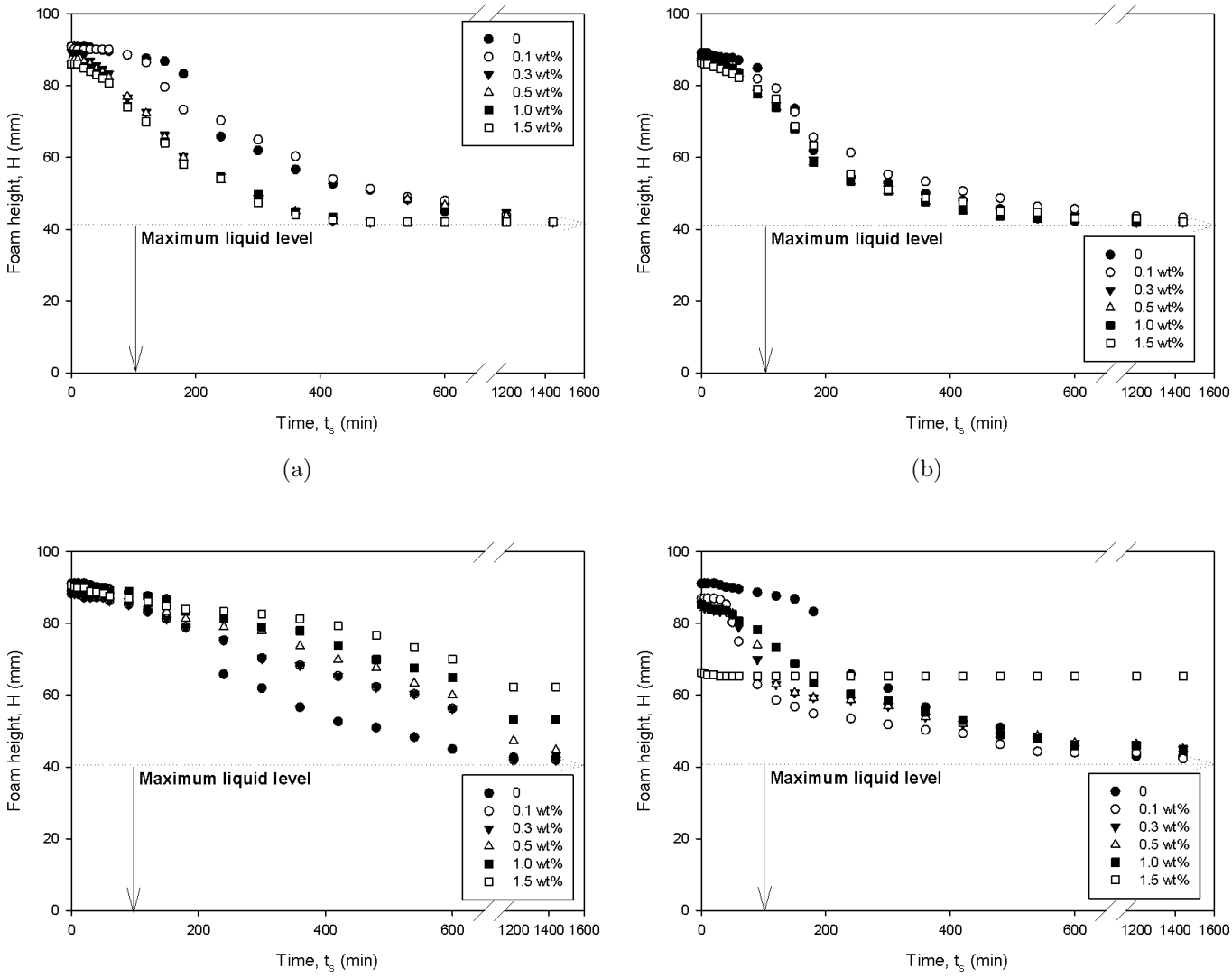

Figure 6.13: Stability of 1.0 cmc C12LAS foam containing (a) hydrophilic; (b) R972; (c) R812; and (d) R202 silica particles.

increases with addition of particles. These observations are independent of the concentration of C12LAS.

Figures 6.12(b) and 6.13(b) show the foam height against time in the foam with addition of R972 particles, at 0.2 and 1.0 cmc C12LAS, respectively. At 0.2 cmc, the rate of foam breakage increases with increasing concentration of silica from 0.1 to 0.5 wt% while there is no foam breakage observed at concentrations of 1.0 and 1.5 wt% silica during the first few hours of foam life. At 1.0 cmc, a more stable foam was observed at 0.1 wt% silica, but a less stable foam was found at higher concentration.

Figures 6.12(c) and 6.13(c) show the foam height against time in the foam with R812 particles, at 0.2 and 1.0 cmc C12LAS, respectively. At 0.2 cmc, the foam curves overlap and foam collapse happens at the same time at low concentrations of silica (0, 0.1 to 0.5 wt%). At high concentrations of particles (1.0 to 1.5 wt%), the foam life is about 5 days, while at lower particle concentrations foam life times are only 12 hours. At 1.5 wt% the foam volume is much smaller than at the other particle concentrations which were considered; however, at this concentration there was no foam collapse found during the first day. At 1.0 cmc, the rate of breakage decreases with increasing concentration of silica. Figures 6.12(d) and 6.13(d) show the foam height against time in the foam with R202 particles, at 0.2 and 1.0 cmc C12LAS, respectively. At 0.2 cmc, the addition of silica reduces the foamability and the foam volume was two third of C12LAS only foam at all particle concentrations. The rate of foam breakage decreases with increasing concentration of silica. There was no foam collapse found at 1.0 and 1.5 wt% within 5 days while C12LAS only foams collapse completely 10 hours after foam formation.

At 1.0 cmc, a reduction of foamability with increasing concentration of silica was also found. When the concentration of silica was varied from 0.1 to 1.0 wt% then the foam height reduced by ten percent; a further increase of the particle concentration to 1.5 wt% led to an initial foam height of about two thirds of the foam without silica.

However, when the concentration of surfactant is low (0.2 cmc), then the reduction of initial foam height when silica are added is much smaller. For a very low particle concentration of 0.1 wt % the initial foam height drops from about 90 mm to 70 mm. When more silica is added the initial foam height remains stable. However, even though the initial foam height appears independent of the particle concentration, the foam stability is not. When the particle concentration is below 1.0 wt% then a faster rate of foam breakage was observed than in the C12LAS only foam. When the particle concentration is 1.5 wt% then the foam shows no collapse during the first day and the total foam life time is 5 days.

In Figure 6.14, foam height is plotted as a function of time at 1.0 cmc CTAB with hydrophilic and hydrophobic silica. In general, at any concentration silica significantly reduce the rate of foam breakage in CTAB foam. With hydrophilic silica, the rate of foam breakage decreases with increasing

concentration of silica as shown in Figure 6.14(a). In Figures 6.14(b), 6.14(c) and 6.14(d), there is no foam breakage when the concentration of silica is over 0.3 wt% and foam life is about one month.

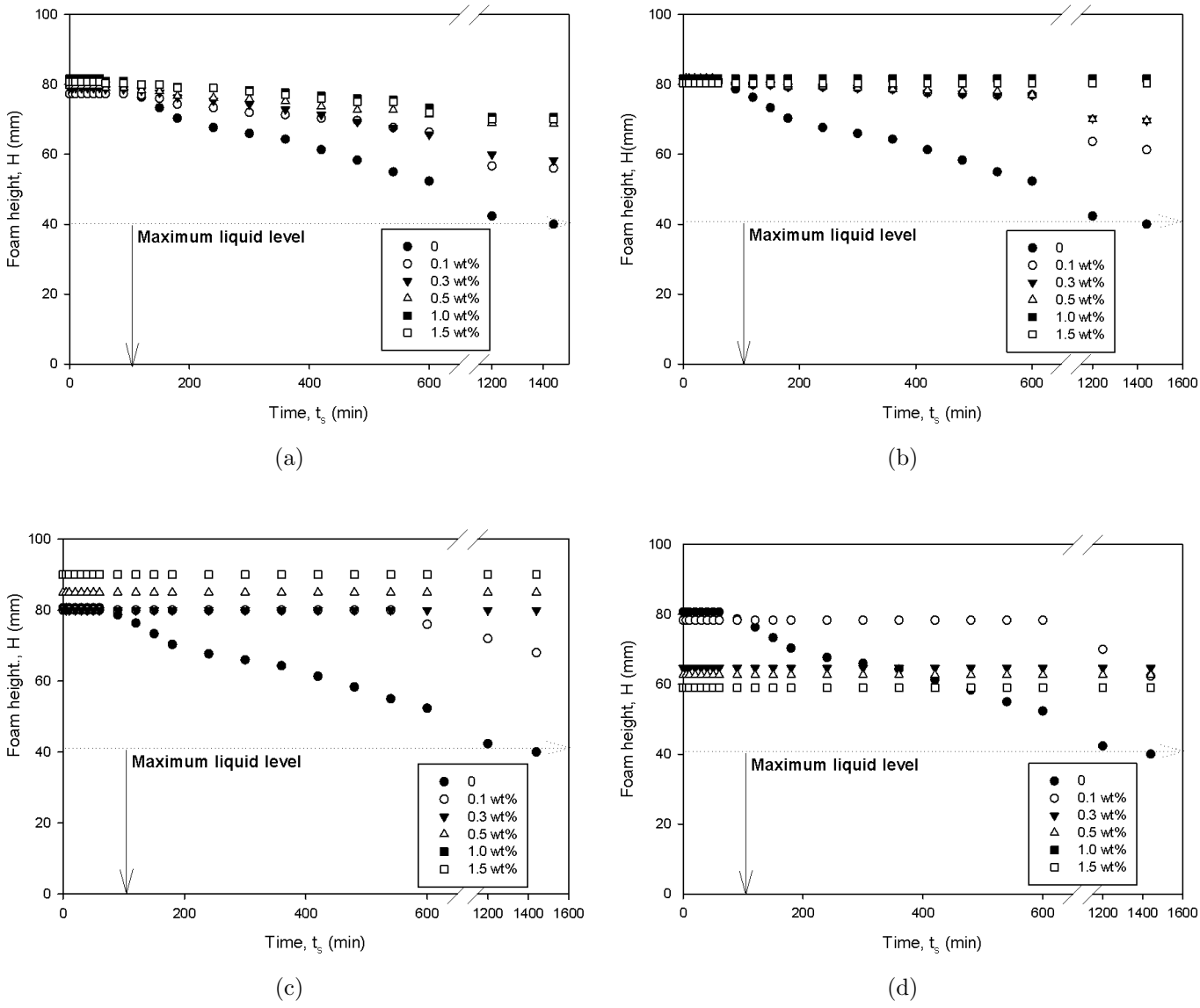

Figure 6.14: Stability of 1.0 cmc CTAB foam containing (a) hydrophilic; (b) R972; (c) R812; and (d) R202 silica particles.

In the foam stabilized by the anionic surfactant (C12LAS), the hydrophilic silica enhance foam stability only at the lower concentration of silica and only slightly. It has been previously reported that a small amount of silica can stay in the foam film and slow down drainage (Pugh, 1996). This decrease of drainage has been used as an explanation for the increased foam stability, when

hydrophilic silica are added. However, there is no reduction of drainage in this experiment, but there is an increase in foam stability in terms of a slower foam collapse, which suggests that there is another explanation for the increase in foam stability as hydrophilic silica are added. A possible explanation is that the hydrophilic silica form a network and hence these aggregates of hydrophilic silica hold the structure of the foam after the drainage is equilibrium.

At lower concentrations, hydrophobic silica act as an anti-foaming agent, but more stable foams are produced at higher concentrations of silica. A possible explanation is that the partially hydrophobic silica are surface active and possess negative charges in the solution. At lower concentrations of silica, the hydrophobic silica compete with the anionic surfactant to stabilize bubbles resulting in lower foam stability at low particle concentration. At higher concentrations, however, the hydrophobic silica take over the surfactant molecules and the foams are only stabilized by particles (without contribution of the surfactant) resulting in extra stable foams.

In cationic surfactant foams (CTAB), the addition of silica always enhances foam stability. Silica particles posses a negative charge and CTAB molecules hold positive charges in the dispersion. Thus, CTAB molecules can attach to particles and modify the surface of particles increasing the hydrophobicity. The addition of silica delays foam collapse because the particles adsorb at the interface and pack closely, thus, making the interface rigid and able to retain sufficient liquid in the foam films. Therefore, silica particles provide another stability mechanism for the foam stabilized by CTAB foam.

Foam Microstructure

In this section, the effects of four different types of silica on the microstructure of foams stabilized by C12LAS and CTAB will be presented. First, the effects on the foam stabilized by a lower concentration of C12LAS (0.2 cmc) and a higher concentration (1.0 cmc) with the addition of the silica are shown. Secondly, the results of the effects on the foam stabilized by CTAB are discussed.

Figure 6.15(a) shows the mean bubble size of foam plotted against the concentration of silica 5 minutes after foam formation in 0.2 C12LAS foam. Under 1.0 wt %, addition of silica do not show significant effects on the mean bubble size, d_{32}, except for R202 and R972 particles more than 1.5

wt%. In this case, d_{32} decreases with increasing concentrations. The mean bubble size is reduced from about 160 to under 50 μm when the particle concentration reaches 0.3 wt%. At a concentration of 1.5 wt%, a much bigger bubble size ($\approx$ 220 μm) is found in the foam with the R972 particles while a much smaller bubble size ($\approx$ 50 μm) is obtained in the foam with R812 and R202 particles. The hydrophilic silica do not affect the bubble size at 1.5 wt%.

Below, the bubble size distributions are shown. A number of observations can be made: the bubble size is significantly reduced at 1.0 and 1.5 wt% of R812 particles compared to other concentrations as shown in Figure 6.16. At lower concentrations ($<$ 1.0 wt%) of R812 particles there are broader bubble size distributions with higher mean bubble sizes. When the concentration is $>$ 1.0 wt% the bubble size distributions move to the left of the spectrum as time passes and also get narrower. After 4 hours standing time, at concentrations $< 1.0wt\%$, the maximum bubble size is about 5000 μm. For concentrations $>$ 1.0 wt%, the bubble size range from few μm to about 100 μm as shown in Figures 6.17(a) and 6.17(b). The images of foams with 1.5 wt% of R812 particles show the evolution of bubble structure in Figure 6.18. 5 minutes after foam formation the bubbles were separated well by thick liquid films. The bubbles still moved up in the bottle due to the liquid still draining away from the foam films. Once drainage has stopped, the air in the smaller bubbles diffuses to larger bubbles as shown in the foam images of 6.18(b) and 6.18(c) which were respectively taken 30 and 60 minutes after foam formation. Four hours after foam formation the largest bubbles start to burst, which results in a smaller mean bubble size and a more uniform bubble size distribution as shown in foam image 6.18(d). The images for 1.0 wt% silica are similar.

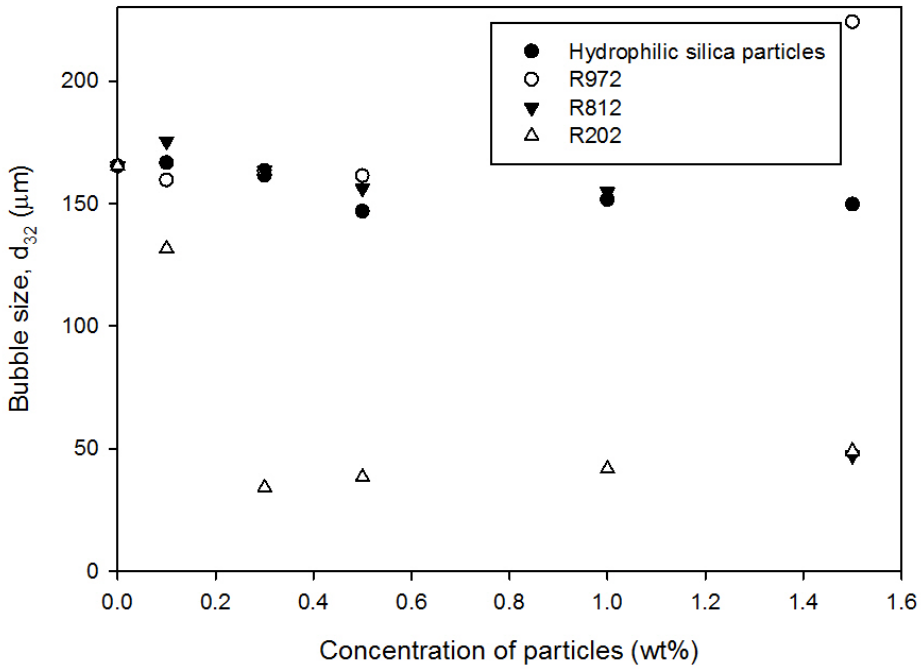

(a)

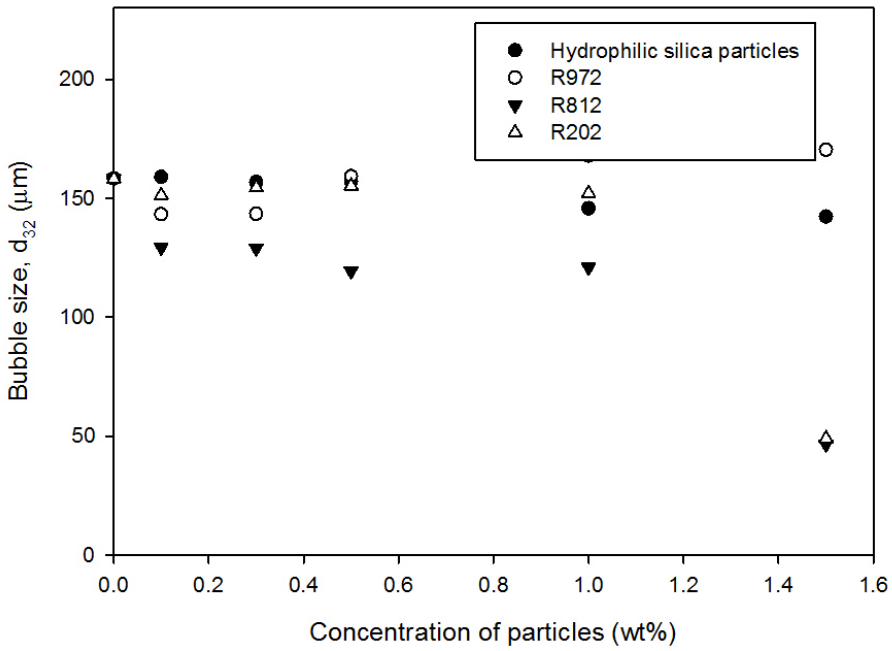

(b)

Figure 6.15: Variation of mean bubble size in foams containing four different types of silica particles after 5 minutes foam formation: (a) 0.2 cmc; (b) 1.0 cmc; C12LAS.

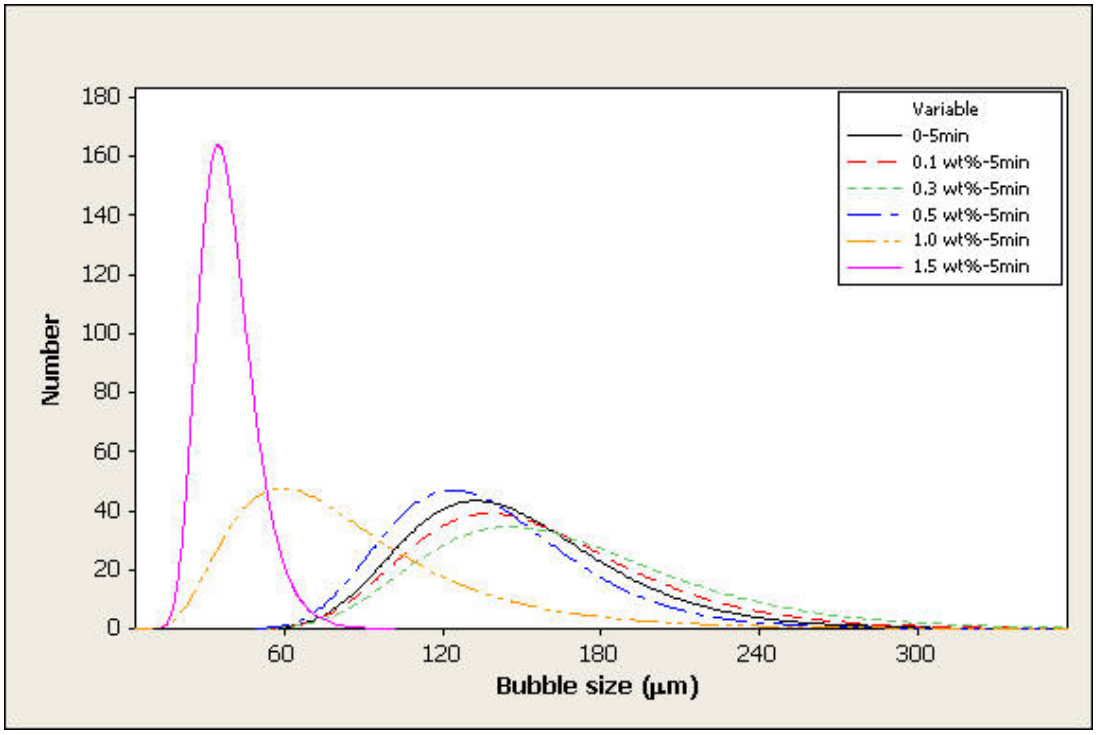

Figure 6.16: Bubble size distribution of foam with addition of R812 silica particles after foam formation 5 minutes.

The d_{32} of foam made from surfactant only is around 150 µm, whereas in the foam with silica it is around 50 µm. In the case of higher concentrations of silica the bubble sizes is about 50 µm which suggests that the foam is mainly formed by particles and the surfactant has a minor contribution. In the foam with R202 particles, similar bubble size distributions to the foams with R972 and R812 particles were observed but fewer particles were needed to reduce the bubble size.

The statistical parameters to describe the bubble size distributions of foam with addition of four types of silica particles in different concentrations are summarized in Tables 6.4. These parameters are used to support the results which are presented above. Hydrophilic and R972 particles have a small effect on inhibiting the bubble size growth when the concentration of C12LAS is low, but have no effect at all at higher concentrations of C12LAS. The bubble size has no clear effect on the foam lifetime.

Skewness and kurtosis are close to zero 5 minutes after the foam has been generated. The values for the foam with addition of silica are very similar to the foam without addition of silica. This indicates that the foam bubbles evolve with time and the addition of these two types of silica has no significant effect on the stability of the foam microstructure. This is different in the foam made

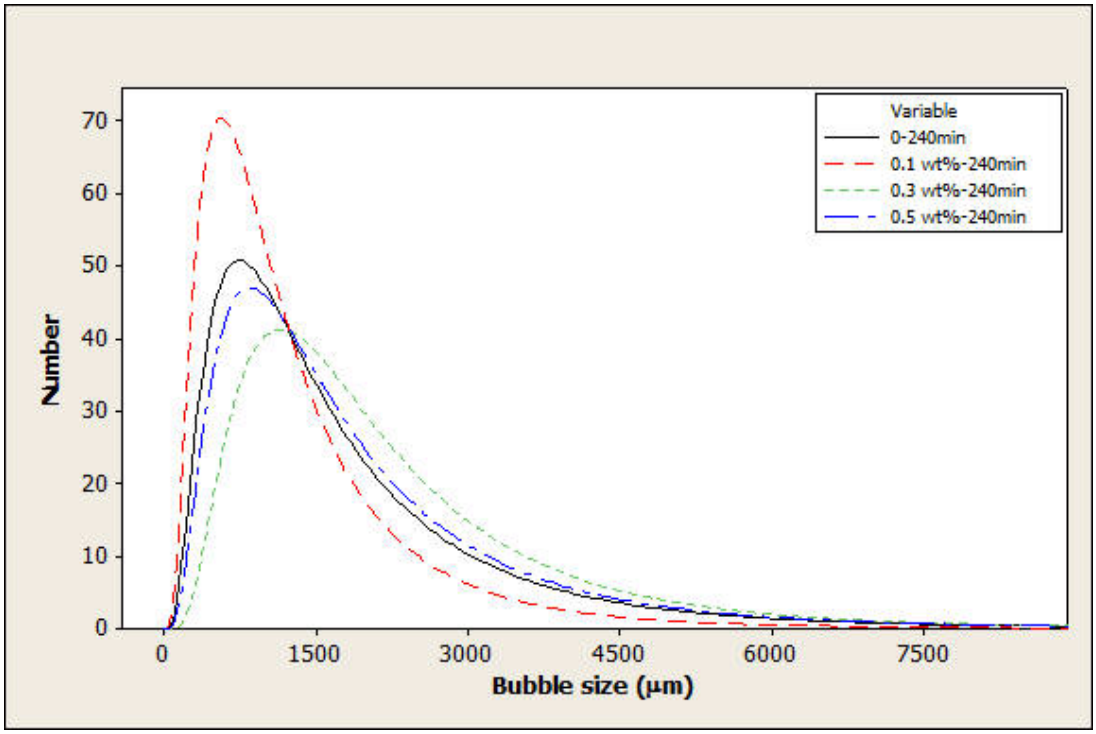

(a)

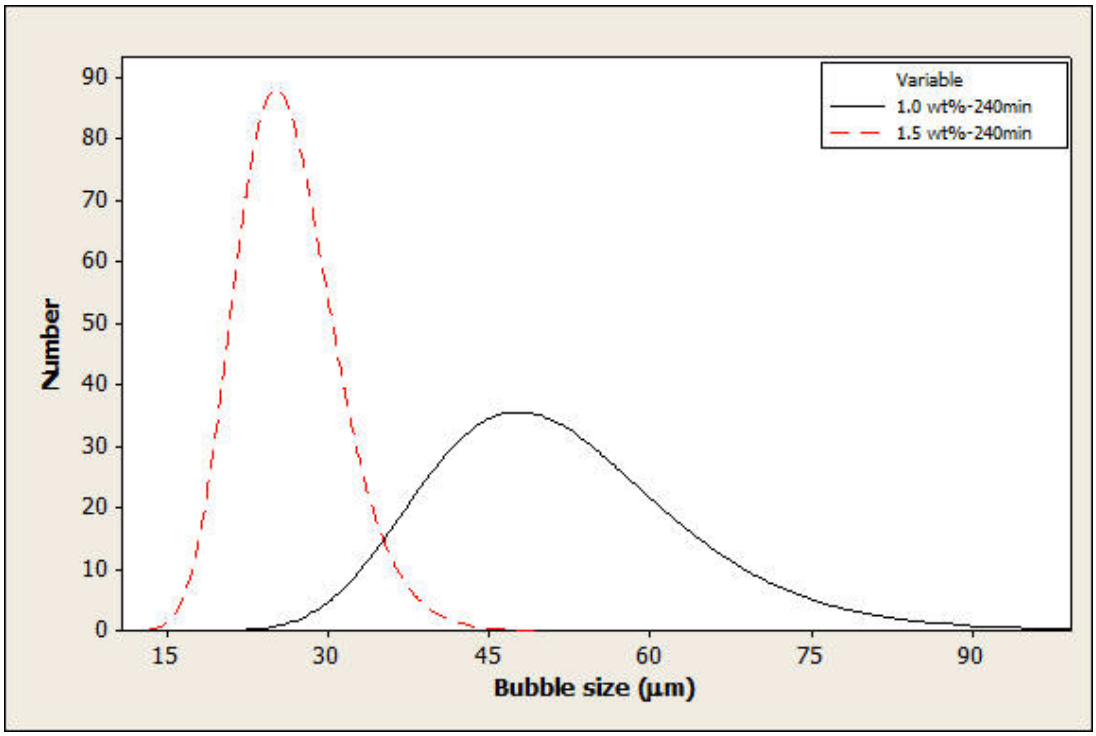

(b)

Figure 6.17: Bubble size distribution of foam with addition of R812 silica particles: (a) after foam formation 240 minutes; 0, 0.1, 0.3, 0.5 wt% (b) after foam formation 240 minutes; 1.0 and 1.5 wt%.

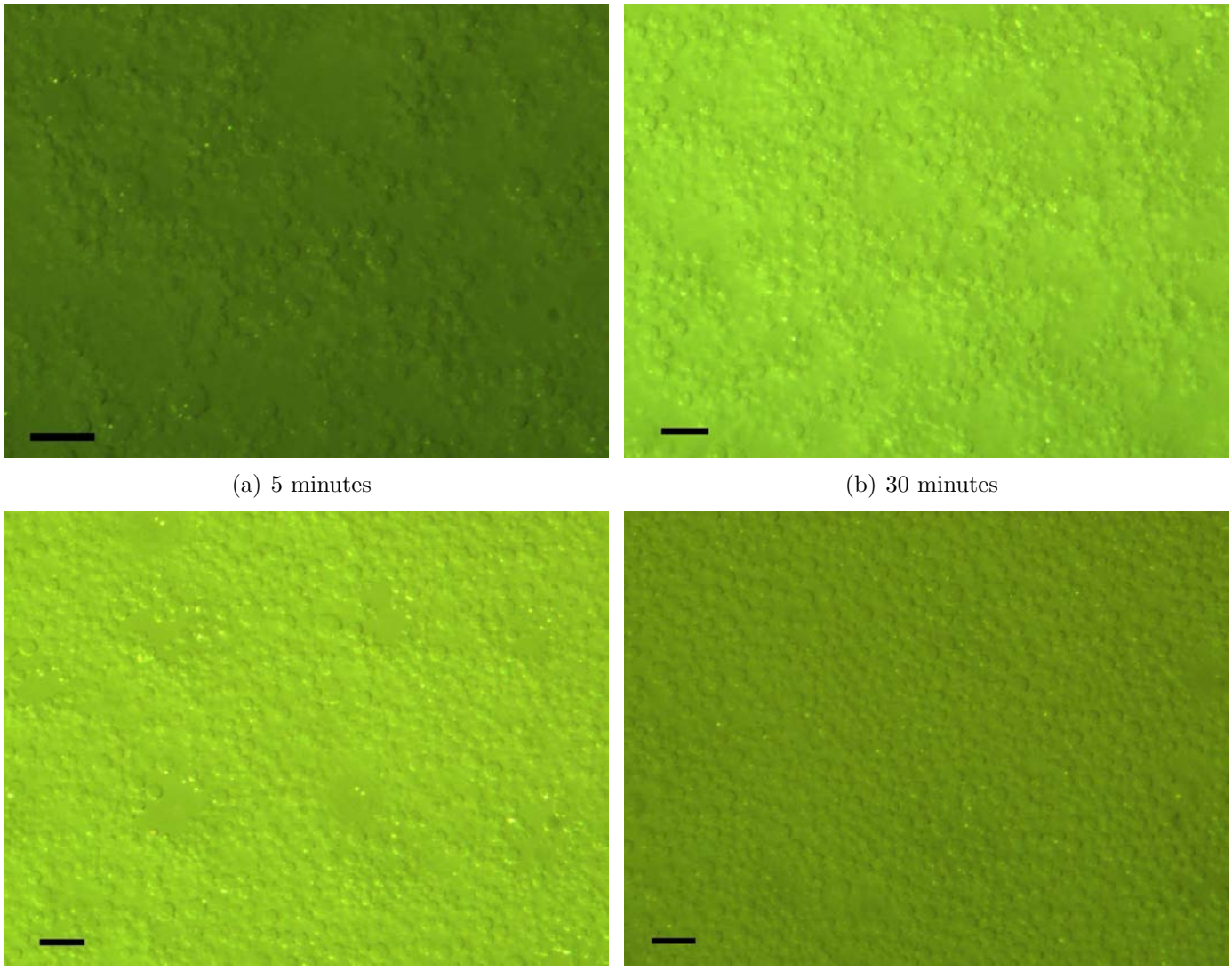

(a) 5 minutes

(b) 30 minutes

(c) 60 minutes

(d) 240 minutes

Figure 6.18: Foam images: 0.2 cmc C12LAS foam with 1.5 wt % R812 silica particles; scale bar=100 μm.

with higher concentrations of R812 and R202 particles. In these case much smaller d_{32}, minimum, maximum and medium bubble sizes were obtained and these values remained constant over time. There is no bubble growth and the foam life is longer. In these distributions, slightly higher skewness and kurtosis were found 5 minutes after foam formation. However, the skewness and kurtosis decrease with time. This indicates that with the addition of these two types of silica the mean bubble size growth decreases while the minimum bubble size increases and the maximum bubble size maintains the same value.

Figure 6.15(b) shows d_{32} plotted against particle concentration 5 minutes after foam formation

in 1.0 cmc C12LAS. In this case, R812 particles can reduce the bubble size from 160 to 120 μm at 1.0 wt% of silica while the rest of the particles has less effect on the bubble size. d_{32} reduces to 50 μm at a concentration of 1.5 wt% with R812 and R202 particles.

The results obtained from the foam stabilized by 1.0 cmc C12LAS with addition of silica show a pattern similar to 0.2 cmc. The differences between these foams stabilized by different concentration of C12LAS are: firstly, hydrophilic and R972 particles do not slow down the bubble growth; secondly, with hydrophobic silica a higher concentration is required to produce a more stable foam. More detail on the foam microstructure of foam at 1.0 cmc C12LAS foam will be presented in below.

The effects of both hydrophilic and hydrophobic silica on the foam produced by the anionic surfactant, C12LAS, have be presented and discussed. Next the effect of these four types silica on the foam microstructure in the foam produced by the cationic surfactant, CTAB, will be presented and discussed in detail.

The mean bubble size of CTAB foam plotted against the concentration of silica 5 minutes after foam formation is shown in Figure 6.19. With addition of hydrophilic silica, the initial mean bubble size first decreases and then increases with increasing concentration of silica. With addition of R972 and R812 particles, the initial bubble size first increases and then decreases with increasing concentration of silica. In R972 particle foam, the mean bubble size increases from 160 to around 200 μm when the particle concentration increases from no particles to 0.5 wt%. It then reduces to around 90 μm when the particle concentration reaches 1.0 wt%. A larger mean bubble size increase was observed in R812 particle foam, the mean bubble size increases from 160 to around 225 μm when the particle concentration is from no particles to 0.3 wt%. Then the mean bubble size reduces to around 45 μm when the particle concentration reaches 1.0 wt%. In R202 foam, the mean bubble size decreases as the silica concentration increases from no particles to 0.5 wt%. However, there is no measurement when the particle concentration is over 1.0 wt% due to poor foam texture.

The statistical parameters of the bubble size distributions of foams with four types of silica in different concentrations are summarized in Table 6.5. In the foam with hydrophilic silica, the initial bubble size decreases when the particle concentration is over 0.5 wt%. However, the hydrophilic silica have no significant impact on the rate of bubble size growth. With R972 particles, the initial mean

Table 6.4: Statistical parameters for bubble size distribution of 0.2 cmc C12LAS foam with: (a) hydrophilic, (b) R972, (c) R812, and (d) R202 silica particles.

(a)

	$d_{10}(\mu m)$	$d_{32}(\mu m)$	S_t	Min(μm)	M(μm)	Max(μm)	S	K
only C12LAS								
5min	147.27	165.22	37.16	53.83	146.00	270.09	0.18	0.02
30min	673.20	852.15	244.90	236.90	636.70	1382.70	0.79	0.35
60min	1127.20	1637.75	530.40	231.00	1079.40	3869.80	1.09	2.84
240min	1862.00	5767.84	1552.00	313.00	1178.00	7280.00	1.38	1.42
0.1 wt%								
5min	149.31	166.52	36.88	62.61	145.22	239.13	0.06	-0.39
30min	534.60	715.00	223.60	171.80	490.70	1217.30	0.67	-0.15
60min	868.90	1469.02	505.80	267.80	687.10	2722.70	1.28	1.15
240min	2019.00	4994.98	1856.00	254.00	1176.00	7873.00	1.41	1.43
0.3 wt%								
5min	143.42	161.50	35.00	56.61	141.87	319.91	1.05	3.34
30min	545.50	757.05	241.20	183.80	492.60	1343.80	0.87	0.31
60min	945.00	1426.39	502.10	242.70	814.10	2469.40	0.90	0.07
240min	2025.00	4453.04	1575.00	254.00	1894.00	9529.00	1.22	3.32
0.5 wt%								
5min	131.94	146.77	31.26	63.39	130.04	240.26	0.53	0.44
30min	536.70	732.29	222.80	147.10	498.00	1435.30	1.19	2.07
60min	777.30	1166.94	408.20	187.10	705.60	1774.50	0.63	-0.55
240min	1894.00	4355.32	1559.00	232.00	1485.00	8295.00	1.59	2.86
1.0 wt%								
5min	134.64	151.55	31.02	85.45	129.58	256.97	2.21	5.77
30min	537.40	640.65	164.60	214.10	513.30	1102.70	0.83	0.69
60min	797.20	1151.64	393.20	127.80	753.50	2037.60	0.58	-0.40
240min	1506.50	3944.56	1272.80	103.50	1096.50	6643.90	1.77	2.95
1.5 wt%								
5min	134.31	149.57	31.86	49.22	134.65	276.35	0.61	1.75
30min	448.20	542.04	144.80	166.30	431.80	959.20	0.71	0.63
60min	778.10	1256.81	436.80	222.70	661.60	2155.70	1.04	0.50
240min	1738.00	4289.51	1494.00	378.00	1160.00	8002.00	1.78	3.48

(b)

	$d_{10}(\mu m)$	$d_{32}(\mu m)$	S_t	Min(μm)	M(μm)	Max(μm)	S	K
only C12LAS								
5min	147.27	165.22	37.16	53.83	146.00	270.09	0.18	0.02
30min	673.20	852.15	244.90	236.90	636.70	1382.70	0.79	0.35
60min	1127.20	1637.75	530.40	231.00	1079.40	3869.80	1.09	2.84
240min	1862.00	5767.84	1552.00	313.00	1178.00	7280.00	1.38	1.42
0.1 wt%								
5min	145.41	159.50	32.97	70.26	144.74	216.87	-0.04	-0.70
30min	708.70	870.99	247.70	271.80	700.00	1438.80	0.33	-0.41
60min	729.40	1094.45	357.90	197.60	648.20	2292.20	1.21	1.77
240min	1268.00	3805.65	1236.50	268.60	683.30	6075.70	1.82	2.93
0.3 wt%								
5min	146.26	163.36	35.43	59.48	144.13	300.35	0.49	1.21
30min	613.50	820.18	254.60	170.60	564.90	1460.00	0.74	-0.06
60min	764.90	1115.37	363.10	220.80	680.60	2378.80	1.07	1.52
240min	1554.20	3595.85	1302.60	301.20	980.40	6474.90	1.33	1.04
0.5 wt%								
5min	147.47	161.21	31.48	74.00	141.04	236.43	0.70	0.16
30min	607.90	854.07	279.30	173.70	563.00	1442.30	0.73	-0.10
60min	728.90	1131.89	383.40	206.70	619.00	2337.30	1.08	1.07
240min	1139.60	3286.65	1095.20	193.70	692.90	5571.40	2.03	4.04
1.0 wt%								
5min	151.24	171.43	39.02	64.61	145.87	312.00	0.58	0.63
30min	604.80	830.23	265.10	179.10	568.90	1431.10	0.74	0.10
60min	712.60	1261.86	433.70	210.60	617.60	2333.30	1.43	2.32
240min	1169.30	3634.61	1192.90	197.60	604.70	6608.60	2.12	4.90
1.5 wt%								
5min	194.70	224.14	54.41	78.78	194.39	379.11	0.35	0.34
30min	608.70	848.22	272.80	182.00	571.00	1386.70	0.82	0.30
60min	703.50	1038.08	322.60	276.10	615.50	2259.60	1.65	3.81
240min	1300.70	3269.37	1124.20	271.00	854.10	5940.40	1.81	3.28

(c)

	$d_{10}(\mu m)$	$d_{32}(\mu m)$	S_t	Min(μm)	M(μm)	Max(μm)	S	K
only C12LAS								
5min	147.27	165.22	37.16	53.83	146.00	270.09	0.18	0.02
30min	673.20	852.15	244.90	236.90	636.70	1382.70	0.79	0.35
60min	1127.20	1637.75	530.40	231.00	1079.40	3869.80	1.09	2.84
240min	1862.00	5767.84	1552.00	313.00	1178.00	7280.00	1.38	1.42
0.1 wt%								
5min	154.91	175.30	40.86	57.04	154.87	300.96	0.13	0.22
30min	734.90	1011.91	320.80	196.90	679.20	1717.60	0.85	0.33
60min	740.90	1242.64	437.70	189.00	663.10	2318.80	1.07	0.81
240min	1353.70	3650.85	1212.90	235.30	927.80	6210.20	2.05	4.58
0.3 wt%								
5min	166.73	163.36	49.28	65.48	163.70	341.30	0.54	0.38
30min	589.50	769.75	228.30	236.10	546.30	1325.50	0.92	0.77
60min	754.40	1275.30	445.40	186.70	640.60	2214.10	1.17	0.77
240min	2223.00	4005.97	1436.00	318.00	1839.00	8404.00	1.15	1.32
0.5 wt%								
5min	137.16	156.15	36.16	61.83	133.96	258.52	0.54	0.04
30min	654.60	864.69	263.10	200.80	608.60	1608.20	0.80	0.42
60min	658.10	1130.56	388.60	186.30	545.90	2107.10	1.35	1.55
240min	1972.00	4215.79	1526.00	349.00	1515.00	7484.00	1.37	1.44
1.0 wt%								
5min	87.12	154.73	52.48	28.78	64.22	300.70	1.55	1.65
30min	72.41	286.94	42.25	12.78	62.04	267.74	1.34	2.47
60min	53.10	479.16	26.51	28.70	48.74	288.87	6.14	46.08
240min	51.60	259.65	12.18	26.17	50.91	96.52	0.87	1.24
1.5 wt%								
5min	38.80	47.13	11.71	18.70	36.70	101.75	1.95	7.02
30min	46.69	57.61	10.76	24.95	45.66	80.09	0.34	-0.07
60min	44.35	55.43	10.44	22.45	42.56	89.81	0.83	1.45
240min	26.37	27.98	4.62	16.32	26.02	43.75	0.33	0.49

(d)

	$d_{10}(\mu m)$	$d_{32}(\mu m)$	S_t	Min(μm)	M(μm)	Max(μm)	S	K
only C12LAS								
5min	147.27	165.22	37.16	53.83	146.00	270.09	0.18	0.02
30min	673.20	852.15	244.90	236.90	636.70	1382.70	0.79	0.35
60min	1127.20	1637.75	530.40	231.00	1079.40	3869.80	1.09	2.84
240min	1862.00	5767.84	1552.00	313.00	1178.00	7280.00	1.38	1.42
0.1 wt%								
5min	119.56	131.58	27.59	51.04	120.65	186.78	-0.01	-0.48
30min	568.40	715.05	202.20	242.40	534.70	1333.30	0.88	0.84
60min	683.30	1176.73	402.10	189.00	613.30	2501.60	1.40	2.75
240min	1988.00	4604.09	1620.00	239.00	1939.00	7866.00	1.62	3.00
0.3 wt%								
5min	29.51	34.02	8.16	14.07	28.04	55.83	0.61	-0.11
30min	32.24	45.77	9.76	10.75	31.16	70.15	1.00	1.95
60min	35.34	42.67	10.79	15.52	33.57	88.41	1.47	4.10
240min	28.03	107.25	6.87	16.44	27.25	57.08	1.14	2.46
0.5 wt%								
5min	32.31	38.33	9.59	10.75	31.16	70.15	1.06	2.19
30min	31.01	37.75	9.98	14.07	28.93	67.53	1.03	1.26
60min	35.37	39.55	8.49	19.61	33.89	60.77	0.75	0.18
240min	27.65	40.56	6.05	14.48	27.13	48.95	0.74	0.98
1.0 wt%								
5min	32.73	41.64	11.40	13.51	29.87	73.89	1.53	2.28
30min	31.19	37.60	9.49	13.51	29.68	79.01	1.44	3.47
60min	31.25	35.17	7.72	14.84	30.15	60.82	0.79	0.87
240min	29.63	33.78	7.56	17.16	28.54	64.77	1.19	2.16
1.5 wt%								
5min	38.46	48.98	15.04	7.10	39.38	80.22	0.19	-0.25
30min	37.78	50.01	16.21	6.15	37.27	77.94	0.21	-0.51
60min	38.00	48.98	12.04	19.36	36.73	91.74	1.31	2.97
240min	34.39	42.78	8.60	19.61	33.05	69.89	1.00	1.74

and maximum bubble size first increases and then decreases with increasing concentration of silica while the minimum bubble size decreases only when the concentration of particle is over 1.0 wt%. At lower concentrations (0.1 and 0.3 wt%), the rate of bubble size growth increases in comparison to CTAB only foam.

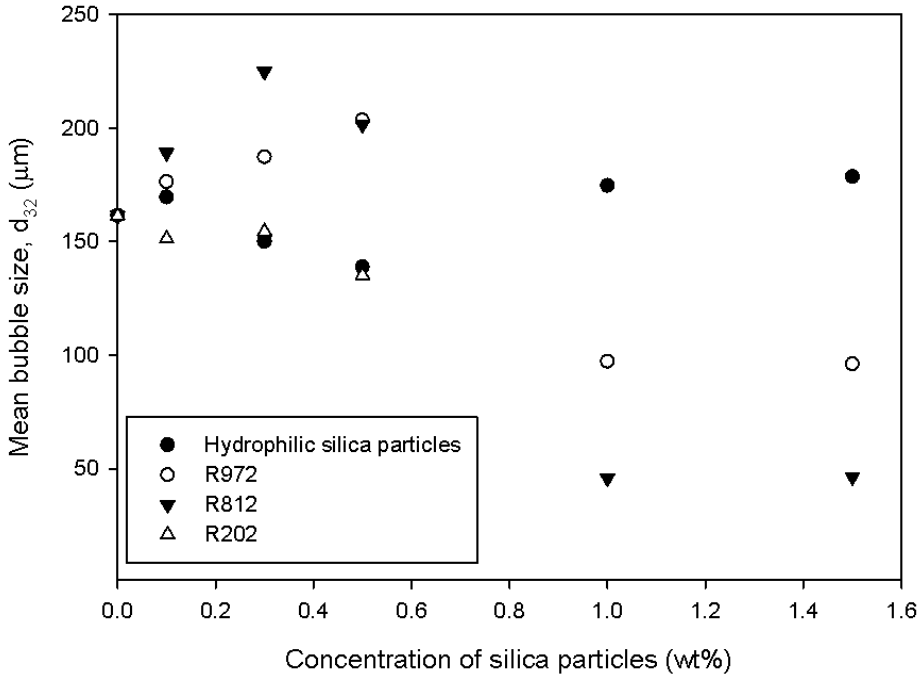

Figure 6.19: Variation of mean bubble size in 1.0 cmc CTAB foams containing four different types of silica particles after 5 minutes foam formation.

At 0.5 wt%, there are bubbles of two sizes 5 minutes after foam formation, not in separate layers as above, but interspersed. The number of larger bubbles is much higher than the smaller bubbles, with very large initial mean and maximum bubble size. This very high initial bubble size subsequently decreases with time mainly due to the larger bubbles bursting while the smaller bubbles still remain in the foam. At higher concentrations (1.0 and 1.5 wt%), the initial mean bubble size is smaller than at lower concentrations which is due to the smaller minimum bubble size of these foams. Also in these two cases a subsequent decrease of the mean bubble size over time was observed, which is again due to the bursting of the larger bubbles.

With R812 particles, a very similar change in bubble size distributions was observed. The initial mean bubble size shows first an increase followed by a sharp decrease of the mean bubble size as the particle concentration is increased. At 0.5 wt%, again two bubble size groups were found. In comparison to the least hydrophobic particle discussed above, the mean bubble sizes were smaller at all concentrations.

With R202 particles, the mean bubble size decreases slightly with increasing concentration of

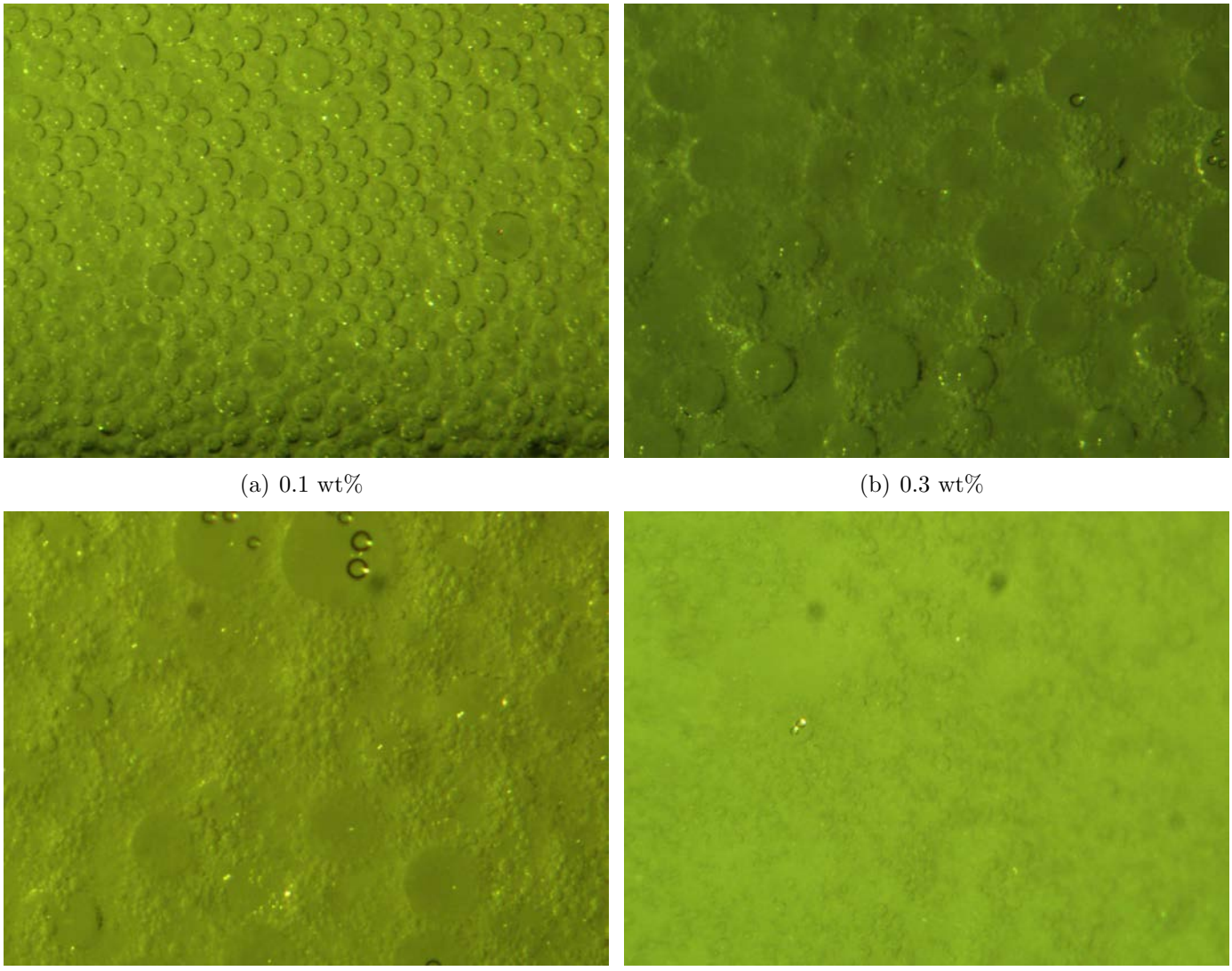

(a) 0.1 wt%

(b) 0.3 wt%

(c) 0.5 wt%

(d) 1.0 wt%

Figure 6.20: Foam images: 1.0 cmc CTAB foam with R812 silica particles.

silica. The rate of bubble size growth increases with silica concentration. It needs to be noted here that there is no data for concentrations higher than 0.5 wt% due to poor foam texture which makes it impossible to measure the bubbles.

In this work, the influence of silica particle concentrations on the stability of surfactant stabilized foam by observing the foam formation, drainage, collapse and bubble size was investigated systematically . In the anionic surfactant foam, the addition of hydrophilic and R972 particle (at the lower concentration) were found to have a negative influence on the stability of foam in the sense that they lead to faster foam collapse and growth of bubble size. Otherwise the addition of the hydrophobic silica significantly improved the stability of foam in the sense that it led to lower drainage, a longer

Table 6.5: Statistical parameters for foam bubble size distribution in CTAB foams containing: (a) hydrophilic; (b) R972; (c) R812; and (d) R202 silica particles.

(a)

	d_{10}(μm)	d_{32}(μm)	S_t	Min(μm)	M(μm)	Max(μm)	S	K
only CTAB								
5min	140.26	161.40	39.93	59.57	141.35	226.78	0.07	-0.67
30min	546.60	458.16	176.40	207.10	546.70	1022.00	0.40	-0.16
60min	805.70	1209.94	405.30	223.50	732.00	2113.70	0.99	0.58
240min	1688.00	3494.24	1342.40	272.20	902.90	4488.20	1.28	1.16
0.1 wt%								
5min	149.70	169.48	38.98	74.78	146.30	254.70	0.35	-0.45
30min	769.30	944.15	266.90	225.90	743.90	1621.60	0.36	-0.17
60min	813.00	1148.77	375.10	231.80	725.90	2024.30	0.79	0.09
240min	1690.98	3497.22	1345.38	275.18	905.88	4491.18	4.26	4.14
0.3 wt%								
5min	135.38	150.03	32.24	55.48	137.09	241.48	0.11	-0.29
30min	683.30	875.04	263.10	220.40	646.50	1411.80	0.48	-0.41
60min	747.10	1067.72	349.50	242.70	680.60	1847.80	0.86	0.16
240min	2001.23	4558.04	1551.00	244.00	1884.00	8854.00	1.32	2.95
0.5 wt%								
5min	125.85	138.78	29.13	53.30	126.17	212.96	0.13	-0.13
30min	442.90	588.12	177.10	125.50	408.80	975.70	0.98	0.52
60min	671.30	891.98	274.50	223.50	615.90	1593.70	0.75	0.22
240min	1854.00	4245.32	1545.00	221.00	1472.00	8202.00	1.48	2.55
1.0 wt%								
5min	154.30	174.65	40.45	64.17	151.43	312.78	0.23	0.15
30min	456.23	540.17	136.28	198.04	427.45	1010.59	0.76	0.95
60min	768.00	1002.81	303.90	251.00	739.20	1704.70	0.68	0.16
240min	1535.50	3845.56	1215.40	104.90	1124.20	7641.90	1.67	2.85
1.5 wt%								
5min	158.19	178.54	44.34	68.06	155.32	316.67	0.40	0.32
30min	460.12	544.06	140.17	201.93	431.34	1014.48	1.04	1.23
60min	771.89	1006.70	307.79	254.89	743.09	1708.59	0.85	0.33
240min	1543.38	3849.45	1219.29	108.79	1128.09	7645.79	1.84	3.02

(b)

	d_{10}(μm)	d_{32}(μm)	S_t	Min(μm)	M(μm)	Max(μm)	S	K
only CTAB								
5min	140.26	161.40	39.93	59.57	141.35	226.78	0.07	-0.67
30min	546.60	458.16	176.40	207.10	546.70	1022.00	0.40	-0.16
60min	805.70	1209.94	405.30	223.50	732.00	2113.70	0.99	0.58
240min	1688.00	3494.24	1342.40	272.20	902.90	4488.20	1.28	1.16
0.1 wt%								
5min	155.01	176.29	41.16	65.83	151.22	270.87	0.36	-0.40
30min	789.70	1172.43	385.70	238.00	724.10	2752.50	1.09	2.50
60min	866.60	1414.79	485.30	223.50	791.60	3027.80	1.19	1.90
240min	1325.32	3568.32	1113.50	232.60	1023.20	4274.70	1.12	2.84
0.3 wt%								
5min	164.38	187.28	42.71	82.26	157.74	320.17	0.83	1.20
30min	663.70	943.23	312.10	191.80	618.80	1558.00	0.72	-0.03
60min	825.30	1519.72	472.30	261.20	743.50	3636.90	2.56	11.89
240min	1322.60	3621.23	1195.20	274.43	998.20	4182.64	0.98	2.23
0.5 wt%								
5min	168.36	203.40	54.28	56.70	162.35	386.09	0.69	0.89
30min	48.79	99.93	26.60	25.57	43.83	211.74	4.80	25.53
60min	40.26	60.01	13.61	21.74	39.13	201.04	8.39	98.15
240min	39.76	59.51	13.11	21.24	38.63	200.54	7.89	97.65
1.0 wt%								
5min	51.91	97.16	29.35	19.48	43.83	213.48	2.88	9.60
30min	51.27	91.60	23.34	19.57	48.35	246.87	5.77	45.79
60min	46.92	51.39	10.09	26.35	45.74	81.57	0.77	1.10
240min	47.50	51.97	10.67	26.93	46.32	82.15	0.67	1.45
1.5 wt%								
5min	50.82	96.07	28.26	18.39	42.74	212.39	0.21	0.06
30min	50.18	90.51	22.25	18.48	47.26	245.78	0.67	0.18
60min	45.83	50.30	9.00	25.26	44.65	80.48	1.33	3.09
240min	46.41	50.88	9.58	25.84	45.23	81.06	1.19	3.33

(c)

	d_{10}(μm)	d_{32}(μm)	S_t	Min(μm)	M(μm)	Max(μm)	S	K
only CTAB								
5min	140.26	161.40	39.93	59.57	141.35	226.78	0.07	-0.67
30min	546.60	458.16	176.40	207.10	546.70	1022.00	0.40	-0.16
60min	805.70	1209.94	405.30	223.50	732.00	2113.70	0.99	0.58
240min	1688.00	3494.24	1342.40	272.20	902.90	4488.20	1.28	1.16
0.1 wt%								
5min	160.16	189.10	47.12	74.87	153.70	351.83	0.96	1.56
30min	811.10	1211.56	410.70	197.60	733.30	2080.40	0.86	0.10
60min	1077.00	2109.37	708.90	266.70	883.10	4493.70	1.81	3.99
240min	1666.70	3665.65	1367.90	267.90	937.20	5012.10	1.56	2.31
0.3 wt%								
5min	198.43	224.89	51.81	86.70	196.78	366.35	0.38	0.05
30min	68.99	428.16	117.82	12.04	26.75	657.48	2.80	7.22
60min	53.83	65.96	15.54	30.78	51.35	177.39	3.30	21.00
240min	55.32	67.45	17.03	32.27	52.84	178.88	4.79	22.49
0.5 wt%								
5min	175.92	201.45	47.99	40.35	166.57	296.09	0.39	0.04
30min	31.67	157.20	23.93	16.39	29.27	349.59	11.95	158.35
60min	27.06	32.10	7.81	10.75	25.81	63.53	1.51	4.30
240min	27.65	32.69	8.40	11.34	26.40	64.12	2.10	4.89
1.0 wt%								
5min	33.10	45.77	12.54	10.75	31.31	113.25	2.84	14.59
30min	33.01	37.52	11.66	17.57	31.54	59.33	4.11	3.39
60min	35.37	39.55	8.49	19.61	33.89	60.77	0.75	0.18
240min	36.06	40.24	9.18	20.30	34.58	61.46	1.44	0.87
1.5 wt%								
5min	33.67	46.34	13.11	11.32	31.88	113.82	3.41	15.16
30min	33.23	38.09	12.23	18.14	32.11	59.90	4.68	3.96
60min	35.45	40.32	9.06	20.18	34.46	61.34	1.32	0.75
240min	36.13	40.81	9.75	20.87	35.15	62.03	2.01	1.44

(d)

	d_{10}(μm)	d_{32}(μm)	S_t	Min(μm)	M(μm)	Max(μm)	S	K
only CTAB								
5min	140.26	161.40	39.93	59.57	141.35	226.78	0.07	-0.67
30min	546.60	458.16	176.40	207.10	546.70	1022.00	0.40	-0.16
60min	805.70	1209.94	405.30	223.50	732.00	2113.70	0.99	0.58
240min	1688.00	3494.24	1342.40	272.20	902.90	4488.20	1.28	1.16
0.1 wt%								
5min	128.08	151.25	26.58	56.70	129.70	192.61	-0.09	-0.39
30min	871.80	1226.57	398.90	249.80	775.70	2265.90	0.80	0.26
60min	1237.40	1943.66	687.50	298.00	1103.70	3458.80	0.78	0.01
240min	1988.00	3996.53	1620.00	239.00	1939.00	7866.00	1.62	3.00
0.3 wt%								
5min	142.03	154.47	30.22	62.52	140.52	225.39	0.15	-0.14
30min	885.90	1282.23	420.20	239.20	832.90	2353.70	0.95	0.93
60min	888.70	1999.86	694.10	186.30	657.80	3504.30	1.69	2.43
240min	1828.03	4002.30	1586.87	186.44	27.25	57.08	1.14	2.46
0.5 wt%								
5min	128.63	135.19	20.78	80.26	128.74	187.91	0.09	-0.18
30min	828.10	1172.23	389.60	196.10	763.90	2147.80	0.65	0.11
60min	923.00	1749.74	621.70	261.20	682.70	2958.40	1.32	1.06
240min	1825.21	3789.96	1426.05	274.48	27.13	48.95	1.74	1.98

foam life smaller mean bubble sizes and a more uniform bubble size distribution. The drainage can be reduced by a factor of ten by addition of hydrophobic silica and foam life can be prolonged to more than five days in comparison to only C12LAS foam. However, a more stable foam containing particles was obtained at low concentrations of surfactants. Also, at 0.2 cmc C12LAS the initial mean bubble size is much more sensitive to the particle concentration, in the sense that the decrease

of the mean bubble size as a function of the particle concentration is much faster. Alargova et al. (2004) reported that the addition of sodium dodecyl sulfate (SDS), an anionic surfactant, significantly reduced the stability of a foam stabilized by rod-shaped SU-8 particles. The explanation was that the oriented adsorption of SDS onto the particles changed the surface properties of the particles from hydrophobic to hydrophilic. This change decreased the affinity of the particles for the interface of gas-liquid. In their study, a high concentration of $10.0wt\%$ of SDS was used.

In the results the addition of particles can destabilize anionic surfactant foam. This can be explained similarly to Alargova by adsorption of the surfactant molecules onto hydrophobic silica which in turn reduces the number of surfactant molecules or their ability to form bubbles. On the other hand, sufficiently high concentrations of hydrophobic silica in the surfactant solution can substitute the surfactant molecules to form the bubbles. Therefore, with hydrophobic silica a different type of foam which consisted of small bubbles and rigid packing of particle-armed surface has been produced. This explains why a sudden drop was observed in mean bubble size.

Zhang, Lan, Liu, Xu and Sun (2008) found that stable foams can be obtained by a combination of CTAB surfactant and Laponite particles in aqueous dispersions. Surfactant concentration and the hydrophobicity of the particles both were important for the stabilization of foams. According to them, the Laponite particles and CTAB system leads to a synergistic stabilization of foams at intermediate surfactant concentrations. They concluded that the hydrophobicity of the particles compared with the electrical property of particles is crucial to obtain stable foams with CTAB/Laponite systems. They obtained the most stable foams by particles with the maximum hydrophobicity (as long as the contact angle is still smaller than 90°). Liu et al. (2009) have also studied the behaviour of foams stabilized by Laponite nano-particles combined with alkylammonium bromides with different alkyl chain lengths. In their article, the synergistic stabilization of foams was promoted by the adsorption of CTAB-modified particles on the bubble surface and the formation of aggregated structures between the armored bubbles and the unabsorbed particles in the bulk phase. The situation in this study is similar to these in that the particles possessed a negative charge which allowed the hydrophobic chain length of CTAB surfactant to attach to and modify the surface. The same results were reported by Zhang, Lan, Liu, Xu and Sun (2008) and Liu et al. (2009). However, a much longer foam lifetime

(over few days) was obtained with R812 and R202 particles in comparison to their foams which only lasted minutes.

In the experiment of cationic surfactant foam containing particles, there was a small increase of the drainage at low concentrations of R202. This was because the hydrophobic particles were modified by the CTAB surfactant and the high degree of hydrophobicity started to destabilize the foam. The contact angle changes as the hydrophobicity changes. Zhang, Lan, Liu, Xu and Sun (2008) showed that foam stability is very sensitive to small changes of the contact angle around 90°. This could explain the results when the particle-surfactant interaction led to a small modification of the contact angle only. The stability of foam was also improved by adding a sufficient concentration (0.5 wt%) of hydrophilic silica. This is probably because CTAB molecules can attach to the surface of hydrophilic silica and hence the hydrophobicity of hydrophilic silica has been modified.

In the case of R812 and R972 particles both can create two levels of bubble sizes at low concentrations (0.3 and 0.5 wt%) in the CTAB solution. The larger ones were produced by the cationic surfactant molecules and the smaller ones were formed by the particles. The mean of the subpopulation of the small bubbles remained constant over a few days, while the larger bubbles disappeared after an hour because of the low detachment energy of the surfactant molecules.

6.2.3 Effect of pH

Zeta potential measurements show that particles are highly charged at high pH and uncharged particles are more hydrophobic than charged ones (Fokkink and Ralston, 1989). It is thus expected that silica particles will become more hydrophilic with increasing the pH. In this section, a series of experiments to study the effect of pH on surfactant stabilized foams with addition of silica is conducted. Three different pH values were used in these experiments: pH 4.5, 7.0 and 10.0. Firstly, The results of pH effect on the foam stabilized by C12LAS with different hydrophobicity particles is discussed. Secondly, the pH effect on the foams stabilized by CTAB foam with addition of different hydrophobicity particles is presented. In these experiments, 1.0 cmc of C12LAS and CTAB is considered for concentrations of particles ranging from 0.1 wt% to 1.0 wt% (see Table 6.1(c)).

Anionic Surfactant: C12LAS

The pH does not affect the foamability of foam stabilized by only C12LAS as shown in Figure 6.21(a). There was no difference in foamability either in the foam produced by C12LAS with addition of either hydrophilic or hydrophobic silica. Also, the pH has no effect on the drainage of foams stabilized by hydrophilic silica or by R972 particles. For this reason only foams that are affected by the change of pH are presented.

At 0.5 wt%, the foam collapsed faster at pH 10 than at lower pH in the foam generated with the addition of R812 particles. The change of pH had no effect on foam collapse at 1.0 wt%, as shown in Figures 6.21(b) and 6.21(c). At lower concentrations of R812, there was no change of foam stability for different pH values. With addition of R202 particles, at 0.1 wt% the foam collapse decreased with increasing pH, as shown in Figure 6.21(d). However, change of pH had no effect on foam collapse at higher concentrations of R202 particles.

There is no significant pH effect on the foam microstructure with the foams produced with C12LAS surfactant only and when the hydrophilic and the least hydrophobic silica are added, which was expected. With increasing hydrophobicity of silica, the mean bubble size can become as low as 30 μm, as discussed above. However, the mean bubble size increases at higher pH in the foam produced with R812. In the foam generated with R202 particles, the mean bubble size remains at around 30 μm and does not change with the pH as shown in Figure 6.21(d).

There was no pH effect on the foam stabilized by C12LAS with addition of hydrophilic and R972 particles. This is expected because the two types of particles are negatively charged and C12LAS is an anionic surfactant. There were also no changes in surface tension and viscosity. Also, in the last section that the partially hydrophobic silica act like surfactants and compete to form the bubbles in foam. Here, these two types of silica do not compete with the surfactant because in the high pH environment both silica are effectively hydrophilic. Therefore the change of pH did not affect foam stability.

Above it has shown that at sufficient hydrophobicity and concentration of silica much more stable foams can be produced; the intermediate and the most hydrophobic, R812 and R202, particles take over the anionic surfactant molecules and form a different type of foam. This is because the

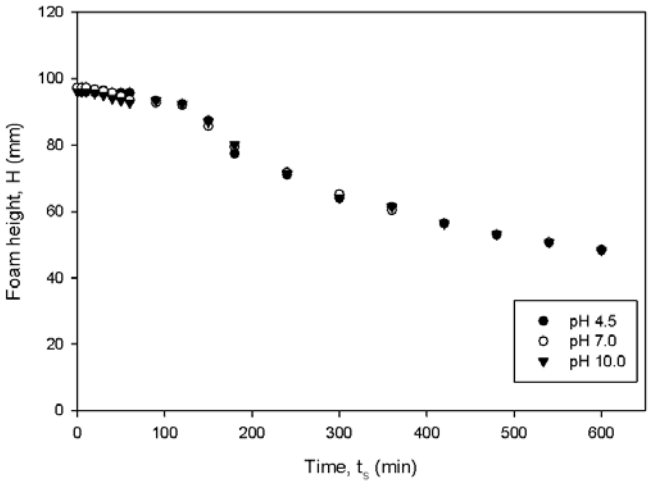

(a) without particles

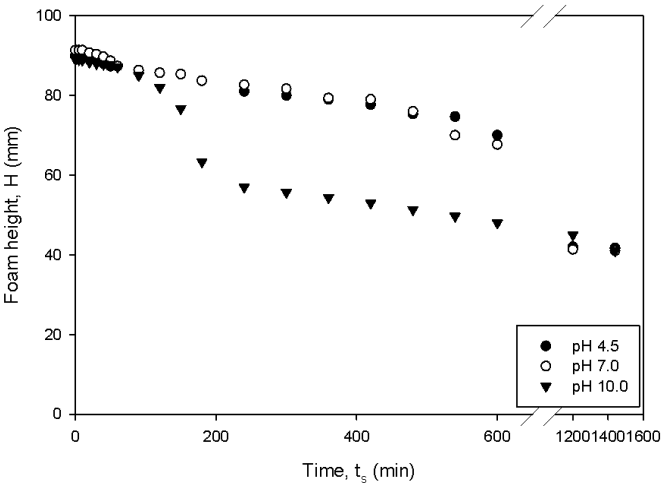

(b) R812 at 0.5$wt\%$

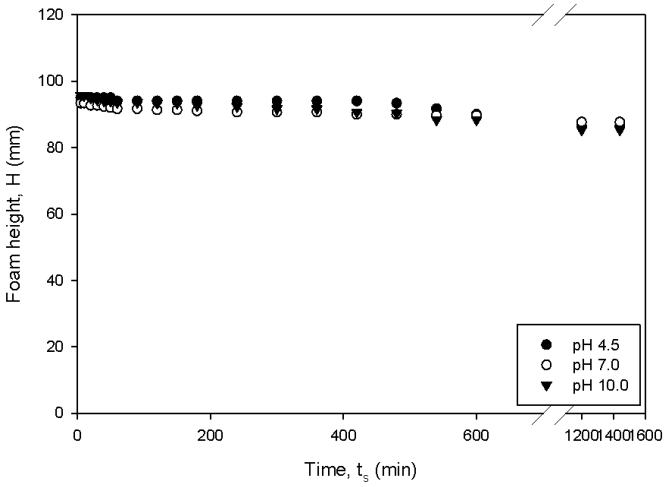

(c) R812 at 1.0$wt\%$

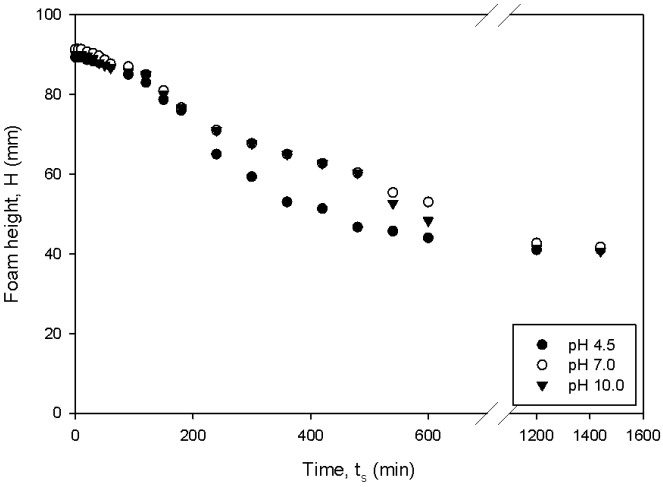

(d) R202at 0.1$wt\%$

Figure 6.21: pH effect on 1.0 CMC C12LAS foam stability.

detachment surface energy of the surfactant molecules is much smaller than that of the hydrophobic silica. The adsorption of surfactant molecules is reversible. In contrast the adsorption of the hydrophobic silica is not reversible, hence, a much more stable foam was formed by the hydrophobic silica. At pH 10, the hydrophobic silica becomes more hydrophilic because of the increasing negative charges. Thus, the hydrophobic silica becomes too hydrophilic to form foam and this leads to fast foam collapse.

Foam produced by R812 particles is much more stable than the anionic surfactant only foam. In this section, the pH has some impact on the foam stability but the difference was only observed at higher values. The reason is that the higher pH can modify the surface of the particles to more hydrophilic which is why a lower viscosity and a small and stable particle aggregate size in the suspensions was observed. Therefore, a shorter foam life was observed in the foam produced by the intermediate silica particles at pH 10 in comparison to the foams at lower pH. However, the change of pH has less effect on the foam produced at higher concentration and under these conditions a more stable foam was generated at pH 10. This might be because R812 particles have not changed to fully hydrophilic and still act like surfactant at higher pH. These particles can still compete with the surfactant molecules to form foam, however, there are not sufficient numbers of particles to form a stable foam. With R202 particles, the pH has no significant effect on foam stability. It might be that the particles were too hydrophobic and there is not enough negative charge from the changing of pH.

Cationic Surfactant: CTAB

Changing the pH had no significant effect on the cationic surfactant foam produced without silica in term of foam formation, drainage, or breakage. Foamability results for foam containing different types of silica at different concentrations are summarized in Figure 6.22. At 0.1 wt%, the foamability is not affected by a change of pH. At higher concentrations (0.3 wt% and 0.5 wt%), the foamability was reduced dramatically with increasing pH in hydrophilic particle foam. In general, the higher the pH the less foam was produced with silica.

The foam height is plotted against time in the foam containing hydrophilic silica at pH 4.8, 7.0

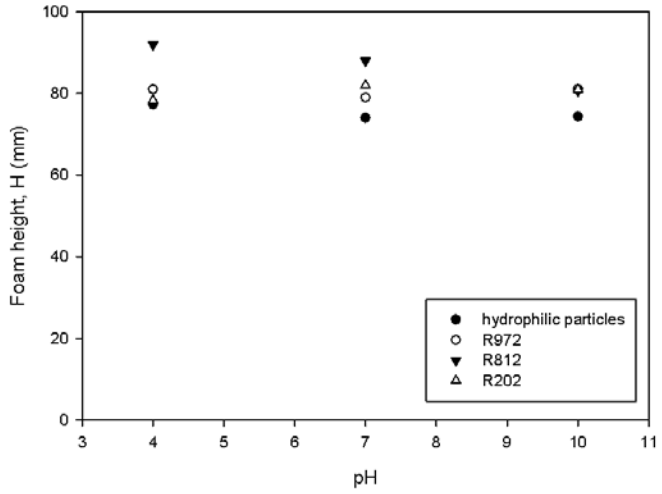

(a) 0.1 wt%

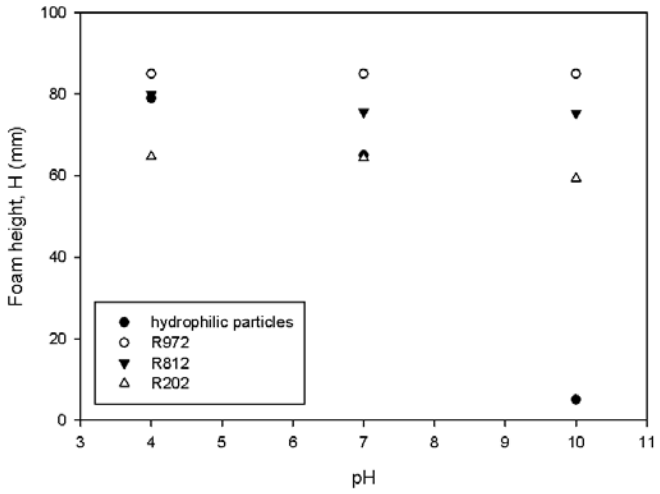

(b) 0.3 wt%

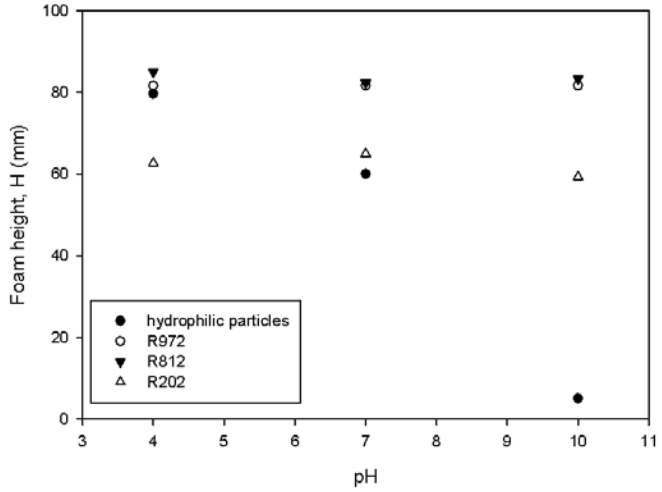

(c) 0.5 wt%

Figure 6.22: Formation of foam containing different types of silica particles in different pH.

and 10.0 in the Figures 6.23(a), 6.23(b), and 6.23(c). At lower concentration of silica, the pH does not affect foam height. With increasing concentration of silica, the higher the pH the earlier the foam collapse sets in, as shown in Figures 6.23(b) and 6.23(c). In the image shown in Figure 6.23(d), at pH 7.0 less foam with 0.5 wt% particles was produced in comparison to pH 4.8, but the liquid drained was clear (there was no particles in the liquid). The foam images shown in Figures 6.24(a) and 6.24(b) show the initial bubble size. The initial mean bubble sizes were 154.9 μm for the foam at pH 4.5 and 285.8 μm for the foam at pH 7.0 at foam standing for 5 minutes. However, after 60 minutes foam standing time the mean bubble size at pH 4.8 was nearly the same as at pH 7.0 namely

1104.6 μm compared to 1094.3 μm at pH 7.0. Despite a similar mean bubble size at both pH values, the bubble size distributions are very different for each pH. At pH 4.8, the bubbles are uniform while there are much smaller bubbles with larger bubbles in the foam at pH 7.0. Longer foam life at pH 7.0 was observed than at pH 4.8 with a much smaller mean bubble size obtained (as shown in Figure 6.24(f)). Based on these foam images and the fact that no particles remained in the liquid, it is clear that a higher foam stability was obtained at pH 7.0 than pH 4.8.

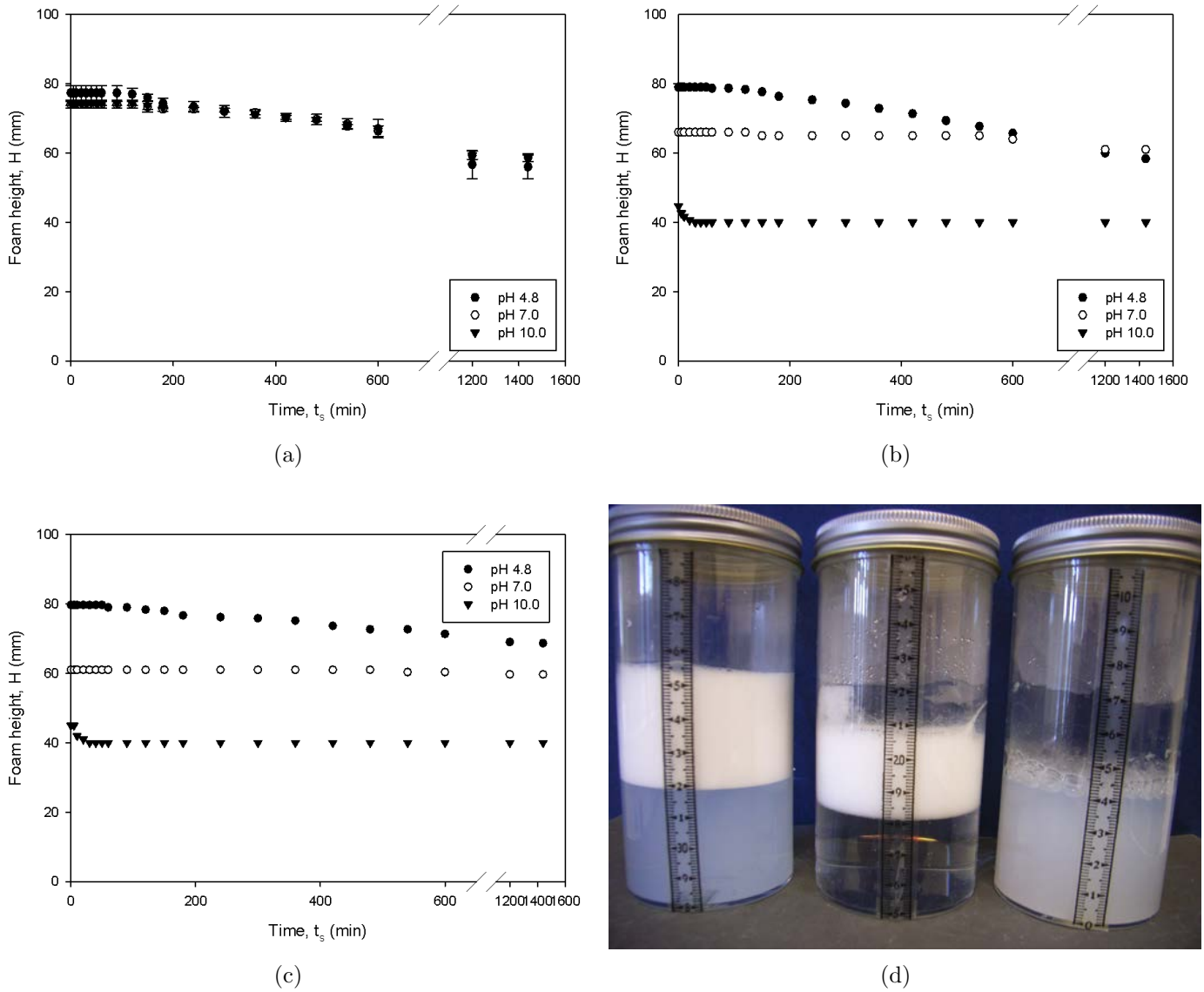

Figure 6.23: CTAB foams containing hydrophilic silica particles at (a) 0.1 wt%; (b) 0.3 wt%; (c) 0.5 wt%; (d) the foam in the sample bottles; the foams are produced at pH 4.8, pH 7.0 and pH 10.0 from the left to right, respectively.

Figures 6.25(a), 6.25(b) and 6.25(c) show the foam height as a function of time at 0.1, 0.3 and 0.5

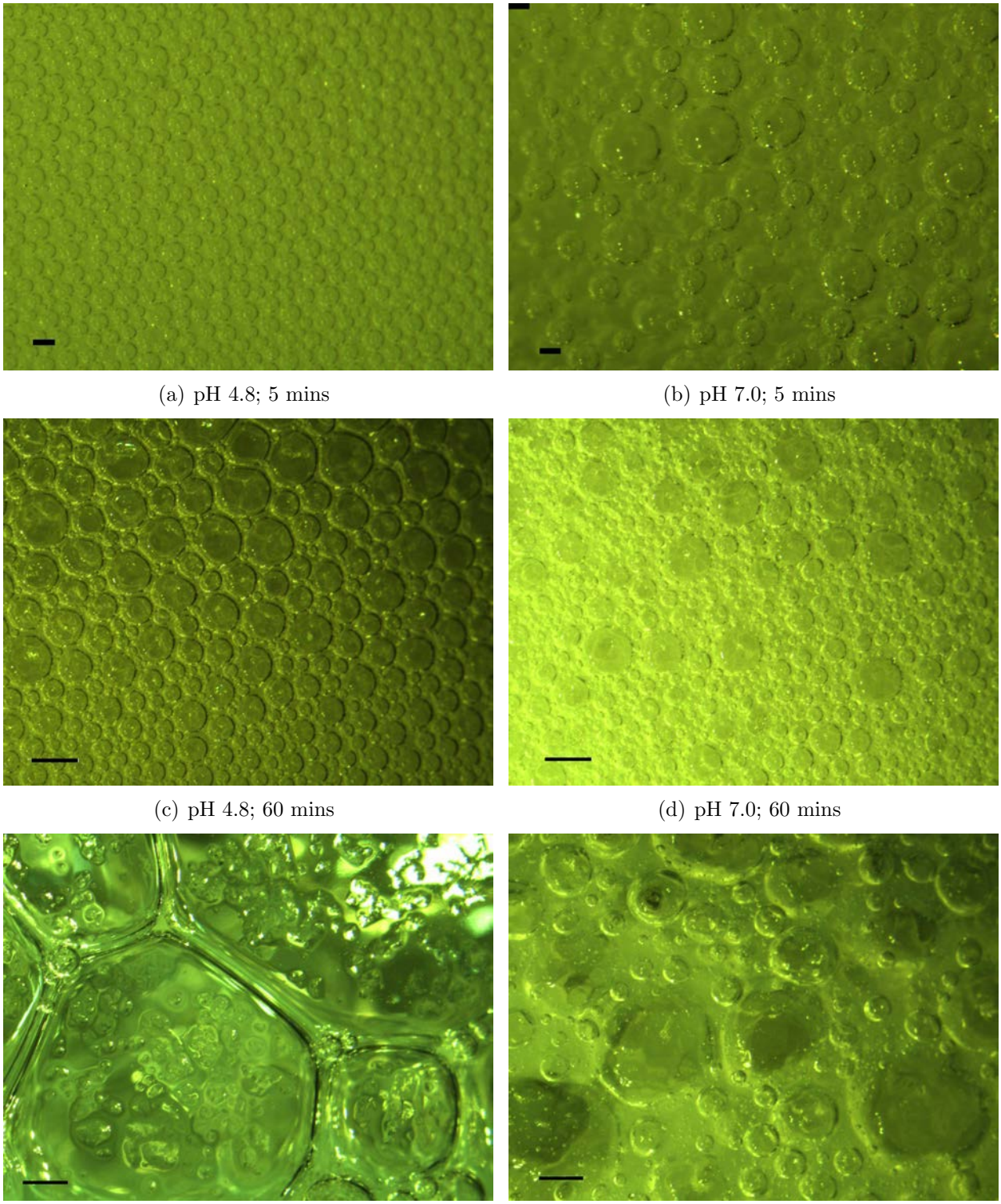

(a) pH 4.8; 5 mins

(b) pH 7.0; 5 mins

(c) pH 4.8; 60 mins

(d) pH 7.0; 60 mins

(e) pH 4.8; 24 hours

(f) pH 7.0; 24 hours

Figure 6.24: Images of foam containing hydrophilic silica particles at pH 4.8 and pH 7.0. Scale bar is 100 μm for the foam images at 5 min and 1 mm for the foam images at 60 min and 24 hours.

wt%, respectively. At 0.1 wt%, the rate of foam breakage increases with increasing pH. At 0.3 wt%, the rate of foam breakage is less sensitive to the pH, but still increasing with increasing pH. At 0.5

wt%, the breakage rate is independent of the pH. A similar result has also been obtained in the foam with R812 particles. In the case of these two hydrophobic silica, the foam stability increased with decreasing pH, increasing concentration of silica, and increasing hydrophobicity of silica. However, for the foam with the third type of particle, R202, the pH has no effect on the concentrations of particles (data not shown).

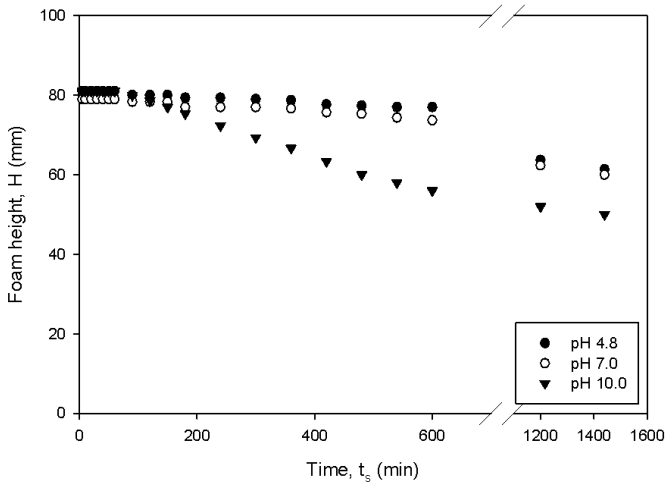

(a) 0.1 wt%

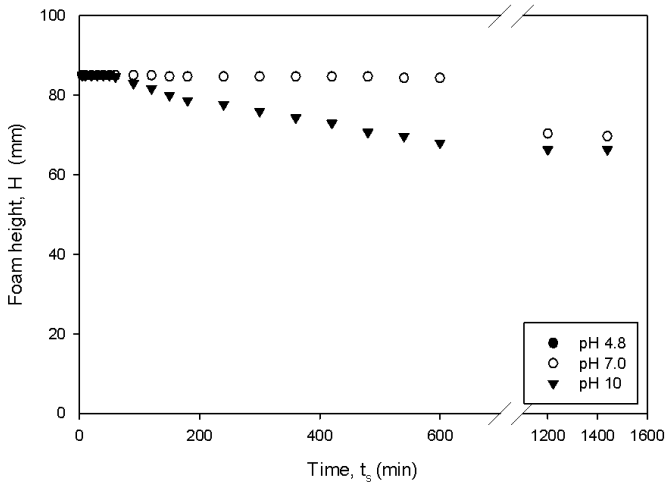

(b) 0.3 wt%

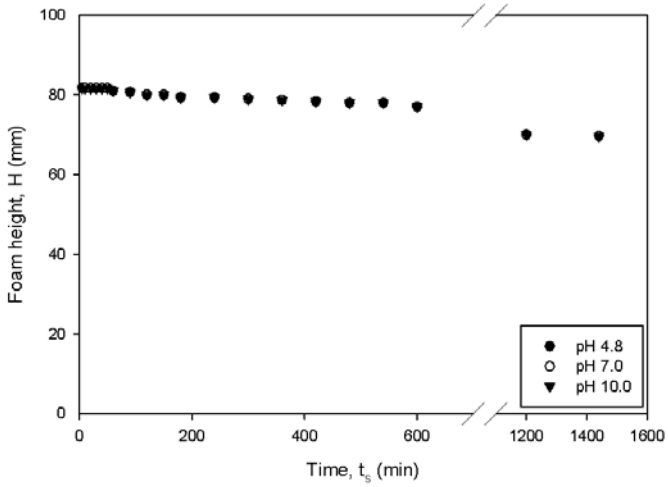

(c) 0.5 wt%

Figure 6.25: Foam containing R972 silica particles at pH 4.5, 7.0, and 10.0 in CTAB surfactant foam.

In a review, Zhang, Lan, Liu, Xu and Sun (2008) reported that CTAB surfactant can be used to modify the surface of particles from hydrophilic to hydrophobic. In these results, foam stability can be enhanced at pH 4.8 by adding hydrophilic particles to the CTAB foam. Foam destabilized at pH

10.0. At pH 4.8 and 7.0 the foams are very heterogeneous with respect to their bubble sizes, that is they contain both very small and very large bubbles.

A possible explanation for this is that the hydrophilic silica are modified by CTAB to more hydrophobic, as suggested by Zhang, Lan, Liu, Xu and Sun (2008), and therefore a more stable foam was formed. When the pH from 4.8 to 7.0 was adjusted, in the higher pH environment the negative charge of the particles is higher. This may lead to a higher attraction between the CTAB surfactant molecules and the hydrophilic particles and result in a much smaller initial mean bubble size and also slower bubble growth. However, if the negative charge becomes very high, as in pH 10, this may also neutralize the external charge of CTAB with the effect that it loses the ability to attach to the hydrophilic particles resulting in poor foamability and foam stability.

6.2.4 Effect of Viscosity

It is well known that foam stability can be enhanced by increasing the bulk viscosity of the system. Also, it has been reported that the liquid holdup in foam increases with liquid viscosity (Deshpande and Barigou, 1999). At higher viscosities, the rate of drainage from the lamellae is reduced, which results in a higher liquid content in the foam.

In this section, the effect of viscosity on the surfactant stabilized foams and mixture of surfactant-particle stabilized foam is investigated. In the previous section, the effect of particle concentrations was investigated. There was a critical concentration where the hydrophobic particles substituted anionic surfactant molecules and started to form foam. These foams were very stable in comparison to surfactant foams. It is interesting to improve the foam stability in the area where foaming is dominated by particles, that is below this critical concentration. Therefore, the concentration of particles at 0.5 wt% was selected and the concentrations of surfactants were both at 1.0 cmc and in these experiments. In these experiments, SCMC was used to increase the viscosity of the solutions and suspensions. Specially, concentrations of 0.08 and 0.1 wt% SCMC were used in the surfactant-particle suspensions.

Foam Formation, Drainage, and Breakage

Figure 6.26(a) shows the foamability of foam produced by C12LAS anionic surfactant solution and with various types of particles. Figure 6.26(b) shows the same for CTAB cationic surfactant solutions and different types of particles. The initial foam volume is substantially reduced with increasing viscosity in both anionic and cationic surfactant foams.

Figure 6.27(a) shows the maximum liquid level, a, as a function of the SCMC concentration in the dispersions with C12LAS; Figure 6.27(b) shows the same for CTAB. In the C12LAS foam, the value of a decreases somewhat as the viscosity increases.

The decrease of a, the liquid holdup level, as a function of SCMC concentration is larger for particles with high hydrophobicity. The value a decreases the most when there are no particles in the foam. In the CTAB foam, the value of a decreases only in the experiments where there is no particles and R202 particles.

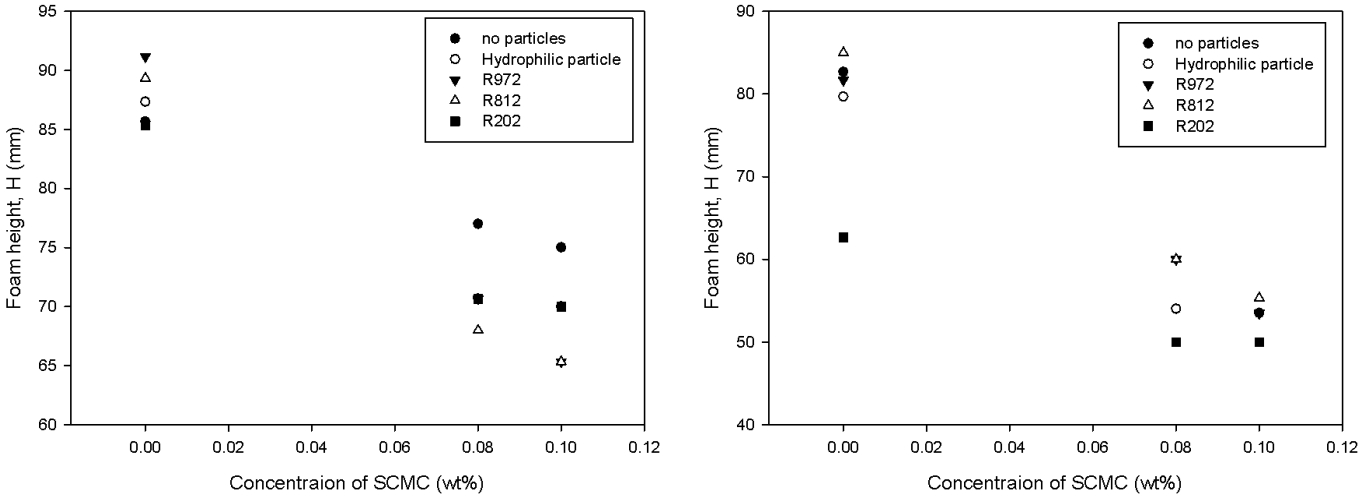

Figure 6.26: Formation of foam containing different type of silica particles in different viscosity liquids: (a) C12LAS; (b) CTAB.

Foam Structure

Figures 6.28(a) and 6.28(b) show the mean bubble size of foam produced in surfactant only solutions. The mean bubble size increased with increasing viscosity in both anionic and cationic surfactant

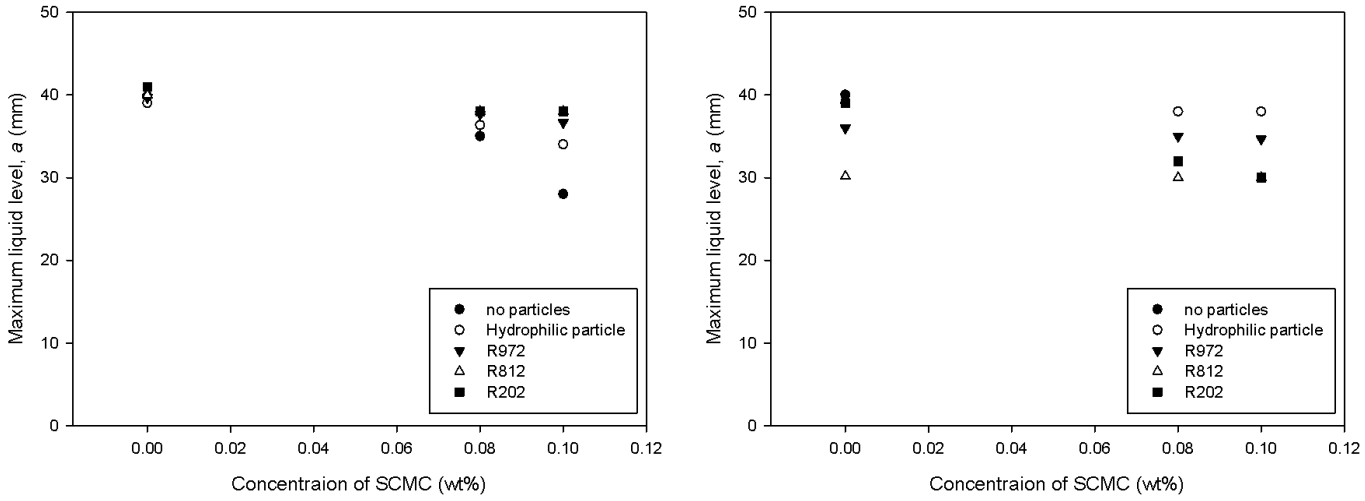

Figure 6.27: Drainage of foam containing different type of silica particles in different viscosity liquids: (a) C12LAS; (b) CTAB.

foams. The growth of bubbles over time slowed down with increasing viscosity. With addition of 0.1 wt% SCMC in anionic surfactant foam, the mean bubble size was reduced from 976 to 175 μm and from 1782 to 407 μm when measured after foam standing times of 30 and 60 mins respectively. In the cationic surfactant foam, with increasing viscosity the decrease of the bubble growth is smaller. The mean bubble size was reduced from 656 to 465 μm at the foam standing time of 30 mins and from 1210 to 763 μm at a foam standing time of 60 mins. After an hour, in the anionic surfactant, the higher viscosity still contributes to more stable foams, in the sense that the bubble size is smaller in the high viscosity sample than in the control without SCMC. This is not the case in the cationic surfactant. In general, at higher viscosities the bubble growth is reduced in anionic surfactant foam.

The mean bubble size of C12LAS foam with addition of silica is summarized in Figure 6.29. A larger initial mean bubble size was obtained from the foam with silica. The growth of bubble size was slowed down with addition of SCMC. Figures 6.29(a) and 6.29(b) show that higher viscosity reduces bubble growth. The mean bubble size at foam standing 30 mins and 0.1 wt% SCMC reduces from 965 and 982 μm to 193 and 298 μm for the foam with hydrophilic particle and R972 particle, respectively. Figures 6.29(c) and 6.29(d) show that higher viscosity is also slowing down the growth of the bubbles in foam with R812 and R202 particles. At 0.1 wt% SCMC, the mean bubble size at foam standing 30 mins reduces from 923 and 1172 μm to 508 and 462 μm (for R812 and R202).

The mean bubble size of CTAB foam with addition of silica is summarized in Figure 6.30. The initial mean bubble size increases with increasing viscosity in CTAB surfactant foam with addition of hydrophilic silica as shown in Figure 6.30(a). During the first 30 minutes, the mean bubble size of foam with no addition of SCMS grows from 138 μm to 588 μm; in comparison, the mean bubble size of foam with addition of 0.1 wt% SCMC increases from 265 μm to 686 μm. In this case, the growth rate of bubbles has been reduced by nearly a factor of two in the higher viscosity. In Figure 6.30(b), the viscosity seems to have no significant impact on the initial mean bubble size. The mean bubble size decreases in the foam without SCMC while the mean bubble size increases in the foam with higher viscosity. Figure 6.30(c) shows that the bubble size decreases with increasing viscosity. The mean bubble size decreases with time in the foam without SCMC. The mean bubble size increases gradually with higher viscosity. Similar results have also been found in the foam with R202 particles.

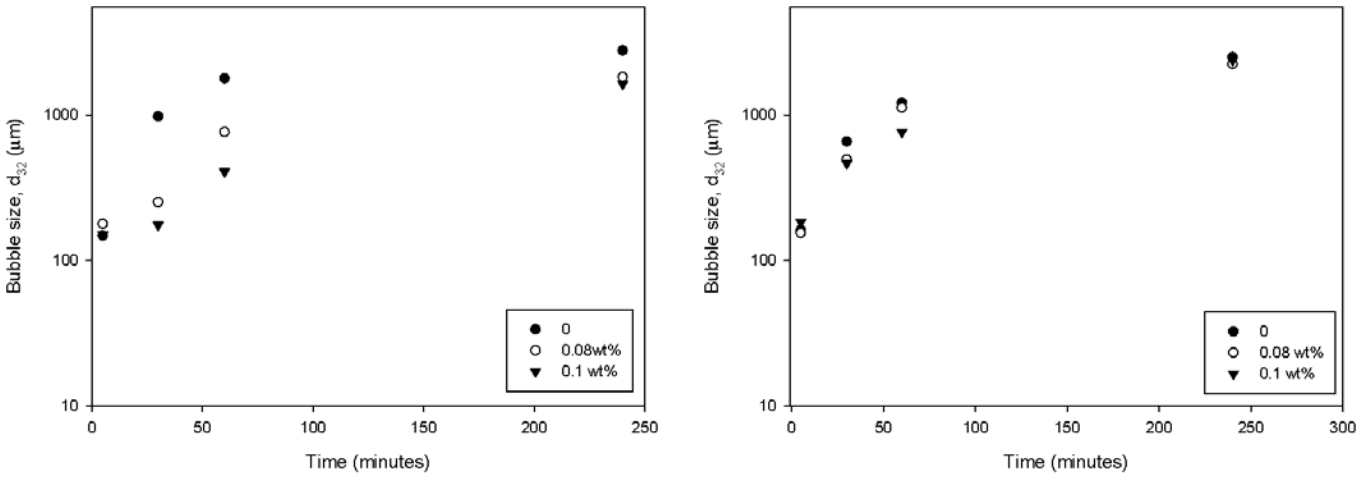

(a) C12LAS (b) CTAB

Figure 6.28: Mean bubble size of foam without silica particles (a) C12LAS; (b) CTAB.

6.3 Conclusions

Two different types of surfactants (anionic surfactant: C12LAS and cationic surfactant: CTAB) were used in this study. Firstly, anionic surfactant have better foamability and stability because of their better ability to lower surface tension as shown in Figure 6.1. In C12LAS foam, two concentrations of surfactant were chosen to understand the effect of silica particles on the foams. At the low

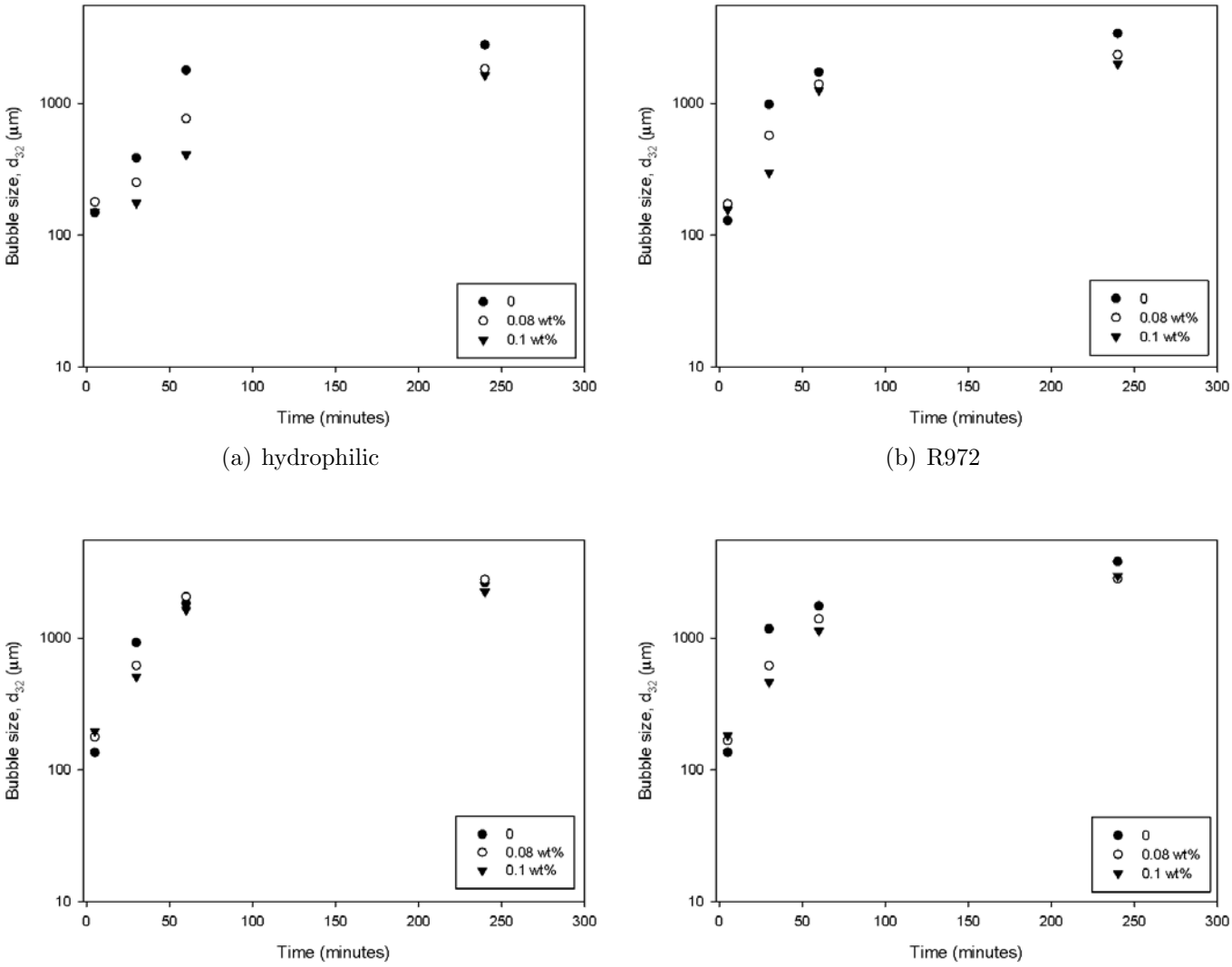

(a) hydrophilic (b) R972

(c) R812 (d) R202

Figure 6.29: Mean bubble size of foam with silica particles in 1.0 cmc C12LAS.

concentration (0.2 cmc), adding low concentration of silica can destabilize foam, whereas addition of high concentration of silica can stabilize foam. The foam stability increases but the foamability decreases with increasing hydrophobicity of silica. In comparison to the foam at higher concentration of surfactant (1.0 cmc), more hydrophobicity and higher concentrations of silica are needed to obtain stable foams. This is because both C12LAS and the particle are negatively charged and they compete to form bubbles in the foams. However, at sufficiently high concentrations of hydrophobic particles, the particles become dominant with respect to determining the properties of the foam. The effects due to the surfactant molecules become secondary. As a result, much more stable foams were obtained.

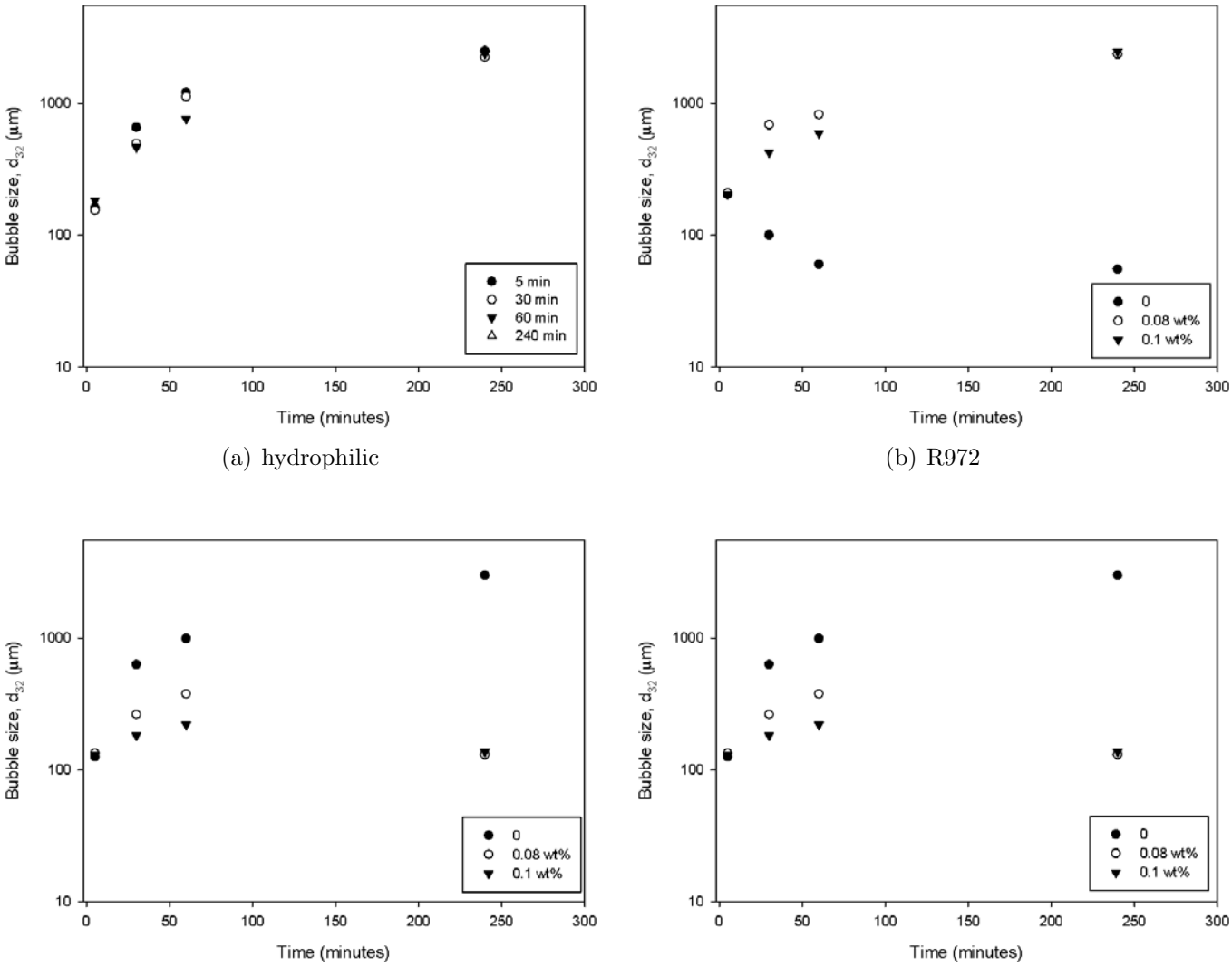

(a) hydrophilic (b) R972

(c) R812 (d) R202

Figure 6.30: Mean bubble size of foam with silica particles in 1.0 cmc CTAB.

In CTAB foams, the foam stability increases with all types of silica and their increasing concentration. An increasing foamability has been obtained with R972 and R812 particles, but a decrease of foamability was found with R202 particles when it is at a high concentration. This can be explained by the fact that the cationic surfactant had opposite charge to the particles. The increasing foamability is because the cationic surfactant molecules can attach to the surface of particles and thus there was a different type of surfactant modified particle to form bubble instead of the competition in between surfactant molecules and particles. The data on the change of foam microstructure also supports previous results. More stable foams consist of smaller bubbles and are formed by the silica.

The pH has no significant influence on the surfactant only foams but it does influence the surfactant foam with hydrophobic silica particles. In general, the foamability and foam stability of foam with silica decreases with increasing pH. This is especially clear in the CTAB foams with silica. From the microstructure, different types of bubbles were produced at different pH. This shows that the hydrophobic silica have lost their hydrophobicity and foams are formed by the surfactant molecules.

The increase of viscosity by adding SCMC definitely contributed to the reduction of the drainage rate, but there is also a great reduction in foamability. The surfactant only foams and C12LAS foams with silica do not differ substantially with respect to the initial foam bubble size. However, both foams show a decrease of the bubble size growth with increasing viscosity. In CTAB foams, a larger initial bubble size combined with a slower bubble growth rate in the foam with hydrophobic silica at higher viscosity foam. The slower bubble growth in both surfactant foams with silica is because there are thicker foam films between bubbles caused by higher viscosity the slows down the drainage. The higher viscosity might inhibit the ability of silica to move freely when they form bubbles. Adding SCMC improves foam stability in the short term.

Chapter 7

Foams Solely Stabilized by Silica Particles

7.1 Introduction

Solid particles can be used instead of colloidal stabilizers or surfactants to stabilize foam. The stability of these foams depends on the particle diameter, shape, concentration, hydrophobicity and also the type of surfactant and stabilizer (Dippenaar, 1982a,b, Tang et al., 1989, Aveyard et al., 1994, Pugh, 1996, Binks, 2002, Pugh, 1996, Sethumadhavan et al., 2002, Alargova et al., 2004, Murray and Ettelaie, 2004, Zhang, Lan, Liu, Xu and Sun, 2008, Zhang, Sun, Dong, Li and Xu, 2008, Liu et al., 2009, Dickinson, 2010). As discussed in detail in chapters 5 and 6, silica particles have been used as both stabilizer and destabilizer in surfactant-stabilized aqueous foams and protein-stabilized foam. Hydrophilic particles increase protein foam stability. This is because hydrophilic particles can accumulate at the plateau borders in the foam film resulting in drainage and also reduced diffusion by creating a network between particles. However, hydrophilic particles can also act as destabilizer in surfactant-stabilized foam depending on the nature of the solution (anionic or cationic surfactants) as shown in previous results. The fully hydrophilic silica particles can be modified into partially hydrophobic silica particles using a chemical coating on their surfaces. These partially hydrophobic silica particles can also alter the stability of both protein-stabilized and surfactant-stablized foams by varying their hydrophobicity and concentration.

Ramsden (Ramsden, 1903) found various inorganic sols to form persistent bubbles more than a century ago. Recently, the foams stabilized solely by partially hydrophobic solid particles have been

a very popular topic because these particles proved to be economically attractive as replacements for conventional surfactants. Blute et al. (2009) have produced foams using industrially manufactured silica nanoparticle sols. Three types of silica particle sols were used one of which is hydrophobic, the others hydrophilic. They showed that a longer foam lifetime was obtained with the hydrophobic silica particles, however, the lifetime of foams produced by all these silica particles is only in the range of seconds to minutes.

Partially hydrophobic particles can act as surfactants and have been used to improve the stability of foams. A key parameter that affects the adsorption of particles appears to be the contact angle which particles exhibit at the interface of gas and water. The energy required to remove the particles from an interface is several orders of magnitude greater than the energy to remove the surfactant molecules when the contact angle is 90 degree. Hence, the particles are irreversibly adsorbed, in contrast to surfactant molecules that adsorb and desorb reversibly (Binks, 2002). Therefore, particulate foam can be much more stable than surfactant foam.

Partially hydrophobic silylated silica particles were used as foam stabilizer to generate bubbles (Du et al., 2003, Dickinson et al., 2004). Salt was also used to fine-tune the hydrophobic character of the particles to further optimize foam formation and stabilization. Suitably hydrophobic particles can be dispersed in water by dispersing particles in a solution of water/ethanol, which allows the more hydrophobic particles to become wetted, then remove the ethanol by repeated sendimentation-redispersion cycles in pure water. However, these silica particles were rather inefficient stabilizers (Dickinson et al., 2004). Irregularly-shaped fine crystalline particles of sodium chloride which were modified into amphiphilic particles by physical adsorption of a cationic surfactant have also been used to stabilize foams (Vijayaraghavan et al., 2006).

In their study, the foaminess increased with the increasing amphiphilic NaCl particle concentration, and a maximum in foaminess was observed experimentally at around 40 vol % in the bulk during suspension boiling, however, they did not not report the foam stability over a long period. When a particle concentration is beyond about 40 vol %, fewer particles attach to the bubble and approach the air-water interface owing to the clustering of amphiphilic particles in the bulk.

Much more stable foams were obtained using a wide variety of solid particles of both nanometer

and micrometer-size. Table 7.1 lists the main recent studies (2004-2010) carried out using solid particles to stabilize foams.

In a review article Binks (2002) summarized results originally reported in Wilson's thesis Wilson (1980). The thesis aimed to understand the key parameters in the formation of particle-stabilized aqueous foams. Anionic charged polystyrene latex particles were used in this study and the particle size ranged from 1.02 to 3.89 μm. In this case foaming depends on the coagulation of the bulk suspension, i.e. the formation of cross-links between the particles. They achieved coagulation by various means, including the addition of salt, cationic surfactant, and by adjusting the pH value.

In subsequent studies Binks and Horozov (2005a) demonstrated that silica particles are sufficient for the stabilization of foam. They studied foam stabilization with five different types of silica particles differing in their hydrophobicity. Of those five types only two could be used to form foam (32% and 20% SiOH) on the surface leading to bubble sizes of around 5-50 μm in both cases. In a later study Binks and Murakami (2006) demonstrated that increasing the hydrophobicity of the stabilizing silica particles at a fixed volume fraction of water (relative to air), equal to 0.056%, can cause phase inversion of air-in-water foams to water in air powder. A fixed mass of 2g of very hydrophobic silica particles (14% SiOH) was used to demonstrate the transformation from dry powder to souffle-like air-in-water foam by increasing the volume of water in a sealed vessel. In yet another study Binks, Duncumb and Murakami (2007) increased the pH to increase the hydrophilicity of hydrophobic particles (at a concentration of 20% SiOH). This induces a transitional phase inversion from a water-in-air powder to an air-to-water foam. Also, they showed that the transformation from an aqueous dispersion to particle-stabilized foam using moderately hydrophobic particles (66% SiOH) can be achieved by increasing the salt concentration. The particles become more hydrophobic as the concentration of salt is increased.

Table 7.1: Literature review

Reference	Type	Size	Modification	Conclusions/Observations
Alargova et al. (2004)	polymer rodlike particles	less than 1 μm and the length of a few tens of micrometers	epoxy-type photoresist SU-8	Foam volume remained the same for more than 3 weeks in closed cylinder and 1 week in open cylinder. When the pressure was reduced, the foam stated increasing the volume and reached twice its initial volume where it remained constant for hours.
Binks and Horozov (2005a)	Fumed silica particles	20-50 nm	Dichlorodimethylsilane (DCDMS)(14%-100% SiOH)	Stable foam can be produced by the silica particles containing 32% and 20% SiOH and the both foamability and foam stability produced by the less hydrophobic silica particles (42% and 51% SiOH) can be improved by the addition of salt.
Binks and Murakami (2006)	Fumed silica particles	20-30 nm	Dichlorodimethylsilane (DCDMS)	Phase inversion of particle-stabilized air-in-water foams to water-in-air powders can be achieved either by increasing the inherent hydrophobicity of the stabilizing silica particles at constant air/water ratio or by increasing the air/water ratio at fixed particle hydrophobicity

Fujii et al. (2006)	Latex particles	Diameter: 780 nm≈1.62 μm		The effect of varying the particle size, latex concentration, and latex surface composition on foam stability were studied in detail. The larger PNVP-PS latexes, the PNVP-PBrS, and the two PNVP-PMMA latexes gave highly stable foams, whereas PEGMA-PS, PNVP-PHPMA, and the charge-stabilized PS latex produced either no foams or foams with inferior long-term stabilities.
Gonzenbach et al. (2006a)	$\alpha - Al_2O_3$, $\delta - Al_2O_3$, ZrO_2, $\beta - Ca_3(PO_4)_2$, SiO_2 and Ti	From 30 nm to 1800 nm	butyric acid, valeric acid, propyl gallate, butyl gallate, butylamine, and hexylamine	Inorganic colloidal particles of various surface chemistries can be partially hydrophobized with tailored amphiphiles to produce wet foams exhibiting high air contents and remarkable stability. High concentrations of such modified particles ($35vol\%$) enabled the stabilization of an enormous air-water interfacial area. Air contents between 45 and 90% and average bubble sizes between 20 and 80 μm. All foams were stable against bubble growth and drainage over days
Binks, Duncumb and Murakami (2007)	Fumed silica particles	20-30 nm	Dichlorodimethylsilane (DCDMS) (20%, 32% and 66% SiOH)	Very hydrophobic particles (20% SiOH) raise their hydrophilicity by increasing the pH and induces a transitional phase inversion from a water-in-air powder to an air-in-water foam. The moderately hydrophobic particles become increasingly hydrophobic with the increasing salt concentration and transformation from an aqueous dispersion to particle-stabilized foam can be achieved.

Binks, Murakami, Armes, Fujii and Schmid (2007)	PS Latex Particles	0.80±0.09 μm	PAA homopolymer	Cationic, flocculated poly(acrylic acid)-coated latex particles can stabilize aqueous foam at low pH. No foam is possible at high pH when the particles are colloidally stable and negatively charged. Defoaming can be achieved simply by increasing the pH of the system after formation.
Gonzenbach et al. (2007)	Alumina powder	28nm ≈ 1800 nm	Short-chain amphiphilic molecules: propionic acid and valeric acid	The microstructure of wet particle-stabilized foams can be tailored in a wide range by adjusting the composition of the initial colloidal suspension (short amphiphile content, particle concentration, pH, ionic strength, and particle size).
Liu et al. (2009)	Laponite RD, a synthetic hectorite	Thickness of 91 nm and diameter about 30 nm	CTAB, TTAB, and DTAB	For surfactants with longer alkyl chain surfactants, stable foams are obtained at lower concentrations.

Binks, Murakami, Armes, Fujii and Schmid (2007) demonstrated that not only silica particles can stabilize aqueous foams at low pH, but also cationic, flocculated poly(acrylic acid)-coated latex particles. They showed that no foam is possible at high pH when the particles are colloidally stable and negatively charged. Defoaming can be simply achieved by increasing the pH of the system after formation.

Gonzenbach et al. (2006a) used several different inorganic colloidal particles which were treated with suitable different short-chain amphiphilic molecules. Later (Gonzenbach et al., 2007) they focused on wet foams produced by hydrophobized aluminium particles and found that high volume particles showed neither bubble growth nor drainage over more than 4 days. The bubble sizes of the wet foams were between 10 and 200 μm and air contents was between 45% and 90%. These results were obtained by varying the coating of the particles using the short-chain amphiphilic molecules (to achieve different amphiphilic properties), the particle concentration, the pH, the ionic strength, and the particle size in the initial suspension. They reported particle concentrations in volume percent (rather than weight percent).

Another type of particle, polymer latex, has also been used to study the stabilization of foam. Fujii et al. (2006) showed that highly stable foam can be produced by PNVP-PS, the PNVP-PBrS, and the two PNVP-PMMA latexes while other types of polymer latex particles produced either no foam or foams with inferior long-term stabilities.

Most of the recent studies used homogenizers or household home mixers to make foam, but there is no work on particle stabilized foam generated by UC. In this study, in addition to high shear mixer UC was also used to produce foams and foams stabilized by silica particles using different foam generation methods is compared. High power ultrasound is known to produce cavitation bubbles in liquids. These bubbles are generated from the gas nuclei and stabilized in the bulk of the liquid or trapped in the vessel walls and solid impurities (Leighton, 1995, Louisnard et al., 2001). The size of the bubbles may be of the order of nanometers or micrometers in diameter depending on the nature of the liquid media and the conditions used in the studies (Louisnard et al., 2001, Cho et al., 2005, Ziga and Aguilera, 2008). Also, higher power ultrasound has become an alternative to many conventional processing steps, such as homogenization, emulsification, degassing, defoaming, reduction of particle

size, pasteurization and solid/liquid separation. The use of an ultrasonic processor is often driven by economic benefits, yet in some cases a unique product functionality can be achieved (Patist and Bates, 2008).

In summary, all investigations of solid particle stabilized foam found that foams can be stabilized by hydrophobic particles. Generally, particles of very high hydrophilicity or hydrophobicity cannot stabilize foam. Hydrophobicity of the solid particles can be controlled by varying the pH and addition of salt. Furthermore, foamability using solid particles that have been prepared with various methods and with various additives have been studied. These studies largely concentrated on the foamability, stability of foams and foam volume, and some of them also considered foam life, drainage, and mean bubble size. However, so far the effect of the particle concentration on the pH and viscosity have not been studied in detail. Especially, there is no research that compares methods of foam generation: mechanical agitation (MA) and ultrasound cavitation (UC).

7.2 Results and discussion

The effect of silica particles on protein and surfactant foams in detail in chapters 5 and 6 is studied. In this chapter, foams stabilized by silica particles only are investigated. The fully hydrophilic particles did not foam. The other three particles are (see Table 3.1 in Chapter 3 for details).

- Weakly hydrophobic silica particle, R972
- Moderately hydrophobic silica particle, R812
- Strongly hydrophobic silica particle, R202

In the results and discussions, the foams produced by MA and UC are compared. A series of experiments varying key parameters of the system were performed. These key parameters are the concentration of silica in water, the degree of hydrophobicity of the silica, the viscosity, and the pH value. It turns out that, all other parameters being equal, the foam generation method (UC, MA) matters.

In section 7.2.4 and 7.2.5 the effects of varying the pH values and the viscosity are investigated. In doing so one method only was considered namely MA simply because it gives better foamability.

7.2.1 Effect of foam generation method and silica particle concentration

In the method of MA, five concentrations of silica particles (0.1, 0.3, 0.5, 1.0, and 1.5 wt%) are considered. There are three concentrations of silica particles (0.1, 0.3, and 0.5 wt%) used in the experiments with UC. The reason for the reduced concentration range in UC is that at room temperature and pressure foam cannot be produced at higher concentration of silica using UC. The foamability, drainage, liquid holdup in foam, foam breakage and foam microstructure are observed and discussed. Surface tension and viscosity of the dispersions have also been investigated to assist in understanding of the behaviour of these foams.

Surface Tension of the Solutions and Dispersions

Partially hydrophobic silica particles act like surfactants. Thus they can lower the surface tension and foams can be produced solely by silica in water. In this section the effect of particle concentrations on the surface tension was quantified; these results should indicate the ability to foam. To determine this the surface tensions of an water-ethanol mixtures (ratio of 20:1) was measured and compared this to the surface tension of pure water. The reason to use the ethanol mixture is that hydrophobic particles would not disperse in pure water, and hence these foams had also ethanol added. The surface tension of the ethanol water mixture will provide a baseline measurement against which the additional effect of added silica particles at various concentrations can be compared.

The surface tensions are measured and they are 72.25 mN/m and 58.48 mN/m for water and the mixture of water and ethanol respectively. There were no differences in surface tension between the mixture of water and ethanol with and without hydrophilic silica. This indicates that hydrophilic silica had no contribution to lower the surface tension. When the hydrophobic silica were dispersed into the mixture of water and ethanol, the surface tensions were all around 55.00 mN/m. The surface tensions of suspensions with hydrophobic silica are lower than those of the mixture of ethanol and water. This indicates that hydrophobic silica particles act like surfactants and the surface tension deceases with hydrophobic silica adding in the suspension. However, there is no difference in surface tension between the three particles with different surface tension.

The surface tension was also measured at concentrations ranging from 0.1 to 1.5 wt%. This

change in concentration resulted only in a small decrease from 55.45 to 54.88 mN/m as the R972 concentration increased. In the R812 and R202 particle dispersions, there were also only a small decrease at lower concentrations ($\leq$ 0.5 wt%). Yet a much larger reduction of the surface tension was found at higher concentrations of those particles (i.e. 1.0 and 1.5 wt%). The values are 52.21 mN/m and 49.89 mN/m for R812 particles, 49.58 mN/m was for R202 particle at a concentration of 1.0 wt%. In general, the higher the concentration of particles in the dispersion was observed, the lower the initial surface tension. Also, the higher the concentration of particles, the faster the surface tension started to drop in these dispersions.

Viscosity of the Solutions and Dispersions

In this section the viscosity of the particle dispersions was measured. Viscosity is an important factor for foam stabilization.

The viscosity was measured using a shear stress-controlled rheometer. Figure 7.1 shows that for the dispersion system at high concentrations the viscosity decreases with increasing shear rate due to the reversible destruction of the structure of the dispersions, which means that the dispersions are shear-thinning fluids. At very low concentrations they are close to being Newtonian, as indicated by a zero slope in Figures 7.1(a) and 7.1(b). The figures also show that the viscosity of the dispersions increased with increasing concentration of R972 and R812 particles. As the concentration increases, there are more interactions between the hydrophobic particles, to the extent that particles tend to aggregate. This results in a stronger network which means a higher viscosity.

There is no results for the R202 particle dispersion for the following reason: In the measurement of viscosity, the gap between the parallel plates needed to be at least 10 times greater than the diameter of the particles in the dispersion. In the dispersion of a very hydrophobic surface on R202 particles, large clusters ($\approx$ 38 μm) were formed in the dispersion (details can be found in Chapter 4). Thus, a large gap between the plates was needed for the dispersion of R202 particles. However, the viscosity of larger particle clusters in water is very low so that the liquid cannot be held in the required gap between the plates at higher shear rates with the lower concentrations of R202 particles.

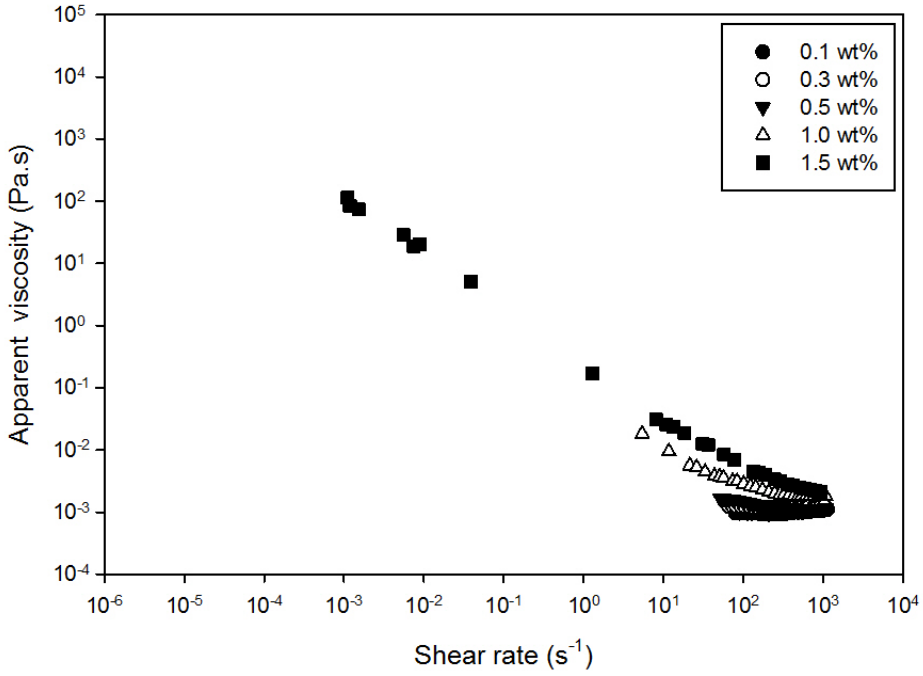

(a) R972

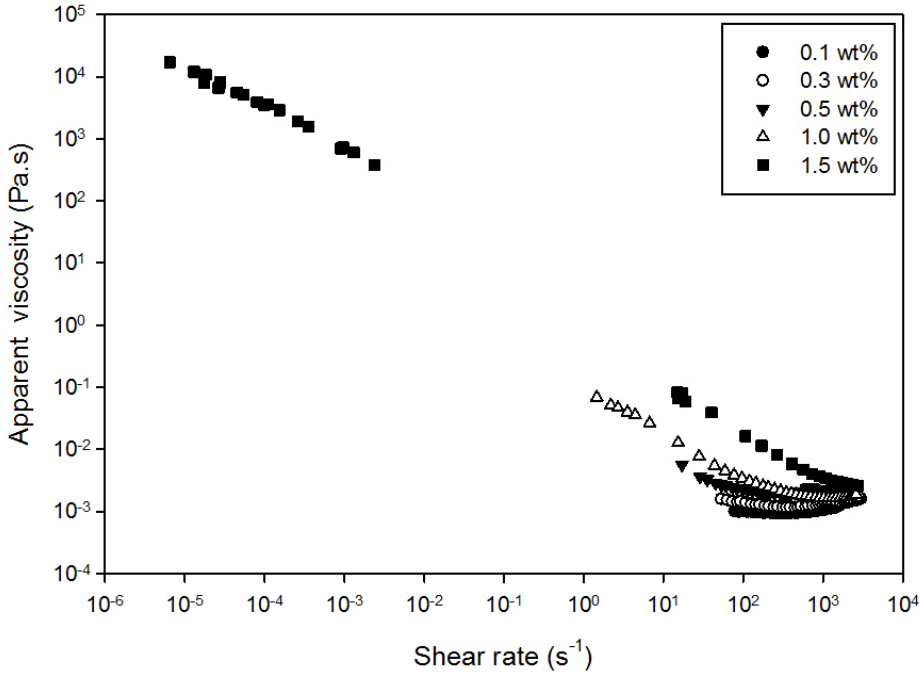

(b) R812

Figure 7.1: Flow curves of hydrophobic silica particle dispersion at different concentrations: (a) R972 (b) R812.

Mathematically, the relationship between the shear rate, γ, the shear stress τ and the viscosity η

can be described by the following power law.

$$\tau = k \cdot \dot{\gamma}^n \tag{7.1}$$

$$\eta = k \cdot \dot{\gamma}^{n-1} \tag{7.2}$$

where k is the consistency coefficient. The exponent n is called the power law index. For a shear thinning fluid: $0 < n < 1$. The more shear-thinning the product, the closer n is to zero. The measurements were fitted to Equations (7.1) and (7.2) to obtain the parameters. The results are summaries in Table 7.2. It was found that for concentrations under 1.0 wt% the particles R972 and R812 particle dispersions can be described by Equation (7.1) with an r^2 confidence of 0.99 or better (see Table 7.2 for details). At lower concentrations R972 and R812 particle dispersions behave as Newtonian fluids indicated by n close to 1. When the concentration of the particles increases then n falls below 1, which means that the fluid is more shear thinning. The parameters of the power model are summarized in Table 7.2. The value of k increases and n decreases with increasing concentration of particles. At the lowest concentrations of particles, the suspensions behave like a Newtonian fluid when $n = 1$. The suspensions become more shear-thinning with increasing particle concentration.

Table 7.2: Power law model parameters for the concentration of silica particle dispersions.

R972	*k (Pa.s)*	n	r^2
0.1 wt%	$9.661*10^{-4}$	1.00	0.9967
0.3 wt%	$9.746*10^{-4}$	1.00	0.9986
0.5 wt%	$3.479*10^{-3}$	0.87	0.9920
1.0 wt%	$4.222*10^{-3}$	0.87	0.9918
1.5 wt%	$4.602*10^{-2}$	0.54	0.9636
R812	*k (Pa.s)*	n	r^2
0.1 wt%	$9.846*10^{-4}$	1.00	0.9979
0.3 wt%	$9.772*10^{-3}$	1.00	0.9956
0.5 wt%	$1.285*10^{-2}$	0.70	0.9780
1.0 wt%	$1.931*10^{-2}$	0.71	0.9833
1.5 wt%	$9.581*10^{-1}$	0.16	0.9257

7.2.2 Foam properties

MA

In this section, the results and the discussion of the foam stabilized by these hydrophobic silica particle using MA is investigated.

Foam Formation and Breakage

Figure 7.2 shows the initial foam height plotted as a function of particle concentration 5 minutes after foam formation. The foamability of foam stabilized by R972 and R812 increased with increasing concentration of particles. The foamability of foam stabilized by R202 hydrophobic particles first increased with increasing concentration and then decreased when the concentration was over 1.5 wt%.

Foamability was approximately the same for R972 and R812 while there was only half the foam volume generated by the R202 particle dispersion. In all three different silica, there was no foam breakage observed for one month.

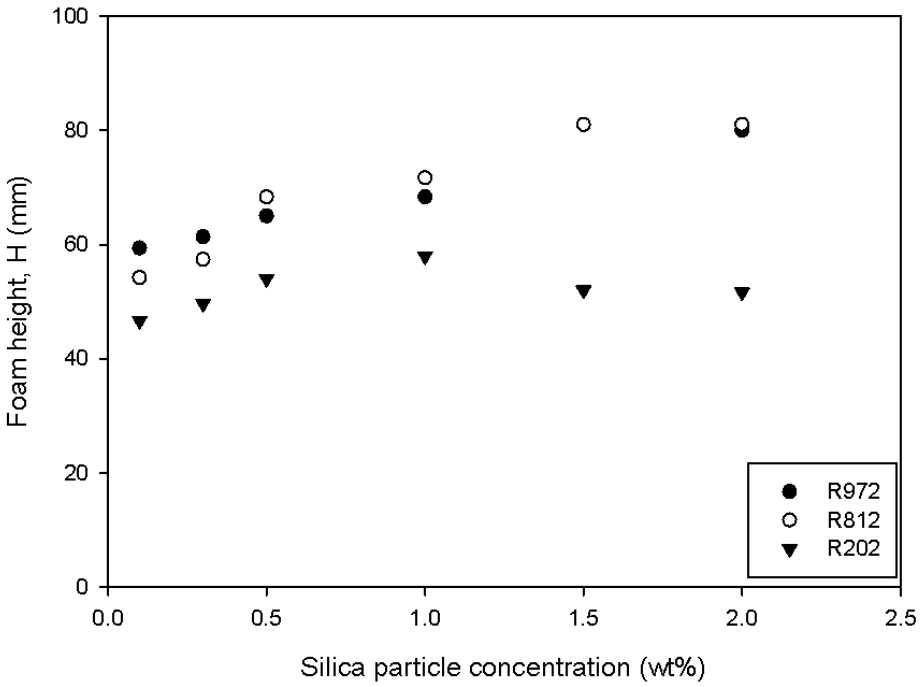

Figure 7.2: Foamability of pure water containing partially hydrophobic silica particles; MA.

Foam Drainage and Liquid Holdup

Drainage almost ended during the first few minutes after formation at lower particle concentrations and the drainage rate declined with increasing particle concentration (see Figures 7.3, 7.4, and 7.5). These drainage curves are well fitted by Equation (3.13) (see page 41) where h is the liquid level, and t_d is the foam drainage time.

The value of a indicates the maximum liquid level and $1/b$ is the time constant. The parameters are listed in the Table 7.3. The maximum liquid level decreases with increasing concentration of particles for all three types of particles and also with increasing hydrophobicity. At higher concentrations of particles, more bubbles can be formed and thus there is more liquid remaining in the foams.

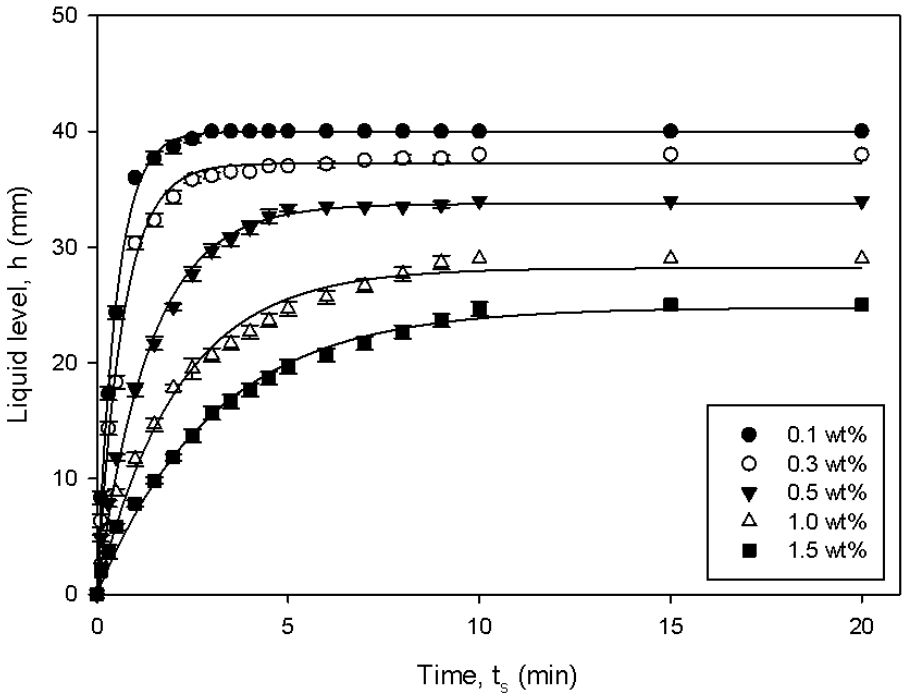

Figure 7.3: Drainage of foam containing silica particles: R972; MA.

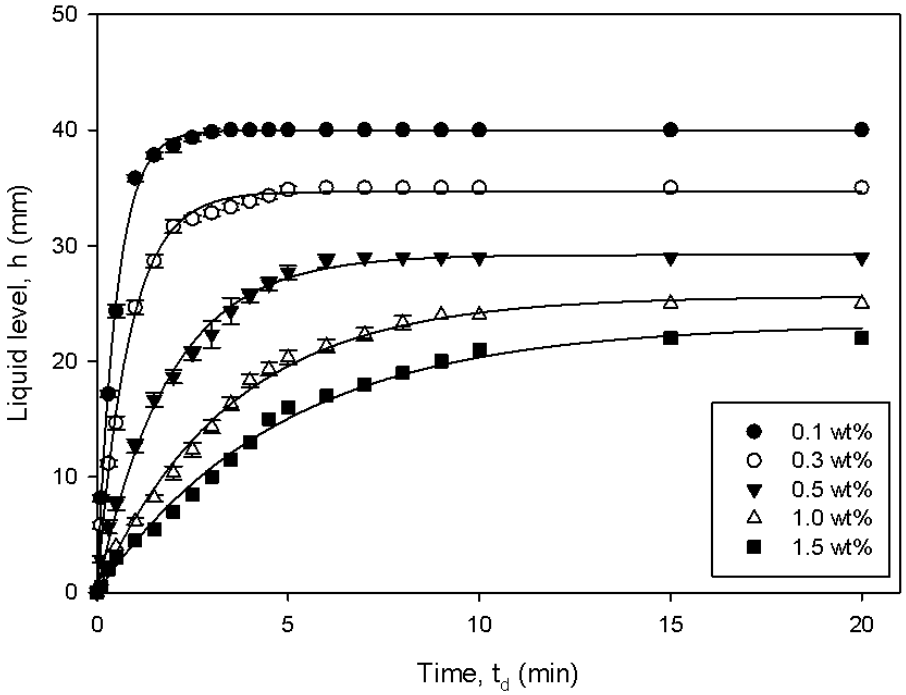

Figure 7.4: Drainage of foam containing silica particles: R812; MA.

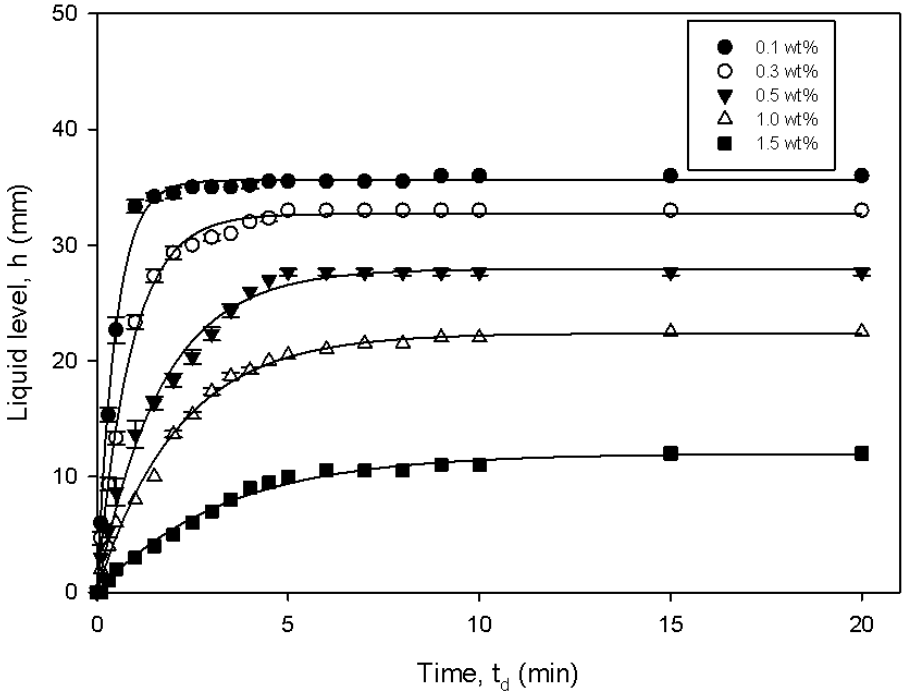

Figure 7.5: Drainage of foam containing silica particles: R202; MA.

Table 7.3: The parameters of the drainage equation at different concentrations of silica particles in dispersion; MA.

R972	a	b	r^2
0.1 wt%	39.8	0.51	0.9981
0.3 wt%	37.23	0.69	0.9979
0.5 wt%	33.75	1.34	0.9924
1.0 wt%	28.29	2.05	0.9919
1.5 wt%	24.89	2.96	0.9953
R812	a	b	r^2
0.1 wt%	39.8	0.51	0.9981
0.3 wt%	34.71	0.82	0.9967
0.5 wt%	29.21	1.78	0.9953
1.0 wt%	25.62	3.46	0.9909
1.5 wt%	23.22	4.79	0.9932
R202	a	b	r^2
0.1 wt%	35.60	0.50	0.9962
0.3 wt%	32.74	0.90	0.9961
0.5 wt%	27.89	1.73	0.9928
1.0 wt%	22.37	2.10	0.9940
1.5 wt%	11.98	3.25	0.9925

In Pugh (1996)'s study, he noted that the drainage rate of foams may be decreased by increasing the bulk viscosity of the liquid from which the foam is prepared. In his study, there are many ways to achieve a higher bulk viscosity, for example adding a solute such as glycerol, liquid paraffin or polyoxyethylene. He also mentioned that adding electrolyte to form a gel network has been proved to halt the drainage. In his study, an alternative way to decrease foam drainage was to increase the surface viscosity by increasing the surfactant concentration in the foaming solution. He explained this is because the denser packing of surfactant molecules at the interface can cause high adhesive or cohesive bonding. Thus, he concluded that the bulk viscosity affects the thinning of thick films whereas the surface viscosity can affect the thinning of the thin films. From the previous experimental result in section 7.2.1 the higher concentrations lead to higher viscosities. Therefore, the decrease of drainage is caused by an increase in bulk viscosity and also an increase in the number of particles adsorbed at the interface.

Next the wetness of these foam stabilized by silica by looking at the the liquid holdup is presented. The liquid holdup is plotted as a function of particle concentration in Figure 7.6. The liquid holdup increases first with increasing concentration of all three types of silica, but with the R972 and R812

particles it stops increasing when the concentration is over 1.0 wt%. It was shown in previous results (see section 7.2.2) that the foamability increases while the drainage decreases with increasing silica concentration. The liquid holdup of the foam produced by the most hydrophobic silica is about twice that of the other two less hydrophobic silica foams. The medium hydrophobic particle foams have higher liquid holdup than the least hydrophobic particle foams at the lower concentrations. The most hydrophobic silica foams have the highest liquid holdup but less foam volume, therefore, much wetter but smaller foam heads were produced.

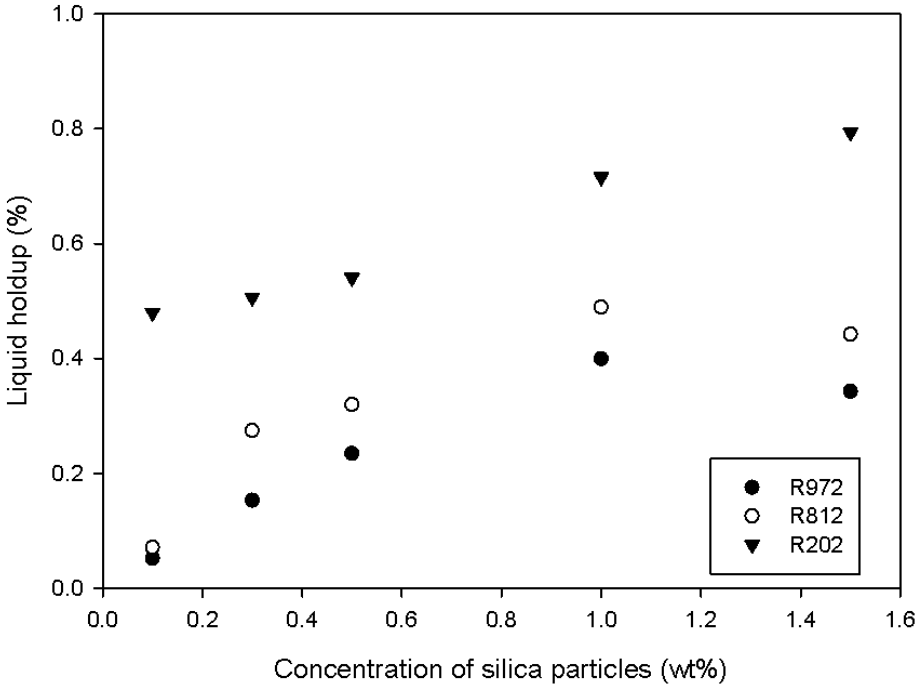

Figure 7.6: Liquid holdup in the foam containing silica particles.

Foam Microstructure

Images of foams stabilized by R972 silica are shown in Figure 7.7. At lower concentrations (from 0.1 wt% to 0.5wt%), the foam consisted of two horizontal layers containing bubbles which had different mean bubble sizes (see Figure 7.8 for a schematic explanation). The mean bubble size in the lower layer was around 30 μm at concentrations from 0.1 wt% to 0.5 wt% while the mean bubble sizes in the upper layer were 3.5 mm, 1.4 mm and 0.9 mm at the silica concentration at 0.1, 0.3 and 0.5 wt%, respectively. The ratios of the height of lower layer foam to the upper layer foam were 0.05, 0.2 and

0.4 at the silica concentration of 0.1 wt%, 0.3 wt% and 0.5 wt%, respectively. In the foam stabilized by R812 particles, similar layers were found. The mean bubble sizes in the lower layer foam were also all around 30 μm while the mean bubble sizes in the upper layer foam were 2.1 mm, 0.8 mm and 0.6 mm at silica concentrations of 0.1 wt%, 0.3 wt% and 0.5 wt%, respectively. The ratios of the lower layer foam and upper layer foam were 0.1, 0.4 and 0.75 at particle concentrations of 0.1, 0.3 and 0.5 wt%, respectively. Above 1.0 wt% silica, foams only consist of micron sized bubbles. The rate of the bubbles in the upper layer foam grows slowly but there was no foam collapse for a week.

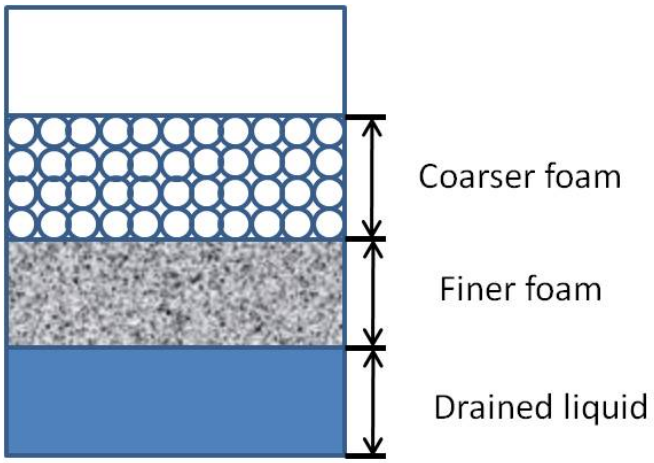

Figure 7.7: Two layers foam produced by lower concentration of silica particles.

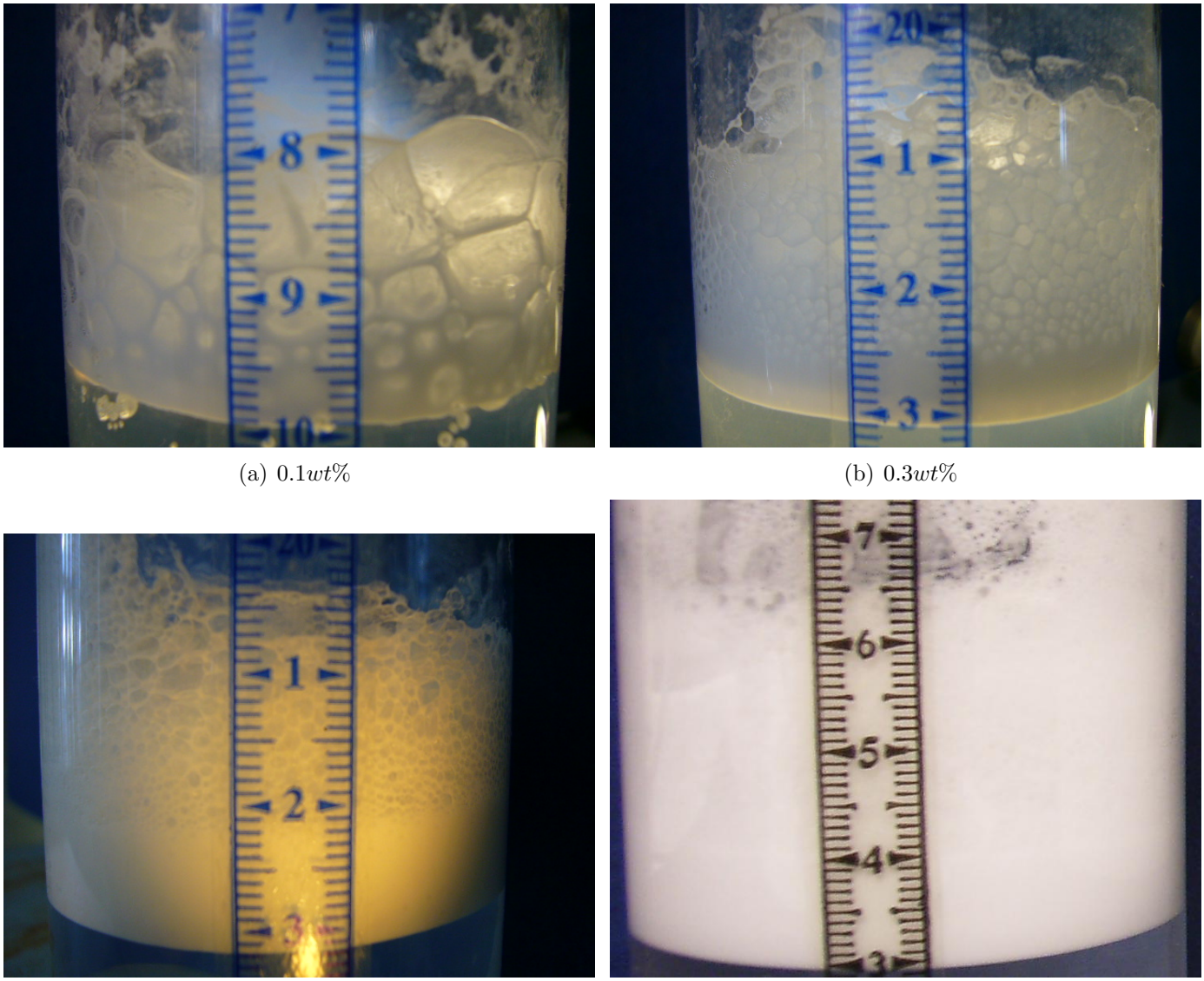

(a) 0.1$wt\%$ (b) 0.3$wt\%$

(c) 0.5$wt\%$ (d) 1.0$wt\%$

Figure 7.8: Foam images; Images of foam stabilized with R972 silica particles.

The bubble growth in the lower layer foam was monitored over time using a camera. The bubble size distribution was determined by looking at 200 bubbles in each image. Figure 7.9 shows typical size distributions of foam stabilized by R812 particles in different concentrations at 5 minutes, a week and a month after foam formation. These bubble size distributions show that the range of bubble sizes are all between about 10 μm to around 75 μm and are not affected by the increasing particle concentrations and time evolution. Figures 7.10(a) and 7.10(b) show how the bubble size varies according to the foam standing time. There is no bubble growth observed within a month. Foam images of R972 and R812 at 0.1 wt% are shown in Figures 7.11 and 7.12. Very similar foams were

found at other concentrations. These bubble size distributions can also be described by the statistical parameters which are summarized in Tables 7.4 and 7.5. It shows that the mean bubble sizes are all around 30 μm to 40 μm. In general, the mean bubble size of foam stabilized by R972 particles is slightly smaller than the foam stabilized by R812 particles. For R812 particles, the bubble size is not affected by an increasing concentration of particles while there is a small increase of the bubble size in the foam stabilized by R972 particles. Positive and close to zero values of skewness were obtained from the bubble size distribution. This indicates that the bubbles are homogenous and there are no larger bubbles in the foam resulting in the median being smaller than the mean bubble diameter d_{10}. The kurtoses are all similar and close to zero. This indicates that the bubble size distributions are close to the normal distribution. For the most hydrophobic silica particles, R202, a mixture of particle clusters and bubbles was generated. Due to the poor foam texture, it was not possible to obtain reasonable microscope images as shown in Figure 7.13.

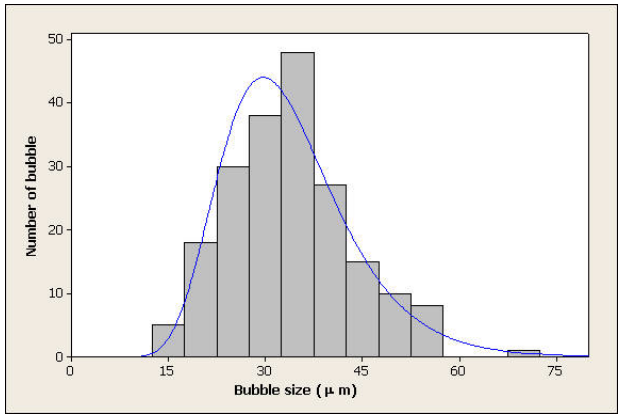

(a) 0.1$wt\%$ - initial

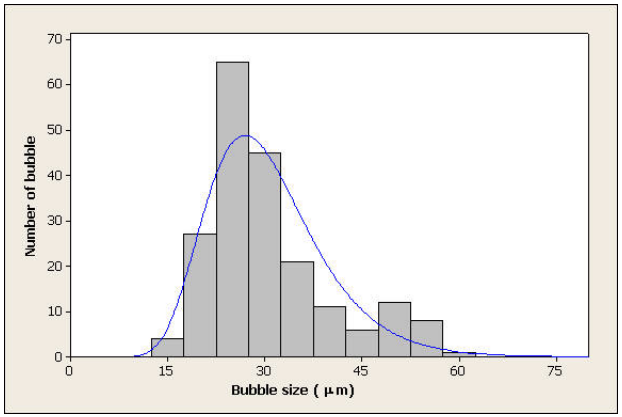

(b) 0.3$wt\%$ - initial

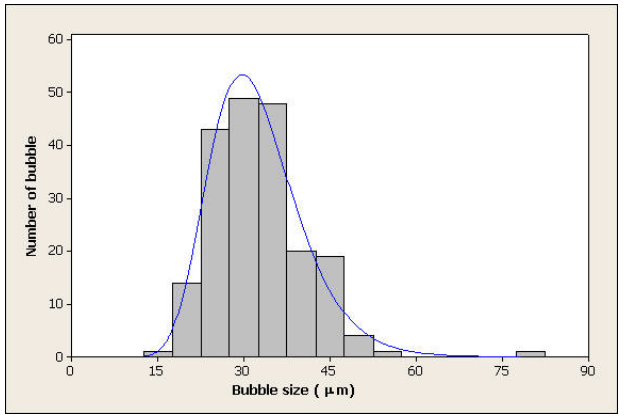

(c) 0.5$wt\%$ - initial

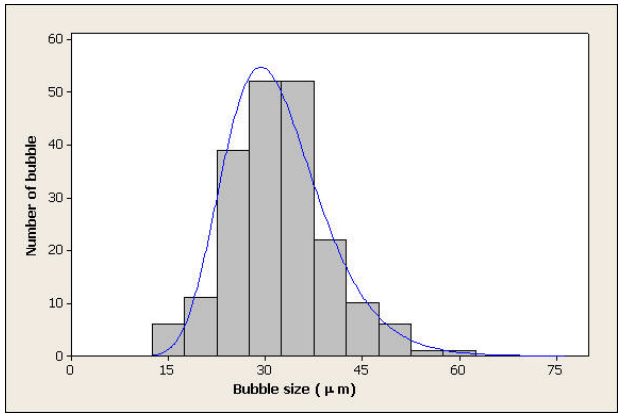

(d) 0.1$wt\%$ - 1 week

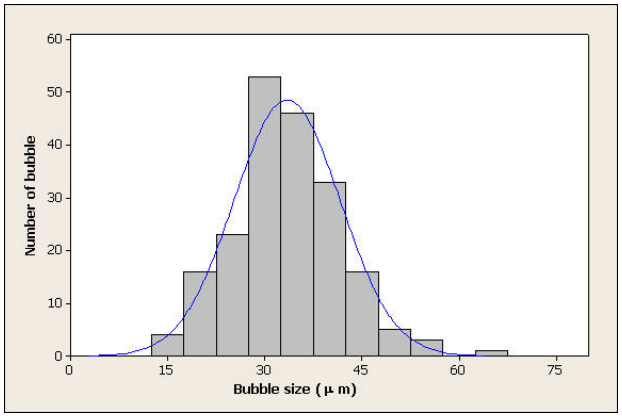

(e) 0.3$wt\%$ - 1 week

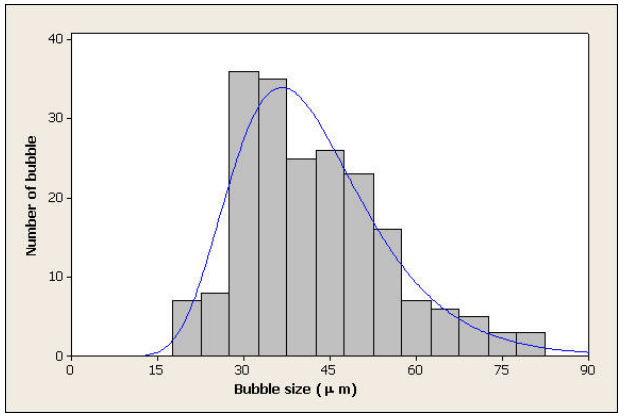

(f) 0.5$wt\%$ - 1 week

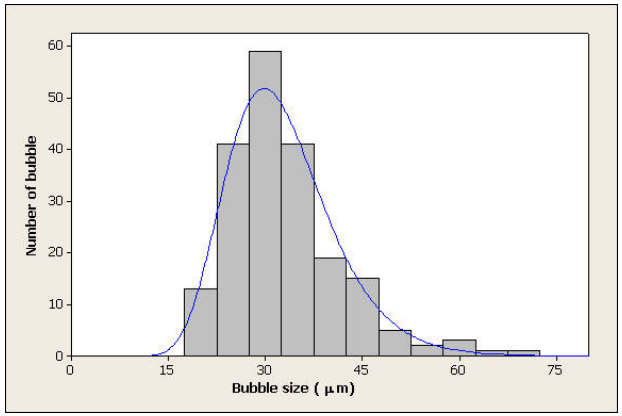

(g) 0.1$wt\%$ - 1 month

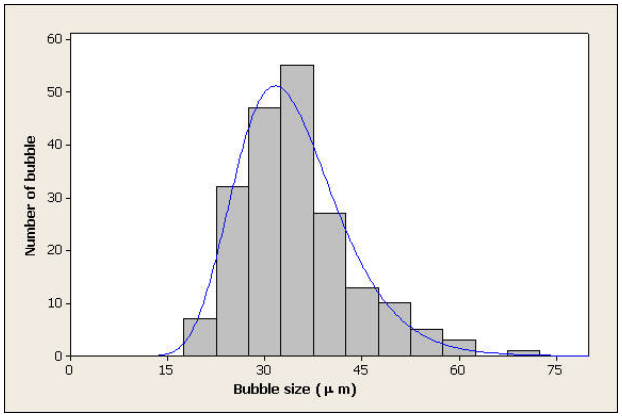

(h) 0.3$wt\%$ - 1 month

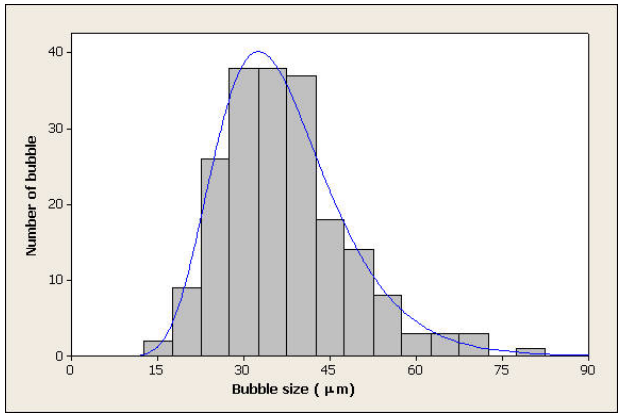

(i) 0.5$wt\%$ - 1 month

Figure 7.9: Bubble size distribution; with R812 silica particles; MA.

Table 7.4: Statistical parameters for foam bubble size distributions of R972.

0.1 wt%	d_{10} (μm)	d_{32} (μm)	StDev	Min (μm)	M (μm)	Max (μm)	S	K
initial	29.74	32.59	6.44	15.17	29.24	53.37	0.72	0.95
1 week	30.44	32.71	5.77	19.46	29.07	53.40	0.85	0.86
1 month	30.09	33.01	6.56	15.33	29.59	54.76	0.69	0.98
0.3 wt%								
initial	28.70	32.00	7.31	10.32	28.73	41.78	-0.39	-0.53
1 week	29.74	31.71	5.40	16.29	29.40	46.57	0.46	0.34
1 month	31.44	33.59	5.84	17.11	30.78	50.03	0.30	-0.07
0.5 wt%								
initial	29.79	32.81	6.70	16.57	28.95	52.06	0.55	0.26
1 week	29.10	32.92	7.48	14.44	28.71	52.54	0.52	0.13
1 month	31.58	34.15	6.37	16.25	30.91	51.68	0.46	0.43
1.0wt%								
initial	30.78	34.95	6.65	17.25	30.55	55.98	0.65	0.47
1 week	31.22	34.52	7.35	16.98	31.21	56.65	0.55	0.85
1 month	32.68	35.05	7.69	17.85	31.25	57.25	0.45	0.24
1.5wt%								
initial	32.38	35.76	7.50	16.57	32.23	52.06	0.25	-0.30
1 week	32.11	37.37	9.32	14.44	32.14	58.95	0.40	-0.33
1 month	33.21	38.13	8.93	15.05	31.51	63.49	0.79	0.20
2 month	32.80	35.36	6.41	20.16	32.05	59.24	0.68	0.76
3 month	32.62	36.61	8.06	18.16	31.35	54.19	0.55	-0.31

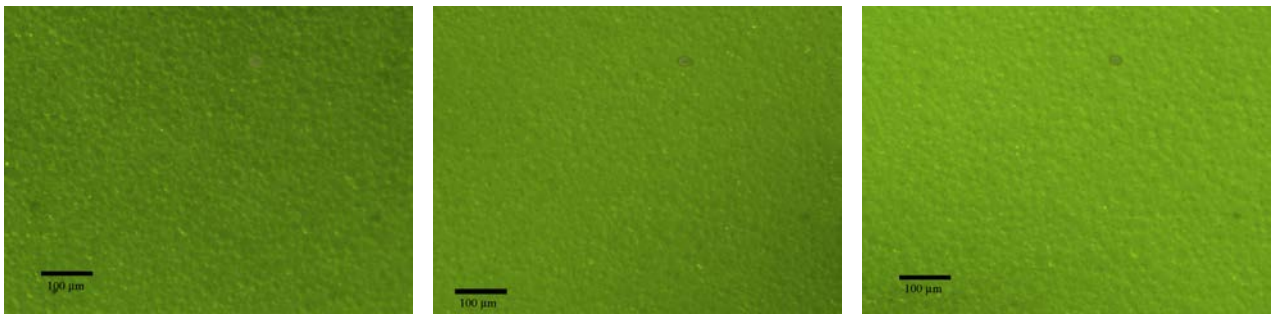

(a) 5 min (b) 1 week (c) 1 month

Figure 7.11: Foam images; Image of foam stabilized with 0.1 wt% R972 silica particles; MA (350x magnification).

At lower concentrations of silica, the lower layer (with smaller particles) is thinner than at high concentrations. A possible explanation of this is that to create smaller bubbles a larger surface area of the film interface is required. This means more silica are required. However, larger bubbles can be produced with lower concentrations of particles. There is also less drainage at higher particle concentrations (see section 7.2.2), which supports this explanation.

Smaller and more bubbles in foams stabilized were expected by the most hydrophobic silica

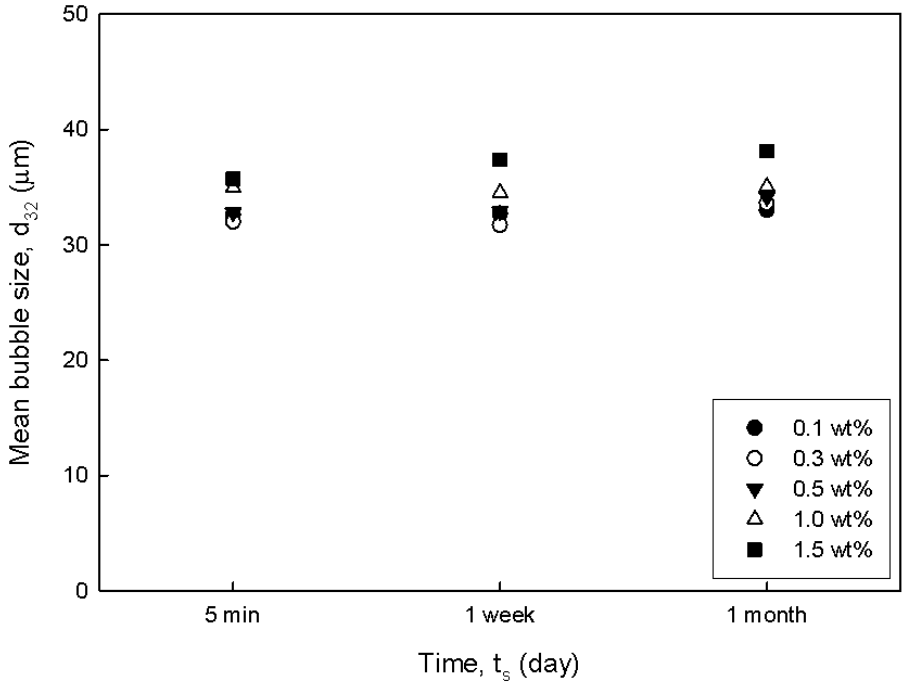

(a) R972

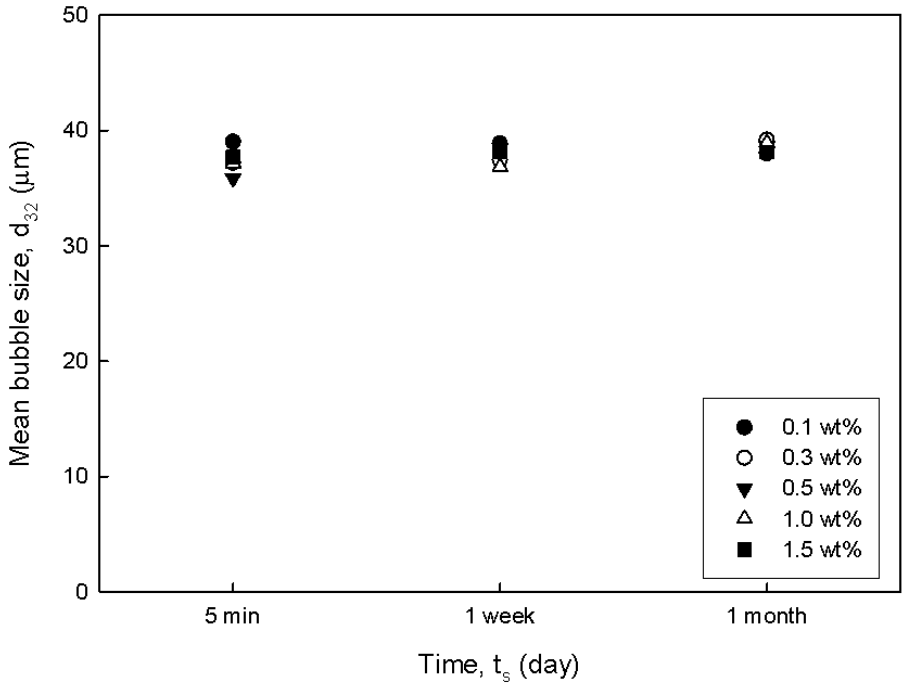

(b) R812

Figure 7.10: Variation of mean bubble size with foam standing time; R972 and R812; MA.

(a) 5 min (b) 1 week (c) 1 month

Figure 7.12: Foam images; Image of foam stabilized with $0.1wt\%$ R812 silica particles; MA (350x magnification).

Table 7.5: Statistic parameters for foam bubble size distribution of R812.

0.1 wt%	d_{10} (µm)	d_{32} (µm)	StDev	Min (µm)	M (µm)	Max (µm)	S	K
initial	33.70	39.03	9.55	13.08	33.31	69.27	0.48	0.37
1 week	34.89	38.86	6.60	20.41	34.15	58.73	0.46	0.66
1 month	32.77	38.01	8.85	17.75	31.07	72.10	1.35	2.00
0.3 wt%								
initial	30.65	37.20	9.69	14.98	28.15	60.03	1.15	0.71
1 week	33.45	37.44	8.21	15.21	33.31	65.24	0.46	0.90
1 month	34.49	39.20	8.73	18.54	32.97	72.32	1.12	1.90
0.5 wt%								
initial	32.32	35.88	7.62	16.54	31.97	55.49	0.43	-0.34
1 week	32.23	38.48	9.91	13.71	31.16	71.24	0.84	0.88
1 month	32.22	38.68	10.11	14.67	31.05	71.65	0.79	0.44
1.0wt%								
initial	32.55	37.15	9.24	15.25	32.21	68.58	1.17	4.10
1 week	32.35	36.85	8.89	15.56	31.35	69.58	0.93	1.15
1 month	35.25	38.95	9.85	16.21	34.58	75.25	1.08	2.36
1.5wt%								
initial	33.15	37.75	8.91	13.08	33.08	57.02	0.27	-0.24
1 week	34.24	38.19	8.21	16.86	33.87	65.24	0.56	0.71
1 month	33.37	38.13	8.93	15.05	31.59	63.49	0.79	0.14
2 month	34.47	38.74	8.61	17.84	33.37	63.68	0.48	-0.18
3 month	34.89	38.78	8.21	16.29	33.96	65.52	0.60	0.39
4 month	34.28	39.20	8.98	16.35	32.50	66.98	0.94	1.12

because of the higher liquid holdup in this case. However, from the microscopy (see Figure 7.13) of the foam microstructure, there were silica clusters and irregularly shaped bubbles. Also in chapter 4 it has been reported that the R202 particles cannot be broken down to sub micron size, as the other two hydrophobic particles; the particle size of the R202 particle suspensions was measured to about 38 µm and 120 nm for R812 and R972 particles, respectively (see section 4.2.2 on page 62). These large particle aggregates prevent the formation of the interface and thus may be the reason

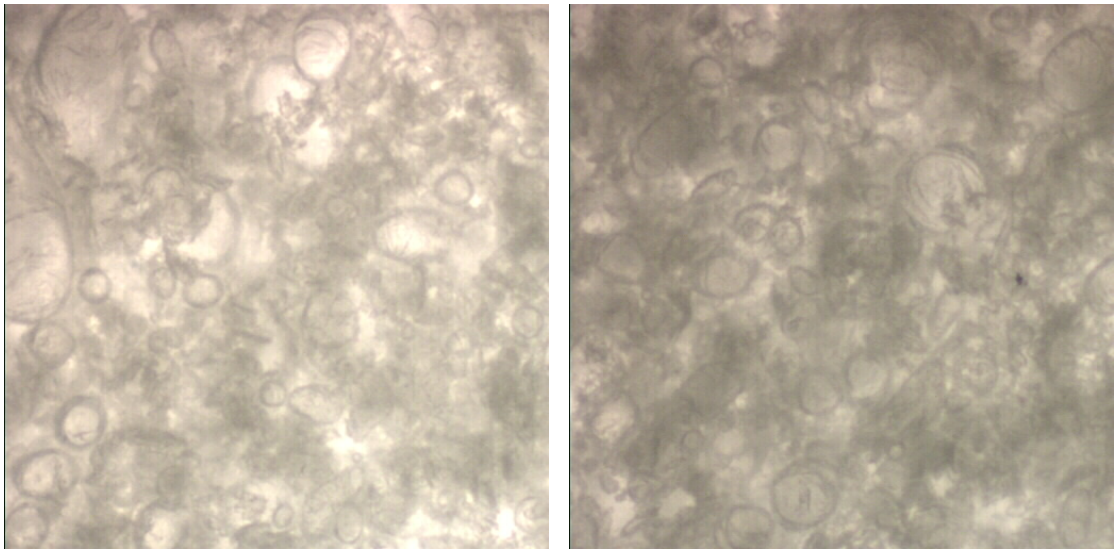

(a) $0.1wt\%$ (b) $0.5wt\%$

Figure 7.13: Foam Images; with $0.1wt\%$ and $0.5wt\%$ R202 silica particles; MA (90x magnification).

why there was less foamability in the case of the most hydrophobic foam.

UC

In this section, the results and the discussion of the foam stabilized by three different types of hydrophobic silica using UC are presented. There are three silica concentrations considered, 0.1 wt%, 0.3 wt% and 0.5 wt%. At higher concentrations no foam was produced.

Foam Formation and Breakage Figure 7.14 shows the foam produced by UC. The initial foam height 5 minutes after foam formation is plotted as a function of the silica concentration. The foamability increases with the concentration of the hydrophobic silica. The suspension of hydrophilic silica does not foam. At a concentration of 0.1 wt%, R812 particles can produce more foam than other types of hydrophobic silica particles. There is no significant difference in foamability between R972 and R812 particle foam but slightly poorer foamability has been found in the foam made from suspension of R202 particle concentrations at 0.3 wt% and 0.5 wt%. Immediately after foam formation, the foam height was recorded and the foam curves remained at a plateau for more than 3 weeks with nearly no breakage at 0.1 wt%, 0.3 wt% and 0.5 wt% in all three different silica.

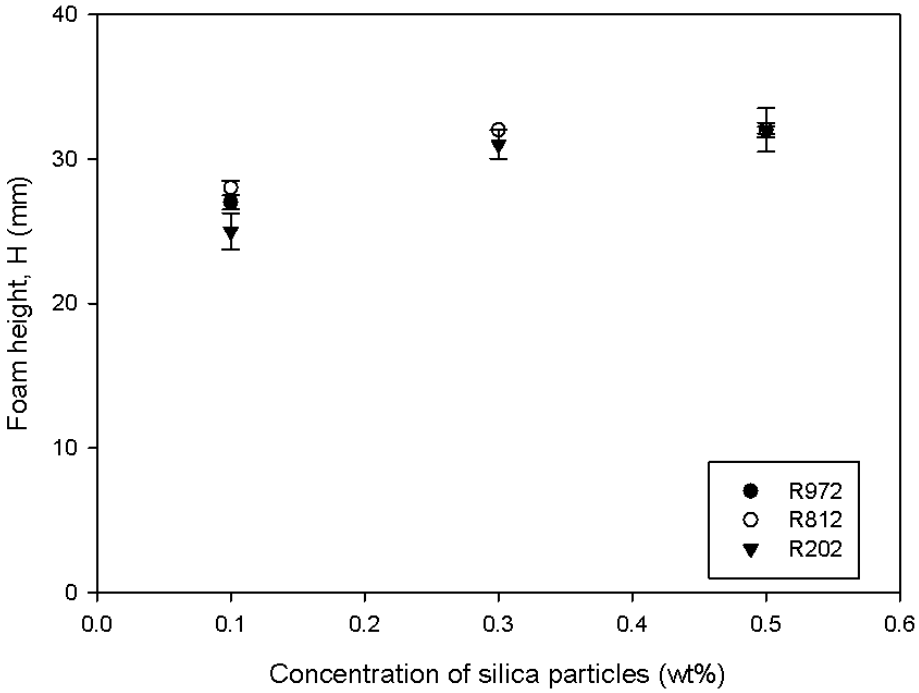

Figure 7.14: Foamability of pure water containing partially hydrophobic silica particles; UC.

Foam Drainage and Liquid Holdup The drainage curves for R972, R812 and R202 silica are plotted in Figures 7.15, 7.16, and 7.17. These curves can be fitted to Equation (3.13). The parameters obtained from the fit are listed in Table 7.6. The maximum liquid level decreases with both increasing concentration and the hydrophobicity of silica particles. Especially, a much lower maximum liquid level was observed with the most hydrophobic particles at 0.5 wt%.

The liquid holdups were plotted against particle concentration in Figure 7.18. The liquid holdup was higher in the foam produced with the lowest concentration for all types of particles and there is not much difference between of 0.3 wt% and 0.5 wt%. A higher liquid holdup was found in the foam produced by the most hydrophobic silica which is again due to the difficulty in breaking up the particle clusters (as in the case of the MA; see section 7.2.2).

Foam Microstructure In this section, the microstructure of foams produced by three different types of hydrophobic silica, R972, R812 and R202 was looked at. The images of the foams produced by these particles are presented.

Figure 7.19 shows the foam images obtained from the foam produced by R972 particles at 0.1

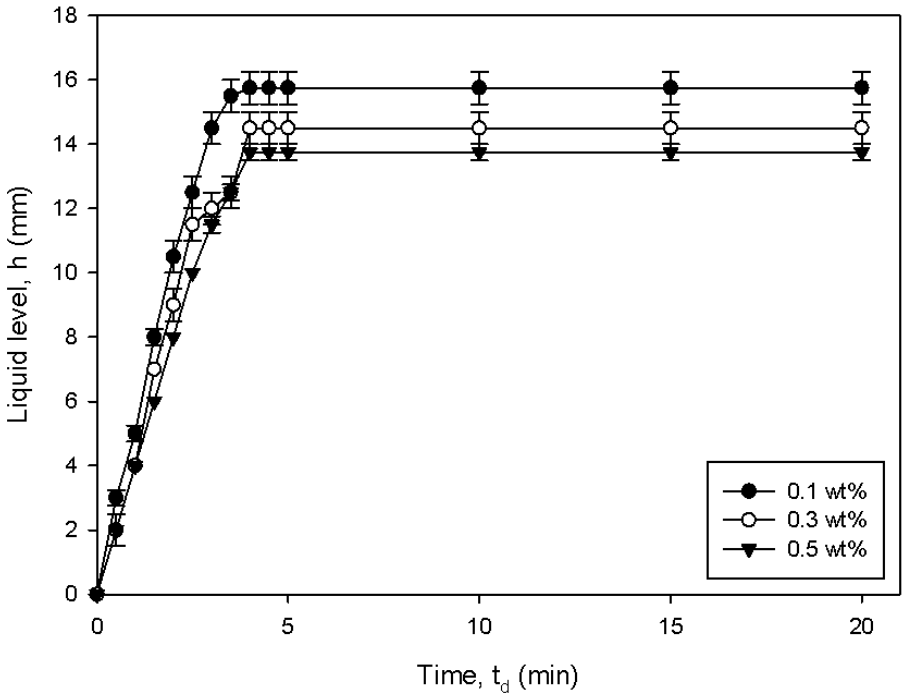

Figure 7.15: Drainage of foam containing silica particles: R972; UC.

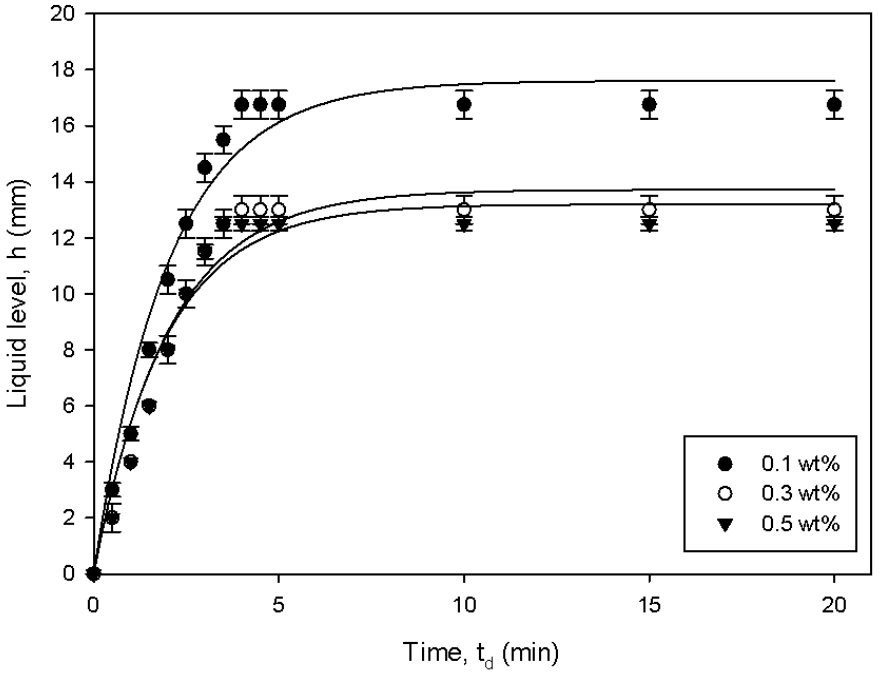

Figure 7.16: Drainage of foam containing silica particles: R812; UC.

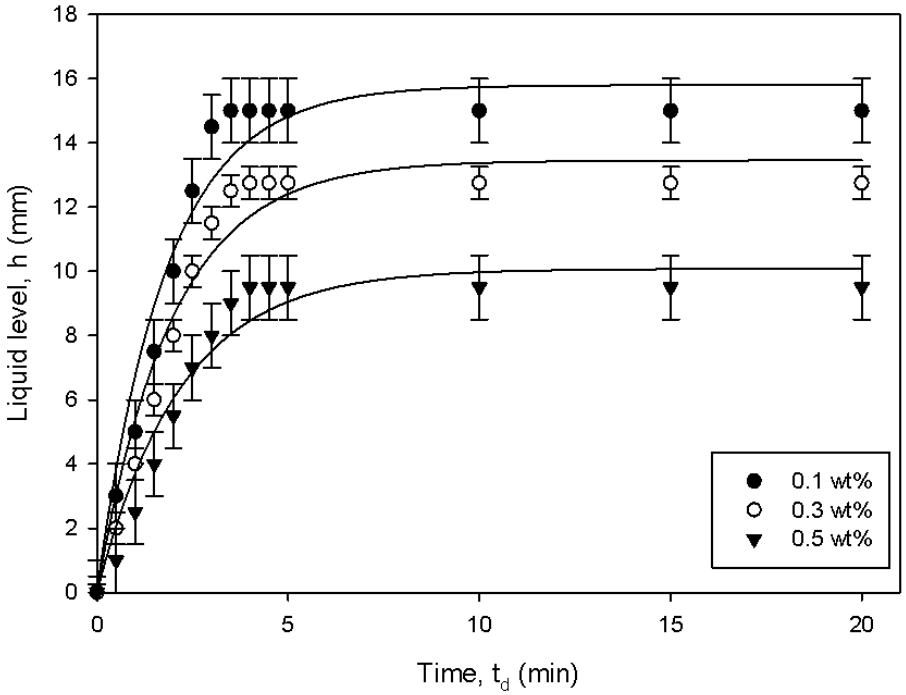

Figure 7.17: Drainage of foam containing silica particles: R202; UC.

Table 7.6: The parameters of the drainage equation at different concentrations of silica particles in dispersion; UC.

R972	a (mm)	b	r^2
0.1 wt%	20.38	2.86	0.9958
0.3 wt%	19.79	3.23	0.9963
0.5 wt%	17.65	3.33	0.9952
R812			
0.1 wt%	22.33	3.23	0.9976
0.3 wt%	17.59	3.23	0.9963
0.5 wt%	16.27	2.86	0.9952
R202			
0.1 wt%	18.63	2.50	0.9948
0.3 wt%	16.90	3.03	0.9958
0.5 wt%	14.61	4.17	0.9949

wt%, 0.3 wt%, and 0.5 wt% at 5 minutes, 1 week and 1 month after foam formation. The bubbles produced at 0.1 wt% are much larger than the ones generated at 0.3 wt% and 0.5 wt% and the bubbles are disproportioned with time can be seen by unaided inspection. Figure 7.20 shows the bubble size distributions and confirms this. It indicates that the bubble size distribution shifts towards the left of the spectrum with increasing concentration of particles. After long standing times the distribution

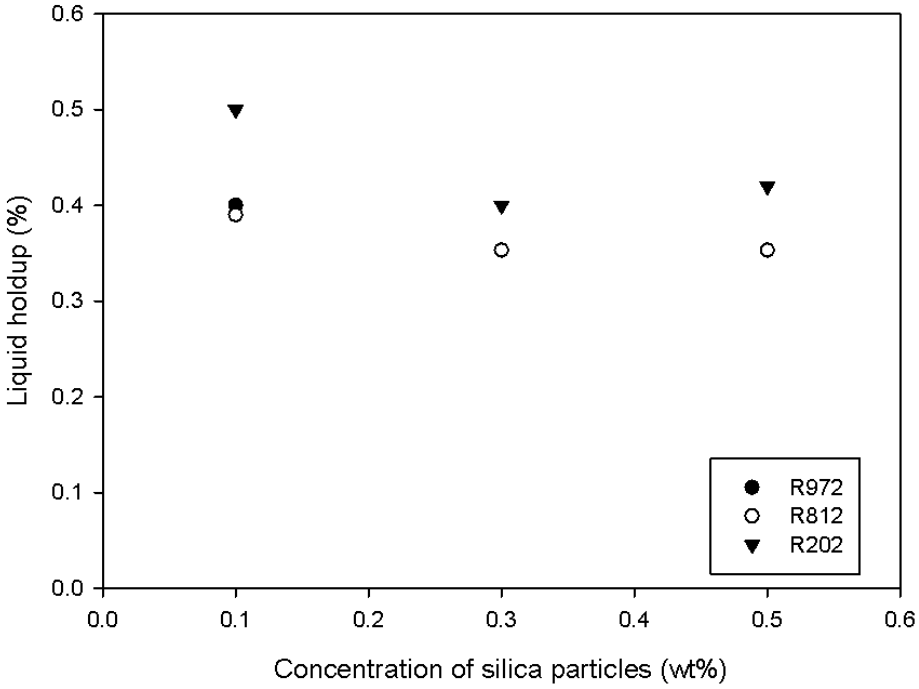

Figure 7.18: Liquid holdup of pure water containing partially hydrophobic silica particles; UC.

shows a longer tail towards the right. The statistical parameters from the these distributions are summarized in the Table 7.7. At 0.1 wt% silica, the mean bubble size, d_{10} decreased with increasing time while d_{32} decreased then increased again with time. At 0.3 wt% and 0.5 wt% silica, the mean bubble size d_{10} and d_{32} both increased with increasing concentration of particle and time. The skewness increases with increasing concentration of particles and with time. This indicates that the bubble size distribution shifts towards the left with a long right hand side tail. The kurtosis also increases with increasing concentration of particles, indicating a sharper peak around the mean.

(a) 0.1$wt\%$ - initial (b) 0.3$wt\%$ - initial (c) 0.5$wt\%$ - initial

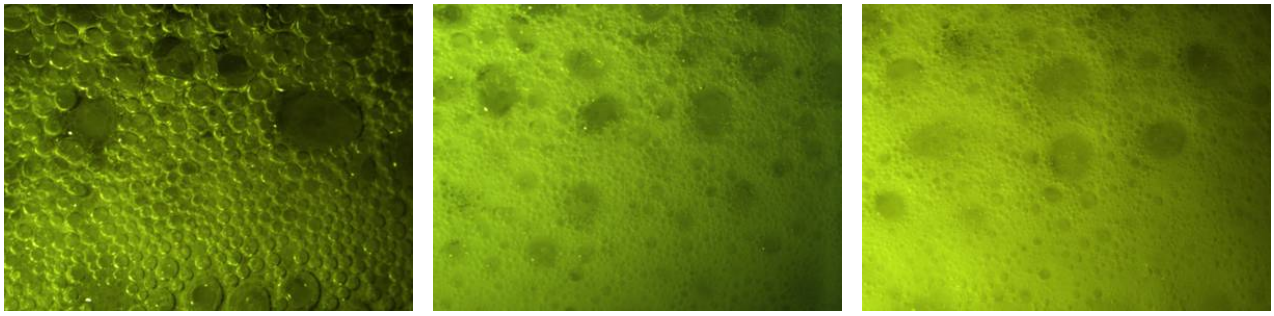

(d) 0.1$wt\%$ - 1 week (e) 0.3$wt\%$ - 1 week (f) 0.5$wt\%$ - 1 week

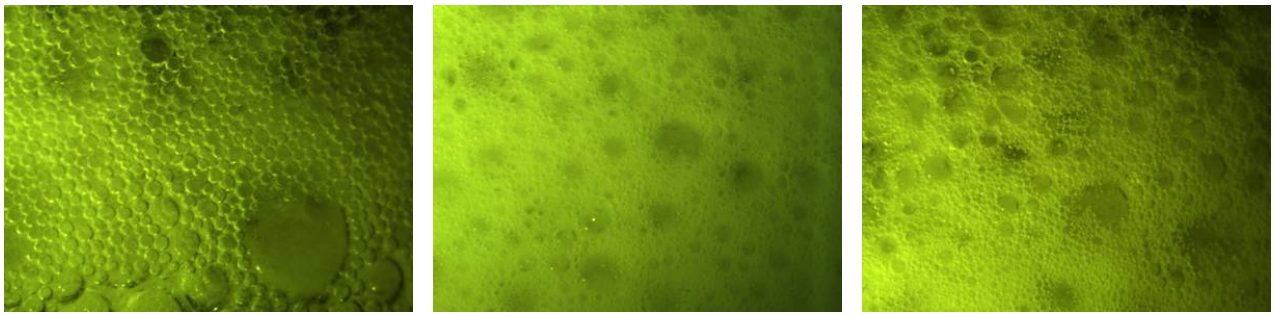

(g) 0.1$wt\%$ - 1 month (h) 0.3$wt\%$ - 1 month (i) 0.5$wt\%$ - 1 month

Figure 7.19: Foam images; with R972 silica particles; UC (7x magnification).

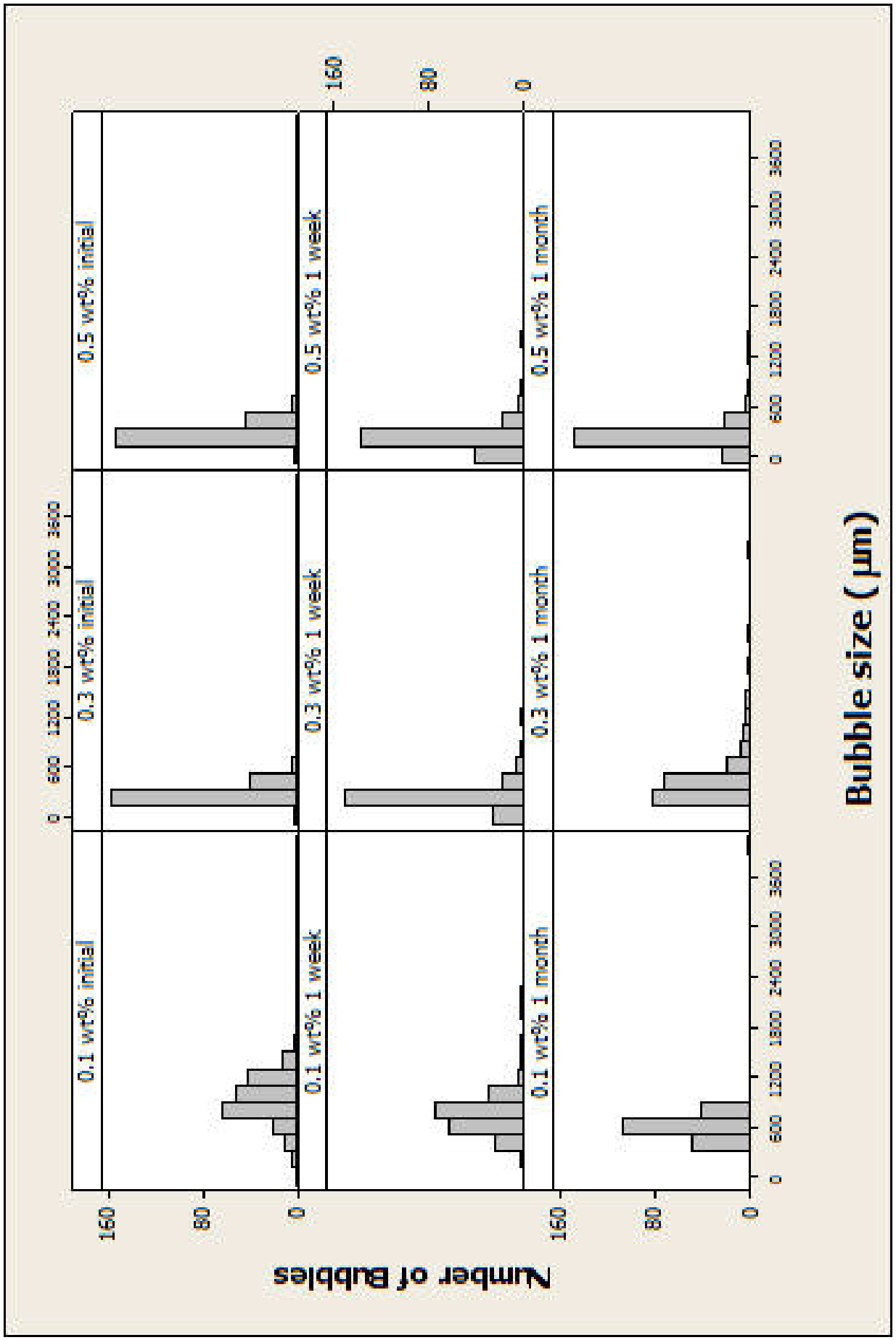

Figure 7.20: Bubble size distribution of R972.

Table 7.7: Statistical parameters for foam bubble size distribution of R972.

0.1 wt%	d_{10} (μm)	d_{32} (μm)	StDev	Min (μm)	M (μm)	Max (μm)	S	K
initial	1045.29	932.70	262.20	259.20	923.50	1674.90	-0.12	0.21
1 week	938.51	745.00	247.70	238.80	715.90	2219.20	1.89	8.27
1 month	1203.98	610.00	262.80	324.70	580.00	3902.40	9.96	124.65
0.3 wt%								
initial	321.57	228.31	101.40	94.76	200.39	634.85	1.14	1.35
1 week	456.32	194.97	132.15	55.97	156.40	1161.89	3.39	17.30
1 month	1368.15	444.80	367.30	131.40	352.20	3294.50	3.84	21.64
0.5 wt%								
initial	308.87	233.00	90.95	92.53	214.00	672.10	1.22	2.57
1 week	553.31	174.94	136.51	61.97	130.56	1424.03	4.83	36.49
1 month	628.72	203.20	163.70	75.00	147.20	1439.00	4.18	23.90

As seen from the foam images and bubble size distributions, the bubbles produced at 0.1 wt% silica after 5 minutes standing time were very uniform in size and separated by thick liquid films. After one week, the bubbles pack closer to each other and are separated by thinner liquid films due to drainage. Also, the gas contained in the smaller bubbles diffused to the larger bubbles and these smaller bubbles reduced their size because of gas diffusion this manifests itself in the presence of a few very large bubbles in the foam image. With the foam standing time increasing to a month, the much larger bubbles burst eventually and only the smaller bubbles remained in the foam. This explains the decrease of the mean bubble size with time in the foam produced at 0.1 wt% silica.

At higher concentrations of silica, much smaller bubbles were generated which grew with time. Although the mean bubble size increases with time, a decrease in minimum bubble size was also observed with time. This is because the smaller bubbles pack closely. When the gas diffuses to the larger bubbles these smaller bubbles still keep their bubble shape.

At higher concentrations of silica there are more particles to create the interface between liquid and air. Therefore, the bubble size is smaller. The mean bubble size at 0.5 wt% is more than 3 times smaller than at 0.1 wt%. In the case of the higher concentrations, after a standing time of 1 month, the larger bubbles are of smaller size than in the 0.1 wt% case. Hence, the kurtosis is lower.

Next, the results of foam microstructure from the foam produced by R812 particles are presented. Figure 7.21 shows the foam images obtained from the foam produced by R812 particles at 0.1 wt%, 0.3 wt%, and 0.5 wt% 5 minutes, 1 week and 1 month after foam formation. Similar to the foam produced by R972 particles, the bubbles produced at 0.1 wt% are much larger than the ones generated

at higher concentrations. A smaller initial mean bubble size and a more uniform distribution was observed at higher concentrations of particles. This is explained by the presence of a sufficient number of silica, as discussed above in the case of MA. In the case of high concentrations a slower disproportionation process was also found. The disproportionation process to be slower in the higher concentrations was observed. As seen in Figure 7.21 after a standing time of 1 month the very large bubbles have completely disappeared in the case of 0.1 wt%. In the higher concentrations they have only reduced in size compared to the foam after 1 week standing time. The bubble size distributions and their statistical parameters are summarized in the Figure 7.22 and Table 7.8. The mean bubble size, d_{10} and d_{32} decreases with decreasing concentration of particles. The mean bubble size, d_{10}, increases, but d_{32} decreases with time. In the case of the R972 foams this can be explained by air diffusion between the bubbles. Increasing skewness and kurtosis were observed with increasing concentration of the particles.

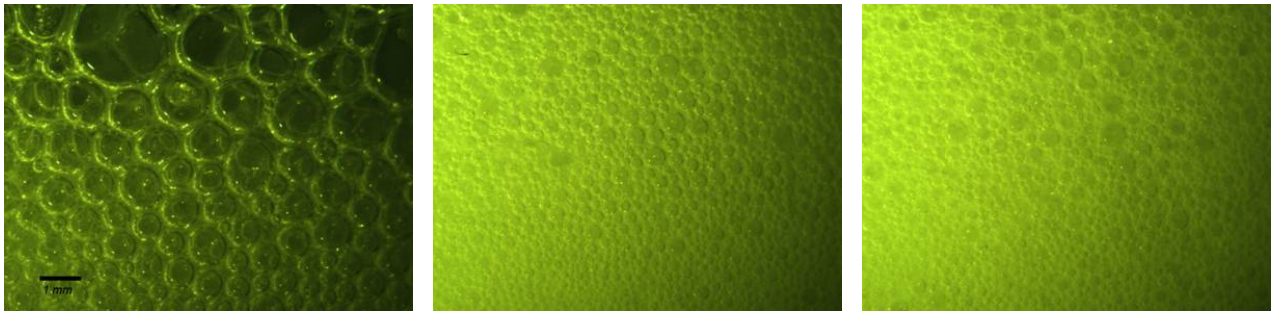

(a) 0.1$wt\%$ - initial (b) 0.3$wt\%$ - initial (c) 0.5$wt\%$ - initial

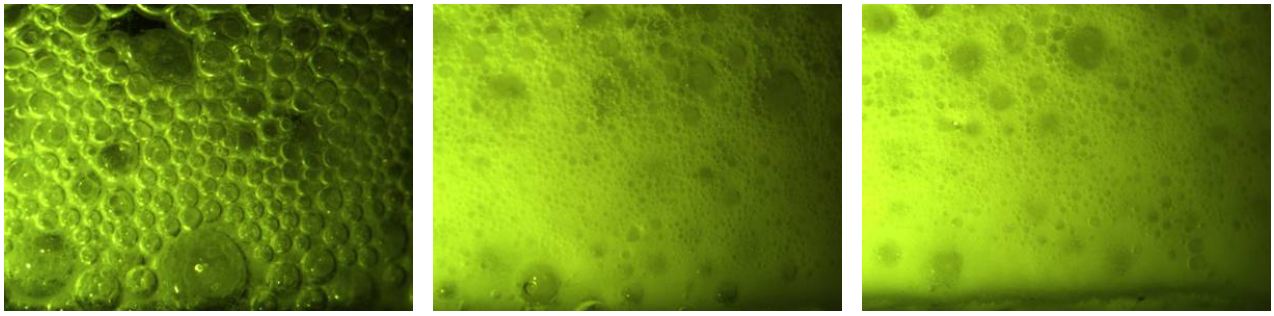

(d) 0.1$wt\%$ - 1 week (e) 0.3$wt\%$ - 1 week (f) 0.5$wt\%$ - 1 week

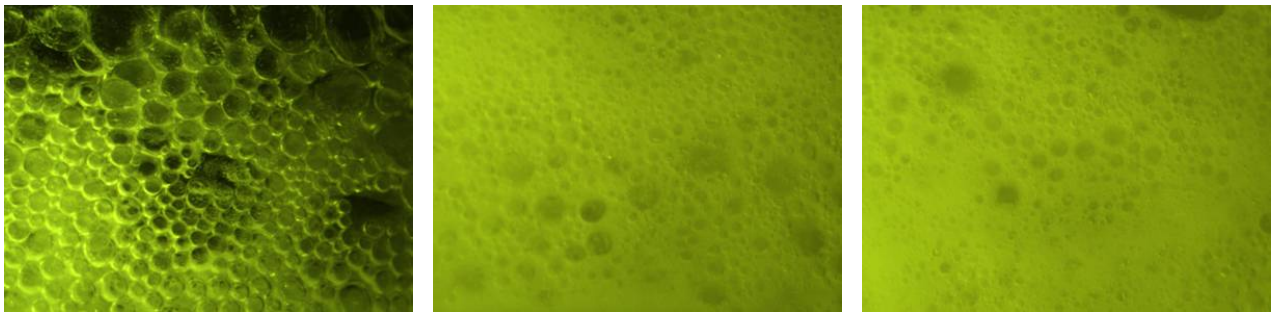

(g) 0.1$wt\%$ - 1 month (h) 0.3$wt\%$ - 1 month (i) 0.5$wt\%$ - 1 month

Figure 7.21: Foam images; with R812 silica particles; UC (7x magnification).

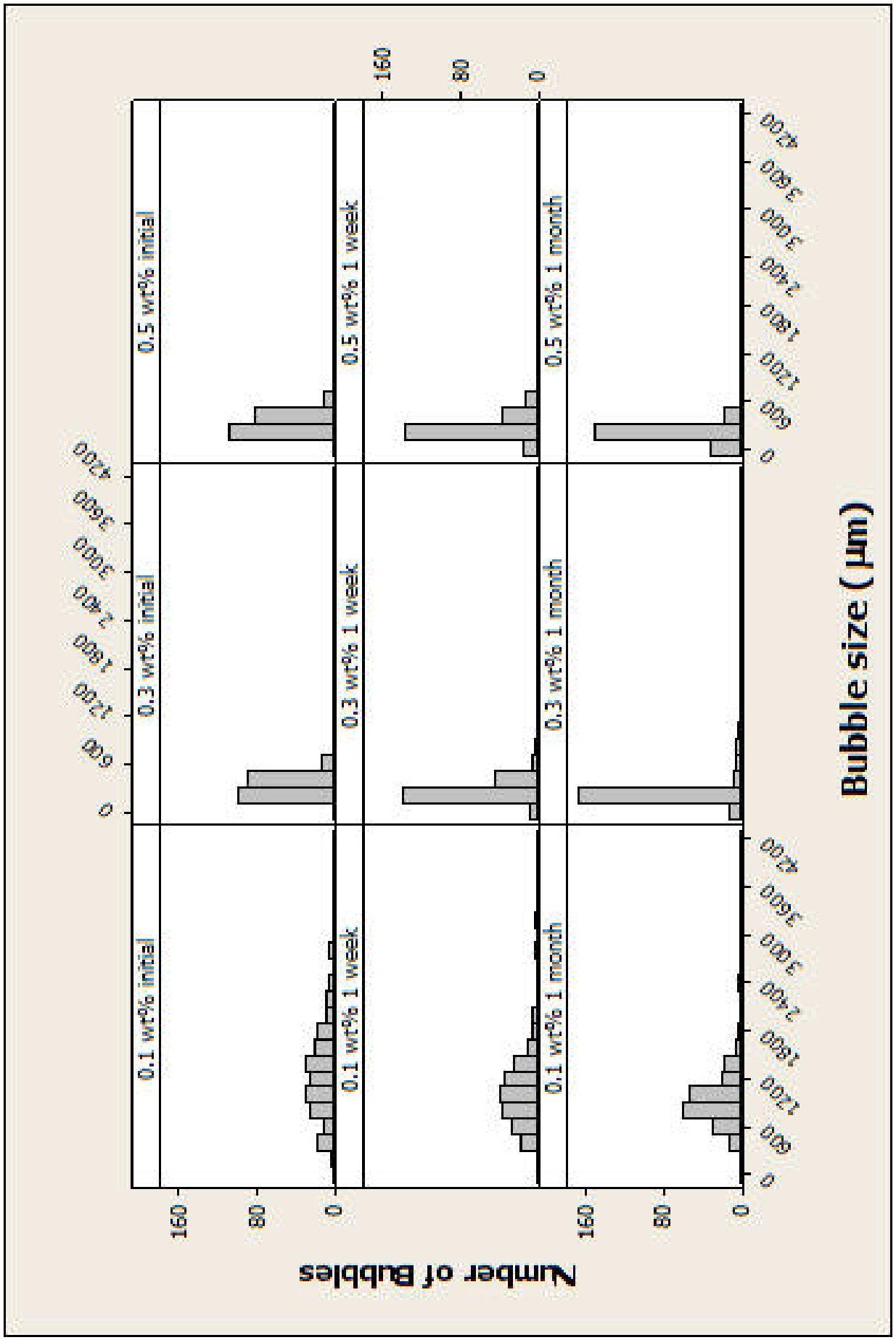

Figure 7.22: Bubble size distributions of R812.

Table 7.8: Statistical parameters for foam bubble size distributions of R812.

0.1 wt%	d_{10} (μm)	d_{32} (μm)	StDev	Min (μm)	M (μm)	Max (μm)	S	K
initial	1918.88	1282.7	607.4	198.4	1273.7	4121.6	0.85	1.98
1 week	1985.33	1076.9	529.1	263.5	1022.9	3689.4	1.96	6.17
1 month	2160.2499	989.1	428.7	353.3	912.2	3327.8	2.34	8.19
0.3 wt%								
initial	393.11	315.53	113.92	105.92	301.98	640.52	0.4	-0.28
1 week	403.49	254.12	128.43	67.81	223.61	851.5	1.8	4.84
1 month	526.49	211.5	153.8	74.3	172.9	979.1	3.22	11.31
0.5 wt%								
initial	378.71	301.7	108.63	114.51	288.33	650.64	0.66	0.25
1 week	415.03	231.32	139.7	58.54	181.72	798.97	1.44	1.78
1 month	286.86	177.03	89.11	71.42	157.25	763.09	2.17	9.05

The images obtained from the foam produced by R202 particles at 0.1 wt%, 0.3 wt%, and 0.5 $wt\%$ and after 5 minutes, 1 week and 1 month standing time are shown in Figure 7.23. Again at lower concentrations of particles we larger bubbles were observed. The bubble size distributions and their statistical parameters are summarized in Figure 7.24 and Table 7.9. The mean bubble size, d_{10} and d_{32} increases with time and decreases with decreasing concentration of particles. Increasing skewness and kurtosis were observed with increasing concentrations of the particles.

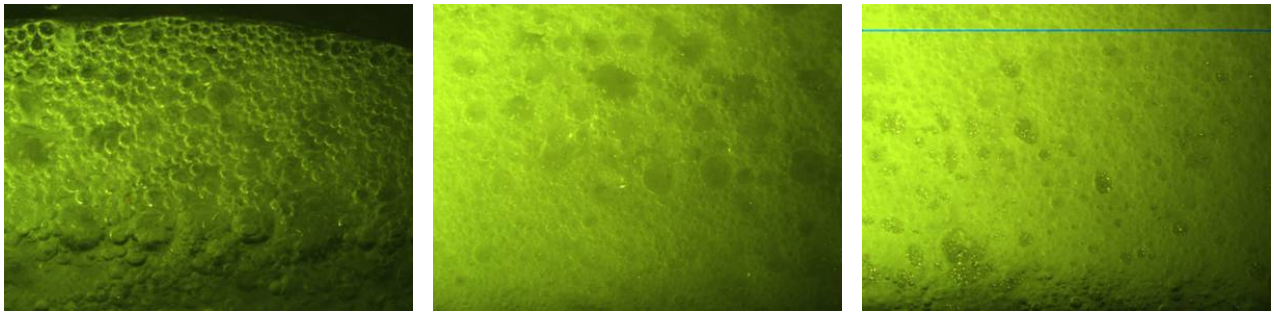

(a) 0.1$wt\%$ - initial (b) 0.3$wt\%$ - initial (c) 0.5$wt\%$ - initial

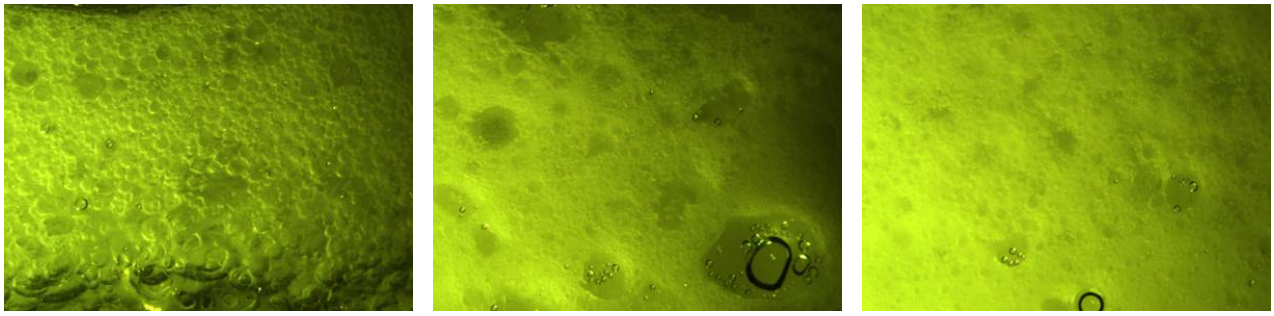

(d) 0.1$wt\%$ - 1 week (e) 0.3$wt\%$ - 1 week (f) 0.5$wt\%$ - 1 week

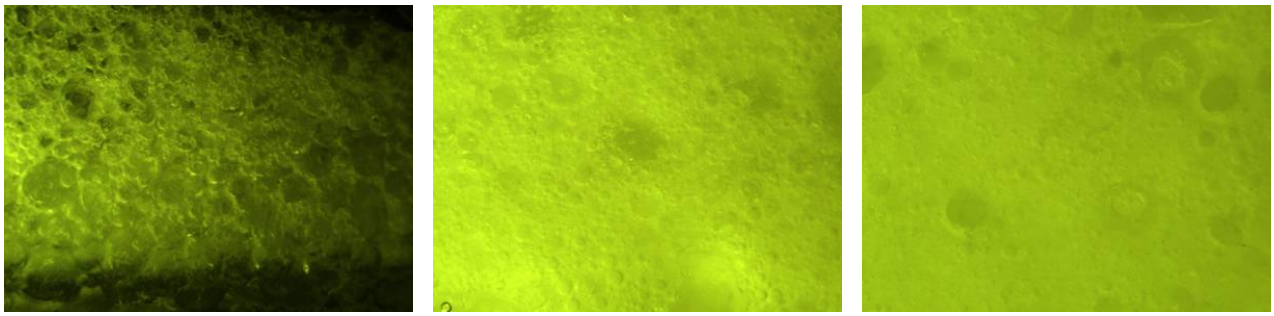

(g) 0.1$wt\%$ - 1 month (h) 0.3$wt\%$ - 1 month (i) 0.5$wt\%$ - 1 month

Figure 7.23: Foam images; with R202 silica particles; UC (7x magnification).

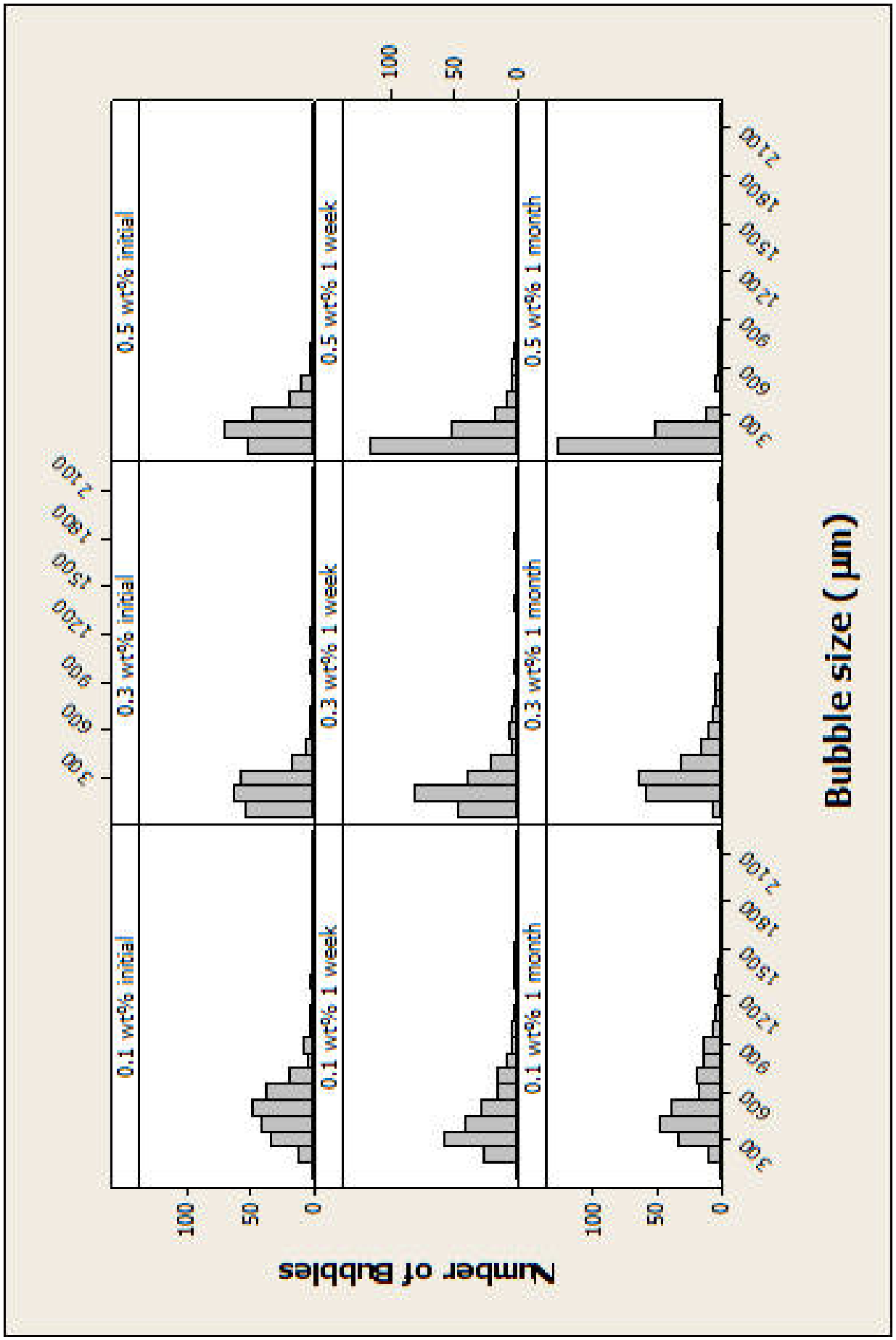

Figure 7.24: Bubble size distributions of R202.

Table 7.9: Statistical parameters for foam bubble size distributions of R202.

0.1 wt%	d_{10} (μm)	d_{32} (μm)	StDev	Min (μm)	M (μm)	Max (μm)	S	K
initial	636.89	497.1	183.5	162	482.4	1298	0.97	1.76
1 week	708.55	455	226.1	158	399.8	1492.6	1.68	3.89
1 month	862.99	545.5	270	189.8	465.3	2231.4	1.98	7.36
0.3 wt%								
initial	451.98	243.1	139.58	65.41	218.46	1162.06	2.6	12.48
1 week	474.55	263.1	194.9	81.4	218.1	1809	4.14	25.21
1 month	840	373.2	245.6	115.6	298	2075.6	3.3	16.33
0.5 wt%								
initial	361.13	238.63	119.51	58.71	215.54	720	1.15	1.34
1 week	362.12	171.69	118.09	51	131.8	737.8	2.15	5.45
1 month	397.61	165.24	110.78	76.91	135.2	843.78	3.84	16.91

After showing the results for these three different types of silica particles at three different concentrations, the foam microstructure varied with the degree of hydrophobicity of the particles is compared. At 0.1 wt%, R202 particles lead to the smallest mean bubbles among these three silica particles and the largest mean bubble size was found in the foam produced by R812 particles. At higher particle concentration, the initial mean bubble size increases with increasing hydrophobicity. This may be because the more hydrophobic particles are packed closer and are strongly adsorbed at the interface of the foam film. At 0.5 wt% silica, UC can produce fine foam with a mean bubble size of 30 μm. In MA, under the same conditions, no fine foam forms. Instead, a mixture of clusters and irregularly shaped bubbles was observed (see Fig 7.13). This difference could be due to the higher local ultrasound energy intensity during foam formation which breaks up clusters while creating the interface. This leads to irreversible absorption of small particles into the interface.

A slower bubble size growth was also observed with increasing hydrophobicity of the silica particles. This might be because the more hydrophobic particles are closer packed and strongly adsorb at the interface of the foam film, which slows down gas diffusion between the bubbles.

7.2.3 Properties of Foam: Comparison between MA and UC

In this section, the foams stabilized by partially hydrophobic silica made with two different methods, MA and UC, are compared. Before discussing the results, it was not possible to use equal volume of dispersion in the UC and the MA experiments. The 100 ml dispersion used in MA did not foam with UC. Thus a smaller amount (30 ml) in all UC experiments is used. Similarly, 30ml would not foam

in MA experiments. In chapter 5 and 6 the same results were reported, namely that the protein and surfactant solutions also do not foam under UC in 100 ml dispersions, although with MA they do. They only foam in a smaller volume dispersion (30 ml). The results show that a better foamability and wetter foam with finer bubbles was produced using MA.

In these particle stabilized foams four main differences between the two generation methods were observed. Firstly, the foams produced by MA have a slightly better foamability at lower concentrations of silica. Secondly, the foams generated by MA are wetter than the foams made by UC. Moreover, the foams produced by MA get wetter with increasing concentration of particles while there is no foam forming using UC at higher concentrations of particles. Thirdly, in comparison to UC a much smaller initial mean bubble size of foams was observed in MA. Fourthly, the most hydrophobic silica can form foams when using UC while poor structure foam was made by MA.

There are a number of possible explanations for these differences and they will be discussed in what follows. In this study a high shear mixer for MA is used and it uses the high speed rotation of the rotor blades to exert a powerful suction which draws the liquid and particles upwards from the bottom of the sample bottle into the centre of the work head. When this process is going on, the dispersion is constantly and vigorously circulated and a lot of air is drawn into the suspension. Thus, there is not only the energy input from the MA but also the extra air drawing to the suspension creating more interface between gas/liquid/solid phases in the process of foam generation. In contrast to UC, an ultrasound probe is inserted into the dispersion. There is no extra air drawn into the dispersion.

The most hydrophobic silica particles cannot be separated into smaller aggregates because there is strong adhesion between particles using ultrasound and it was not possible to use MA to break down hydrophobic silica particles without the dispersion starting foaming as shown in chapter 4. However, in this chapter, a much lower concentration ($\geq 0.5wt\%$) was used to produce foam. Fewer particles (lower concentration) may need less energy input to separate the particle aggregates.

In the case of MA, breakdown of hydrophobic particles is even poorer. The larger clusters cannot form bubbles as they have lost the amphiphilic property. A small amount of hydrophobic silica particles are shattered (fractured) out from the edge of big particle clusters. These form some bubbles, in an effectively low concentration dispersion. Therefore, a mixture of bubbles with irregular

shapes and silica particle aggregates are found in the foams produced by MA. It needs to be noted here that at very low concentrations foam without larger clusters can be produced by UC. This indicates that the most hydrophobic silica particles can be broken down into the size range which allows formation of bubbles.

7.2.4 Effect of pH

From previous sections, MA is the better foaming method for foams stabilized by partially hydrophobic silica particles only. Therefore, in this section, only MA as the foam generation method to study the effect of pH was used. First the effects of pH from the measurement of zeta potential, particle aggregate size and viscosity of these dispersions were studied. A series of experiments was conducted to investigate the effect of pH on foams stabilized by three different hydrophobic silica particles, each at two concentrations, 0.5 wt% and 1.0 wt%. The natural pH values of these suspensions (i.e. dispersion in water without adding sodium hydroxide) ranges from pH 5.4 to 5.8 (depending on the silica particles dispersed in distilled water). In these experiments the pH values were varied from natural to pH 10.

Physical Properties of Dispersions

Particle size and zeta potential It is well-known that the charge on silica particle surfaces in water is dependent on pH (Iler, 1979). Zeta potential measurements show that particles are highly charged at high pH. Uncharged surfaces are more hydrophobic than charged ones (Fokkink and Ralston, 1989). It is thus expected that silica particles will become more hydrophilic when increasing the pH. Thus, the pH has great influence on the stability of aggregation, flow and sedimentation of the dispersions. The variation of the zeta potential with dispersion pH is shown in Figure 4.19(a). The zeta potential decreases with an increase in pH because the ions react with the surface of the silica particles and then increase the particle surface charge density. All particles in aqueous media are known to carry a surface charge and attract oppositely charged ions in solutions. Therefore to be able to neutralize the negative charge of the silica particles, free cations in the aqueous phase tend to diffuse near the negatively charged surface of the particles in response to the electrical potential. The

stability (the ability to prevent clusters) of the silica particles depends on their surface charge. The hydrophobic silica particles considered in this section are negatively charged at all pH. However, the attraction of the hydrophobic force can be much greater than the the repulsion due to the negative charge at low pH and when the hydrophobicity is high. Therefore, the most hydrophobic silica particles, R202, aggregate to larger clusters of micron size in all pH and the less hydrophobic silica particles aggregate to micron size cluster in the lower pH only as shown in Figure 4.19(b).

Surface Tension Figure 7.25 shows the surface tension of three types of hydrophobic silica particles at natural pH (vary from pH 5.4 to 5.8) and pH 10 plotted against time. For R972 and R812 particles, the surface tension first increases then decreases at the natural pH. The first increase is due to the evaporation of the ethanol contained in the dispersion of silica particles, and the decrease was caused by the denser particle packing at the interface of liquid and air (please see the detail in section 7.2.1). However, the surface tensions of R972 and R812 particles increase with time when the pH is at 10.0. It shows the same behavior as fully hydrophilic particles dispersed into the mixture of ethanol and water. The reason for this is that hydrophobic particles become more hydrophilic at higher pH (Binks, Duncumb and Murakami, 2007). R202 particles also show a higher surface tension at higher pH, however, they do not behave the same as the other types of hydrophobic particles. At higher pH the surface tension first increases and then decreases, whereas with the less hydrophobic particles, the surface tension always increases.

Viscosity

The viscosity of the dispersions decreased considerably with increasing pH. An explanation is that, as the pH increases, the negative ions increase. Therefore, they repel each other, causing the particles to move further apart causing the gel network to become weaker.

Table 7.10 lists the parameters obtained when the power law model (7.1) is used to analyze these flow curves. The data is well fitted by the model ($r^2 > 0.99$). With increasing pH the viscosity decreases while the value of n increases from about 0.86 to about 1. This means that with increasing pH the dispersions change from being shear-thinning to Newtonian.

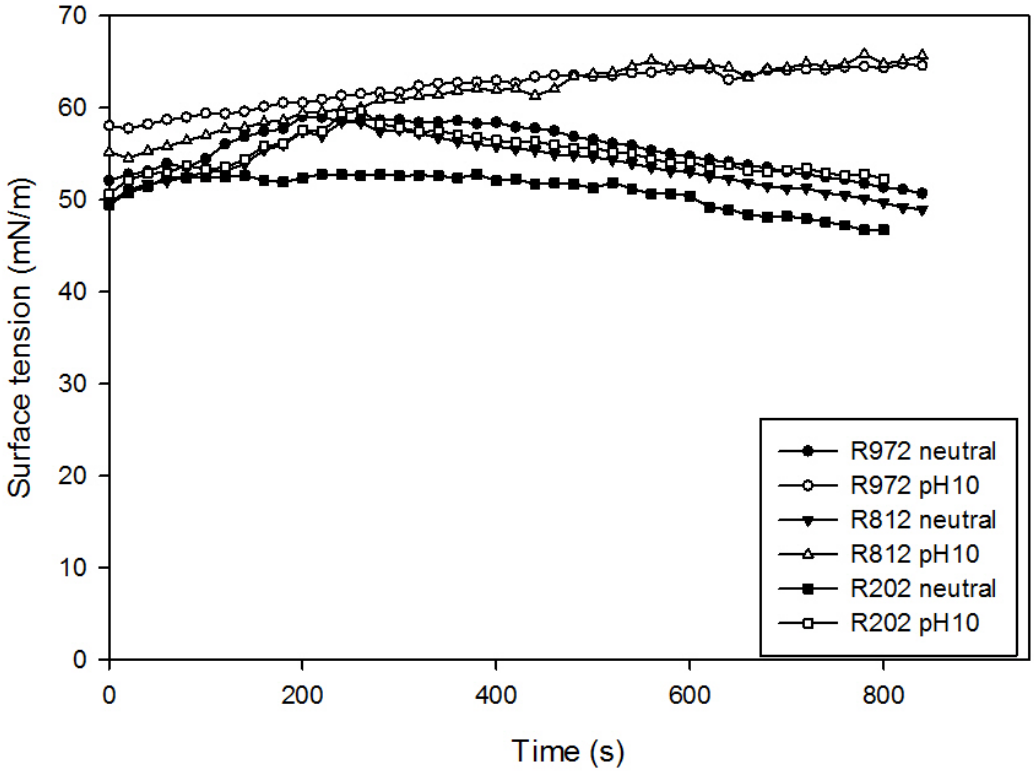

Figure 7.25: Surface tension of dispersion at different pH.

Foam Formation, Drainage, Liquid Holdup, and Collapse

Figures 7.26(a) and 7.26(b) show the foam height immediately after formation as a function of silica particle type for concentrations of 0.5 wt% and 1.0 wt%, respectively. The foamability of foam stabilized by R972 and R812 silica particles decreases with increasing pH values at both concentrations. There is no significant effect with the foam produced by the R202 particles at the concentration of 0.5 wt% but a small difference is observed at a concentration of 1.0 wt%.

Table 7.10: Power law model parameters for the effect of pH on silica particle dispersions.

R972			
Neutral pH	***k (Pa.s)***	**n**	**r^2**
0.5 wt%	$3.479*10^{-3}$	0.87	0.9844
1.0 wt%	$4.932*10^{-3}$	0.85	0.9896
pH7			
0.5 wt%	$1.673*10^{-3}$	0.94	0.9976
1.0 wt%	$2.475*10^{-3}$	0.90	0.9978
pH10			
0.5 wt%	$5.342*10^{-4}$	1.09	0.9991
1.0 wt%	$7.104*10^{-4}$	1.07	0.9994
R812			
Neutral pH	***k (Pa.s)***	**n**	**r^2**
0.5 wt%	$1.285*10^{-2}$	0.64	0.978
1.0 wt%	$1.931*10^{-2}$	0.71	0.9833
pH7			
0.5 wt%	$6.407*10^{-3}$	0.80	0.9902
1.0 wt%	$5.473*10^{-3}$	0.82	0.9987
pH10			
0.5 wt%	$6.442*10^{-4}$	1.04	0.9990
1.0 wt%	$9.355*10^{-4}$	1.03	0.9992

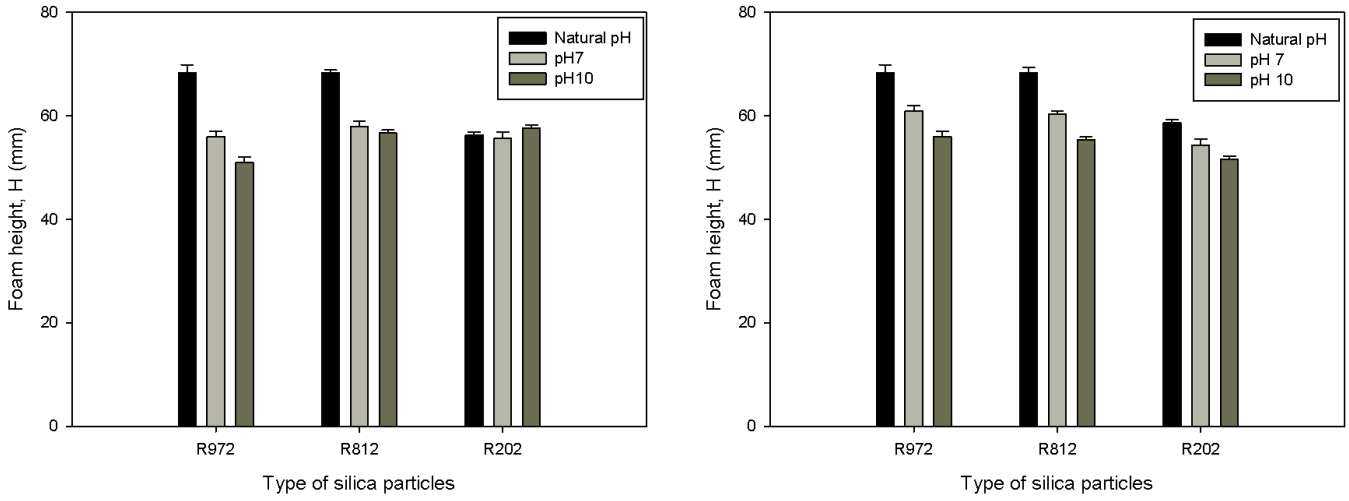

(a) $0.5wt\%$ (b) $1.0wt\%$

Figure 7.26: Foamability of pure water containing 0.5 wt% and 1.0 wt% partially hydrophobic silica particles in different pH values; MA.

The maximum liquid level, a, is obtained from the drainage curves which are fitted by Equation 3.13. The parameter a is plotted as a function of silica particle type as shown in Figures 7.27(a) and

7.27(b). Drainage takes about 20 minutes at pH 4 and pH 7 while drainage almost ended during the first few minutes after formation at higher pH. The maximum liquid level increases with increasing pH in the foam stabilized by R972 and R812 particles but there is no significant difference in the foam stabilized by R202 particles.

In Figures 7.28(a) and 7.28(b) the liquid holdups are plotted against silica type with various pH. In general, the liquid holdup in the foams with 1.0 wt% is higher than 0.5 wt%. In the foam stabilized by R972 and R812 foams, wetter foams were produced at pH 4 and 7. At pH 10, the amount of liquid holdup is much less than at low pH. Specifically, in the case of 0.5 wt% it is less than 10% and less than 20 % in the case of 1.0 wt%, respectively. The liquid holdup of the foam produced by R202 particle is higher than in the other two types of hydrophobic particles. 62 % liquid holdup can be achieved at a particle concentration of 1.0 wt% with the foam stabilized by R202 particles at pH 10.

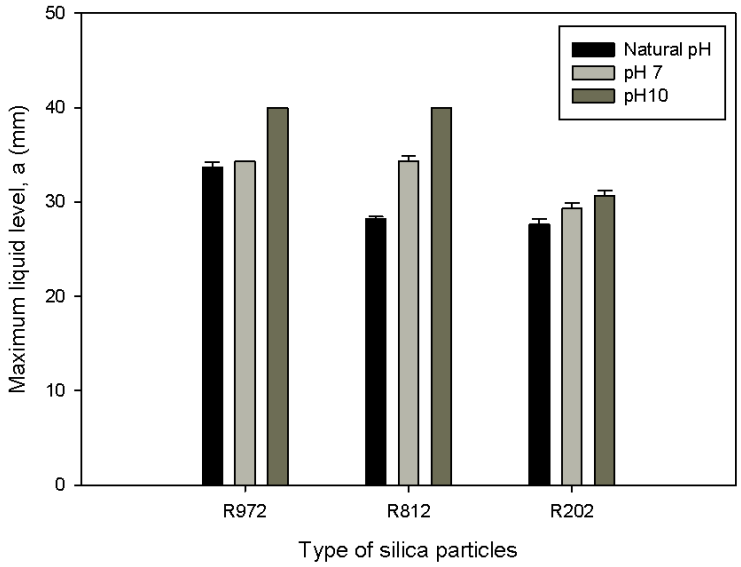

(a) $0.5wt\%$

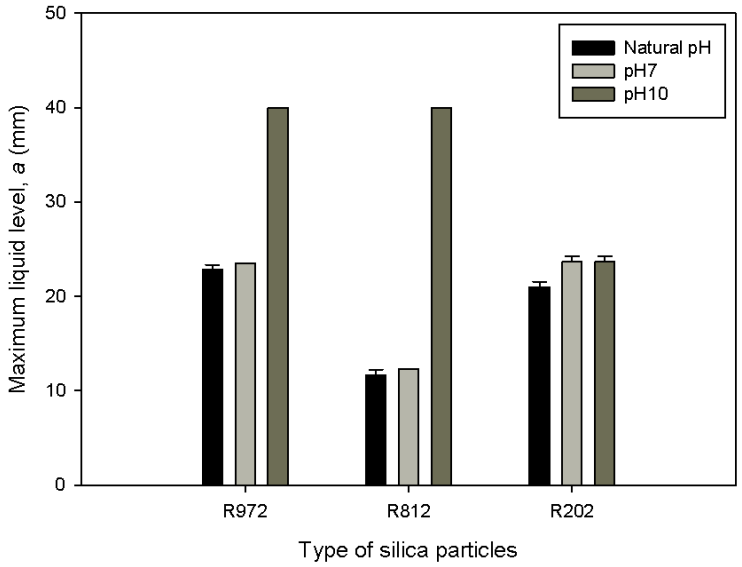

(b) $1.0wt\%$

Figure 7.27: Drainage of pure water containing 0.5 wt% and 1.0 wt% partially hydrophobic silica particles at different pH values; MA.

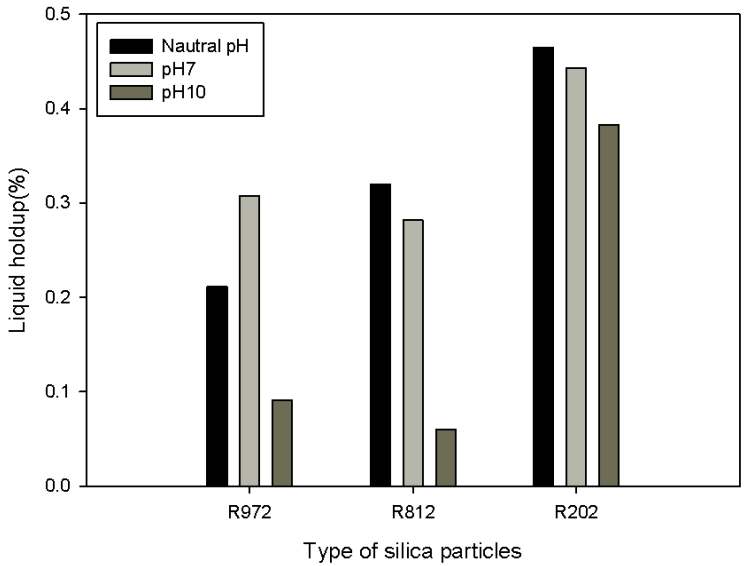

(a) $0.5wt\%$

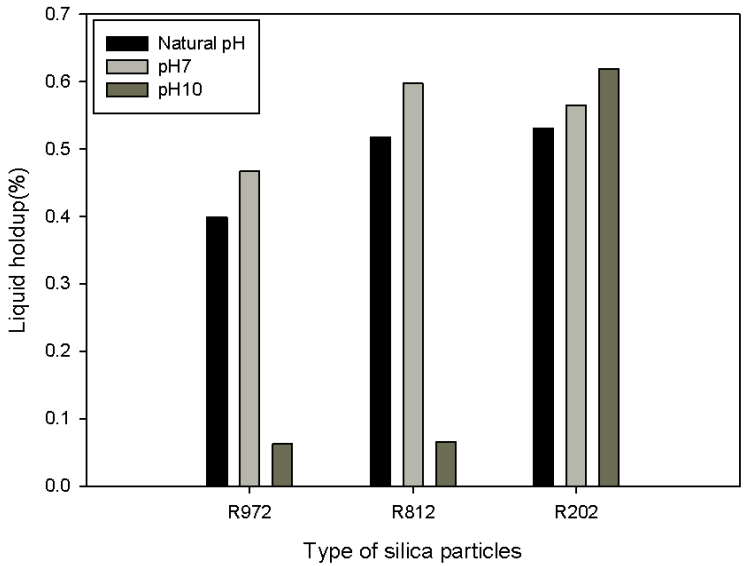

(b) $1.0wt\%$

Figure 7.28: Liquid holdup of pure water containing 0.5 wt% and 1.0 wt% partially hydrophobic silica particles at different pH values; MA.

The foams stabilized by only particles are shown in Figures 7.29(a), 7.29(b) and 7.29(c). There is no foam collapse observed in foams stabilized by R972 and R812 at their natural pH for over a month, but at pH 10 the foam collapses within a few days. The foams stabilized by R202 particles seem unaffected by the pH. At pH 5.8, pH 7 and pH 10, these foams are stable and no collapse is observed for months.

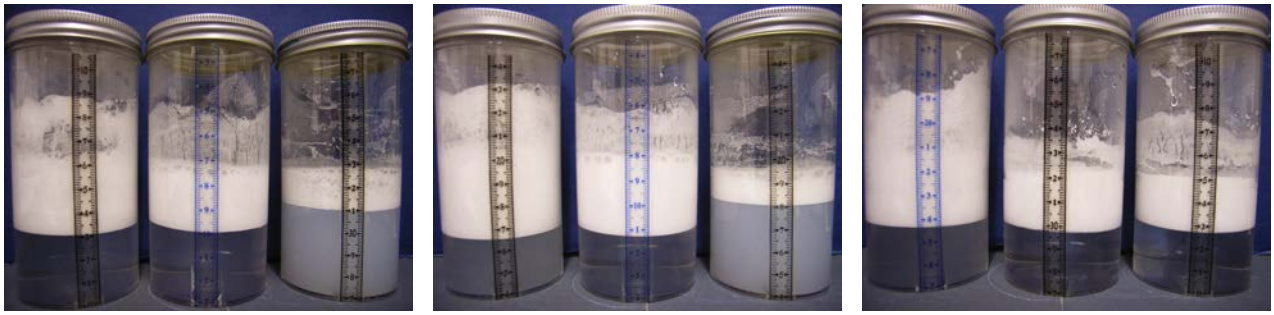

(a) (b) (c)

Figure 7.29: Foam stabilized by silica particles at various pH (a) R972 (b) R812 (c) R202 (in the each individual image; the left one is natural pH (5.4-5.8); the middle one is pH 7; and the right one is pH 10.

Foam Microstructure

Figures 7.30(a), 7.30(b), 7.31(a), and 7.31(b), show Sauter mean diameter, d_{32}, as a function of foam standing time in the foams stabilized by R972, and R812 silica at concentrations of 0.5 wt% and 1.0 wt%. At lower particle concentrations, the initial mean bubble size of the foam stabilized by R972 are around 30 μm at natural pH and pH 7. A much larger initial mean bubble size, ≈200 μm, is obtained at pH 10 as shown in Figure 7.30(a).

Sauter mean diameter, d_{32} increases with time at pH 10. At natural pH and pH 7 there is no bubble growth. The bubble size distribution curves of the foams produced at pH 7 are shown in Figure 7.32(a). From 5 minutes to 30 minutes after generation the curves shift to the right hand side of the spectrum with time. After 30 minutes, there is little further change, and the curves for 60 and 240 minutes are barely distinguishable from the 30 minutes curve. Similar bubble size distribution are also found in the foam at natural pH.

In Figure 7.30(b), the initial mean bubble sizes are also around 30 μm in the foam stabilized by 1.0 wt% R972 particles. It is similar to the foam made with 0.5 wt% R972 particles. At natural

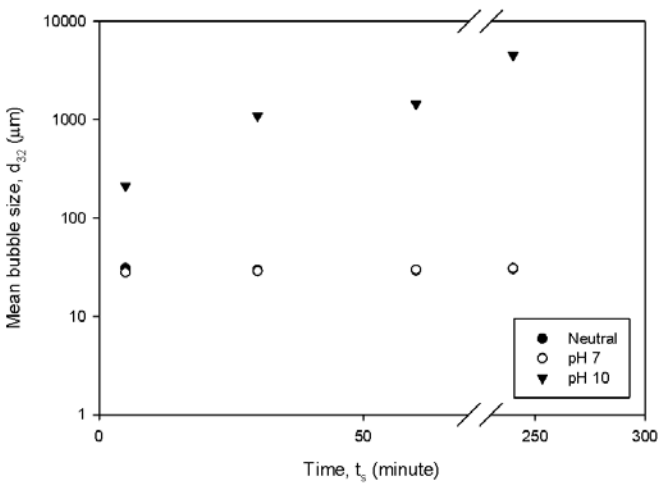

(a) 0.5wt%

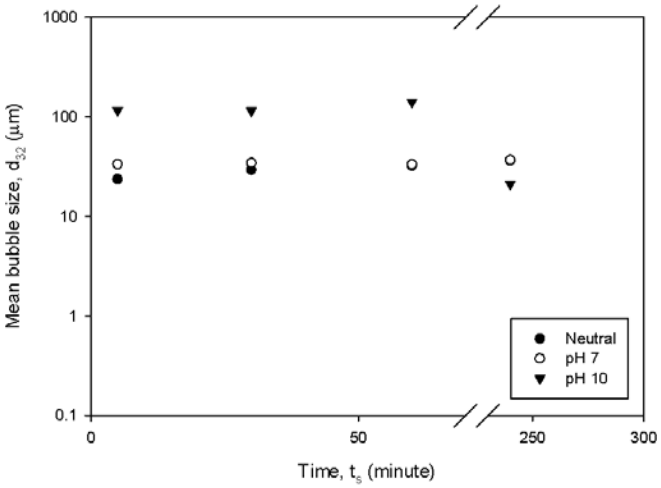

(b) 1.0wt%

Figure 7.30: Variation of mean bubble size with foam standing time at different pH; R972 silica particles.

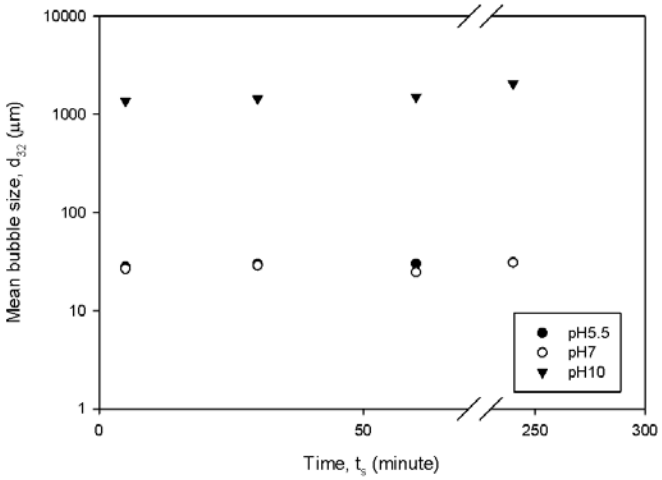

(a) 0.5wt%

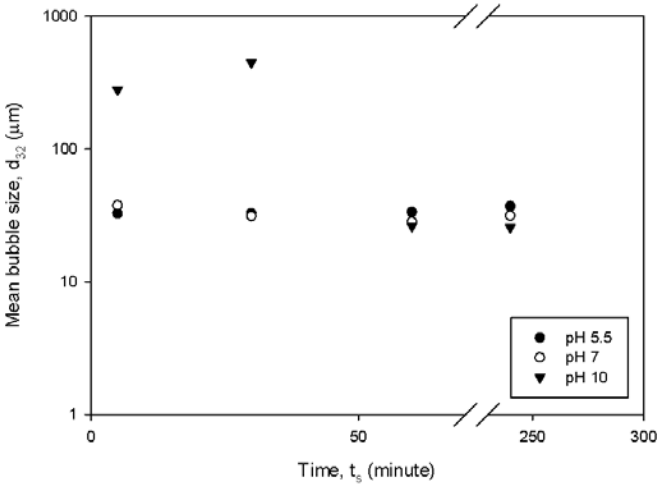

(b) 1.0wt%

Figure 7.31: Variation of mean bubble size with foam standing time at different pH; R812 silica particles.

pH and pH 7, it shows a stable period of no bubble growth. At pH 10, the initial mean bubble size is around 100 μm; under these conditions the mean bubble size remains constant for an hour and then drops to ≈21 μm. The bubble size distributions at the natural pH , pH 7, and pH 10 are shown in Figure 7.32(b). The curves get narrower and shift to the left of the spectrum with time increasing, as exemplified by the foam images in Figure 7.33. At pH 10.0, the bubble sizes are

initially heterogenous. With time increasing, the larger bubbles grow and burst in the foam. There are only smaller bubbles left in the foam after 4 hours, and the distribution is more even.

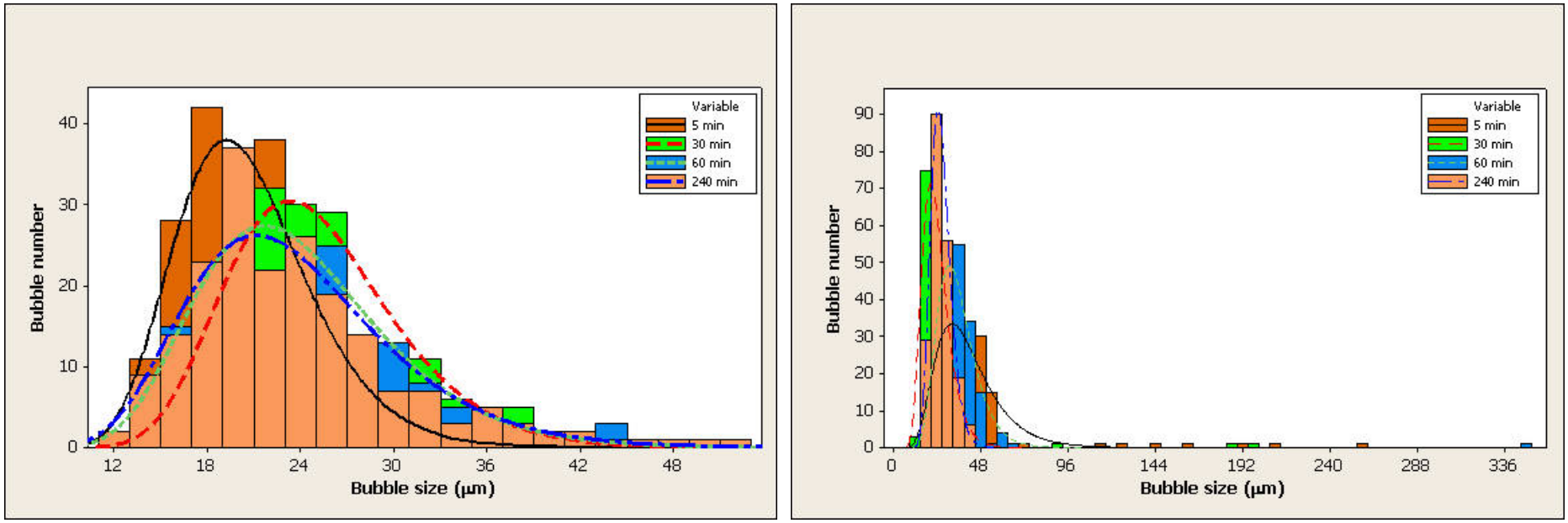

(a) $0.5wt\%$ at pH7

(b) $1.0wt\%$ at pH10

Figure 7.32: Bubble size distributions; R972 silica particles at pH7.

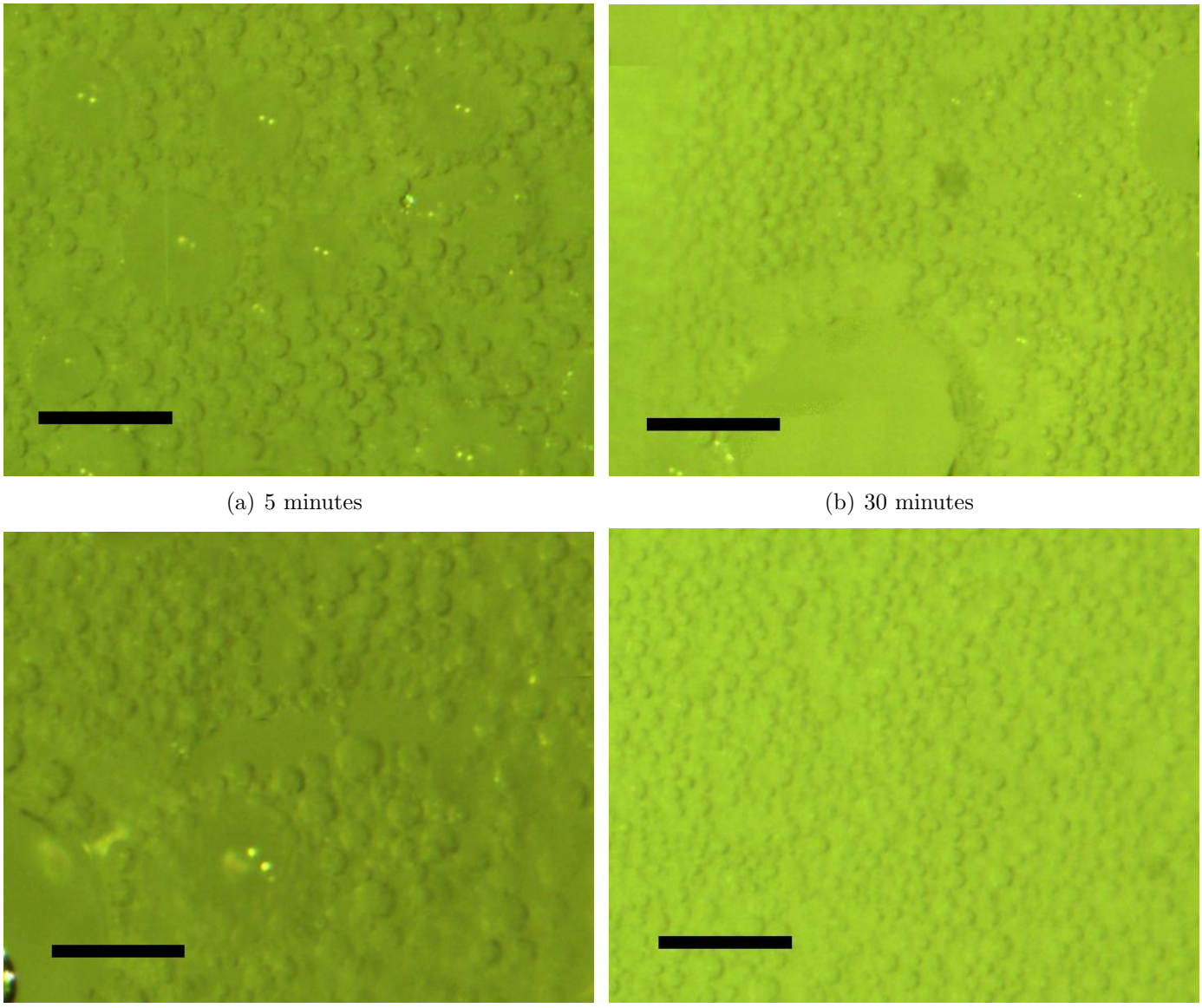

(a) 5 minutes

(b) 30 minutes

(c) 60 minutes

(d) 240 minutes

Figure 7.33: Foam Images; with R972 silica particles; pH10; the scale bar = 100 μm (350x magnification).

Sauter mean diameter, d_{32} of foams stabilized by R812 particles at natural pH and pH 7 are all around 30 μm in both concentrations as shown in Figures 7.31(a) and 7.31(b). At pH 10, the initial mean bubble sizes are 1370 and 280 μm in concentrations of 0.5 wt% and 1.0 wt%, respectively. At the lower concentration of R812 silica particles, d_{32} increases by a factor of 2 in four hours. At the higher concentration of R812 particles, the mean bubble size drops to 25.7 μm.

At natural pH, there are mainly clusters of silica particles and isolated bubbles as shown in Figure 7.34(a). At pH 7, the mixture contains fewer particle aggregates and a mix of irregular and round

bubbles as shown in the foam images in Figure 7.34(b). At pH 10.0, a fine and uniform foam was generated by the most hydrophobic silica particles as shown in the foam image in Figure 7.34(c). Therefore, here the mean bubble size plotted against time at pH 10 was presented as shown in Figure 7.35.

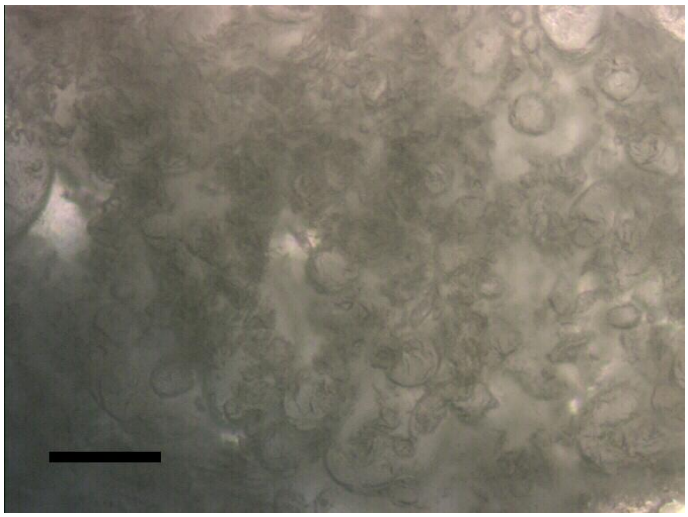

(a) pH5.5

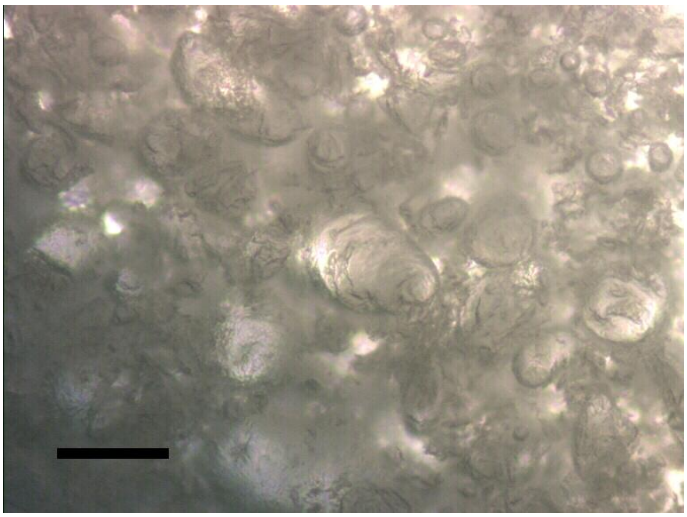

(b) pH7

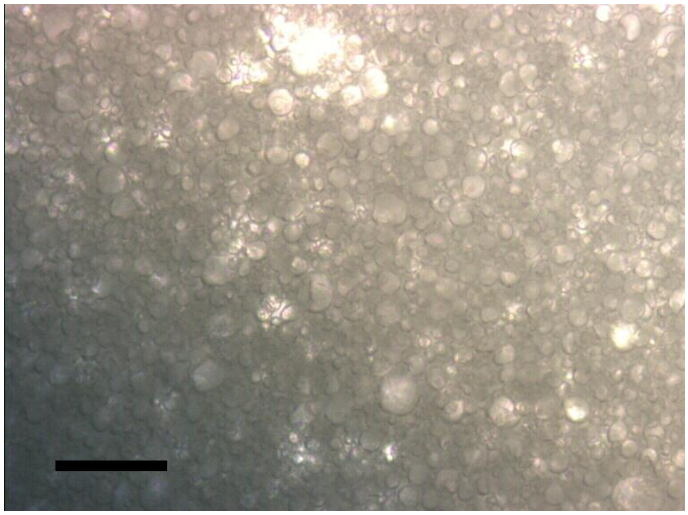

(c) pH10

Figure 7.34: Foam Images; with 1.0$wt\%$ R202 silica particles; the scale bar = 100μm (200x magnification).

Summary of Findings

The foaming properties are strongly affected by the properties of the hydrophobic silica particle dispersions (Gonzenbach et al., 2006a). Therefore, the properties of these dispersions before foaming

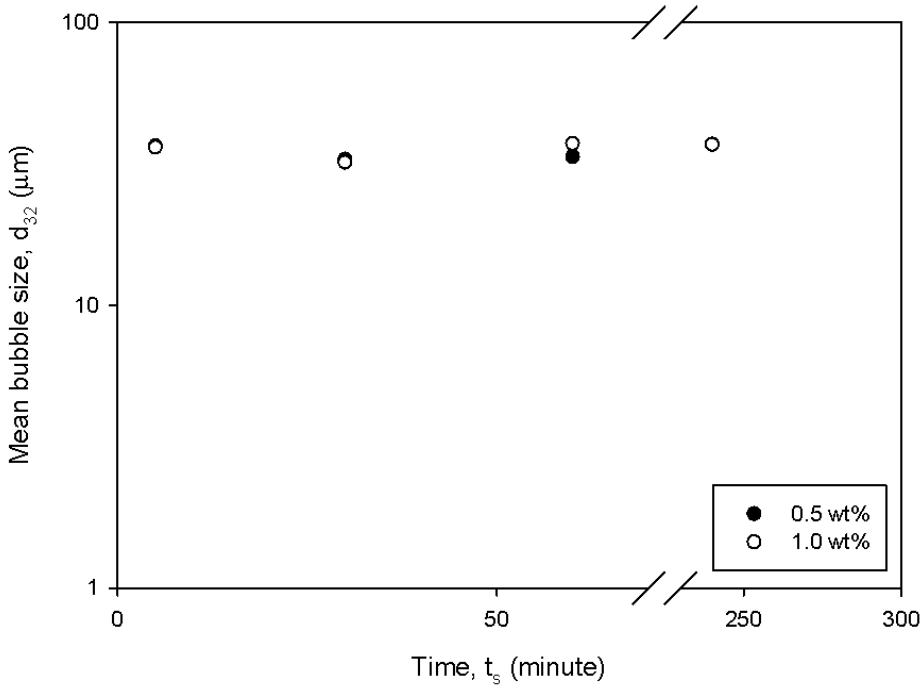

Figure 7.35: Variation of mean bubble size with foam standing time at pH10; R202 silica particles.

was looked at. The surface tension varied with the pH. Figure 7.25 shows the surface tension as a function of time for both hydrophilic particle and hydrophobic particle dispersion. At high pH, the hydrophobic particles behave like hydrophilic particles as far as the surface tension is concerned. At natural pH, the surface tension of the hydrophobic particles first increases with time, then decreases while the surface tension of hydrophobic particles increases only. A possible explanation is as follows: The hydrophilic silica particles prefer the liquid phase. Evaporation of the ethanol leads to a decrease of the surface tension. Once all the ethanol is evaporated, the dispersion has the surface tension of water. In the case of hydrophobic particles, the ethanol also disperses, but the hydrophobic particles adsorb at the surface of the liquid-air interface which lowers the surface tension. Hence, evaporation of ethanol and adsorption are opposed to one another. Moreover, the water in the drop evaporates as well which causes a denser and closer packing of the particles at the interface of the drop, leading to a further decrease of the surface tension (The pendant drop method to measure the surface tension was used, and see details in Chapter 3).

The viscosity of R972 and R812 particle dispersions decreases with increasing pH, but there is no change found in the viscosity in the most hydrophobic particles as shown in Table 7.10. This indicates that the R972 and R812 particles increase in hydrophilicity with increasing pH; under these conditions the viscosity is also similar to the viscosity of the fully hydrophilic particles.

The least and medium hydrophobic particles can form extra stable foams with a very small bubble size in natural pH and pH 7. However, when the pH is adjusted to a higher pH 10, then their foamability is less, the liquid holdup is significantly reduced and the foams are much more unstable.

In contrast R202 particles produce again a poor foam quality, with a mixture of bubbles and clusters even at natural pH (see Figure 7.34). However, at pH 10 micron sized bubbles without particle aggregates can be formed with the most hydrophobic particles (see Figure 7.34). The highest liquid holdup is always found in the foam produced by the strongly hydrophobic particles under all conditions, but at natural pH and pH 7.0 all particles show a poor foam texture, which is most probably due to to large size of the particle aggregates.

While the lightly and moderately hydrophobic particles did not foam well at pH 10, the strongly hydrophobic particles had the highest liquid holdup and a fine and uniform bubble size at pH 10.

This is because at pH 10 the hydrophobicity was optimally balanced by the pH value for the R202, but R972 and R812 are too hydrophilic to foam well.

7.2.5 Effect of Dispersion Viscosity

Pradhan and Khilar (1994) and Laheja et al. (1998) have investigated the effect of polymer additives that change the viscosity of the solution. They considered sodium carboxymethyl cellulose (SCMC), which has the effect of increasing the viscosity. They found that the foam stability (drainage half-life) increases with the concentration of SCMC. In this section, the effect of viscosity on foam stabilized by silica and SCMC is studied. R972 and R812 particles at a concentration of 1.0 wt% and two concentrations of SCMC (0.08 and 0.1 wt%) were used.

In Figures 7.36(a) and 7.36(b), the viscosity of the dispersions increased with increasing concentration of addition of SCMC and hydrophobicity of the particles. The data of shear stress and shear rate were well fitted by Equation (7.1). The parameters are summarized in Table 7.11. The viscosity increases with addition of SCMC and concentration of silica particles. A value of $n < 1$ indicates that the dispersion is shear-thinning fluid.

Table 7.11: Power law model parameters for silica particle dispersions with addition of SCMC.

R972			
0.08 wt% CMC	***k (Pa.s)***	**n**	**r^2**
no particles	$3.657*10^{-2}$	0.91	0.9989
0.5 wt%	$3.334*10^{-2}$	0.91	0.9994
1.0 wt%	$3.738*10^{-2}$	0.89	0.9997
0.1 wt% CMC			
0.5 wt%	$4.897*10^{-2}$	0.90	0.9992
1.0 wt%	$5.633*10^{-2}$	0.90	0.9991
R812			
0.08 wt% CMC	***k (Pa.s)***	**n**	**r^2**
0.5 wt%	$3.518*10^{-2}$	0.94	0.9989
1.0 wt%	$4.904*10^{-2}$	0.92	0.9981
0.1 wt% CMC			
0.5 wt%	$4.904*10^{-2}$	0.92	0.9981
1.0 wt%	$8.511*10^{-2}$	0.83	0.9999

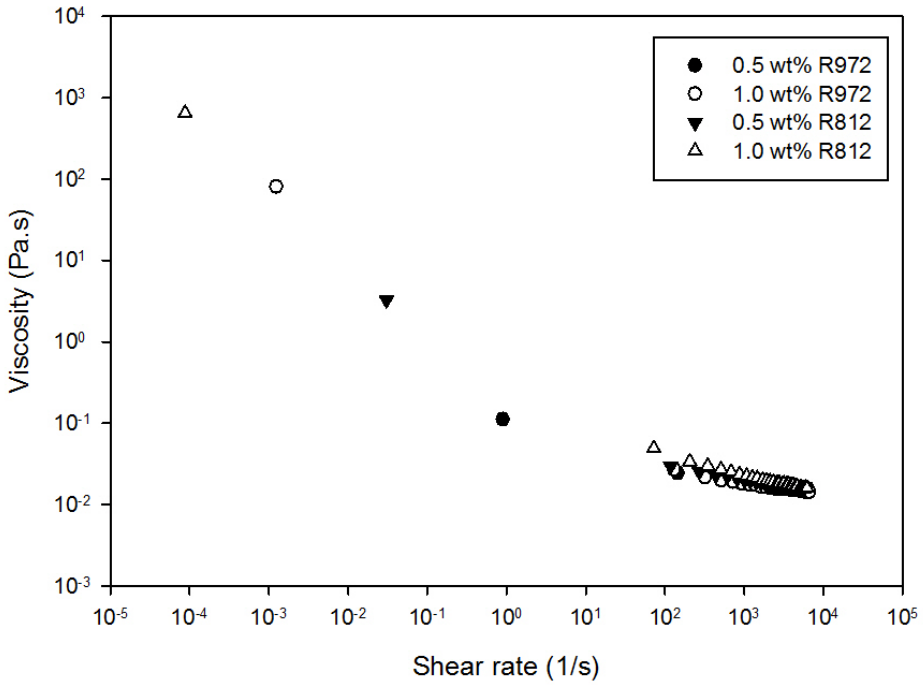

(a) $0.08wt\%$

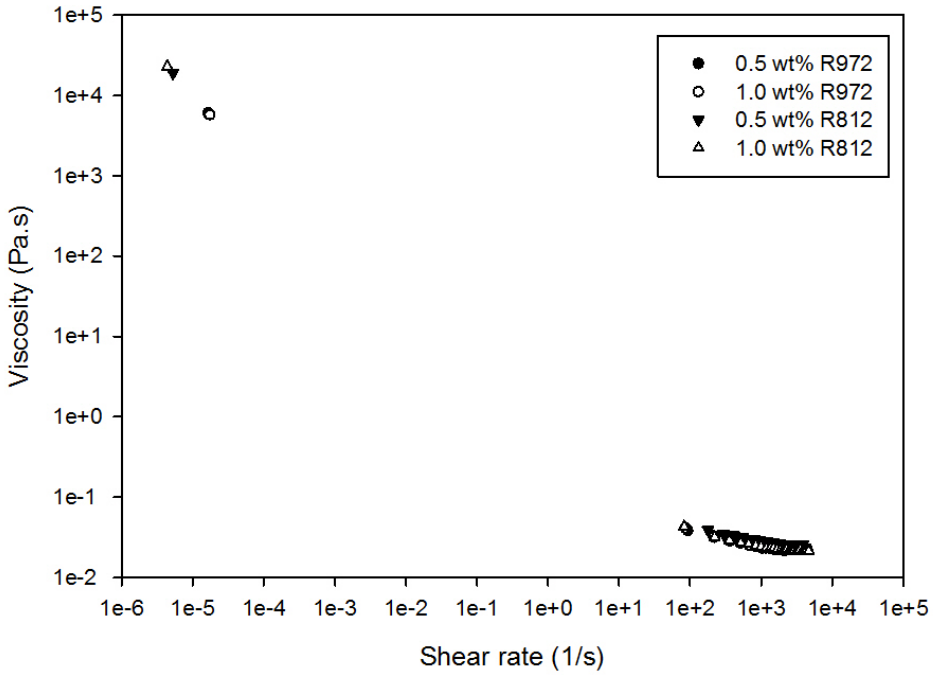

(b) $0.1wt\%$

Figure 7.36: Flow curves of viscosity-modified hydrophobic silica particle dispersions.

Foam Formation and Breakage

Figure 7.37 shows that the addition of SCMC has significantly reduced the foamability of foam stabilized by R972 and R812 particles whose foam volumes are reduced by nearly half and two thirds respectively. The foam head was plotted as a function of time in Figures 7.38(a) and 7.38(b). There was no significant foam collapse observed within a week.

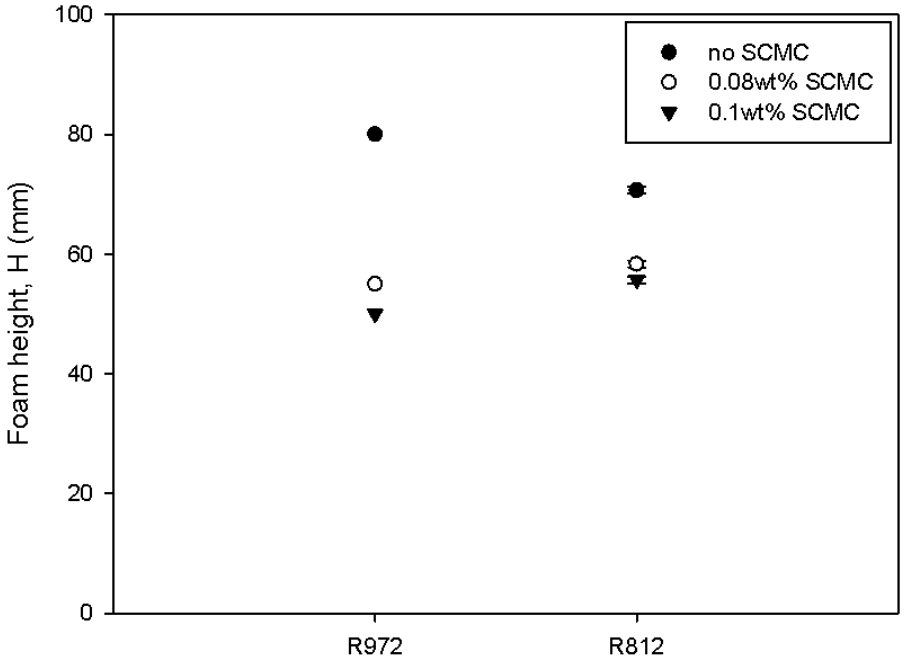

Figure 7.37: Effect of SCMC on foamability of foam containing R972 and R812 silica particles.

Foam Drainage and Liquid Holdup

Figures 7.39(a) and 7.39(b) show the liquid level as a function of time. They show that the drainage of both hydrophobic silica particles decreases significantly with increasing viscosity. In the foam stabilized with R972 particles, drainage almost stops after the first 10 minutes without any SCMC added. With addition of SCMC in the foam a much slower drainage is observed. The drainage ends about an hour after foam formation.

In the foam stabilized with R812 particles there was no drainage observed during the first few minutes in the foam with added SCMC. The drainage was slowed down by more than a factor of two

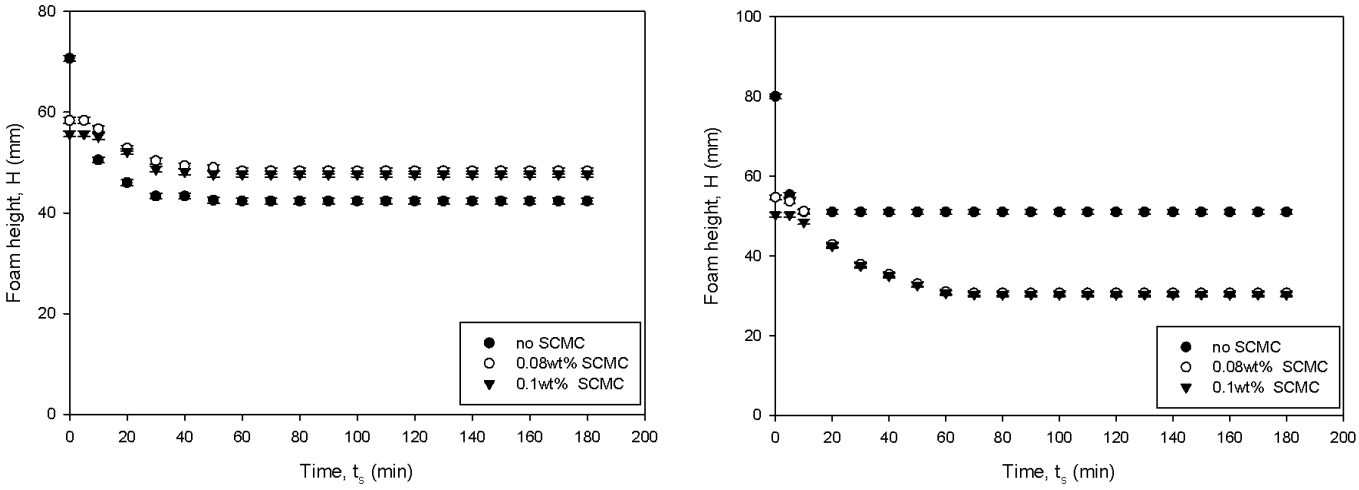

(a) R972 (b) R812

Figure 7.38: Effect of SCMC on breakage of foam containing R972 and R812 silica particles.

when SCMC was added. Figure 7.39(c) shows an increase in the liquid holdup in foams stabilized by R972 and R812 particles. The foam stabilized by R812 particle has a slightly higher liquid holdup than the foam produced by R972 particles. At 0.08 wt% SCMC, both foams stabilized by R972 and R812 particles show a twofold increase of the liquid content compared to particle foams without added SCMC. A further increase of SCMC concentration to 0.1 wt% only led to a relatively small further increase of the the liquid hold-up.

Foam Microstructure

5 minutes after foam formation the Sauter mean bubble size of R972 foams was 30.5, 16.7, and 18.7 μm for SCMC concentrations of 0, 0.08, and, 0.1 wt%, respectively. In foams stabilized by R812 the Sauter mean size was 23.4, 14.5, and 15.7 μm at SCMC concentrations of 0, 0.08, and 0.1 wt% SCMC, respectively. The images of foams stabilized by R972 and R812 particles are shown in Figures 7.40 and 7.41. The bubble size distributions of these foams are shown in Figure 7.42. Bubble size, d_{10} and d_{32}, decreases with addition of silica particles but there was no further reduction in the bubble size when the concentration of SCMC was increased. These foams were very stable and there was no bubble growth within a week.

Increasing viscosity by addition of SCMC causes a significant reduction in the drainage rate, mean

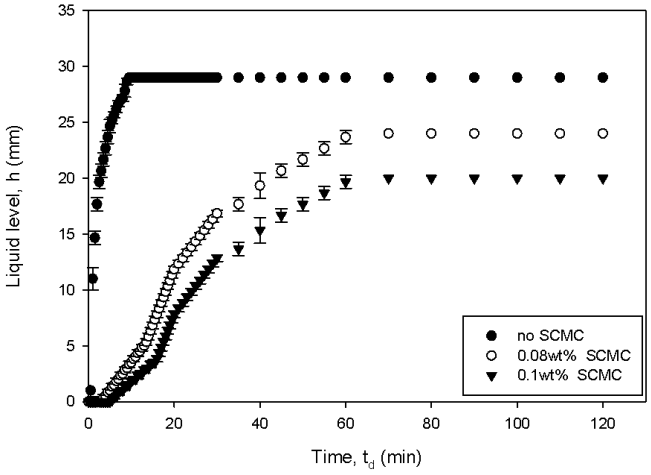

(a) R972

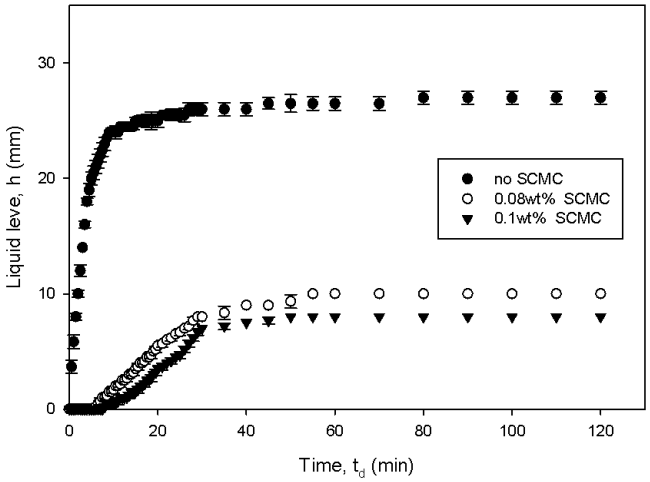

(b) R812

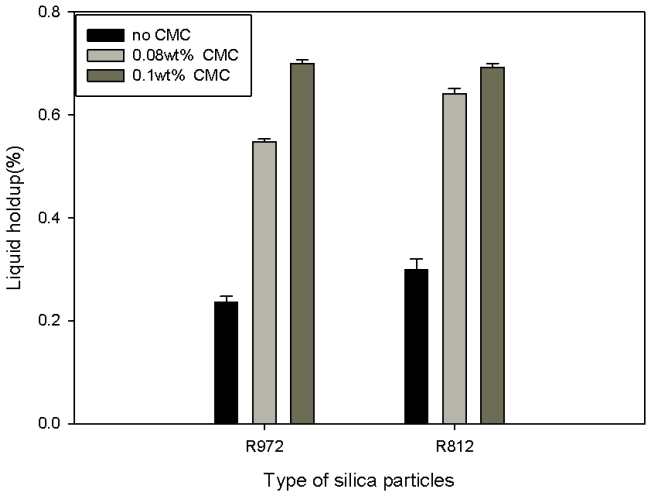

(c) liquid holdup

Figure 7.39: Effect of SCMC on: (a) Drainage of foam containing R972 silica particles. (b) Drainage of foam containing R812 silica particles (c) Liquid holdup of foam containing R972 and R812 silica particles.

bubble size, and an increase in liquid holdup in the foam stabilized by hydrophobic silica particles. However, less foamability was found.

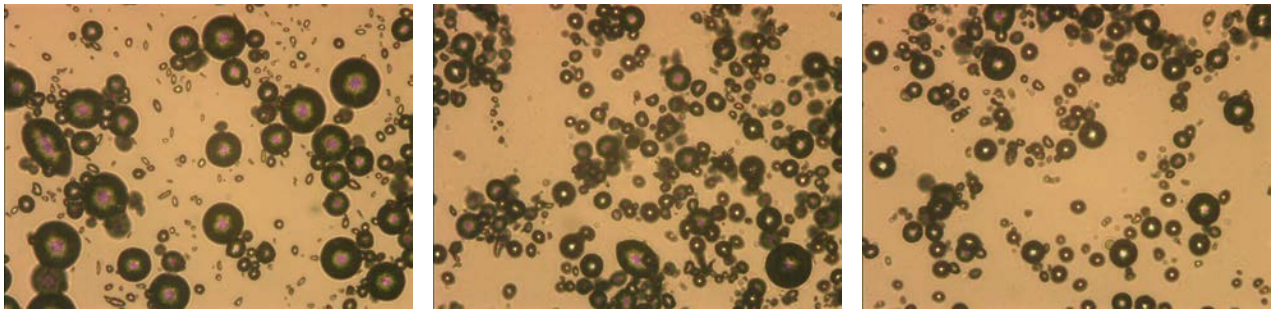

(a) only R972 particles (b) 0.08 wt% SCMC (c) 0.1 wt% SCMC

Figure 7.40: Foam Images; with R972 silica particles; MA (200 x magnification).

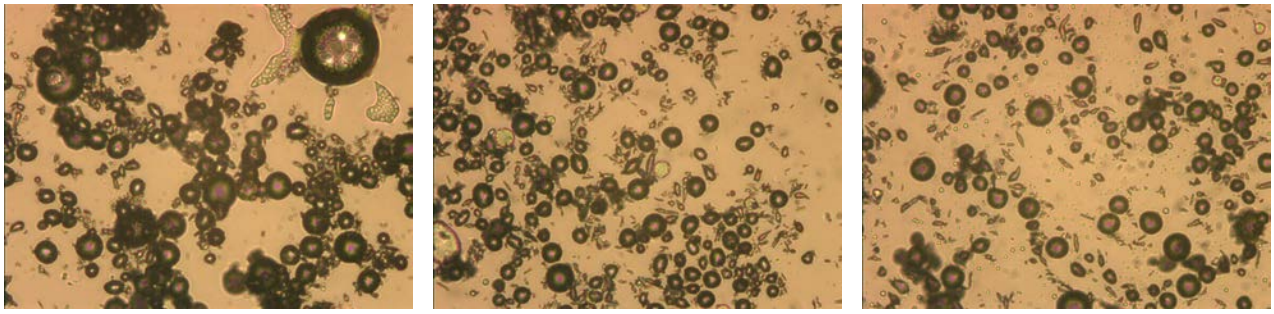

(a) only particles (b) 0.08 wt% SCMC (c) 0.1 wt% SCMC

Figure 7.41: Foam Images; with R812 silica particles; MA (200 x magnification).

Rheology of Foam Stabilized by Hydrophobic Silica Particles

In this section, foam stabilized by R812 particles only, as well as the R812 foam with addition of 0.1 wt% SCMC to study the foam rheology. These particles were chosen because they produce the most stable foams.

Wall slip test Figure 7.43 shows the evolution of instantaneous viscosity recorded at the imposed shear stress of 200 Pa and different plate gap sizes. The sample used contains 5.0 wt% of R812 particles. The gap size does not make a measurable difference to the viscosity evolution curves, which means that there is no wall slip.

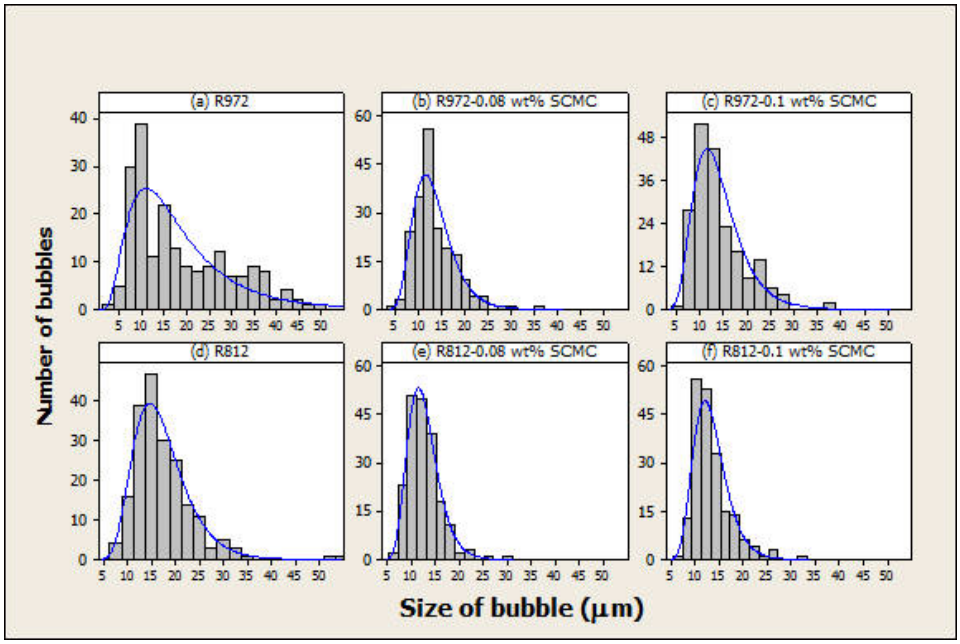

Figure 7.42: Bubble size distribution (a) R972 particles only (b) R972 particles with 0.08 wt% SCMC (c) R972 particles with 0.1 wt% SCMC (d) R812 particles only (e) R812 particles with 0.08 wt% SCMC (f) R822 particles with 0.1 wt% SCMC.

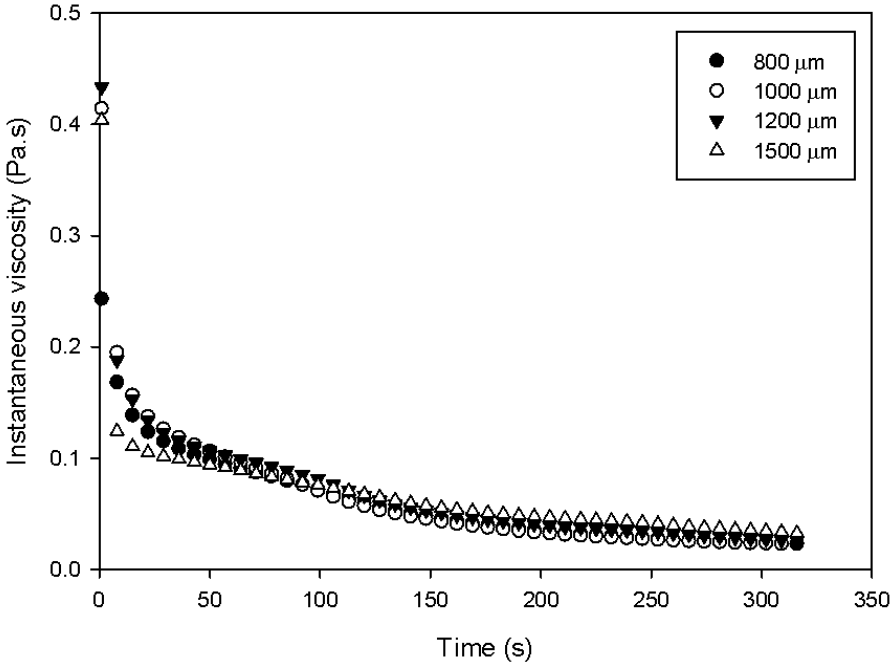

Figure 7.43: Evolution of instantaneous viscosity of R812 particle stabilized foam at different gap sizes using parallel plate geometry. Applied shear stress=200Pa

Constant Shear Stress Tests The constant shear stress tests on the foam was performed; the resulting shear rate and thus instantaneous viscosity were recorded over time. Figures 7.44 and 7.45 show the shear rate and corresponding instantaneous viscosity evolution curves of foam under different constant shear stresses. Overall, the shear rate evolution curves of the foam under a constant shearing stress could be divided into 3 categories depending on the magnitude of shear stress imposed:

1. **Low Shear Stress ($<$ 25 Pa)** Below a shear stress of 25 Pa, the instrument would not register any measurement. It is because the particle-stabilized foam is quite rigid and a shear stress below 25 Pa is not sufficient to shear the foam.

2. **Intermediate shear stress (25-40 Pa)** The shear rate increases gradually to reach a steady state, as shown in Figure 7.44. In Figure 7.45, the corresponding instantaneous viscosity of foam decreased to a plateau region where it stayed constant.

3. **High shear stress (50-70 Pa)** Initially, the shear rate increases sharply with time, particularly at high shear stresses. When the applied shear stress is over 70 Pa, the rheometer could no longer record data because the geometry overspeeds. This is because there was no foam structure left but only the mixture of silica particles and liquid. The foam was shear-thinning before its structure was destroyed completely.

Figures 7.46 and 7.47 show the shear rate and corresponding instantaneous viscosity evolution curves of the R812 silica particles stabilized foam with addition of 0.1 wt% under different constant shear stresses. Unlike the foam stabilized by R812 silica particles only, the response of foam with addition SCMC was found to be dependent of the shear stress but independent on shearing time. It could also be divided into three classes:

The observations discussed above show that the foam stabilized by silica particles only changes depending on the shear stress and shearing time over a range of different shear stresses. For shear stress less than 25 Pa, the foam is simply too rigid to shear; for shear stress over 50 Pa, the foam is too fragile to shear. Hence, measurements of the shear rate were not possible in these ranges. Only in the range of 25-40 Pa the shear rate could be determined reliably. An increase in the shear rate and a drop in the viscosity as a function of time were found. This indicates that the foams are

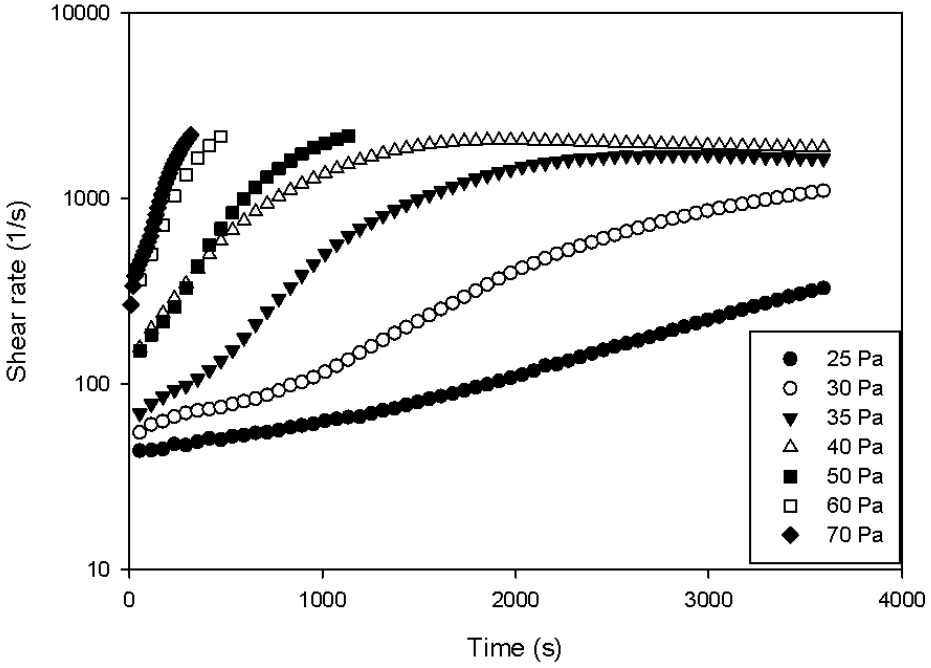

Figure 7.44: Shear rate evolution curves of R812 stabilized foam under application of a constant shear stress.

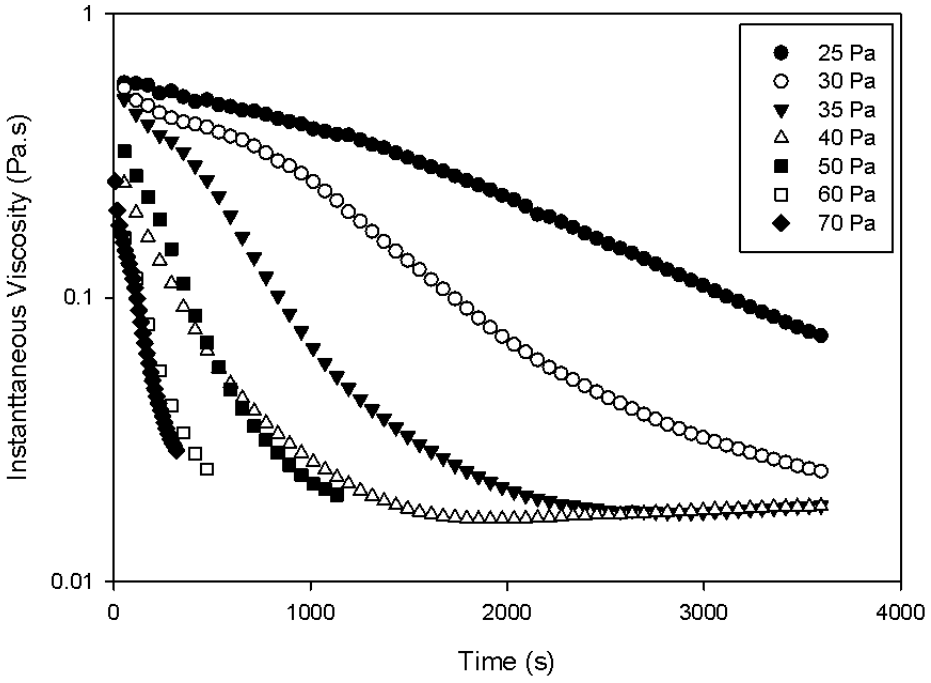

Figure 7.45: Instantaneous viscosity evolution curves of R812 stabilized foam under application of a constant shear stress.

shear-thinning. The transition from solid-like to liquid-like behaviour can be called *melting process* and this transition happens faster with increasing shear stress. This corresponds to a faster decrease of the instantaneous viscosity evolution curves. The foam stabilized by particles with addition of SCMC can be sheared at lower shear stress and higher shear stress than the foam stabilized by particles only. There is no sudden drop or increase in recorded shear rate or instantaneous viscosity.

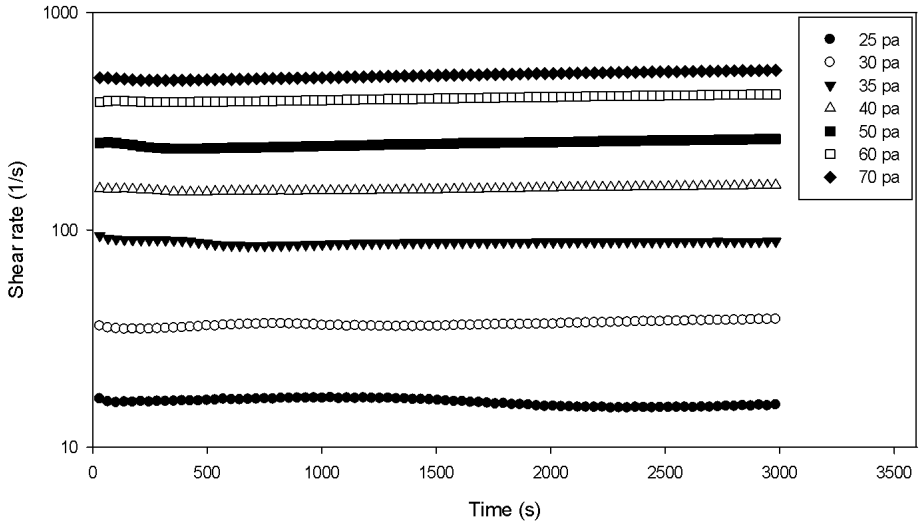

Figure 7.46: Shear rate evolution curves of R812 stabilized foam with addition of 0.1wt% of SCMC under application of constant shear stress.

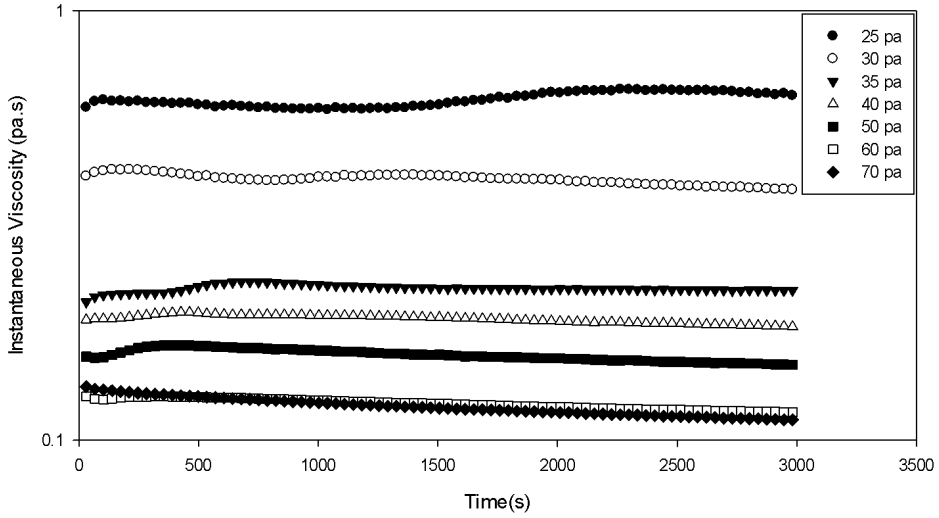

Figure 7.47: Instantaneous viscosity evolution curves of R812 stabilized foam with addition of 0.1 wt% of SCMC under application of constant shear stress.

Lim (2005) studied Gillette foam in detail. Gillette foam is a commercial brand of shaving foam. Shaving foams are aqueous foams. They consist of polydisperse gas bubbles packed in a smaller amount of water containing surfactants or other surface-active macromolecules. The bubble size of Gillette foam is about 30 μm. In the study, the author investigated the response of foam to a range of imposed shear stresses and found qualitatively very similar viscosity evolution curves as shown above in Figure 7.45. The author interpreted the decrease of the viscosity over time as a consequence of the destruction of bubbles in the sample. The higher the shear stress, the faster the bubbles are destroyed, and hence the faster the drop of the viscosity. In this study a similar behaviour in the foam stabilized by silica particles only but within a narrower range of imposed shear stress was observed. Therefore, the behaviour of the foam stabilized by R812 silica particles only could also be explained in the same way: when a low shear stress ($\leq$ 25 Pa) is applied to the foam stabilized by silica particles only, there is no plate movement and no data are recorded. This however, can be interpreted. It indicates that there is no macroscopic foam flow in the sample for the shear stress imposed. This is because the bubbles are rigid. This rigidity is a consequence of the bubbles being encapsulated in a particle network. This interpretation is supported by previous observation (see section 7.2.1) that under the same conditions there is no bubble growth within a month and hence no coarsening process either.

Sharing Lim's explanation, not only the imposed shear stress leads to a coarsening of the foam, and hence a reduces the rigidity of the foam. This coarsening process manifests itself in an increasing shear rate over time. The foam starts to flow when the imposed shear stress and exceeds a threshold strain and initiates bubble movement and coarsening. Hence only when the imposed shear stress is higher than or equal to 25 Pa then the rheometer can be used to measure the shear rate and the viscosity.

When a shear stress of 25 Pa is applied, then the viscosity decreases only slightly with time as shown in Figure 7.45. In the light of the this can be interpreted as a a process of bubble rearrangement coupled with a coarsening process. For higher shear stresses this coarsening process is much faster, which manifests itself in the rapid decrease of the viscosity over time. In these experiments, the shear rate qualitatively mirrors the instantaneous viscosity, as can be established by comparison of Figures

7.45 and 7.44 Above a shear stress of 70 Pa the shear rate data stopped because the geometry was overspeeding. This is caused by the bubble structure being destroyed and a complete collapse of the foam when only liquid and particles remained.

The foam with addition of SCMC shows very different behaviour from the foam only stabilized by particles only (see Figures 7.46 and 7.47). The viscosity evolution curves in this case are constant. With increasing imposed shear stress, the shear rate increases and the corresponding viscosity decreases.

Comparing the qualitative features of the stress test of foams with and without SCMC, added SCMC appears to lead to more robust bubbles. The addition of SCMC to the foam provides more strength to the bonding and flexibility between particles and therefore the foam can be sheared at lower shear stresses and also higher shear stresses without destroying the foam structure. This conclusion can be made and based on the time-independence of the instantaneous viscosity evolution curves in the case of added SCMC. This indicates that in this case there is no bubble coarsening due to the imposed shear stress. This could be due to the fact that adding SCMC alters the foam structure. Specifically, the bubbles in the foam with addition of SCMC are smaller with a lower foam volume indicating a denser foam in comparison to the bubbles produced by particles only.

Flow Curves The results from the foam stabilized by only R812 particles obtained in the constant stress shearing tests in the previous section show that the foam rheology under the application of an external shear is time-dependent; the shear rate depends on the shear stress applied and also the shearing time. Therefore, the instantaneous foam viscosity obtained in these tests can only be used when the shear stress and duration of shear at this stress is specified. The foam flow curves in this study are constructed by extracting the shear rate and viscosity registered at different stress values at specific shearing times.

Figure 7.48 shows the flow curves of particle stabilized foam at specific shearing times. The flow curves are plotted in three different ways: shear stress vs. shear rate; instantaneous viscosity vs. shear stress; and instantaneous viscosity vs. shear rate. The results to Lim's study can be compared. In Lim's study, the Gillette foam rheology can be divided into three regions on the flow curve namely (i) lower shear Newtonian, (ii) shear thinning and (iii) higher shear Newtonian region.

In the experiments, region (*ii*) the shear thinning region was observed. This can concluded from the particular shape of the flow curves, that is the graph that plots the instantenous viscosity as a function of shear rate in Figure 7.48. The data in these graphs is the same as above in the viscosity evolution curves and the shear rate evolution curves.

The flow curves of foam stabilized by only R812 silica particles show the viscosity decreasing with shear rate. This establishes that the foam stabilized by only particles is shear-thinning over the whole region measured. The reason for the absence of a Newtonian regime may be as follows: Bubbles produced by surfactant are more flexible than the particle stabilised foams. The irreversible absorption of particles at the interface of bubbles and the particle network may provide a long term stability of the foam but decreases the flexibility of bubble rearrangement. Once the imposed shear stress is over a certain value, the foam becomes very fragile and the transition process of solid-like to liquid-like behaviour happens very quickly under shearing.

The flow curves of foam stabilized by R812 particles with addition of SCMC constructed at shearing time of 1 min, 5 min, 10 min, 15 min and 30 min are shown in 7.49. These curves almost overlap because the addition of SCMC has changed the foam to time-independent as discussed in the previous section.

Dynamic Stress Sweep Test In this section, the viscoelastic properties of foams are investigated. Since the theory of dynamic test is based on the assumption that material deforms in a linear manner, it is thus important that all the tests are done in the linear domain of the material. this linear viscoelastic region in a foam stabilized by particles only by imposing an oscillating stress ranging from 0.01 to 60 Pa to the sample was determined. The resulting storage (elastic) modulus, G' and loss (viscous) modulus, G" were then recorded. Figure 7.50 shows the variation of the moduli with the oscillating stress imposed. A clear plateau in G' and G" was obtained in the range of shear stress from 0.01 to 20 Pa, indicating the linear viscoelastic region of particle stabilized foam. The storage modulus, G' was much higher than the loss modulus, G". This was expected because of the tight packing of the bubble matrix in the foam structure; the foam exhibited a predominantly solid-like behaviour.

The elastic modulus G' was constant up to and including a pressure of 20 Pa, but showed a

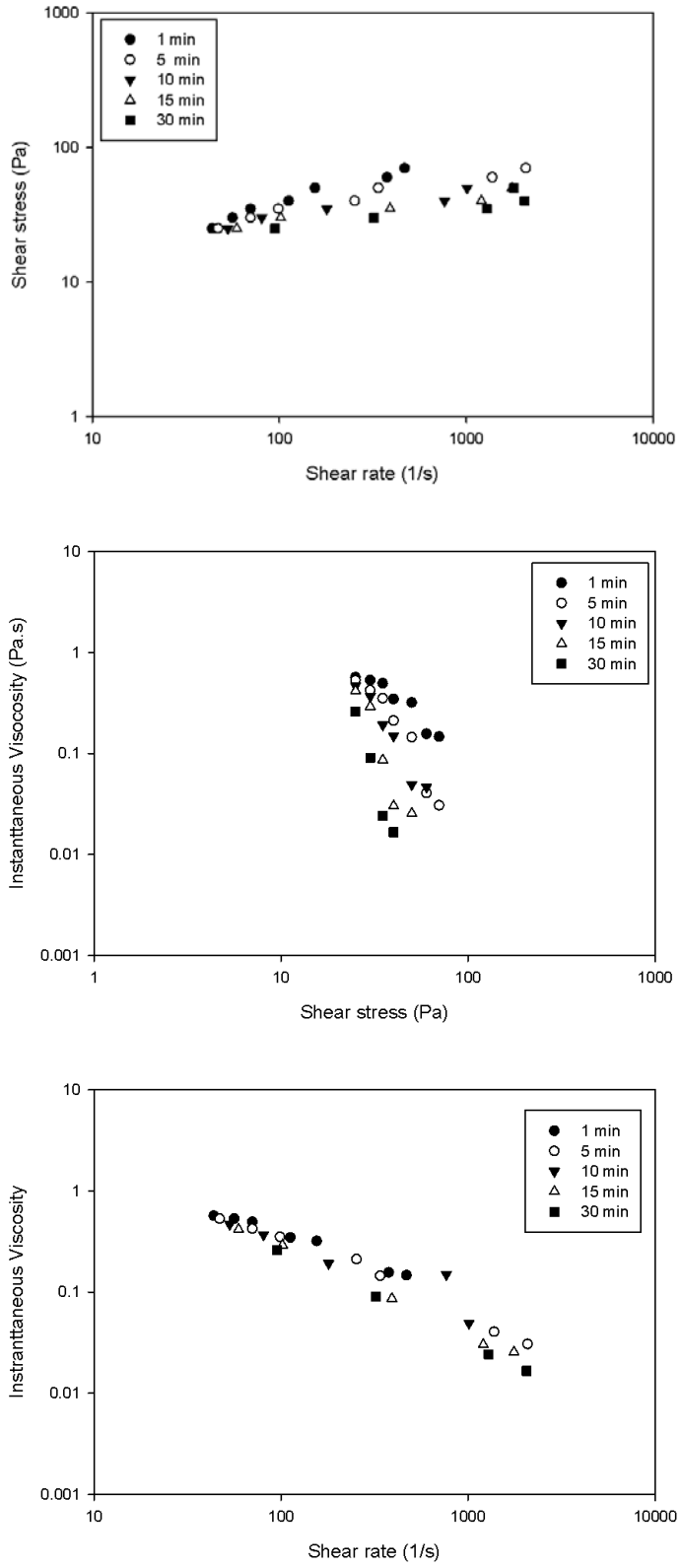

Figure 7.48: Flow curves of foam stabilized by R812 silica particles only at specific shearing time: (a) shear stress vs. shear rate; (b) instantaneous viscosity vs. shear stress; (c) instantaneous viscosity vs. shear rate.

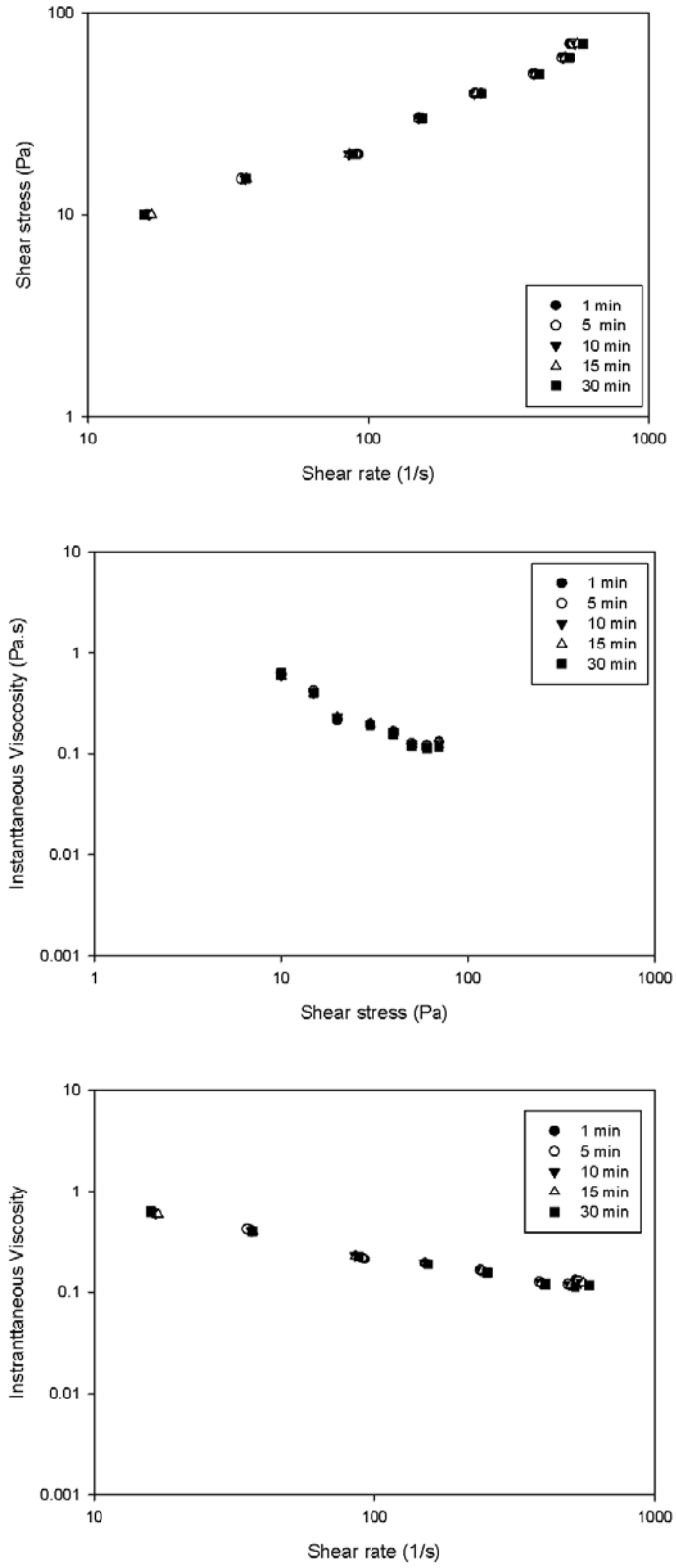

Figure 7.49: Flow curves of foam stabilized by R812 silica particles with $0.1wt\%$ SCMC only at specific shearing time: (a) shear stress vs. shear rate; (b) instantaneous viscosity vs. shear stress; (c) instantaneous viscosity vs. shear rate.

marked decline for 30 Pa. Also, there was a crossover between G' and G" at this critical stress. G" was found to be higher than the G' beyond this shear stress. Note that the crossover point corresponds to the minimum shear stress (in the measurements of the instantaneous viscosity above) to induce foam flow. This confirms the interpretation that shear stresses < 20 Pa cannot induce bubble re-arrangements and hence further suggests that bubbles of particle foams are very rigid.

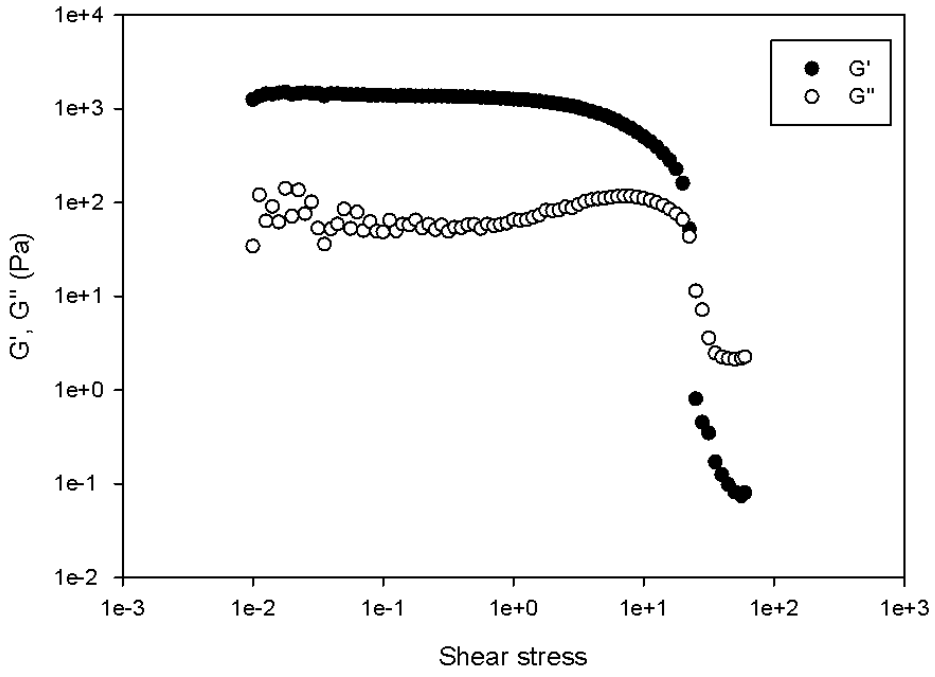

Figure 7.50: Linear viscoelastic region of foam stabilized by only R812 silica particles in the stress sweep test.

Figure 7.51 shows the variation of storage modulus, G' and loss modulus, G" at imposed shear stresses from 0.001 to 200 Pa in foam stabilized by R812 silica particle with addition of SCMC. In this case, the storage modulus decreases but the loss modulus keeps constant with increasing shear stress. A possible explanation is that the addition of SCMC has changed the foam properties to liquid-like behaviour because a high liquid holdup and smaller bubble size in this foam was observed.

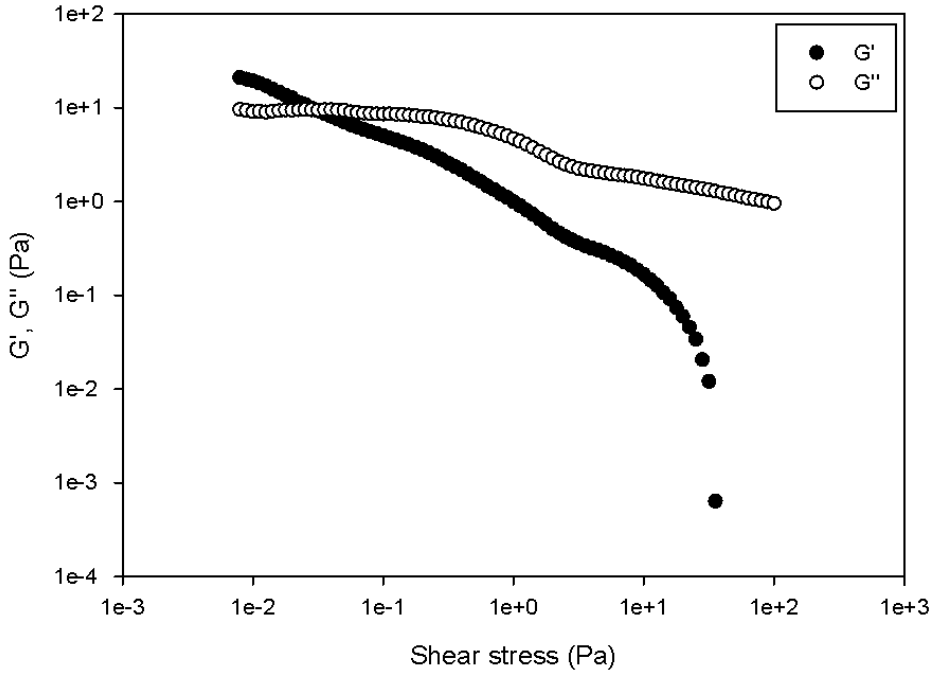

Figure 7.51: Foam stabilized by only R812 silica particles with 0.1wt% SCMC in the stress sweep test.

7.3 Conclusions

Four types of hydrophobic silica particles with different hydrophobicity were used to stabilize foams. UC and MA were use to make foams and the properties of the foams were compared.

A number of key observations emerged. Firstly, foamability as measured by the foam height generated in the column increased with the concentration of hydrophobic particles with both methods of foam generation. In general, an intermediate degree of hydrophobicity gave optimum foamability, whilst no foam could be produced with fully hydrophilic particles. Foam drainage was initially fast but stopped completely after the first ten minutes. Increasing silica concentration or the degree of particle hydrophobicity led to higher liquid holdups as the drainage rate was dramatically reduced.

Secondly, the foams generated using UC were drier. At low particle concentrations, the mean foam bubble size was of the order of 1 mm, but at higher concentrations a mean bubble size of about 300 μm was generated. The more hydrophobic particles also led to a coarser foam texture. These ultrasound generated foams were rather stable with significant changes in foam height only beginning to occur after a month. The bubble size distribution, however, started to evolve almost immediately

after foam generation was completed, leading to approximately a doubling in mean bubble size after a month.

Thirdly, the foams generated in the high shear mixer were considerably wetter than the ultrasound generated foams. At lower concentrations of silica particles, there were two layers of different mean bubble size foams produced. At all particle concentrations, the bubble size distributions generated by the high shear mixers were much narrower than those generated by UC, with a mean bubble size of the order of 30 μm; thus, three times finer and more uniform foams were obtained by MA. The foams exhibited an ultra high stability with no drainage or changes detected in foam height or mean bubble size over a month. After a period of 4 months, the bubble size distribution did evolve significantly leading to a considerable growth in bubble size. However, the foam height still remained constant and there was still no significant drainage occurring. The most hydrophobic particle clusters which could not be broken up into the sub-micron size range, even when pre-dispersed by high intensity ultrasound, produced foam with a poor texture in this case. This may be attributed to the existence of a bimodal particle cluster size distribution with the smaller aggregates ($\approx 0.3\mu m$) forming foam, whilst the larger aggregates ($\approx 20\mu m$) not being able to stabilize foam bubbles.

Fourthly, a much less stable foam was generated at pH 10 with lightly and intermediated hydrophobic silica particles. At pH 10, the foam bubble size distributions were much broader and a much larger mean bubble size was obtained with the least and intermediate hydrophobic silica particles. However, a better foam texture, with a mean bubble size of the order of 30 μm can be produced at higher pH with the most hydrophobic silica particles. Fifthly, much wetter and denser foams were obtained by adding SCMC. With all types of hydrophobic silica particles, a smaller mean bubble size of foam was produced in a higher viscosity dispersion.

In the foam rheology study, constant shear stress tests showed that the behaviour of the foam stabilized by R812 silica particles only is dependent on both time and shear stress, however, the R812 particle stabilized foam with addition of SCMC is independent of time and dependent on applied shear stress only. The transition of solid-like to liquid-like behaviour was found in the foam stabilized by particles only. The particle stabilized foam with addition of SCMC has no such transition region. The flow curves of both foams were constructed by extracting the data obtained at different shearing

time intervals. There is no yield stress as Lim reported. However, unlike Lim only one clear region was found. The curves are all lying in the shear thinning region. In this region, the foam flowed like liquid and hence the liquid-like behaviour.

The foam stabilized by only particles was found to have an elastic modulus which was much higher than viscous modulus. However, with addition of SCMC to foam does not have a linear viscoelastic region because the elastic modulus decreases with increasing shear stress.

Chapter 8

Conclusions

8.1 Conclusions

This thesis set out to study firstly the de-agglomeration of silica particles and secondly the stability of foams by investigating: (i) the effects of silica particles on proteins foams; (ii) the effects of silica particles on surfactants foams; and (iii) foams solely stabilized by silica particles.

The first and foremost conclusion of re-dispersing particles into suspensions is that hydrophilic silica particles can easily re-disperse into a well suspended and homogeneous suspension using a relatively low input while hydrophobic silica particles need significantly larger energy input. For the foam studies, hydrophilic particles stabilize protein foams while hydrophobic silica particles destabilize them. In surfactant stabilized foams, the hydrophobicity of particles plays different roles in foam stability. In the foam solely stabilized by particles, hydrophilic particles alone cannot generate foam. On the other hand, foams generated by hydrophobic particles are extremely stable.

8.1.1 The De-agglomeration of Silica Particles

- In the de-agglomeration process, particle size distributions can be divided into three stages. The first stage is that the aggregates of particles are larger than 1 μm and the single peak of size distribution stays in the right hand side of the spectrum. The size distribution shifts to the left but remains mono-modal with increasing energy input. In the second stage, the size distribution starts to split into two peaks. One stays on the right hand side of the spectrum

and the other stays on the left. 1 μm is the split point. In the third stage, the particle size distribution becomes mono-modal peak again and sits only in the micron size range. It can shift more to the left which means a further decrease of the average aggregate size with increasing energy input.

- Two re-dispersing methods were used and compared: ultrasound cavitation (UC) and mechanical agitation (MA). It was found that using MA to separate aggregates is faster and requires less energy than using UC when the aggregates were larger than 1 μm. Under 1 μm size, UC breaks down aggregates size to 106.5 μm, while mechanical agitation reduces the size to around 140.0 μm at an energy input of 3800 kJ/kg in ultrasound cavitation.

- With increasing hydrophobicity of the silica particles, much more energy input is needed to pull the aggregates apart. R972 particles (lightly hydrophobic) need nearly 10 times more energy input to break the aggregates to micron size range than the hydrophilic particles. With R812 particles (moderately hydrophobic), the emergence of a bimodal particle distribution coincides with the appearance of bubbles that are trapped in the suspensions. With R202 particles (strongly hydrophobic), the aggregate size can be reduced but the size distribution never reaches a bi-modal distribution or a single peak in the sub-micron-range. The bubble generation was unavoidable in these dispersions.

- Hydrophilic particles can easily disperse into suspension in ranging pH between 2 to 12 and the suspension was stable for two months. With increasing pH, hydrophobic particles can be separated. Once the hydrophobic particles break into micron size, the suspensions are stable for longer periods (a day).

- The particle size of R972 and R812 can be altered by adjusting the pH and by adding ionic surfactant. R972 particles can be broken into sub-micron size at a pH between 4 to 12 in 0.2 cmc C12 LAS and R812 can be separated into sub-micron size at pH between 7 to 12. In comparison to only water, adding C12LAS and SDS enhanced the ability of re-dispersing these hydrophobic particles. R812 can be broken into sub-micron size with adding CTAB at pH 10 and 12.

8.1.2 The Effects of Silica Particles on Proteins Foams

- In comparing the two foam generation methods used, UC can produce finer protein stabilized foam with less energy input into the system
- A much better foamability was found in casein foams than in whey foams. Foam stability and foam life are similar. Addition of hydrophilic particles enhanced the stability of whey protein foams.
- Addition of hydrophilic particles increased foam stability and foam life, whereas addition of hydrophobic particle destabilized the foams.
- When adding hydrophilic particles, a higher liquid holdup with smaller initial bubble size and slower bubble growth was generated by UC at a concentrations of particles under 1.0 wt%. UC is a method that allows lower energy use and shorter generation time to produce foam with and without addition of silica particles. However, the drawback is that it can only be used when the dispersion volume is small and in low viscosity materials.
- A better foamability but a shorter foam life was found at pH 10 in whey protein foam. At pH 7, the foam made by MA collapsed in 30 minutes while there is no such observation in the foam made by UC. The structure of protein may be altered by UC.

8.1.3 The Effects of Silica Particles on Surfactants Foams

- C12LAS and CTAB were used in this study. At 0.2 cmc C12LAS foam, addition of low concentrations of hydrophobic particles destabilizes the foams, whereas addition of a high concentration of hydrophobic particles stabilizes foams. Foam stability increases but the foamability decreases with increasing hydrophobicity of particles. At 1.0 cmc C12LAS foam, more hydrophobic particles are needed to stabilize foams.
- In CTAB foams, foam stability increases when either hydrophilic or hydrophobic silica is added. Increasing silica concentration enhances foam stability. Addition of R972 and R812 particles

increases foamability whereas a decrease of foamability was observed in the foam with R202 particles.

- The pH has no significant influence on surfactant stabilized foams but it does have an effect on the surfactant foam with hydrophobic particles. In general, the foamability and foam stability of foam with particles decreases with increasing pH. This is especially apparent in the CTAB foams with particles. From the microstructure, there are different types of bubbles produced at different pH. It shows that the hydrophobic particles have lost their hydrophobicity and foam is formed by the surfactant molecules.

- In general, the increase of viscosity by adding SCMC reduces drainage rate, but there is also a great reduction in foamability.

8.1.4 Foams Solely Stabilized by Silica Particles

- In general, R812 particles (moderately hydrophobic) gave optimum foamability, whilst no foam could be produced with fully hydrophilic silica particles. Increasing particle concentration and degree of hydrophobicity led to higher liquid holdups as the drainage was reduced dramatically.

- Comparing UC and MA, the foams generated by UC were drier than the ones produced by MA but still with a substantial liquid holdup. The mean bubble size increased from 300 μm to 1 mm when the concentration of particles decreased from 0.5 wt% to 0.1 wt%. These foams were stable with significant changes in foam height only beginning to occur after a month.

- The foams generated by MA were considerably wetter than UC generated foams. Under 1.0 wt% of particles, there were two layers of different mean bubble size foams and the upper layer of foam decreases with increasing concentration of particles. The lower layer of foam contains smaller bubbles which are about 30 μm while the upper layer bubbles were of the order of mm. The foams exhibited ultra high stability with no drainage or changes detected in foam height or bubble size distribution over a month.

- With R972 and R812 particles, a much less stable foam was produced above pH 10. However, a more regular shaped foam texture was achieved than at lower pH. At pH 10 R202 particles

can produce foams with a mean bubble size of 30 μm. A smaller mean bubble size and a wetter foam was obtained with increasing viscosity.

- In the foam rheology study, the viscosity of R812 particles stabilized foam depends on both time and shear stress. However, when SCMC is added then it is independent of time. A transition from solid-like to liquid-like behaviour was found in the foam without addition of SCMC. The bubbles were rigid at low shear stress but extremely fragile at higher shear stress.

Bibliography

Alargova, R. G., Warhadpande, D. S., Paunov, V. N. and Velev, O. D. (2004). Foam superstabilization by polymer microrods, *Langmuir* **20**(24): 10371–10374.

Aoki, M., Ring, T. A. and Haggerty, J. S. (1987). Analysis and modeling of the ultrasonic dispersion technique, *Advanced Ceramic Materials* **2**(3A): 209–212.

Assar, G. and Burley, R. (1984). *Encyclopaedia of Fluid Mechanics, vol. III*, Gulf Publishing.

Ata, S., Ahmed, N. and Jameson, G. J. (2002). Collection of hydrophobic particles in the froth phase, *International Journal of Mineral Processing* **64**(2-3): 101–122.

Ata, S., Ahmed, N. and Jameson, G. J. (2004). The effect of hydrophobicity on the drainage of gangue minerals in flotation froths, *Minerals Engineering* **17**(7-8): 897–901.

Aveyard, R., Binks, B., Fletcher, P. and Rutherford, C. (1994). Measurement of contact angles of spherical monodisperse particles with surfactant solutions, *Colloids and Surfaces A: Physicochemical and Engineering Aspects* **83**(1): 89–98.

Beneventi, D., Carre, B. and Gandini, A. (2001). Role of surfactant structure on surface and foaming properties, *Colloids and Surfaces A: Physicochemical and Engineering Aspects* **189**(1-3): 65–73.

Bergeron, V. (1997). Disjoining pressures and film stability of alkyltrimethylammonium bromide foam films, *Langmuir* **13**(13): 3474–3482.

Bhakta, A. and Ruckenstein, E. (1997a). Decay of standing foams: drainage, coalescence and collapse, *Advances in Colloid and Interface Science* **70**: 1–124.

Bhakta, A. and Ruckenstein, E. (1997b). Drainage and coalescence in standing foams, *Journal of Colloid and Interface Science* **191**(1): 184–201.

Bikerman, J. J. (1973). *Foams*, Springer-Verlag New York Inc.

Binks, B. P. (2002). Particles as surfactants–similarities and differences, *Current Opinion in Colloid & Interface Science* **7**(1-2): 21–41.

Binks, B. P., Desforges, A. and Duff, D. G. (2007). Synergistic stabilization of emulsions by a mixture of surface-active nanoparticles and surfactant, *Langmuir* **23**(3): 1098–1106.

Binks, B. P., Duncumb, B. and Murakami, R. (2007). Effect of pH and salt concentration on the phase inversion of particle-stabilized foams, *Langmuir* **23**(18): 9143–9146.

Binks, B. P. and Horozov, T. S. (2005a). Aqueous foams stabilized solely by silica nanoparticles, *Angewandte Chemie-International Edition* **44**(24): 3722–3725.

Binks, B. P. and Murakami, R. (2006). Phase inversion of particle-stabilized materials from foams to dry water, *Nature Material* **5**: 865.

Binks, B. P., Murakami, R., Armes, S. P., Fujii, S. and Schmid, A. (2007). pH-responsive aqueous foams stabilized by ionizable latex particles, *Langmuir* **23**(17): 8691–8694.

Binks, B. P. and Rodrigues, J. A. (2007). Enhanced stabilization of emulsions due to surfactant-induced nanoparticle flocculation, *Langmuir* **23**(14): 7436–7439.

Binks, B. P., Rodrigues, J. A. and Frith, W. J. (2007). Synergistic interaction in emulsions stabilized by a mixture of silica nanoparticles and cationic surfactant, *Langmuir* **23**(7): 3626–3636.

Binks, B. P. and Whitby, C. P. (2005). Nanoparticle silica-stabilised oil-in-water emulsions: improving emulsion stability, *Colloids and Surfaces A: Physicochemical and Engineering Aspects* **253**(1-3): 105–115.

Binks, P. B. and Horozov, S. T. (2005b). Aqueous foams stabilized solely by silica nanoparticles, *Angewandte Chemie-International Edition* **44**: 3722–3725.

Blute, I., Pugh, R. J., van de Pas, J. and Callaghan, I. (2009). Industrial manufactured silica nanoparticle sols. 2: Surface tension, particle concentration, foam generation and stability, *Colloids and Surfaces A: Physicochemical and Engineering Aspects* **337**(1-3): 127–135.

Bos, M. A. and van Vliet, T. (2001). Interfacial rheological properties of adsorbed protein layers and surfactants: a review, *Advances in Colloid and Interface Science* **91**(3): 437 – 471.

Bremmell, K. E., Jameson, G. J. and Biggs, S. (1999). Adsorption of ionic surfactants in particulate systems: flotation, stability, and interaction forces, *Colloids and Surfaces A: Physicochemical and Engineering Aspects* **146**(1-3): 75–87.

Briggs, T. (1995). *Foams: Theory, measurements, and applications*, Marcel Dekker Inc, chapter Foams for firefighting, p. 465.

Britten, M.and Lavoie, L. (1992). Foaming properties of proteins as affected by concentration, *Journal of Food Science* **57**(5): 1219–1241.

Burley, R. and Shakarin, M. (1992). An experimental study of foam rheology in straight capillary tubes, *International Journal of Engineering Fluid Mechanics* **5**(2): 115–141.

Chapel, J.-P. (1994). History-dependent hydration forces measured between silica surfaces, *Journal of Colloid and Interface Science* **162**(2): 517 – 519.

Cherry, J. and McWatters, K. (1981). Whippability and aeration, *Protein functionality in food*, pp. 147–149.

Cho, S.-H., Kim, J.-Y., Chun, J.-H. and Kim, J.-D. (2005). Ultrasonic formation of nanobubbles and their zeta-potentials in aqueous electrolyte and surfactant solutions, *Colloids and Surfaces A: Physicochemical and Engineering Aspects* **269**(1-3): 28–34.

Cooke, T. F. and Hirt, D. E. (1995). *Foams: Theory, mesurements, and applications*, Marcel Dekker Inc, chapter Foam wet processing in the textile industry, p. 339.

Creighton, T. H. (1993). *Proteins: structures and molecular properties*, San Francisco: W. H. Freeman.

Deshpande, N. and Barigou, M. (1999). Foam formation, drainaage, and collapse in the presence of antifoams, *The Fourth Italian Conference on Chemical and Process Engineering, Florence, Italy* pp. May 2–5.

Dickinson, E. (1986). Mixed proteinaceous emulsifiers: review of competitive protein adsorption and the relationship to food colloid stabilization, *Food Hydrocolloids* **1**(1): 3 – 23.

Dickinson, E. (1989). Food colloids – an overview, *Colloids and Surfaces* **42**(1): 191–204.

Dickinson, E. (1992). *An introduction to food colloids*, Oxford University Press, Oxford.

Dickinson, E. (2010). Food emulsions and foams: stabilization by particles, *Current Opinion in Colloid Interface Science* **15**(1-2): 40–49.

Dickinson, E., Ettelaie, R., Kostakis, T. and Murray, B. (2004). Factors controlling the formation and stability of air bubbles stabilized by partially hydrophobic silica nanoparticles, *Langmuir* **20**(20): 8517–8525.

Dickinson, E., Ettelaie, R., Murray, B. S. and Du, Z. (2002). Kinetics of disproportionation of air bubbles beneath a planar air-water interface stabilized by food proteins, *Journal of Colloid and Interface Science* **252**(1): 202 – 213.

Ding, P. and Pacek, A. W. (2008). Effect of pH on deagglomeration and rheology/morphology of aqueous suspensions of goethite nanopowder, *Journal of Colloid and Interface Science* **325**(1): 165–172.

Dippenaar, A. (1982a). The destabilization of froth by solids. I. the mechanism of film rupture, *International Journal of Mineral Processing* **9**(1): 1–14.

Dippenaar, A. (1982b). The destabilization of froth by solids. II. the rate-determining step, *International Journal of Mineral Processing* **9**(1): 15–22.

Du, Z., Bilbao-Montoya, M. P., Binks, B. P., Dickinson, E., Ettelaie, R. and Murray, B. S. (2003). Outstanding stability of particle-stabilized bubbles, *Langmuir* **19**: 3106–3108.

Eskandar, N. G., Simovic, S. and Prestidge, C. A. (2007). Synergistic effect of silica nanoparticles and charged surfactants in the formation and stability of submicron oil-in-water emulsions, *Phys. Chem. Chem. Phys.* **9**: 6426 – 6434.

Exerowa, D. and Kruglyakov, P. M. (1998). *Foams and Foam Films: theory, experiment, application: Studies in interface science, vol 5*, Elsevier.

Fokkink, L. G. and Ralston, J. (1989). Contact angles on charged substrates, *Colloids and Surfaces* **36**(1): 69 – 76.

Frye, G. C. and Berg, J. C. (1989). Antifoam action by solid particles, *Journal of Colloid and Interface Science* **127**(1): 222–238.

Fujii, S., Iddon, P. D., Ryan, A. J. and Armes, S. P. (2006). Aqueous particulate foams stabilized solely with polymer latex particles, *Langmuir* **22**(18): 7512–7520. PMID: 16922528.

Ganzevles, R. A., Cohen Stuart, M. A., Vliet, T. v. and de Jongh, H. H. (2006). Use of polysaccharides to control protein adsorption to the air-water interface, *Food Hydrocolloids* **20**(6): 872–878.

Gao, M. and Forssberg, E. (1995). Prediction of product size distributions for a stirred ball mill, *Powder Technology* **84**(2): 101 – 106.

Garrett, P. (1993). *Defoaming, Surfactant Science Series vol. 45*, Marcel Dekker Inc.

Goff, H. D. and Hill., A. R. (1993). *Dairy Chemistry and Physics*, VCH Publishers, New York, chapter Dairy Science and Technology Handbook, Vol. 1, Principles and Properties, pp. 1–81.

Gonzenbach, U., Studart, A., Tervoort, E. and Gauckler, L. (2006a). Stabilization of foams with inorganic colloidal particles, *Langmuir* **22**(26): 10983–10988.

Gonzenbach, U., Studart, A., Tervoort, E. and Gauckler, L. (2007). Tailoring the microstructure of particle-stabilized wet foams, *Langmuir* **23**(3): 1025–1032.

Gonzenbach, U. T., Studart, A. R., Tervoort, E. and Gauckler, L. J. (2006b). Stabilization of foams with inorganic colloidal particles, *Langmuir* **22**(26): 10983–10988.

Gonzenbach, U. T., Studart, A. R., Tervoort, E. and Gauckler, L. J. (2006c). Ultrastable particle-stabilized foams, *Angewandte Chemie-International Edition* **45**(21): 3526–3530.

Grabbe, A. and Horn, R. G. (1993). Double-layer and hydration forces measured between silica sheets subjected to various surface treatments, *Journal of Colloid and Interface Science* **157**(2): 375–383.

Graham, D. E. and Phillips, M. C. (1979). Proteins at liquid interfaces : I. kinetics of adsorption and surface denaturation, *Journal of Colloid and Interface Science* **70**(3): 403–414.

Gulseren, I., Guzey, D., Bruce, B. D. and Weiss, J. (2007). Structural and functional changes in ultrasonicated bovine serum albumin solutions, *Ultrasonics Sonochemistry* **14**(2): 173–183.

Gunzey, D., Gulseren, I., Bruce, B. and Weiss, J. (2006). Interfacial properties and structural conformation of thermosonicated bovine serum albumin, *Food Hydrocolloids* **20**(5): 669–677.

Hammershoj, M., Prins, A. and Qvist, K. B. (1999). Influence of pH on surface properties of aqueous egg albumen solutions in relation to foaming behaviour, *J. Sci. Food Agric.* **79**(6): 859–868.

Horozov, T. S. (2008). Foams and foam films stabilised by solid particles, *Current Opinion in Colloid & Interface Science* **13**(3): 134–140.

Hudales, J. B. M. and Stein, H. N. (1990). The influence of solid particles on foam and film drainage, *Journal of Colloid and Interface Science* **140**(2): 307–313.

Hunter, T. N., Pugh, R. J., Franks, G. V. and Jameson, G. J. (2008). The role of particles in stabilising foams and emulsions, *Advances in Colloid and Interface Science* **137**(2): 57–81.

Iler, R. K. (1979). *The Chemistry of Silica*, Wiley-Interscience, New York, chapter Chapter 1.

Jambrak, A. R., Mason, T. J., Lelas, V., Herceg, Z. and Herceg, I. L. (2008). Effect of ultrasound treatment on solubility and foaming properties of whey protein suspensions, *Journal of Food Engineering* **86**(2): 281–287.

Ji, Y.-Q., Black, L., Koster, R. and Janek, M. (2007). Hydrophobic coagulation and aggregation of hematite particles with sodium dodecylsulfate, *Colloids and Surfaces A: Physicochemical and Engineering Aspects* **298**(3): 235–244.

Kam, S. I. and Rossen, W. R. (1999). Anomalous capillary pressure, stress, and stability of solids-coated bubbles, *Journal of Colloid and Interface Science* **213**(2): 329 – 339.

Kippax, P. (2005). Measuring particle size using modern laser diffraction techniques, *Paint and Coating Industry magazine* .

Kloek, W., Van Vliet, T. and Meinders, M. (2001). Effect of bulk and interfacial rheological properties on bubble dissolution, *Journal of Colloid and Interface Science* **237**(2): 158–166.

Kosmulski, M. (2001). *Chemical properties of material surfaces*, Marcel Dekker Inc.

Kralchevski, P., Nikolov, A., Wasan, D. T. and Ivanov, I. (1990). Formation and expansion of dark spots in stratifying foam films, *Langmuir* **6**: 11801189.

Kuropatwa, M., Tolkach, A. and Kulozik, U. (2009). Impact of pH on the interactions between whey and egg white proteins as assessed by the foamability of their mixtures, *Food Hydrocolloids* **23**(8): 2174–2181.

Kusters, K. A., Pratsinis, S. E., Thoma, S. G. and Smith, D. M. (1993). Ultrasonic fragmentation of agglomerate powders, *Chemical Engineering Science* **48**(24): 4119–4127.

Kusters, K. A., Pratsinis, S. E., Thoma, S. G. and Smith, D. M. (1994). Energy–size reduction laws for ultrasonic fragmentation, *Powder Technology* **80**(3): 253–263.

Laheja, A. P., Basak, S., Patil, R. M. and Khilar, K. C. (1998). Experimental observations on drainage of foams generated using micellar solutions of anionic, cationic, and nonionic surfactants, *Langmuir* **14**(2): 560–564.

Lakkis, J. and Villota, R. (1990). *Food emulsions and foams: Theory and practice*, American Institute of Chemical Engineers, New York, chapter A study on the foaming and emulsifying properties of whey protein hydrolysates, pp. 87–111.

Lan, Q., Yang, F., Zhang, S., Liu, S., Xu, J. and Sun, D. (2007). Synergistic effect of silica nanoparticle and cetyltrimethyl ammonium bromide on the stabilization of o/w emulsions, *Colloids and Surfaces A: Physicochemical and Engineering Aspects* **302**(1-3): 126–135.

Langevin, D. (2000). Influence of interfacial rheology on foam and emulsion properties, *Advances in Colloid and Interface Science* **88**(1-2): 209 – 222.

Lee, S.-Y., Morr, C. V. and Ha, E. Y. (1992). Structural and functional properties of caseinate and whey protein isolate as affected by temperature and pH, *Journal of Food Science* **57**(5): 1210–1229.

Leighton, T. G. (1995). Bubble population phenomena in acoustic cavitation, *Ultrasonics Sonochemistry* **2**(2): S123–S136.

Lim, K. and Barigou, M. (2005). Pneumatic foam generation in the presence of a high-intensity ultrasound field, *Ultrasonics Sonochemistry* **12**(5): 385–393.

Lim, K. S. (2005). *Studies of foam microstructure and rheology*, University of Birmingham.

Liu, Q., Zhang, S., Sun, D. and Xu, J. (2009). Foams stabilized by laponite nanoparticles and alkylammonium bromides with different alkyl chain lengths, *Colloids and Surfaces A: Physicochemical and Engineering Aspects* **355**: 151–157.

Louisnard, O., Lyczko, N., Espitalier, F., Urzedowski, M., Vargas-Hernandez, Y. and Sanchez-Romero, C. (2001). High bubble concentrations produced by ultrasounds in binary mixtures, *Ultrasonics Sonochemistry* **8**(3): 183–189.

Magrabi, S., Dlugogorski, B. and Jameson, G. (1999). Bubble size distribution and coarsening of aqueous foams, *Chemical Engineering Science* **54**(18): 4007–4022.

Marinova, K. G., Basheva, E. S., Nenova, B., Temelska, M., Mirarefi, A. Y., Campbell, B. and Ivanov, I. B. (2009). Physico-chemical factors controlling the foamability and foam stability of milk proteins: Sodium caseinate and whey protein concentrates, *Food Hydrocolloids* **23**(7): 1864 – 1876.

Mason, T. J. (1999). *Sonochemistry*, Oxford University Press.

Mason, T. J. and Lorimer, J. P. (2002). *Applied sonochemistry*, Weinheim, Wiley-VCH.

Mende, S., Stenger, F., Peukert, W. and Schwedes, J. (2003). Mechanical production and stabilization of submicron particles in stirred media mills, *Powder Technology* **132**(1): 64 – 73.

Meste, M., Colas, B., Simatos, D., Closs, B., Courthaufon, J.-L. and Lorient, D. . (1990). Contribution of protein flexibility to the foaming properties of casein, *Jounal of Food Science* **55**: 1445.

Midmore, B. R. (1998a). Preparation of a novel silica-stabilized oil/water emulsion, *Colloids and Surfaces A: Physicochemical and Engineering Aspects* **132**(2-3): 257–265.

Midmore, B. R. (1998b). Synergy between silica and polyoxyethylene surfactants in the formation of o/w emulsions, *Colloids and Surfaces A: Physicochemical and Engineering Aspects* **145**(1-3): 133–143.

Monsalve, A. and Schechter, R. S. (1984). The stability of foams: Dependence of observation on the bubble size distribution, *Journal of Colloid and Interface Science* **97**(2): 327 – 335.

Morrison, I. D. and Ross, S. (2002). *Colloidal dispersions: suspensions, emulsions, and foams*, A John Wiley & Sons, Inc., Publication.

Murray, B. S. (2007). Stabilization of bubbles and foams, *Current Opinion in Colloid & Interface Science* **12**(4-5): 232 – 241.

Murray, B. S. and Ettelaie, R. (2004). Foam stability: proteins and nanoparticles, *Current Opinion in Colloid & Interface Science* **9**(5): 314–320.

Mutilangi, W. M. and Kilara, A. (1985). Functional properties of heat-denatured whey proteins. II. emulsifying and foaming properties, *Milchwissernschaft* **40**: 391.

Pacek, A., Ding, P. and Utomo, A. (2007). Effect of energy density, pH and temperature on de-aggregation in nano-particles/water suspensions in high shear mixer, *Powder Technology* **173**(3): 203–210.

Patel, P. and Fry, J. (1987). *Development in food protein 5*, Elsevier Applied Science, Oxford, chapter The search for standardized methods for assessing protein functionality, p. 299.

Patino, J. M. R., Delgado, D. N. and Fernandez, J. (1995). Stability and mechanical strength of aqueous foams containing food proteins, *Colloids and Surfaces A: Physicochemical and Engineering Aspects* **99**(1): 65–78.

Patist, A., Axelberd, T. and Shah, D. O. (1998). Effect of long chain alcohols on micellar relaxation time and foaming properties of sodium dodecyl sulfate solutions, *Journal of Colloid and Interface Science* **208**(1): 259–265.

Patist, A. and Bates, D. (2008). Ultrasonic innovations in the food industry: From the laboratory to commercial production, *Innovative Food Science & Emerging Technologies* **9**(2): 147–154.

Paulsson, M. and Dejmek, P. (1992). Surface film pressure of β-lactoglobulin, α-lactalbumin and bovine serum albumin at the air/water interface studied by wilhelmy plate and drop volume, *Journal of Colloid and Interface Science* **150**(2): 394–403.

Pradhan, M. S. and Khilar, K. C. (1994). Stability of aqueous foams with polymer additives: III. measurements and calculations of stability of foams generated at different pressures, *Journal of Colloid and Interface Science* **168**(2): 333–338.

Prins, A., Bos, M., Boerboom, F. J. G. and van Kalsbeek, H. K. A. I. (1998). *Proteins at liquid interfaces*, Elsevier Sciences, Amsterdam, chapter Relation between surface rheology and foaming behavior of aqueous protein solutions, pp. 221–266.

Prud'homme, R. K. and Khan, S. A. (1995). *Foams: Theory, measurements, and applications*, Marcel Dekker, Inc.

Pugh, R. (1996). Foaming, foam films, antifoaming and defoaming, *Advances in Colloid and Interface Science* **64**: 67–142.

Pugh, R. (2005). Experimental techniques for studying the structure of foams and froths, *Advances in Colloid and Interface Science* **114-115**: 239 – 251. Dedicated to the Memory of Dr Hans Joachim Schulze.

Ramsden, W. (1903). Separation of solids in the surface-layers of solutions and 'suspensions' (observations on surface-membranes, bubbles, emulsions, and mechanical coagulation) - preliminary account, *Proceedings of the Royal Society* **72**: 156.

Reiss-Husson, F. and Luzzati, V. (1966). Small-angle x-ray scattering study of the structure of soap and detergent micelles, *Journal of Colloid and Interface Science* **21**(5): 534–546.

Ridley, M. (2006). *Genome*, New York, NY: Harper Perennial.

Rieger, M. (1995). *Foams: Theory, mesurements, and applications*, Marcel Dekker Inc, chapter Foam in personal care product, p. 381.

Rosen, M. J. (1989). *Surfactants and Interfacial Phenomena*, John Wiley & Sons, Inc.

Rossen, W. R. (1995). *Foams: Theory, mesurements, and applications*, Marcel Dekker Inc, chapter Foams in enhanced oil recovery, p. 413.

Saint-Jalmes, A., Peugeot, M.-L., Ferraz, H. and Langevin, D. (2005). Differences between protein and surfactant foams: Microscopic properties, stability and coarsening, *Colloids and Surfaces A: Physicochemical and Engineering Aspects* **263**(1-3): 219 – 225. A collection of papers presented at the 5th European Conference on Foams, Emulsions, and Applications, EUFOAM 2004, University of Marne-la-Vallee, Champs sur Marne (France), 5-8 July, 2004.

Sanchez, C. C. and Patino, J. M. R. (2005). Interfacial, foaming and emulsifying characteristics of sodium caseinate as influenced by protein concentration in solution, *Food Hydrocolloids* **19**(3): 407–416.

Sauter, C., Emin, M., Schuchmann, H. and Tavman, S. (2008). Influence of hydrostatic pressure and sound amplitude on the ultrasound induced dispersion and de-agglomeration of nanoparticles, *Ultrasonics Sonochemistry* **15**(4): 517–523.

Sauter, C., Pohl, M. and Schuchmann, H. P. (2006). Ultrasound for dispersion nanoparticles, *12th European Conference on Mixing, Bologna* .

Schwarz, S. and Grano, S. (2005). Effect of particle hydrophobicity on particle and water transport across a flotation froth, *Colloids and Surfaces A: Physicochemical and Engineering Aspects* **256**(2-3): 157–164.

Sethumadhavan, G., Bindal, S., Nikolov, A. and Wasan, D. (2002). Stability of thin liquid films containing polydisperse particles, *Colloids and Surfaces A: Physicochemical and Engineering Aspects* **204**(1-3): 51–62.

Suslick, K. (1988). Ultrasound: Its chemical, physical, and biological effects, *in* K. Suslick (ed.), *Homogeneous sonochemistry*, New York, pp. 123–163.

Suslick, K. S. and Grinstaff, M. W. (1990). Protein microencapsulation of nonaqueous liquids, *Journal of the American Chemical Society* **112**(21): 7807–7809.

Tamura, T., Takeuchi, Y. and Kaneko, Y. (1998). Influence of surfactant structure on the drainage of nonionic surfactant foam films, *Journal of Colloid and Interface Science* **206**(1): 112 – 121.

Tang, F.-Q., Xiao, Z., Tang, J.-A. and Jiang, L. (1989). The effect of SiO2 particles upon stabilization of foam, *Journal of Colloid and Interface Science* **131**(2): 498–502.

Teilum, K., Olsen, J. G. and Kragelund, B. B. (2011). Protein stability, flexibility and function, *Biochimica et Biophysica Acta (BBA) - Proteins & Proteomics* **1814**(8): 969–976.

Timothy, J. M. and Dietmar, P. (2002). *Practical sonochemistry: power ultrasound uses and applications, 2nd Edition*, Horwood.

Tkachenko, N. H., Yaremko, Z. M., Bellmann, C. and Soltys, M. M. (2006). The influence of ionic and nonionic surfactants on aggregative stability and electrical surface properties of aqueous suspensions of titanium dioxide, *Journal of Colloid and Interface Science* **299**(2): 686–695.

Verwey, E. and Overbeek, J. (1948). *Theory of the stability of lyophobic colloids*, Elsevier, Amsterdam.

Vigil, G., Xu, Z., Steinberg, S. and Israelachvili, J. (1994). Interactions of silica surfaces, *Journal of Colloid and Interface Science* **165**(2): 367 – 385.

Vijayaraghavan, K., Nikolov, A. and Wasan, D. (2006). Foam formation and mitigation in a three-phase gas-liquid-particulate system, *Advances in Colloid and Interface Science* **123-126**: 49–61.

Wang, W., Zhou, Z., Nandakumar, K., Xu, Z. and Masliyah, J. H. (2004). Effect of charged colloidal particles on adsorption of surfactants at oil-water interface, *Journal of Colloid and Interface Science* **274**(2): 625–630.

Weaire, D. and Hutzler, S. (1999). *The physics of foams*, Clarendon Press, Oxford.

Wiggers, F. N. (2001). *The flow and drainage of foams and films*, PhD thesis, University of Birmingham.

Wilde, P. (2000). Interfaces: their role in foam and emulsion behaviour, *Current Opinion in Colloid & Interface Science* **5**(3-4): 176–181.

Wilson, J. C. (1980). *A study of particulate foams. phd thesis*, Master's thesis, University of Bristol.

Yotsumoto, H. and Yoon, R.-H. (1993a). Application of extended DLVO theory: I. stability of rutile suspensions, *Journal of Colloid and Interface Science* **157**(2): 426–433.

Yotsumoto, H. and Yoon, R.-H. (1993b). Application of extended DLVO theory: II. stability of silica suspensions, *Journal of Colloid and Interface Science* **157**(2): 434–441.

Zhang, S., Lan, Q., Liu, Q., Xu, J. and Sun, D. (2008). Aqueous foams stabilized by Laponite and CTAB, *Colloids and Surfaces A: Physicochemical and Engineering Aspects* **317**(1-3): 406–413.

Zhang, S., Sun, D., Dong, X., Li, C. and Xu, J. (2008). Aqueous foams stabilized with particles and nonionic surfactants, *Colloids and Surfaces A: Physicochemical and Engineering Aspects* **324**(1-3): 1–8.

Zhou, Z., Xu, Z., Finch, J., Masliyah, J. and Chow, R. (2009). On the role of cavitation in particle collection in flotation - a critical review. II, *Minerals Engineering* **22**(5): 419 – 433.

Ziga, R. and Aguilera, J. (2008). Aerated food gels: fabrication and potential applications, *Trends in Food Science and Technology* **19**(4): 176–187.